12-2015

Investigation of the Inherent Chemical, Structural, and Mechanical Attributes of Bio-Engineered Composites Found in Nature: Alligator Gar's Exoskeleton Fish Scales

Wayne Derald Hodo
University of Arkansas, Fayetteville

Investigation of the Inherent Chemical, Structural, and Mechanical Attributes of Bio-Engineered Composites Found in Nature: Alligator Gar's Exoskeleton Fish Scales

A dissertation submitted in partial fulfillment
of the requirements for the degree of
Doctor of Philosophy in Engineering

by

Wayne D. Hodo
Auburn University
Bachelor of Science, 1997
Mississippi State University
Master of Science in Civil Engineering, 2006

December 2015
University of Arkansas

This dissertation is approved for recommendation to the Graduate Council.

_____
Dr. R. Panneer Selvam
Dissertation Director

_____   _____
Dr. Kevin D. Hall   Dr. John F. Peters
Committee Member   Committee Member

_____   _____
Dr. Ernie Heymsfield   Dr. Min Zou
Committee Member   Committee Member

ABSTRACT

The U.S. Army has determined a huge cost savings of up to 51% can be accomplished by reducing the gross vehicle weight, for their personnel carrier, by 33%. To cut cost, composite materials are needed. Man-made composites can have superior material properties (high-strength, high-fracture toughness, and lightweight), but they are prone to delamination at the glued-layered interface. In contrast, fish scale is a natural composite that has the same material properties and, additionally, tend not to delaminate.

The focus of this study was to learn how nature integrates hard and soft materials at each length scale to form a layered composite that better resists delamination. Previous research conducted by others had suggested that from the nano-to-millimeter length scale the individual components of the fish scale are glued to form layers in the composite. My research provided a detailed description, using novel experiments, to explain how hard and soft materials have been mixed/integrated at each length scale, optimized by volume fractions, and subtly vary material properties. The material variations were compared to mechanical properties of modulus, hardness, and for the first time energy dissipation.

(a)   The combination of the hard (inorganic minerals) and soft (polymer-like organic collagen fibers) are integrated instead of being glued at the nano scale. At the micron scale for the two-layered composite the outer dental enamel (hard) layered interface uses a saw tooth shaped joint to connect to the inner bone (hard open-like foam) layer. At the millimeter scale the material and mechanical properties are gradually graded through the thickness, away from the interface.

(b)   Within each layer, at the micron scale, there are subtle variations in materials. However, the outer dental enamel (hard) layer has 90-percent hard (inorganic minerals), 10 percent (polymer-like organic collagen fibers), by volume. Whereas, the inner bone (hard open-like foam) layer has 60 percent hard (inorganic minerals) and 40 percent (polymer-like organic collagen fibers), by volume.

(c)   Because hard and soft materials are mixed/integrated within the layers from the nano-to-micro length scales; along with property away from the interface at the millimeter scale the local stresses that lead to delamination are reduced.

ACKNOWLEDGEMENTS

I would like to first acknowledge the University of Arkansas' Graduate School and Civil Engineering Department for affording me the opportunity to pursue a basic scientific research topic that is typically thought to be non-traditional to most Civil Engineering PhD curriculums. I would like to thank my PhD committee: Drs. R. Panneer Selvam (Chair), Kevin Hall (Member), Ernie Hyemsfield (Member), John Peters, (Member), and Min Zou (Member). Each committee member provided their diverse perspectives as researchers and professionals, which were both instrumental in the execution of my research topic.

I would like to acknowledge the USACE-ERDC and its Military Engineering Research Program for providing financial support. I would like to thank all of my loyal family, friends, and colleagues who stuck by me and supported me unconditionally throughout this enduring process. I would like to thank God and my parents for giving me the mental and physical resolve to be able to achieve one of the most important milestones of my lifetime. I would like to especially thank Dr. John Peters, my long-time colleague, mentor, and advocate, for all the words of wisdom, encouragement, and jokes he provided so I would stay motivated to overcome any obstacle and continue marching along the path of success.

I am very grateful for being able to complete the long journey to the mountaintop. This process has truly taught me professionalism and life skills that I could not have learned otherwise. With the achievement of my PhD, I now truly understand the dedication and sacrifice it requires to become a philosopher. Now that one chapter of my life has ended, it's time to start anew. It's time for me to start living life again by going off and doing great, rewarding things for years to come.

DEDICATION

I would like to dedicate this body of work to my parents Mrs. Ruby Hodo and Wilbur Hodo (Deceased).

TABLE OF CONTENTS

LIST OF FIGURES

LIST OF ABBREVIATIONS AND TERMS

Abbreviations	Terms
$\alpha\text{-}Al_2O_3$	Aluminum Oxide
2σ	Two Standard Deviations
AASHTO	American Association of State Highway and Transportation Officials
$AgC_{22}H_{43}O_2$	Silver Behenate
AFM	Atomic Force Microscopy
Al	Aluminum
ATR	Attenuated Total Reflectance
ATR-FTIR	Attenuated Total Reflectance- Fourier Transform Infrared Spectroscopy
B-Ap	Bio-Apatite
C/B-Ap	Collagen + Bio-Apatite
C	Carbon
Ca	Calcium
$CaCO_3$	Calcium Carbonate
CO_3	Carbonate
CBR	California Bearing Ratio
CH_x	Hydrocarbons
Cl	Chlorine
COOH	Carboxyl
CP	Cross-Polarization
CP-CH	Cross-Polarization Carbon-Hybridized
CP-CSA	Cross-Polarization Chemical Shift Anisotropy

CP-DD	Cross-Polarization Dipolar De-phasing
CP-DDD	Cross-Polarization Dipolar De-phasing Difference
CP-TOSS	Cross-Polarization Total Carbon Speciation
Cryst.	Crystals
DEM	Discrete Element Method
DMA	Dynamic Mechanical Analysis
DOE	Design of Experiments
Deter.	Determination
D_S	Contact Damping
D_m	Machine Damping
DTI	Drop Tower Impact
E'	Storage Modulus
E''	Loss Modulus
EELS	Electron Energy Loss Spectroscopy
EPMA	Electron Microprobe Analyzer
ERDC	Engineer and Research Development Center
F	Fluorine
F_0	Harmonic Force Amplitude
FEA	Finite Element Analysis
FEM	Finite Element Method
Fe	Iron
FIB	Focused Ion Beam
FTIR	Fourier Transform Infrared Spectroscopy
G	Gravitational Constant

Ge	Germanium
H	Hydrogen
h_0	Harmonic Displacement
H	Hypothesis
HAADF	High Angle Annular Dark Field
HAp	Hydroxyapatite
HR-SEM	High Resolution Scanning Electron Microscopy
INI	Instrumented Nanoindentation
IRE	Internal Reflection Element
ITZ	Interfacial Transition Zone
K	Potassium
k_f	Finite Stiffness
k_s	Spring Stiffness
m	Mass
Mg	Magnesium
Mn	Manganese
μm-UC	Micropillar Uniaxial Compression
μm-XANES	Microcomputed Synchrotron X-Ray Absorption Near Edge Structure
μm-XCT	Micro X-Ray Computed Tomography
μm-XEDS	Microcomputed X-Ray Energy-Dispersive Spectroscopy
μm-XRD	Microcomputed Synchrotron X-Ray Diffraction
μm-XRF	Microcomputed Synchrotron X-Ray Fluorescence
Mg	Magnesium
Mn	Manganese

N	Nitrogen
Na	Sodium
NIH	National Institutes of Health
O	Oxygen
OH$^-$	Hydroxide
P	Phosphorus
PO$_4$	Phosphate
PBS	Phosphate-Buffered Saline
ppm	Parts-Per-Million
Prot.	Protein
ROI	Return on Investment
S	Contact Stiffness
S	Sulfur
Si	Silica
Sr	Strontium
Speciat.	Speciation
SS-NMR	Solid-State Nuclear Magnetic Resonance
STEM	Scanning Transmission Electron Microscopy
STEM-HAADF	Scanning Transmission Electron Microscopy-High Angle Annular Dark Field
STEM-EELS	Scanning Transmission Electron Microscopy-Electron Energy Loss Spectroscopy
tan Φ	Phase Lag or Phase Angle
TEM	Transmission Electron Microscopy
Ti	Titanium

TGA	Thermal Gravimetric Analysis
UC	Uniaxial Compression
UT	Uniaxial Tension
Var.	variables
Zn	Zinc

CHAPTER 1: INTRODUCTION

1.1 Motivation

As a result of recent budget restraints, the U.S. Army has looked to reduce production

cost for some of its military assets. For example, the Army has determined a huge cost savings

can be accomplished by reducing the gross vehicle weight for the Mine-Resistant Ambush

Protected (MRAP) personnel carrier by thirty-three-percent (Joint Light Tactical Vehicle, 2015).

The MRAP weighs [7-15] tons and cost [300 -550 (base models)] $k/vehicle to build (Mine-

Resistant Ambush Protected, 2015). Whereas, the next generation Joint Light Tactical Vehicle

(JLTV) is expected to weigh [4.5-10] tons and [230 -270 (base models)] $k/vehicle] to build

(Joint Light Tactical Vehicle, 2015). To be able to cut cost up to fifty-one-percent while

maintaining military personnel safety, engineered composite materials will need to be used.

Engineered composite (inhomogeneous) materials are well known for their superior structural

properties. Composites are attractive because they can have the superior structural properties of

being impact/penetration resistant, lightweight, high-strength, high-stiffness, and can provide

good fatigue and corrosion resistance, Figure 1.1 (Structural Composites and Sandwhich Panels,

2015). Additionally, engineered composites are multilayered systems that have interfaces that are

glued. In the general sense, composite materials are defined as two or more physically and

chemically distinct materials which, when combined, have improved properties over the

individual materials (Strong, 2008). When comparing engineering composites to other structural

materials such as steel, concrete, and foams, we find: (a) steel has high-strength, high-fracture

toughness, but is extremely heavy, (b) concrete has high-strength, but is very brittle, has little

fracture toughness and is very heavy, (c) foam is impact resistant, lightweight, but has low

fracture-toughness, and low-strength.
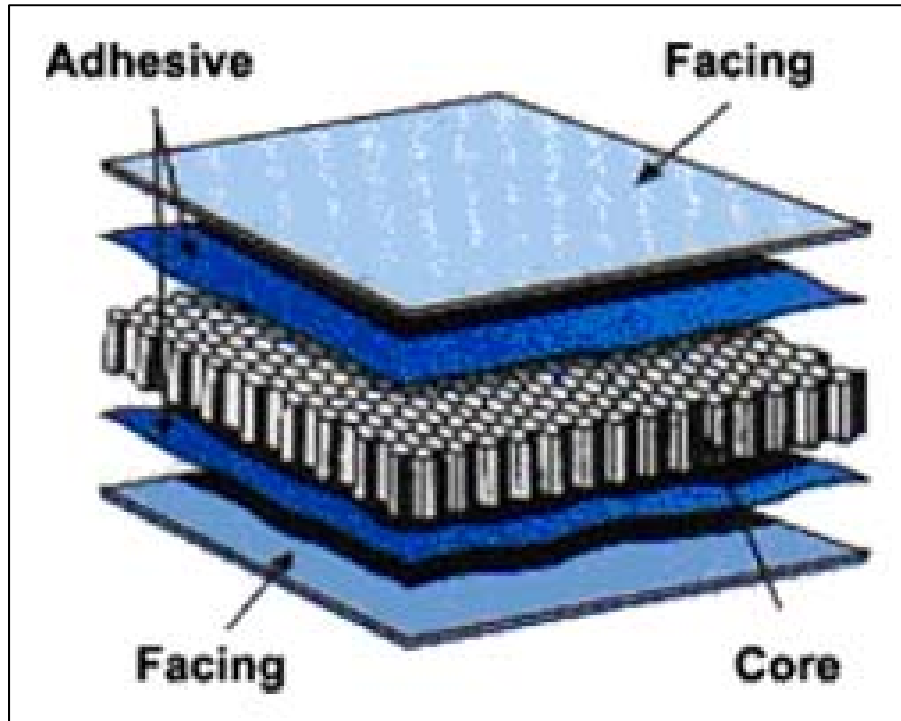
Figure 1.1 Schematic of multilayered composite material system
(Structural Composites and Sandwhich Panels, 2015).

Although composites are promising and offer mutual exclusive material properties (high-

strength, high-fracture toughness, and lightweight) that are not found in other structural

materials, they are prone to delamination at the glued layered interface. Usually man-made

engineered composites tend to delaminate when impacted because the glued layers de-bond.

Delamination at layer interfaces is the primary mechanism that leads to the failure of composite

materials, Figure 1.2 (Makhecha, 2005; Columbia Accident Investigation Board, 2003). As an

example, if engineered composites are used as sandwich panels on space shuttles, they can

become damaged by impact. As an outcome of the impact damage, the glued sandwich panels

may delaminate and fail almost instantaneously if exposed to the extreme thermal temperatures

and weight of gravity, causing the shuttle to explode. (Makhecha, 2005; Columbia Accident Investigation Board, 2003).

Figure 1**.2** Composites fail by delamination when impacted, foam-tile delamination led to Columbia space shuttle disaster (Columbia Accident Investigation Board, 2003).

In contrast to man-made composites, most superior performing materials (high-strength, high-toughness, and lightweight) found in nature are layered composite systems that use a two-component mixture of materials that are integrated at each length scale from the nano-to-millimeters to form what is called a (hierarchal structure). From the nano to micron length scale the hard materials (similar to metals) are mixed with soft materials (similar to polymers) then varied by volume fractions, spatial proximity, and directional placement in the layers to produce

3

a delamination resistant composite system. These delaminate resistant biocomposite structures [e.g., alligator gar (*Atractosteus spatula*) exoskeleton fish scale] have mechanical properties that vastly exceed the properties of their relatively weak constituents Figure 1.3 (Wegst, U., Schecter, M., Donius, A., and Hunger, P., 2010). Shown in Ashby's chart "a," Figure 1.3, are the specific values (that is, normalized by density) of strength and stiffness (or Young's modulus) for both natural and synthetic materials.
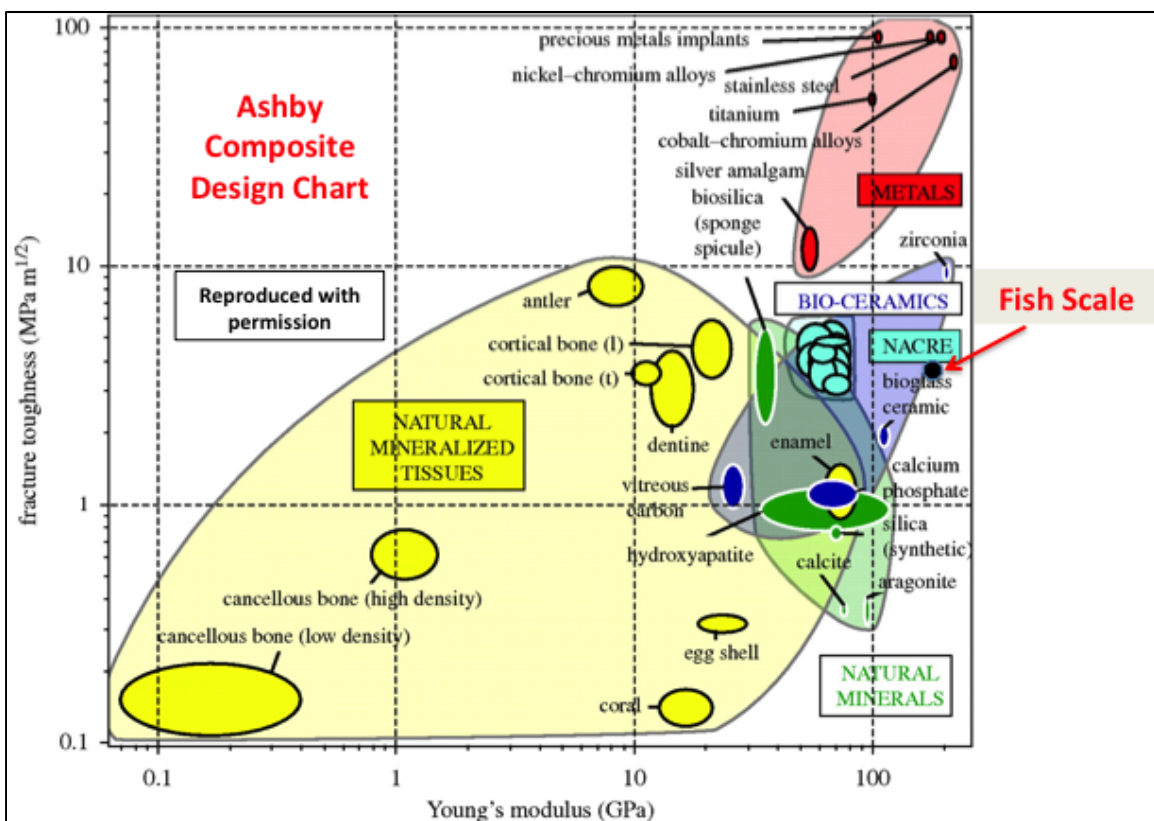
Figure 1.3 Ashby design chart of mechanical properties showing fracture toughness plotted against Young's modulus for natural and engineered composite materials (Wegst, U., Schecter, M., Donius, A., and Hunger, P., 2010).

At the millimeter scale after integrating the hard and soft material, the natural composites can have values of strength and toughness that are very comparable to those of most metals and alloys.

Specifically, shown in Figure 1.3, the engineering properties of the fish scales two individual layer components are similar to the outer dental enamel (hard) and inner cancellous bone (soft-sponge-like foam). The hard enamel is lightweight, has high-strength but is brittle and has a low fracture toughness. Whereas the sponge-like cancellous bone is lightweight, but it is soft, low-strength and has low fracture toughness. However, when the (hard) enamel is mixed with the (soft) sponge-like cancellous bone, they combine to make a lightweight fish scale layered composite that has high-strength with good fracture toughness whose engineering properties are comparable to metal alloys.

1.2 Problem

Most superior performing materials found in nature possess a hierarchal composite structure. The formation of the weak individual constituents found in fish scale composite is a function of its environmental conditions (i.e., water temperature and soluble minerals). Within each layer, at the micron scale, there are subtle variations in the spatial proximity and directional placement of the hard and soft materials. The fish scale is made up of 90 percent hard (inorganic minerals) and 10 percent soft (polymer-like organic collagen fibers) by volume. However, knowledge is lacking on how nature integrates hard and soft materials at each length scale to form a layered composite that is lightweight has high-strength with good fracture toughness but does not delaminate.

1.3 Scientific Objective

The objective of this research effort is to: (a) Investigate how nature might produce a composite made from a hard (inorganic mineral) and soft (polymer-like organic fibers) to form a layered structure that exhibits superior performing delamination resistance when externally loaded. (b) Explain how the hard and soft materials are integrated in the fish scale to form a

layered structure that is lightweight and has high-strength with good fracture toughness so they may not delaminate. (c) Suggest what fish scale design principles can be applied to the design of man-made engineered composite systems.

1.4 Hypothesis (*H*)

The hypothesis (*H*) is that the fish scales resist cracks and delamination because of the mixing and integration of materials occurring at millimeter, micron, and nano scales. Evidently, the fish scale's hard (inorganic minerals) and soft (polymer like organic fibers) material volume fractions and variations within the layers reduces the local stresses that lead to delamination and crack formation caused by impact/penetration.

1.5 Approach

To meet the objectives of this research effort and to test the hypothesis, I further experimentally investigated from the nano-to-millimeter length scale the delamination resistant mechanisms in fish scale. At each length scale a detailed description was provided of how the hard and soft materials were mixed, what were the material variations within the layers, and what effect did the materials and variations have on mechanical properties in the composite system.

1.6 Research Innovation

Previous research conducted by others has suggested that from the nano-to-millimeter length scale the individual components of the fish scale are glued rather than being integrated to form layers in the composite. However, sufficient evidence had yet to be provided that neither proves nor disproves the suggested assumption. The innovation of this research is that for the first time a detailed description was provided as to how hard and soft materials are mixed and integrated at each length to form a layered structure. In addition my research provided details on

6

how the hard and soft materials vary by volume fractions, spatial proximity, and directional placement within the layers. Furthermore, the material variations were compared to mechanical properties of modulus, hardness, and for the first time energy dissipation were used to explain why the natural composite has high strength, good toughness, and may not delaminate.

As an additional outcome of my research, to be able to meet my research objective and sufficiently test the hypothesis, a fundamental material science approach was used to develop an experimental protocol. Currently, there are no satisfactory standard combined protocols for investigating the material integration, local mechanical properties, material variation and integration at each length scale (millimeter, micron, and nano). Therefore, the development of the experimental protocol was needed so that the material variation and integration from the nano-to-millimeter length scale could be adequately explained. The experimental protocol used in this research is based on fundamental principles as opposed to the applied research methods of trial and error. The approach used here makes use of design concepts rather than iterative techniques that are employed across the engineering and scientific communities.

1.7 Organization of Thesis

Chapter 2 of this document provides a detailed overview of the current state of knowledge for exoskeleton fish scales and the experimental methods used in the characterization of bio-composites. Chapter 3 describes the experimental plan, materials, and methods used in this study. Chapter 4 provides the experimental data, analysis, and results for type, integration, and variation of materials, and mechanical properties for the layers at each length scale. Chapter 5 discusses the specific questions raised by the hypothesis, insight provided for the biological design principles, and suggested methodologies for developing bioinspired engineered

composite designs that exhibit advanced high-performance. Chapter 6 provides the summary,

contributions/conclusions, from this research, and offers recommendations for future work.

CHAPTER 2: STATE-OF-KNOWLEDGE

2.1 Advanced Engineered Composites Overview

Advanced engineered composites have been widely used by public and private sectors for marine, automotive, transportation, and aerospace industries (Gururaja 2012). In general, composites are used because no single structural material can be found that has all of the desired characteristics to meet the demands for specific applications. Engineered composites are robust and are often preferred by designers because individual materials are used in concert for the enhancement of performance characteristics. For instance, heterogeneous (dissimilar) carbon fiber–reinforced polymers (CFRP's) materials are used wherever high strength-to-weight ratio and rigidity are key to performance such as in airplane wings (Jones, 1999). The wings must be light for air flight and durable enough to resist torsion, compressive, tensile, shearing, and flexural failure.

In recent years, the composites that are in use are comprised of advanced materials and typically function under extreme operating conditions. For example, high earthquake areas, subzero temperature environments, nuclear blast, or instances of penetration effects caused by mid-to-high rate situations are the extreme conditions in which the composites should be able to perform well. Therefore, the myriad of attributes advanced composites offer that may be used to meet designers tailored requirements are: (a) tailorable physical and mechanical properties (e.g., anisotropic strengthening, toughness, durable, lightweight, high stiffness/crush resistance, strength-to-weight ratios and complex geometries, (b) conductive properties (e.g., optical or electrical ranging from none, to low, to high), (c) corrosion resistance, (d) thermal/flammable resistance, and (e) renewability/recyclability (Gibson, 1994).

2.2 Current Limitations of Advanced Engineered Composites

One of the most critical aspects when designing composites is to prevent de-bonding/ delamination of layers and at interfacial transition zones (ITZ's) of dissimilar materials. For example, engineered sandwich panel composites have the superior properties of being lightweight and temperature resistant and have been consistently used on space shuttle surfaces; thereby making space travel possible. However, an accident occurred, on February 1, 2003, during the Columbia space mission when the surface layer of the composites panel space shuttle received impact damage from a foreign object. As an outcome of the impact damage, the composite panel became unglued and delaminated. The space shuttle could no longer perform as designed. Failure occurred almost instantaneously because the damaged de-bonded surface areas were exposed to the extreme thermal temperatures (3000 °F) and gravity of at least 5G (where G is the gravitational constant is approximately equal to $6.674 \times 10-11$ N m^2/kg^2), causing the shuttle to explode. (Makhecha, 2005; Columbia Accident Investigation Board, 2003).

The capability to prevent composites from delaminating has eluded designers. Engineered composites are vulnerable to delamination when impacted or penetrated (Qiao, Yang, and Bobaru, 2008; Geubelle and Baylor, 2008). Delamination at the interface is the primary mechanism that leads to the failure of composite materials (Tippetts, 2005). The interface is an important factor controlling the stiffness, strength, and fracture properties for composite materials at the macro scale (Needleman, 1989). Because of expanding needs for new high performance materials that are cheaper and environmentally acceptable, researchers have turned to nature for answers by investigating superior performing biological materials.

2.3 Biological Materials Overview

Over the last two decades, both design engineers and researchers have turned to nature with the hopes of understanding how biological materials are efficiently created to have superior properties such as high-strength, high toughness, and lightweight (Wegst and Ashby, 2004). Researchers have learned nature does not design structures rather it designs for functionality using whatever materials are indigenous to the geographical location. Functionality is what dictates the formation of the structure (Srinivasan, Haritos, and Hedberg, 1991; Weiner, Addadi, and Wagner, 2000). From an evolutionary standpoint, the biological materials adapted to their environment by enhancing their functionality in response to external stimuli. The adaptation by biological organisms has traceable developmental processes documenting how the systems adjust to their ever-changing surroundings. The motifs that are common in the development of biological materials, shown in Figure 2.1 I summarized the previous research efforts as to how the three integrated stages occur (Goodsell, 2004; Oyen, 2011 Ehrilich, 2010; Luz and Mano, 2009; Sarikaya, Fong, Frech, and Humbert, 1999).

The three sequential occurring stages are *External Stimuli*, *Phase Ordering*, and *Structural Formation*. *Stage I* is where nature acquires indigenous materials to be used for its constructs. Biological materials routinely make use of the commonly available periodic elements: carbon(C), nitrogen (N), calcium (Ca), hydrogen (H), oxygen (O), silica (Si), phosphorus (P), iron (Fe), and magnesium (Mg), which then form into proteins and minerals (Meyers, Chen, Lin, and Seki, 2008). Nature uses the same periodic elements to serve different purposes in the structural development process. For instance, the periodic elements of Ca, C, and O can form calcium carbonate ($CaCO_3$).

11
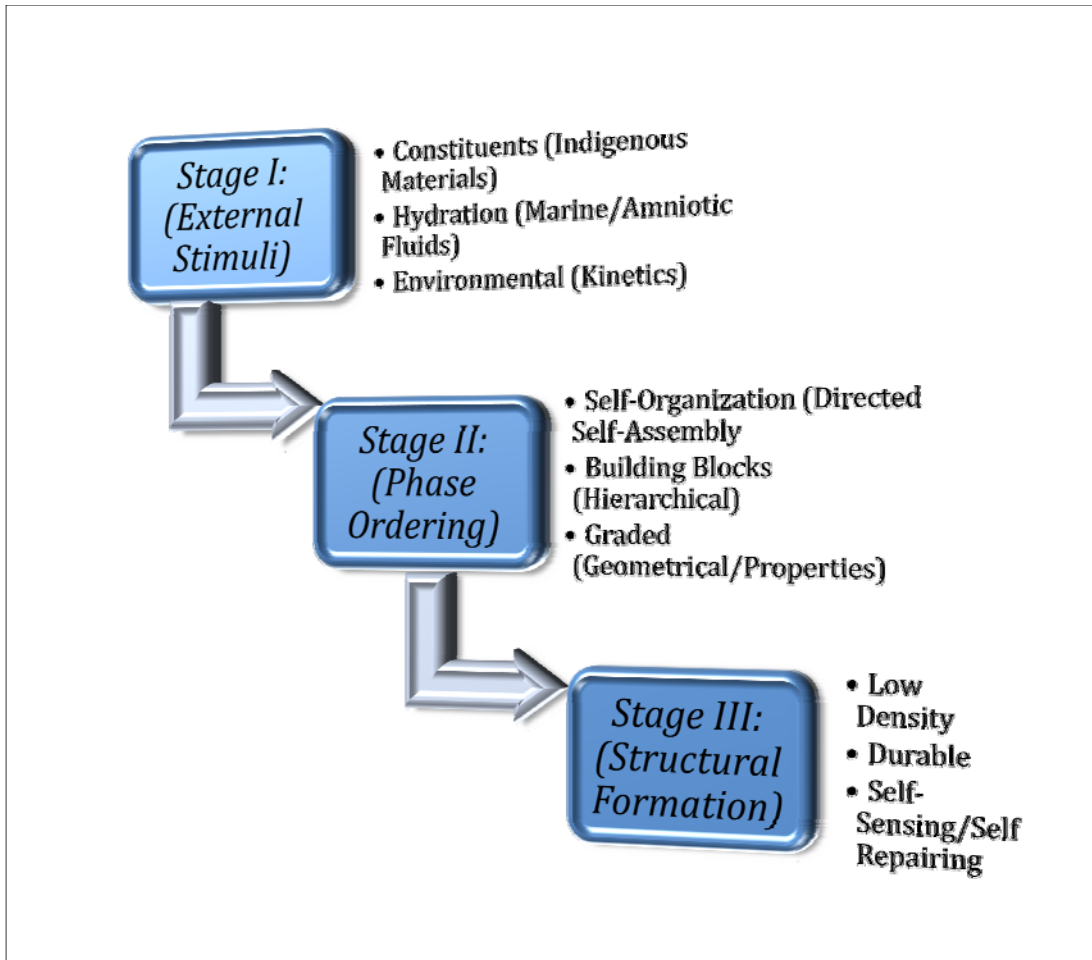
Figure 2.1 Three integrated stages of developmental processes
for adaptive biological materials.

In the Nacre *(Mother of Pearl)* layer for the mollusks seashells, $CaCo_3$ is the main

molecule that drives the structural formation of high-strength mineralized aragonite layers within

the seashell, Figure 2.2. Yet, in bone and tooth, $CaCO_3$ assumes the role of solubilizing agent

used for promoting ion transport within the hydroxyapatite molecule. The hydroxyapatite

molecule is the primary constituent responsible for developing the high-strength mineralized

structural layers found in bone and tooth (Goodsell, 2004; Ehrilich, 2010; Meyers, Chen, Lin,

and Seki, 2008).
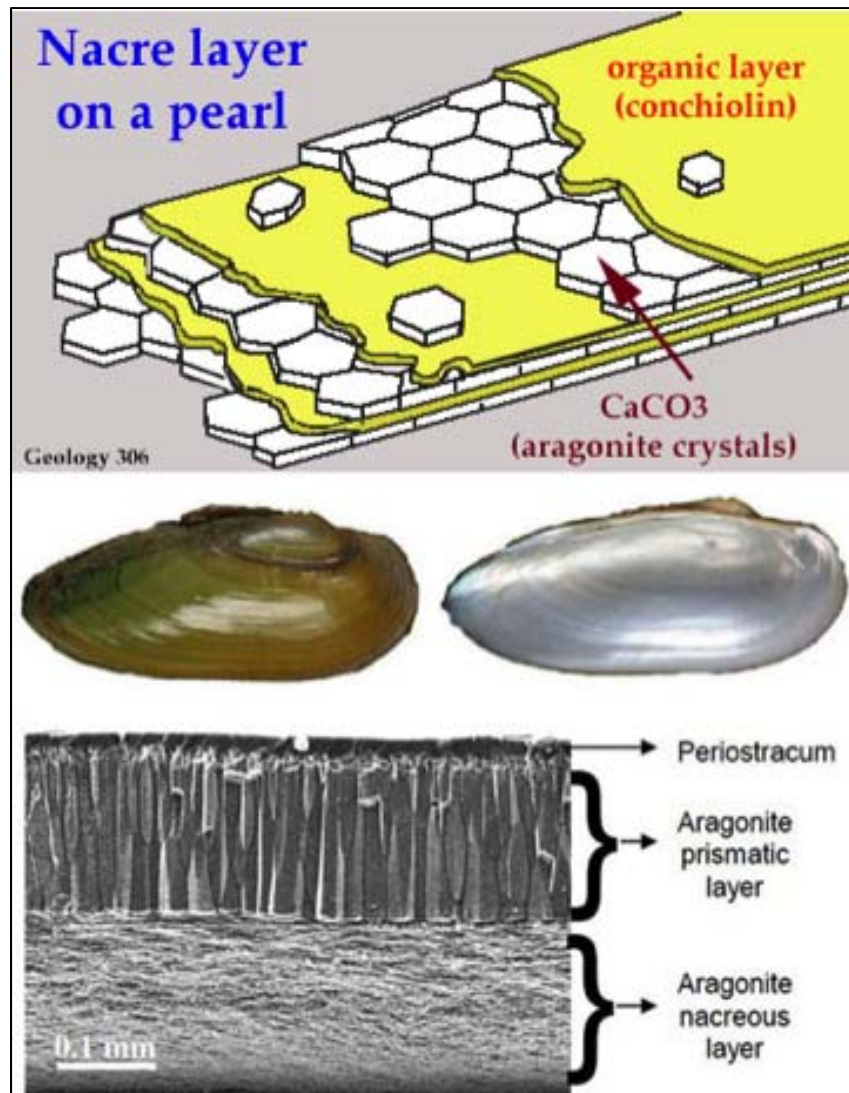
Figure 2.2 Schematic and scanning electron microscope images
of the structural arrangement for aragonite crystal layers
found in nacre (Meyers, Chen, Lin, and Seki, 2008).

Another important aspect of all biological material formation is the hydration state.

Nature uses hydration to facilitate the organism's development starting from the incubation

period through the end of cessation. The environmental conditions provide the efficient energy

source to drive the reaction kinetics, usually occurring at ambient temperature with standard

pressure and hydration states as determined by the required functionality (e.g., structural

formation/geometry and mechanical property development). More importantly, nature responds

to the environmental conditions to maintain a delicate balance between the role the periodic elements play in the construction and functionality of the organisms.

Next, *Stage II* begins with self-organizing the media and metrics defined in *Stage I*. The entity then uses the directed self-assembly process to attach the building blocks at each length scale with the variation in how the materials are integrated. In *Stage II*, the way materials are mixed, distributed, and integrated plays a key role in the amplification of properties that governs the formation of the multifunctionality for the system. The amplification of properties is very complex and unique for each length scale starting from the atomic level through the macro level (one-angstrom to one-millimeter) depending on the characteristic length for the system.

After nature has systematically gathered, organized, and measured the ingredients within the confines of the environmental constraints, as denoted in *Stages I-II*, finally *Stage III* can begin. The construction of biological material structure encompasses several aspects of formation. Biological materials, specific to structures that have undergone the biomineralization process, develop characteristics during formation of being low density, durable, self-sensing, and able to repair themselves when damaged (Mann, 2001).

2.4 Mineralized Biological Composites

A mineralized biological composite constitutes two phases: hard (inorganic minerals) matrix phase integrated with a soft (polymer-like organic fiber reinforcement phase) (Dunlop and Fratzl, 2010; Baohua and Huajian, 2010; Wegst, Bai, Saiz, Tomsia, and Ritchie, 2015; Dubey and Tomar, 2010; Yang, Chen, McKittrick, and Meyers, 2012). Scientists discovered the biomineralized composites are advanced because of their length scale dependent material ordering, grading of mechanical properties, and functional role, and have exhibited superior performance under extreme conditions (Meyers, Chen, Lopez, Seki, and Lin, 2011; Fratzl, 2007).

14

Subsequent to the scientist's discovery, design engineers have become fascinated with the novel characteristics and the possibilities of learning from nature how to synthesize bioinspired materials and structures for use in engineering applications (Barthelat, 2007a; Bhushan, 2009). Examples of superior performing advanced mineralized biological composites are bone, teeth, and exoskeleton fish scales (Chen, McKittrick, and Meyers, (2012)).

2.4.1 Exoskeleton Fish Scale

Material designers are in need of multifunctional composite materials that can readily meet a variety of in-service requirements (e.g., mechanical, sensing, or repairing) (Hanus and Harris 2013). Exploring simpler structured biomaterials other than bone and tooth is advantageous and can have a huge payoff for the composites community (Hanus and Harris 2013). Exoskeleton fish scales are another one of Mother Nature's biomineralized analogues that exhibit superior performance characteristics. Scientists are extremely challenged with the characterization, interpretation of processes, and functionality of the complex biomineralized systems such as nacre, bone, and tooth. By investigating less complex biological constructs, there is a greater chance for designers to use "biomimicry" or "bioinspiration" for synthesizing, designing, and manufacturing superior performing advanced composites.

Designers are frequently challenged when vetting new composite materials systems, especially those biological material composites deemed superior performing in nature. The new composites will need to: (a) meet engineering requirements, (b) have performance characteristics that are scalable from the nano to macro level, (c) be affordable to produce, and (d) be environmentally safe. By studying the less complicated structure of exoskeleton fish scale, designers are more likely to develop future advanced composites materials that can better meet

the challenging need to maintain the nation's infrastructure, aircraft, and automobiles. Also, the fish scale can be used as a stepping-stone for understanding more complicated material systems.

Designers have recently shown great interest in studying exoskeleton fish scales for potential use in a wide variety of engineering applications. Researchers have observed that the protective biomineralized hard outer layer seems to function as body armor for the fish (Bruet, Song, Boyce, and Ortiz, 2008a; Song, Reichert, Kallai, Gazit, Wund, Boyce, and Ortiz, 2010). The fish scales are especially attractive for study because it is relatively simple and involves fewer discrete layers, yet the fish scale exhibits superior mechanical response and has comparable nanoindentation moduli with bone and tooth (Oyen, 2011; Chen, Lin, Yang, Lopez, Li, Olevsky, and Meyers, 2011). From a design engineer's vantage point, when fewer components are incorporated there is higher probability the composite's design will: (a) meet specifications, (b) require less optimization, and (c) can ultimately be manufactured. Therefore, the designer is more likely to develop a superior performing advanced composite structure with the in-service lifecycle maintenance requirements that are manageable and affordable (Hoa, 2009; Ashby, 2007; Salonitis, Pandremenos, Paralikas, and Chryssolouris, 2010). The remaining portion of this section will discuss the current state of knowledge for the exoskeleton fish scale.

Nature has synthesized the scales of fish to serve many purposes attracting several researchers in their studies of evolution, functions, structures, and properties (Chen, McKittrick, and Meyers, 2012; Sire, 1989a; Sire, 1989b; Sire, 1995a; Sudo, Tsuyuki, Ito, and Ikohagi, 2002; Richter and Smith, 1995; Wiley, 1976; Williamson, 1849; Alfaro, Gonzales, and Ferrara, 2008; Bartol, Gharib, Weihs, Webb, Hove, and Gordon, 2003; Raschi and Tabit, 1992). Although several classes of fish have been investigated, scientists/observationists have been able to only find one fish scale group that form extremely hard, high-strength exterior biomineralized

lightweight layers, Figure 2.3 (Yang, Chen, Gludovatz, Zimmermann, Ritchie, and Meyers, 2013a; Goodrich, 1907).
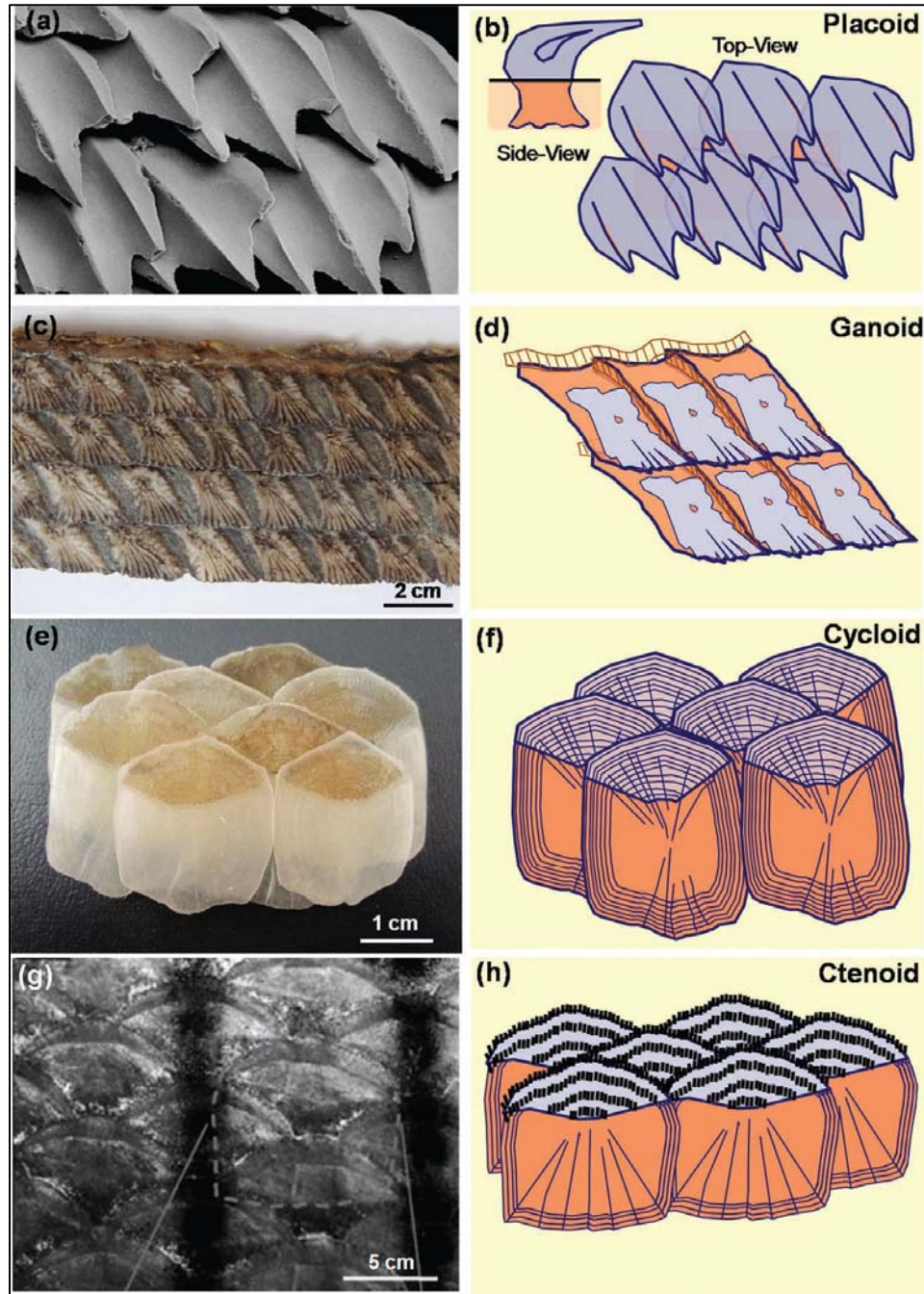
Figure 2.3 Images of different fish scale types and their overlaps;
(a)–(b) Placoid, (c)-(d) Ganoid, (e)-(f) Cycloid, (g)-(h) Ctenoid.
(Cosmoid scales not shown) (Yang, Chen, Gludovatz,
Zimmermann, Ritchie, and Meyers, 2013a).

The bony fish scale group is called ganoid. Ganoid scales are found in the Actinopterygii: gar and birchir fish class. The inception of both fish happened during the "Cretaceous" time period, occurring [66–144] million years ago (Gottfried, Krause, June 1998; Daget, Gayet, Meunier, and Sire, 2001). The fish developed before the continental plates broke apart to form the African, South American, and Asian continents. As a result, the birchir and gar had widespread distribution in locations as diverse as Spain, India, Cuba, and North and Central America (Gayet, Meunier, 1991; Domingo, Grimes, Soler-Gijón, López-Martínez, 2009; Kumar, Rana, and Paliwal, 2006; Smith, Grandstaff, and Abdel-Ghani, 2006; Gayet, Meunier, and Werner, 2002). Table 2.1 presents the speciation and general structural features for the gar and birchir fish that have been studied (Allison, et al. 2013; Yang, Chen, Gludovatz, Zimmermann, Ritchie, and Meyers, 2013a; Géraudie, 1988).

The ganoid scales are multilayered with mechanically graded modulus and hardness properties. The outermost layer is the strongest with strength decreasing and toughness increasing for innermost layers (Allison, et al. 2013). The scales are diamond-shaped, with the outer edges of the scale being thinner to allow overlapping, Figure 2.4 (Shark, 2015). Peg-and-socket joints along with sharpey fibers connect the adjacent overlapping scales, Figure 2.5 (Bruet, Song, Boyce, and Ortiz, 2008a). The overlapped connectors create a layer of uniform thickness that matches the scales' interior orthogonal thickness, Figure 2.6.

Although the ganoid scales of the gar and birchir fish have very similar speciation and general structural features, the two fish have differing structural layer arrangements. Examples of differing structural layer arrangements for the Senegal birchir (*Polypterus senegalus*) and Mississippi alligator gar fish (*Atractosteus spatula*) are illustrated in Figures 2.7 and 2.8, respectively (Bruet, Song, Boyce, and Ortiz, 2008a). The most commonly reported layer labels

18

Table 2.1. Speciation and general structural features for gar and birchir fish
(Allison, et al. 2013; Yang, Chen, Gludovatz, Zimmermann, Ritchie,
and Meyers, 2013a; Géraudie, 1988).

	Fish Species	
Speciation Profile	**Gar**	**Birchir**
Temporal Range	Late Cretaceous–Recent	Cretaceous–Recent
Kingdom	Animalia	Animalia
Phylum	Chordata	Chordata
Class	Actinopterygii (Ray-Finned Fishes)	Actinopterygii (Ray-Finned Fishes)
Sub-Class	Neopterygii	Cladistia
Order	Lepisosteiformes	Polypteriformes
Family	Lepisosteidae	Polypteridae
Genera	[1]*Atractosteus*; *Lepisosteus*	[1]*Polypterus*; *Erpetoichthys*
Structural Member	Bone/Tooth/Scale	Bone/Tooth/Scale
Constituent Materials	Hydroxyapatite Mineral; Collagen Fibers	Hydroxyapatite Mineral; Collagen Fibers
Structural Features	- Biomineralized; - Multilayered; - Hierarchical - Functionally Graded - Composite	- Biomineralized; - Multilayered; - Hierarchical - Functionally Graded - Composite
[1]Most frequently studied.		

are provided for each fish type. Earlier layer designations provided by observationists have

varied. For instance, the work discussed in Smith (2006) pointed out there has been a long-

standing debate since the 1850s whether or not the *polypterus* is a three- or four-layered system.

In recent years, because of advanced microscope technology, the number of layers found

in each fish type has been determined with more certainty (Bruet, Song, Boyce, and Ortiz,

2008a; Allison, et al. 2013; Yang, Chen, Gludovatz, Zimmermann,Ritchie, and Meyers, 2013a).

The Mississippi alligator gar fish scale has been shown to have two-layers (outer ganoine + inner
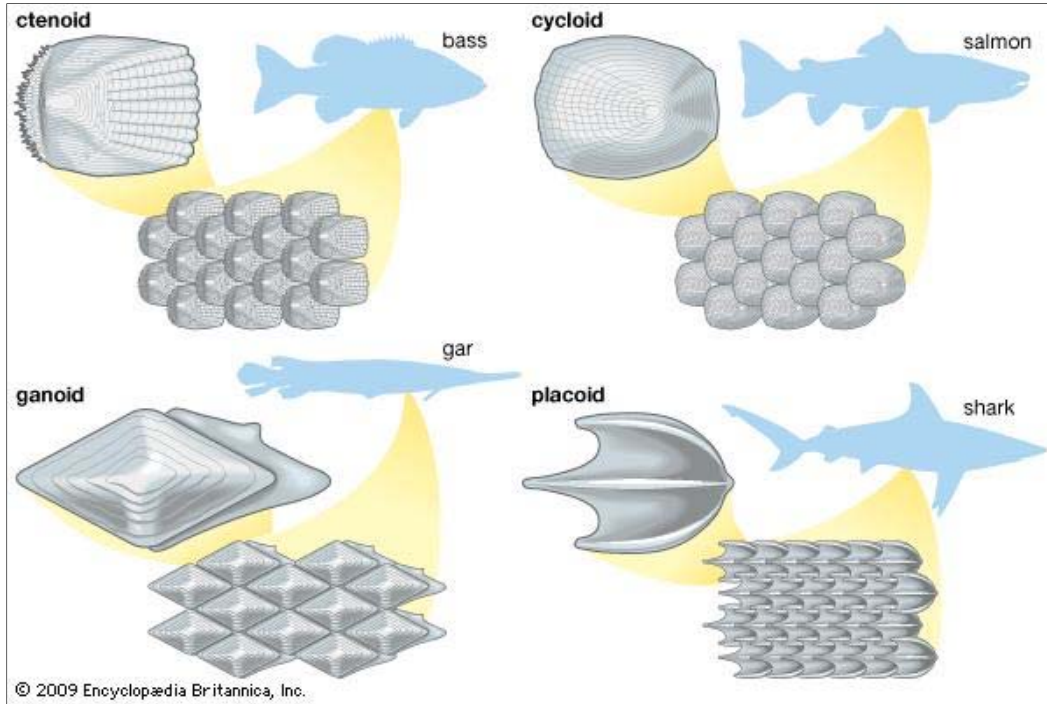
Figure 2.4 Images of different fish scale types and their shapes (Shark, 2015).
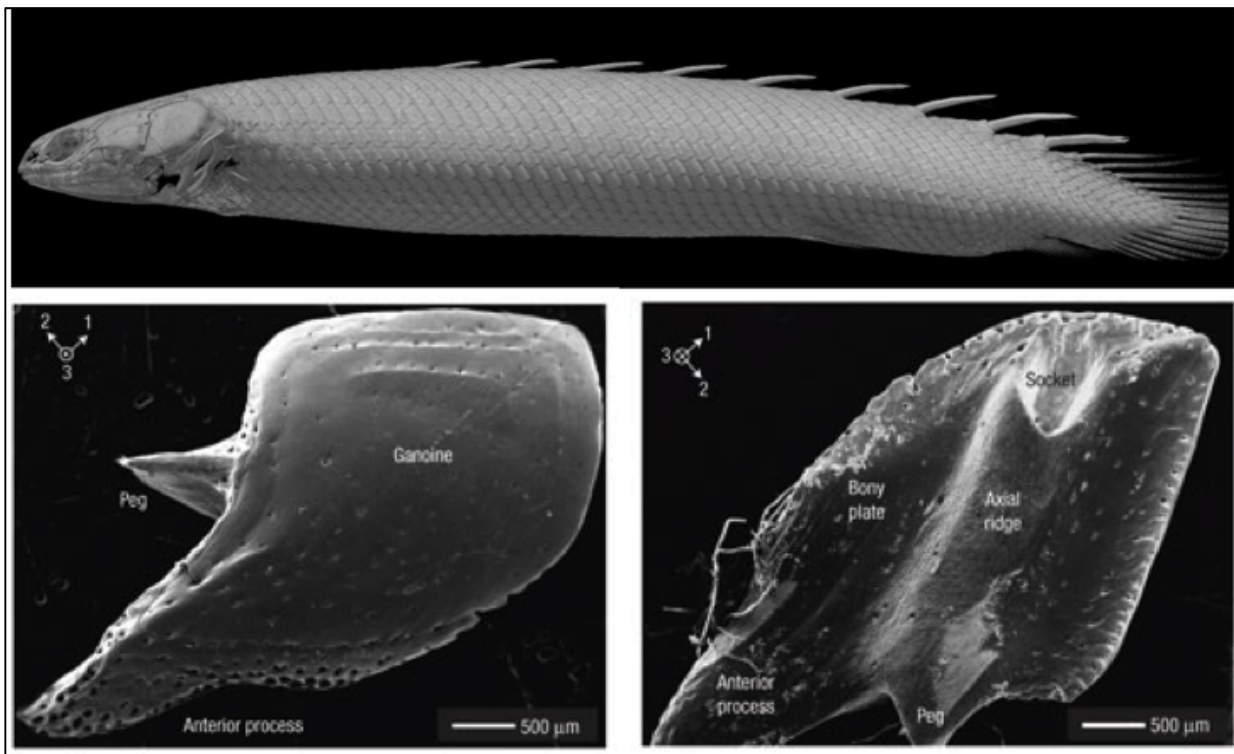
Figure 2.5 Birchir fish with peg and socket connecting scales
(Bruet, Song, Boyce, and Ortiz, 2008a).

Figure 2.6 3-D printed prototype demonstrating peg-and-socket joint connecting the adjacent overlapping birchir ganoid scales [Images courtesy of the U.S. Army's Institute for Soldier Nanotechnology located at Massachusetts Institute of Technology].
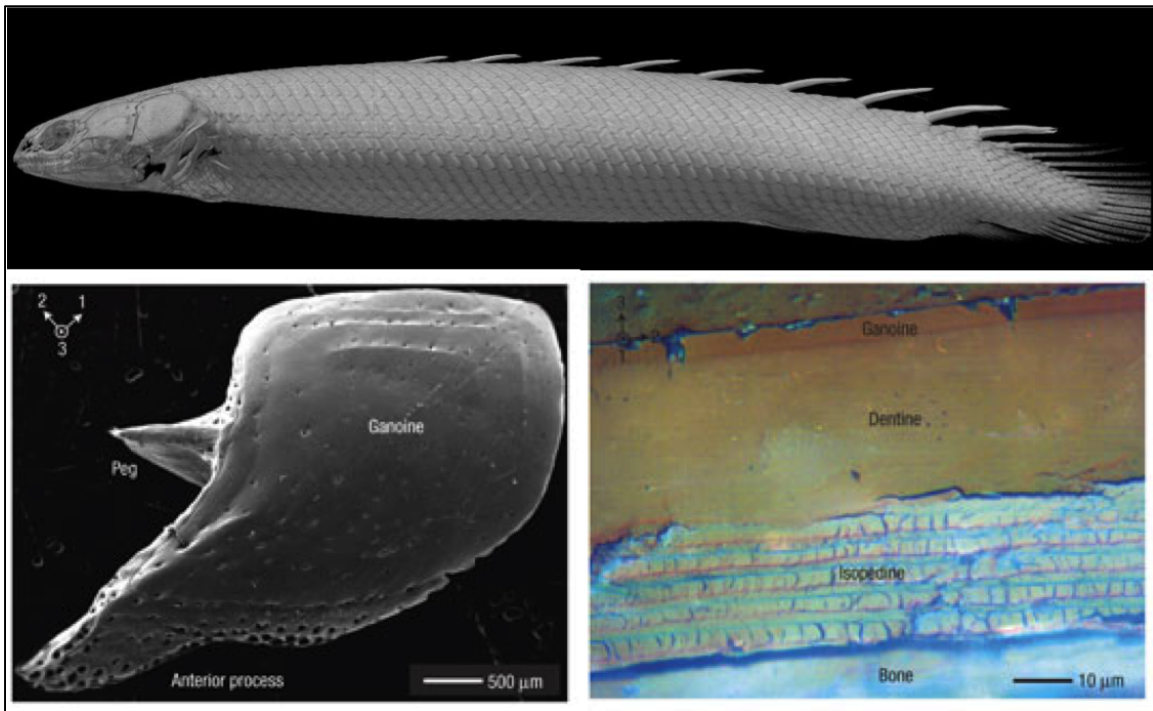
Figure 2.7 Structural layer arrangements for the Senegal birchir (*Polypterus senegalus*) (Bruet, Song, Boyce, and Ortiz, 2008a).

lamellar bone) and the Senegal birchir fish scale has four-layers (outermost ganoine + 1st inner dentine + 2nd inner isopedine + inner most bone) (Bruet, Song, Boyce, and Ortiz, 2008a; Allison, et al. 2013; Yang, Chen, Gludovatz, Zimmermann, Ritchie, and Meyers, 2013a).
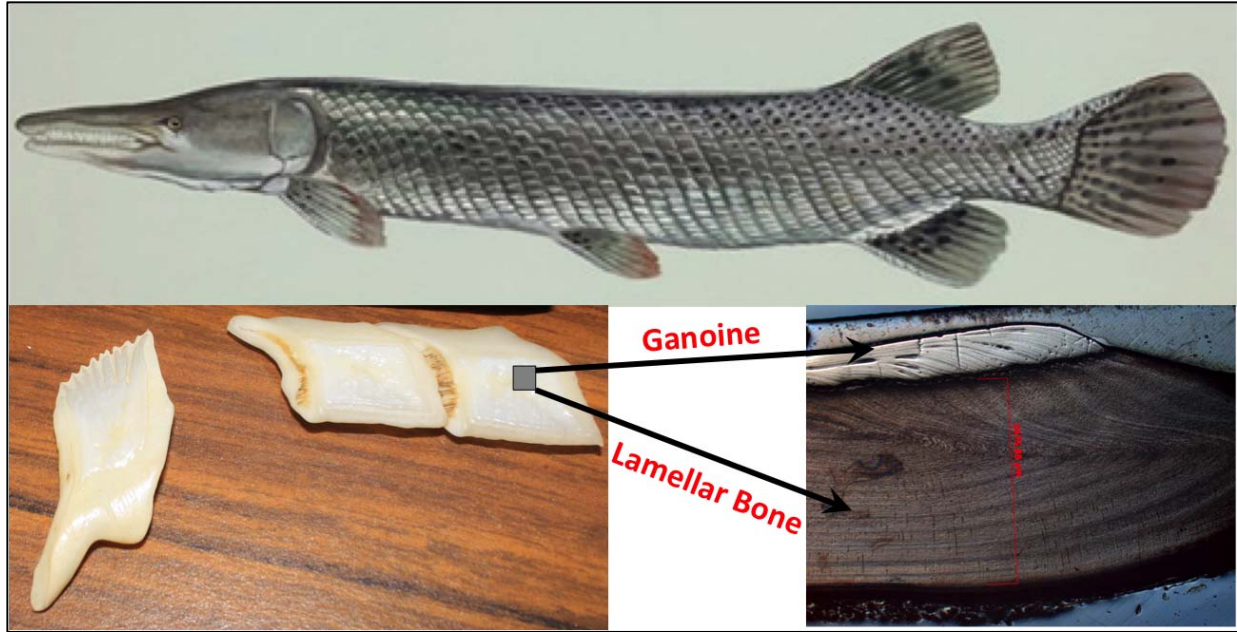
Figure 2.8 Structural layer arrangements for the Mississippi alligator gar fish (*Atractosteus spatula*) [Images courtesy of the U.S. Army's Engineer Research and Development Center (ERDC)-Geotechnical and Structures Laboratory (GSL) located in Vicksburg, Mississippi].

However, the comparisons made to other better understood biological materials are still open for questions. Observers have long debated the dissimilarities and resemblances of the structure and formation/growth mechanisms for each individual fish and also when comparing the birchir to the gar fish, along with other biomineralized composite materials such as bone and tooth (Williamson, 1849; Goodrich, 1907; Wiley, 1976; Géraudie, 1988; Sire, 1989a; Sire, 1989b; Gayet, Meunier, 1991; Sire, 1995a; Gottfried, Krause, June 1998; Daget, Gayet, Meunier, 2001; Gayet, Meunier, and Werner, 2002). Subsequently, the debate has led researchers to postulate the inherent mechanical response is directly related to the fish's intrinsic structure arrangement and chemical composition. The general postulate has been proven many times over, however, the structural specific layer make-up, formation, and growth mechanisms for the two fish scales are still not clear (Smith, 2006; Géraudie, 1988).

From a detailed review of literature, the material compositional differences in the two

fish are subtle. Also, there are few differences in the local mechanical properties (elastic modulus

and hardness) determined from nanoindentation experimentation. Elastic modulus and hardness

appears to be similar within the ganoine layers and when taking measurements across the

interface into the dentin layers and lamellar bone for the birchir and gar fish, see Figures 2.9 and

2.10, respectively (Bruet, Song, Boyce, and Ortiz, 2008a; Allison, et al. 2013; Yang, Chen,

Gludovatz, Zimmermann, Ritchie, and Meyers, 2013a; Yang, Gludovatz, Zimmermann, Bale,

Ritchie, and Meyers, 2013b); although, from microindentation experiments and simulations, the

measured global response indicates the birchir is better at resisting uniaxial loading when

compared to the gar, see (corresponding) Figures 2.11 and 2.12, (Bruet, Song, Boyce, and Ortiz,

2008a; Song, Oriz, Boyce, 2011; Chandler, Allison, Rodriguez, Moser, and Kennedy, 2014).
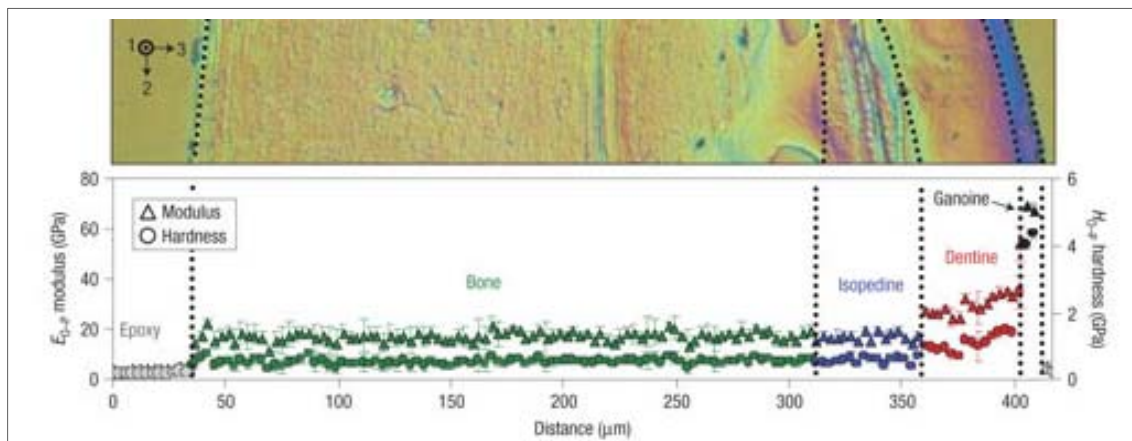
Figure 2.9 Illustration of nanoindentation measured elastic modulus and
hardness for Birchir fish scale (Bruet, Song, Boyce, and Ortiz, 2008a).

Evidently, increased resistance is attributed to the number of layers found in the birchir.

Such use of layered structures is well known to design engineering. For example, pavement

design makes use of the principle of starting with the highest modulus materials on the surfaces

followed by successively decreasing modulus layers to redistribute and dissipate stress and

23
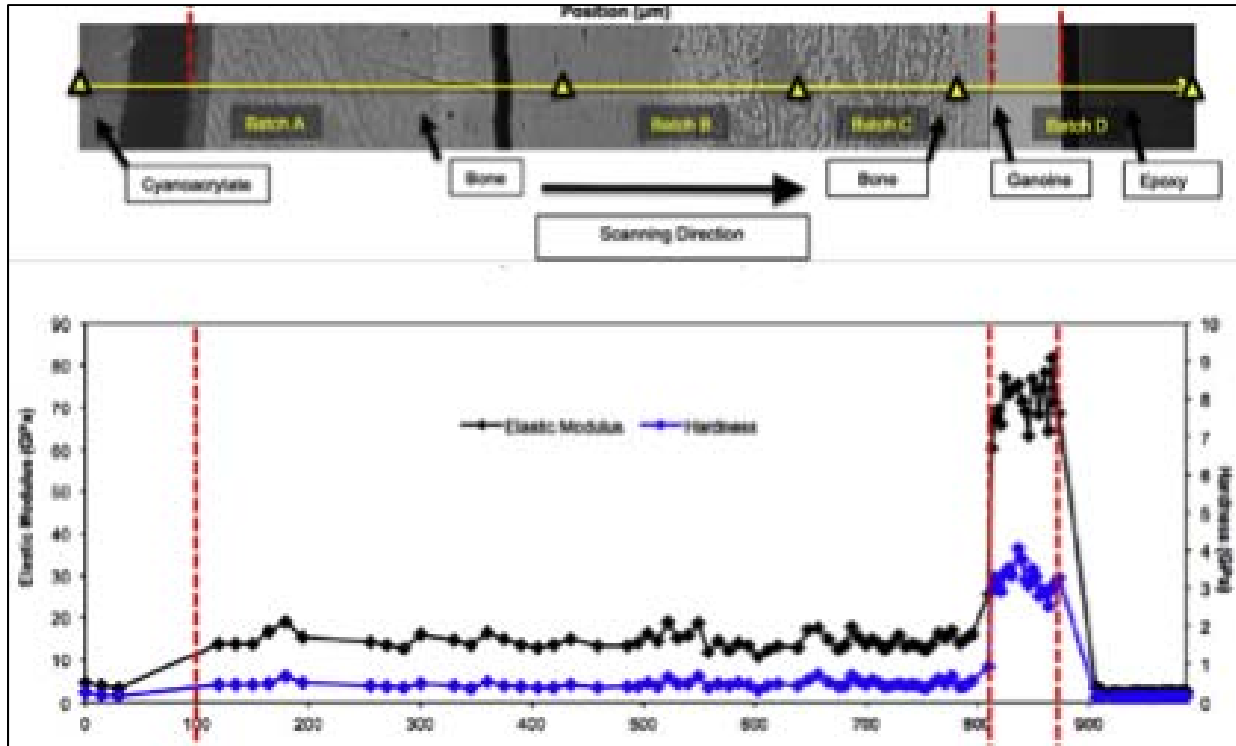
Figure 2.10 Illustration of nanoindentation measured elastic modulus
and hardness for gar fish scale (Allison, et al. 2013).

deformation. More generally, civil engineers incorporate highly heterogeneous geological

materials in construction such as foundations, slopes, and retaining walls. The design procedures

include stress and deformation design/analysis for load transfer of point loads laterally and

vertically through the layers as uniformly distributed loads. As an example, Table 2.2 outlines the

often-used methods and theories by the civil engineers' communities that may be relevant to the

biomaterials research community when understating the stress transfer mechanisms exhibited by

layered and hierarchically graded composites (Mallick. and El-Korchi, 2009; Huang, 1993;

Yoder and Witczak, 1975; Timoshenko and Lessels, 1925; Lambe, and Whitman, 1969; Terzaghi,

1943; Das, 1990; Das, 1994; AASHTO, 1993; Ashish, Mehta, Cleary, Guo, Musumeci, Zapata,

and Kettleson, 2011; Brill, 1998; Bull and Singh, 1990; Chou, 1997; Hammonds, 1997;

Hammonds; Ioannides, and Korovesis, (1990); UFC 03-260-02, 2001b; Westergaard, 1925).
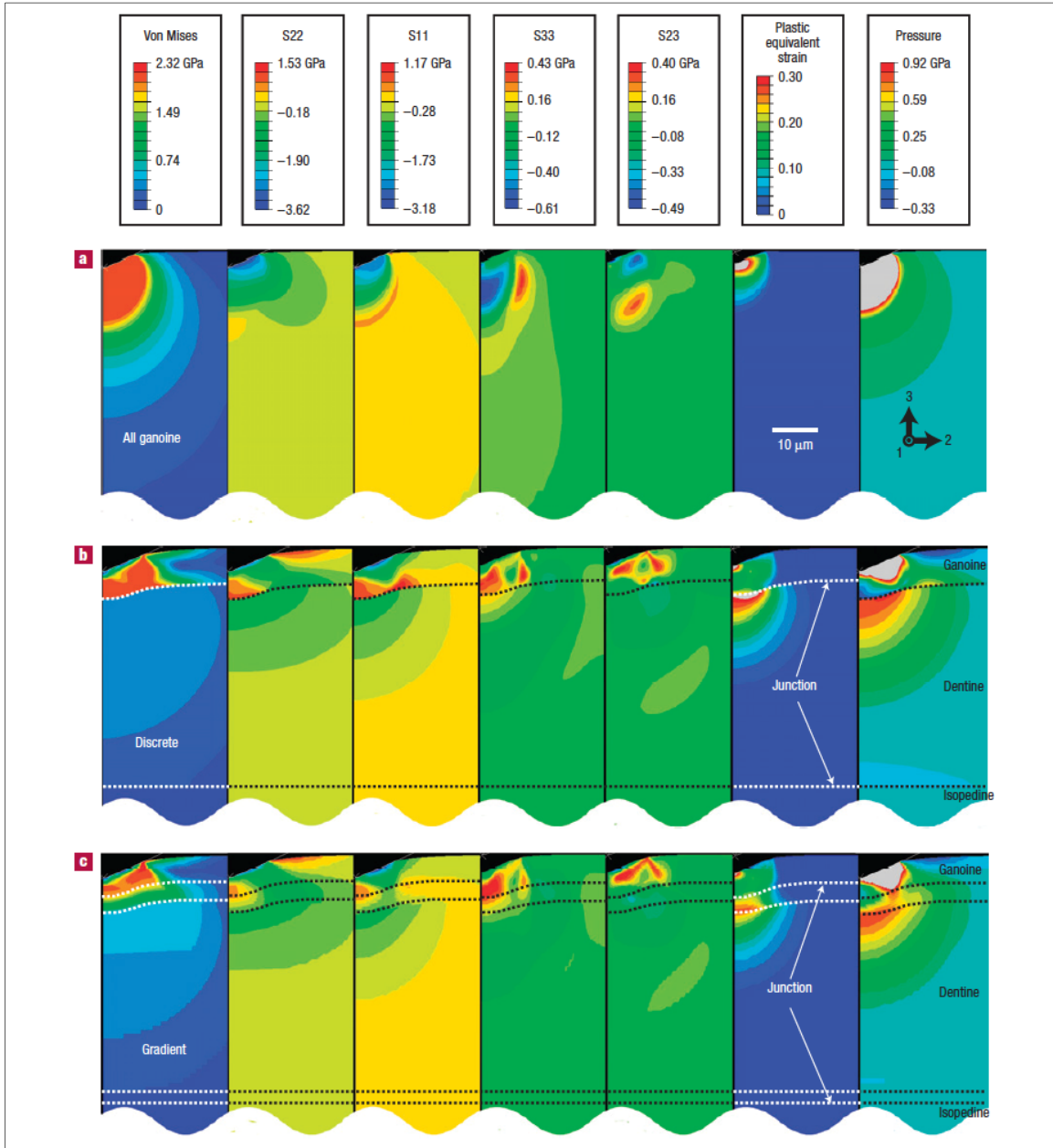
Figure 2.11 Microindentation simulation contours of stress, plastic strain and pressure fields of a birchir scale via multilayered finite element analysis (FEA) simulations. In "a"– "c," finite element analysis predictions of von Mises stress field, S22 (normal stress on the plane perpendicular to the 2 axis), S11 (normal stress on the plane perpendicular to the 1 axis) and pressure at a maximum depth when fully loaded, and S23 (shear stress on the plane perpendicular to the 3 axis acting in the 2 direction), S33 (normal stress on the plane perpendicular to the 3 axis) and plastic equivalent strain after fully unloaded for three models: all ganoine (a), discrete (b) and gradient (c) models for 1-N-maximum-load indentation (Bruet, Song, Boyce, and Ortiz, 2008a).
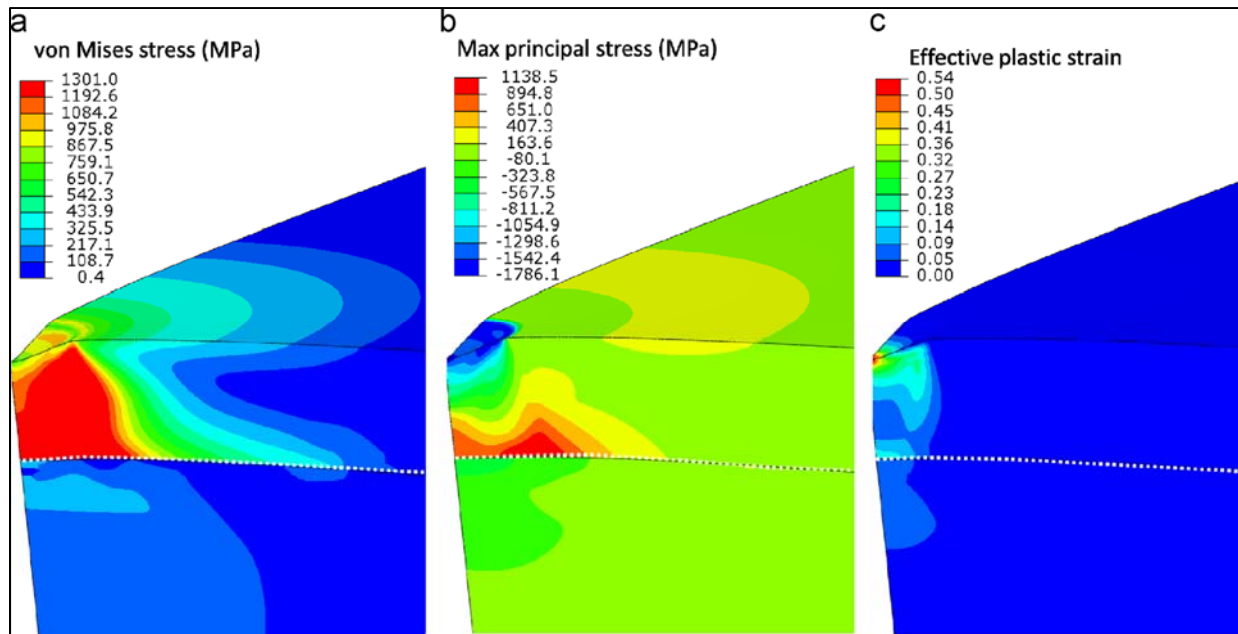
Figure 2.12 Microindentation simulation contours of stress, plastic strain and pressure fields of a gar scale via multilayered FEA simulations. When the indentation force is 10-N. (a) von Mises stress, (b) maximum principal stress, (c) effective plastic strain (Chandler, Allison, Rodriguez, Moser, and Kennedy, 2014).

Table 2.2 Example methods for understanding load transfer in highly heterogeneous geological materials used in civil engineered structures (Huang, 1993; Yoder and Witczak, 1975; Timoshenko and Lessels, 1925; Lambe, and Whitman, 1969; Terzaghi, 1943; Das, 1990; Das, 1994; AASHTO, 1993; UFC 03-260-02, 2001b; Westergaard, 1925).

	Theories	**Applications**
Design/Analysis Methods		
CBR Pavement Design	• Boussinesq approximation • Layered Elastic	Stress distribution in soils and flexible pavements
AASHTO Pavement Design	• Boussinesq approximation • Layered Elastic • Westergaard analysis	Load transfer and stress distribution in flexible/rigid pavements
Foundation Design	• Terzaghi's	Shear deformation determination near soil surface
Retaining Wall Design	• Rankin • Coulomb's	Lateral/vertical earth pressure determination at soil depths

Upon further inspection, both birchir and gar ganoine layers have similar moduli and are effective in redistributing the microindentation point load through the layers' interfacial zones for the immediate underlying layers. The uniqueness of the gar fish scale is the ganoine-bone layers have a modulus mismatch, which acts to effectively transfer load across the interface, allowing the layered composite to remain undamaged when at the similar microindentation load levels, Table 2.3 (Chandler, Allison, Rodriguez, Moser, and Kennedy, 2014).

In man-made systems, one of the most critical aspects when designing composites is to prevent de-bonding/delamination of layers and at interfacial transition zones (ITZ) of dissimilar materials. The modulus mismatch for the dissimilar materials leads to de-bonding/delamination at the ITZ causing premature shear failure. Therefore, the source of delamination resistance in ganoid fish scales is particularly attractive for additional research.

Table 2.3 Microindentation experimental observations for birchir and gar scales, under different load levels (Chandler, Allison, Rodriguez, Moser, and Kennedy, 2014).

	Microindentation Loads (N)		
	≈ 0.5	≈2.0	≈10.0
Fish Type			
Birchir	No cracking	Ring cracking at the edge of the indentation imprint	Already damaged
Alligator Gar	No cracking	No cracking	Ring cracking at the inside and outside of indentation imprint, interface cracking at the ganoine–bone junction, vertical cracking in ganoine layer

2.4.2 Role of Material Hierarchy in Fish Scale and Other Biomineralized Composites

The formation/growth processes/functions may differ across the wide variety of biomineralized composites (e.g., fish, bone, tooth). Uniquely, the secret to nature's superior performing composite structures appears to be attributed to the materials hierarchy. Many biocomposites are complex structures that have arisen from millions of years of evolution, maintaining relatively simple chemical composition at ambient conditions, while modifying its physical geometrical structure (Bruet, 2008b). Naturally occurring biomineralized composite structures rely upon their hierarchical structure, rather than different composition, to provide exceptional mechanical properties such as high stiffness, toughness, and crack resistance. Remarkably, stiffness and toughness are examples of mutually exclusive properties for lightweight manufactured materials (Ritchie, 2011).

The toughness of the functionalized constituents making up the biocomposite systems is several magnitudes greater than that of the individual component materials. As an example, illustrated in Figure 2.13 is the hierarchical structure of collagen, which scans over different material length scales, from nano to macro. The macroscopic mechanical material behavior is controlled by the interplay of properties throughout various scales (Buehler, 2007). Recent studies have shown that the desirable engineering properties of exceptional flexural stiffness, toughness, and adhesion are readily found in flaw tolerant biomaterials (Gao, Ji, Buehler, Yao, 2004).

The exoskeleton of fish scales has a hierarchical biocomposite structure, which is thin, lightweight, and durable. Nature has chemically/geometrically engineered the exoskeleton fish hierarchal structure to include bulk properties of strength and ductility that are several orders of magnitude higher than those found within the discrete structural units of hydrated collagen fibers
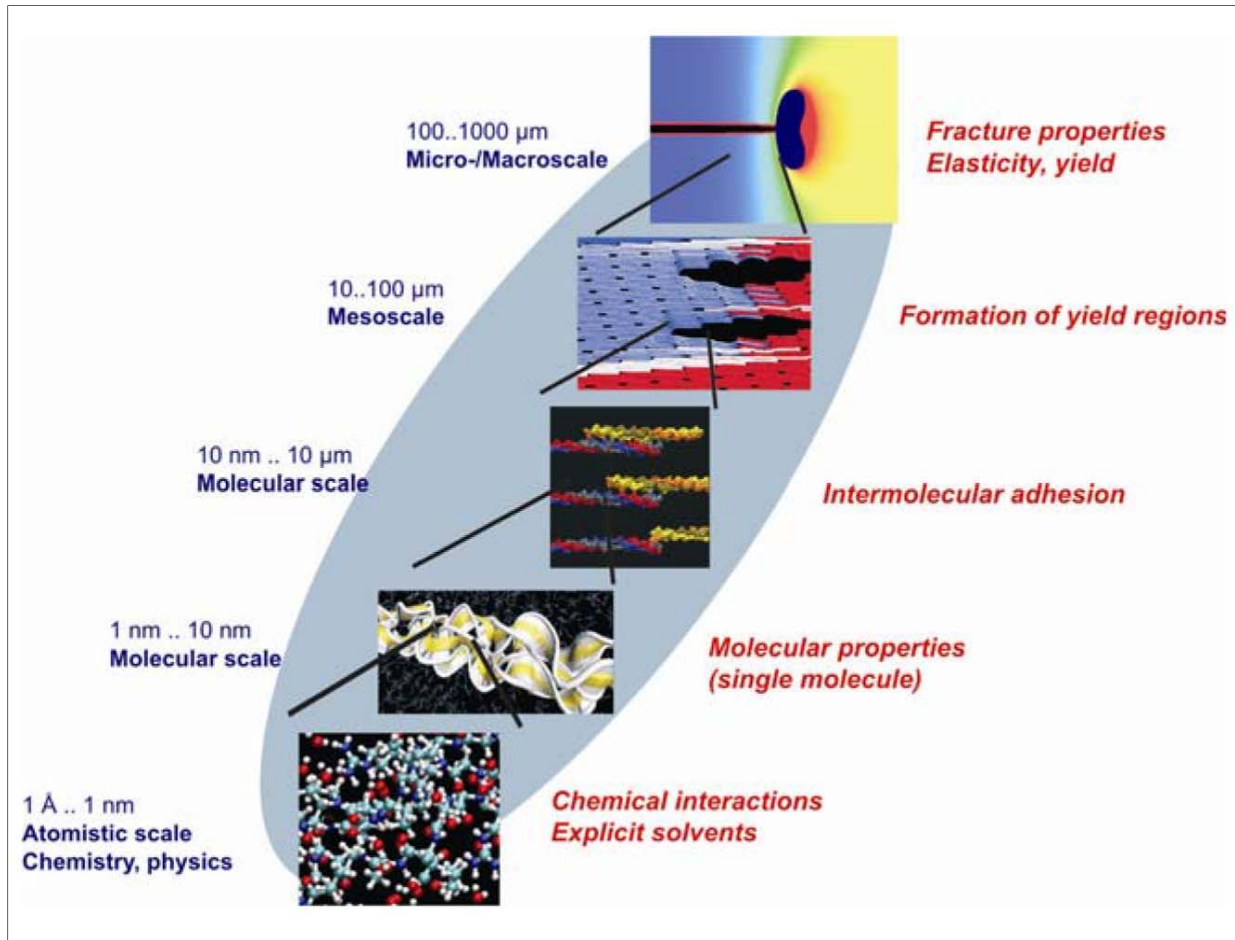
Figure 2.13 Overview of hierarchical structure of collagen, which scans over different material length, scales, from nano to macro (Buehler, 2007).

and hydroxyapatite minerals. Note that the use of these weak constituent materials is a limitation imposed on biological systems by the ambient water temperature and requirement for soluble minerals. Typically, the inorganic phase of hard hydroxyapatite mineral matrix is interfaced with embedded polymer-like, soft organic collagen fibers reinforcement phase. The discrete molecular units of hydroxyapatite crystals and bundled collagen fibers form a structural unit at the characteristic length scale of approximately one-micron (Ochsner, and Ahmed, 2011; Nudelman, Pieterse, George, Bomans, Friedrich, Brylka, Hilbers, de With, and Sommerdijk, 2010). Independently these phases are weak but when combined in the appropriate volume fractions

29

they form an extremely high-strength, high toughness biocomposite system that is also

lightweight (Barthelat and Espinosa, 2007b).

2.4.3 Challenges of Measuring Chemical Composition, Structural Arrangement, and Mechanical Attributes within Materials Hierarchy from Experimental Laboratory Methods

Recently, researchers have set forth the goal to analyze/design/prototype composite

structures that have been inspired by nature (Bruet, Song, Boyce, and Ortiz, 2008a; Song,

Reichert, Kallai, Gazit, Wund, Boyce, and Ortiz, 2010). Nature has used self-assembly to

meticulously form its complex structure (Chung, Oh, Kwak, Lee, Meyer, Wang, Hexemer, and

Lee, 2011; Sarikaya, Fong, Frech, and Humbert, 1999). The limited constituent's nature uses in

the formation of robust hierarchical structures is one of the features of nature that has gained

researchers attention. To be able to meet the researchers' goals, the biocomposite system must

first be reverse engineered. Reverse engineering can help with the understanding of how, what

are the inherent chemical, morphological, and mechanical attributes that can lead to such

enhanced performance and multi-functionality.

However, using laboratory experimental methods to probe the material hierarchy of

biomineralized composites is challenging. The challenges are due to three aspects of multi-scale

investigation. Firstly, even though researchers understand that several hierarchical levels exist in

the composite material, it is not obvious how the structure spans across many orders of

magnitude of spatial scales (Aizenberg, Weaver, Thanawala, Sundar, Morse, Fratzl, 2005).

Secondly, by not knowing how many hierarchical levels exist, determining which experimental

methods are appropriate is difficult. What is clear is no single experiment will sufficiently

elucidate the attributes for the materials' multi-length scale mixing, integration, and variation

(Bauerlein, Behrens, Epple, and Pickett-Heaps, 2007). Lastly, because the soft and hard materials

at each length scale in biomineralized composites exhibit gradual variation in material properties,

the researcher is challenged with developing a robust experimental plan that may better aid in identifying the subtle attributes for relevant mechanisms observed at each length scale and across scales (Beniash, 2011).

2.5 Biological Composite Materials Summary

Biological materials are well organized and exhibit superior property characteristics of lightweight, high strength, high toughness, and energy absorbency. Nature does not design structures rather it adapts to achieve niche functionality using whatever materials are indigenous to the geographical location. The functionality is what dictates the formation of the structure. Biological organisms adapt to environmental changes by enhancing their functionality. Biomineralized composites have exhibited superior performance under extreme conditions. Examples of superior performing advanced mineralized biological composites are bone, teeth, and exoskeleton fish scales. The characterization, interpretation of processes, and functionality of the more complex biomineralized systems such as nacre, bone, and tooth is difficult. The composites are advanced, because of hierarchical ordering, grading of properties, and multifunctionality. However, researchers are having difficulty explaining what the attributes are that is leading to superior performance. By investigating less complex ganoid exoskeleton fish scale, there is a greater chance for designers to use "biomimicry" or "bioinspiration" for synthesizing, designing, and manufacturing superior performing advanced composites.

2.6 Overall State-of-Knowledge Summary

Advanced engineered composites have been successfully used in several applications with a wide range of materials. However, there are several limitations in the design and manufacturing of advanced engineered composites. Advanced composites are susceptible to delamination. In particular, civil engineers are in need of multifunctional composite materials

that can readily meet a variety of in-service requirements (e.g., mechanical, sensing, or repairing). Because of the impending need, designers are probing nature for solutions. By investigating the superior performing less complex fish scale, insights may be gained on how to best meet the engineer's needs.

The literature review has shown extensive research efforts have been performed to characterize fish scale. From literature it was found each layer, at the micron scale, has subtle variations in the placement of the hard and soft materials. The fish scale is made up of 90 percent hard (inorganic minerals) and 10 percent soft (polymer-like organic collagen fibers) by volume. However, knowledge is lacking on how nature integrates hard and soft materials at each length scale to form a layered composite that is lightweight and has high-strength with good fracture toughness but does not delaminate. Additionally, knowledge gaps exist because past researchers were limited: (a) equipment technology was not available adding to the difficulty in quantifying descriptions, isolating mechanisms which led to interpretations of results being based on idealized cartoon illustrations, (b) no characterization standard protocol exists for probing the multiscale and the experimental methods used all operate at different wavelengths of energy and different physical principles which led to difficulty obtaining coherent descriptions at given length scales from disparate data sets, and (c) the researcher did not anticipate the experimental results would be used to build, calibrate, and validate computational models which led to some of the subtle details of the fish scale being overlooked. Therefore, more comprehensive investigations are needed to understand how nature incorporates similar hard and soft materials that have been optimized so that a layered delamination resistant composite system may be produced.

The following Chapter 3 describes the details of experimental techniques employed in this current research effort. Also provided in the next chapter is a discussion as to what criteria were used to select the experimental methods. The selected methods are thought to provide the best opportunity for obtaining the type, variation and integration of materials, and mechanical properties that best describe the gar fish scale inherent qualities.

CHAPTER 3: EXPERIMENTAL DESIGN METHODOLOGY

3.1 Formulation of Hypothesis (*H*)

The rationale for the experimental program is tied to the problems associated with testing the hypothesis. The difficulty with any hypothesis is that it is stated sufficiently precise so that its nullification is possible through experiment (Wheeler and Ganji, 2001). Accordingly, the hypothesis will be reviewed in some detail before describing the experimental program.

The hypothesis *(H)* is the fish scales are effective in resisting cracks, dissipating energy, and transferring loads across interfaces because of the grading of the composite layer properties. The purpose, of *H*, is to test if there is a significant difference in the material above, below, or between layers. In addition to using the experimental program to test, *H*, the program must verify the following: (a) interfaces exists, and (b) the layers are graded.

3.2 Purpose of Experiments for Testing Hypothesis (*H*)

When deriving basic questions from a reverse engineering approach to ascertain the fish scale characteristics, the questions should lead to the selection of experiments that can be used to provide evidence and test *H*. Moreover, the overarching purpose of the experiments is to answer the following fundamental questions:

(a) How are natural nano-composite systems assembled?

(b) How do the layer thickness and the functionalized gradient properties interact to achieve high toughness?

(c) What are the design principles of natural armor systems?

(d) How can these design principles be applied to the design of man-made engineered composite systems?

34

3.3 Questions Developed from Hypothesis (*H*)

A reverse engineering approach is used to test the hypothesis that fish scales are effective in resisting cracks, dissipating energy, and transferring loads across interfaces because of the grading of the composite layer properties. By using a reverse engineering approach, scientific questions can be developed that may be answered with experimental evidence and test *H*. If the primary scientific questions are developed sufficiently, secondary questions will often arise. When both the primary and secondary scientific questions can be answered with experimental evidence sufficiently, the information can be used to develop scientific theories.

Scientific theories use many observations and have volumes of experimental evidence that can be applied to unrelated facts and new relationships. Also, theories are flexible enough to be modified if new data/evidence is introduced. Furthermore, if sufficient evidence has been gathered to develop theories, researchers can begin asking tertiary questions such as: (a) are the results repeatable, (b) are the results equipment-operator dependent, or (c) are the results predictable? Meaning they follow directly from primary and secondary results. If the tertiary questions can be answered with sufficient experimental evidence, scientific laws can be established. In this current investigation the primary, secondary, scientific, and ancillary questions that have been formed from *H* are as follows:

3.3.1 Primary Scientific Questions

    (a)   The primary question is determining how the chemical and morphological nature of the layering and thickness of the interface may affect the mechanical response?

    (b)   What is the chemical composition?

    (c)   What is the structure?

    (d)   Does the structure have layers?

(e)   Are structural layers identifiable, if so how many?

(f)   Are the structural layers graded?

(g)   To what extent can mechanical measurements, chemical composition, and structural morphological measurements be used to understand load transfer across layered interfaces and energy dissipation throughout the layers?

3.3.2 Secondary Scientific Questions

(a)   If the structural layers are graded, to what extent?

(b)   Is the observed morphology the reason for the graded properties in the fish scale?

(c)   Is the measured chemical composition the reason for the graded properties in the fish scale?

(d)   Is the chemical composition and morphology interrelated, if so to what extent?

(e)   Is fish scale composite system's chemical composition and morphological hierarchically arranged?

(f)   If there is a hierarchal arrangement, to what extent are the mechanisms observable/measurable?

(g)   Does the hierarchal arrangement lead to the development of the graded structure?

(h)   What role does the hierarchal arrangement have in mechanical measurements, to what extent?

3.3.3 Ancillary Questions

(a)   Are there routine analytical and experimental approaches that have been used in the past that are relevant to the questions asked, if so, can they readily be applied in this research effort?

(b)   What are the attributes and limitations for the known analytical and experimental approaches?

(c)   Are there alternative analytical and experimentally viable approaches if routine methods are not available?

(d)   Is there reasonable information found in literature that can be used to compare the measured results and/or can help fill identified knowledge gaps?

(e)   Does the design of experiments (DOE) provide sufficient overlap between analytical and experimental methods for supplemental comparison of the measured phenomena/mechanisms?

(f)   What is a reasonable data collection plan that provides sufficient information?

(g)   Does the DOE and data collection plan provide sufficient evidence to test H?

(h)   In addition to testing H, does the DOE provide contingencies for further investigation of new discoveries that have been deemed necessary to address critical knowledge gaps?

(i)   What is the return-on-investment (ROI) for conducting additional experiments? Are the additional experiments cost effective? Will the additional efforts advance the community of practice for experimentation and specimen preparation? Are the additional experiments critical for advancing the body of knowledge in biomaterials, biomimicry/bioinspired design, and manufacturing?

3.4 Selection of Experiments for Testing Hypothesis (H)

3.4.1 Criteria for Selecting Experimental Methods

Ideally, when selecting experimental methods for biological characterization, consideration should be given on how to best mimic in situ conditions which can allow the

specimen to remain in a pristine, undamaged, and unaltered state. Often times, the specimens are unavoidably damaged during preparation for experimentation. Thus, verification methods must be incorporated in experimental program that can help determine sources of uncertainty in the specimen, preparation, experimental equipment, and forensic analysis technique.

The following considerations were used in developing the criteria for selecting experimental methods: (a) What is thought to be known about the fish scale? (b) Which methods have been used previously to investigate fish scales or other similar biomineralized materials along with their attributes? (c) Which methods can be used to identify the fish scale's hierarchal structure? (d) Which methods can be used to speciate the fish scale biochemistry? (e) Which methods provide bulk versus local measurements? and (f) Which methods provide overlap, can be used to confirm others methods?

(a)   Recall, being discussed in Chapter 2, knowledge of the fish scale formation processes is limited. However, past researchers have reported the sub-units of the fish scale are made up of apatite crystals and collagen fibers (Chen, Lin, Yang, Lopez, Li, Olevsky , and Meyers, 2011; Yang, Chen, McKittrick, and Meyers, 2012; Allison, et al. 2013; Yang, Chen, Gludovatz, Zimmermann, Ritchie, and Meyers, 2013a; and Yang, Gludovatz, Zimmermann, Bale, Ritchie, and Meyers, 2013b). In addition, since the sub-units are derived from soluble geological minerals then there is a likelihood the minerals themselves have a known structural class in terms of crystallographic diffraction, thermal gravimetric signature, x-ray, and electron patterns (Yang, Gludovatz, Zimmermann, Bale, Ritchie, and Meyers, 2013b). Furthermore, previous research has shown the biomineralized scales to exhibit property grading with very little change in composition so the sub-units may also

38

have identifiable packing arrangements, grain shape, grain size distributions, and unique grain orientations at interfaces throughout the hierarchal levels (Chen, Lin,Yang, Lopez, Li, Olevsky , and Meyers, 2011; Allison, et al. 2013; Yang, Chen, Gludovatz, Zimmermann, Ritchie, and Meyers, 2013a; and Yang, Gludovatz, Zimmermann, Bale, Ritchie, and Meyers, 2013b).

(b-f) Table 3.1 lists twenty-eight experimental characterization methods that have been commonly used to investigate the structural, chemical, and mechanical attributes of fish scales or other similar biomineralized materials (Lee, Novitskaya, Reynante, Vasquez, Urbaniak, Takahashi, Woolley, Tombolato, Chen, and McKittrick, 2011; Torres, Troncoso, Nakamatsu, Grande, and Gomez, 2008; Tai, Qi, and Ortiz, 2005; Bruet, Song, Boyce, and Ortiz, 2008a; Yang, Gludovatz, Zimmermann, Bale, Ritchie, and Meyers, 2013b; Garrano, La Rosa, Zhang, Niu, Tay, Majd, and Arola, 2012; Landis, 1995; Ikoma, Kobayashi, Tanaka, Walsh, and Mann, 2003; Lin, Wei, Olevsky, and Meyers, 2011; Song, Reichert, Kallai, Gazit, Wund, Boyce, and Ortiz, 2010; Chang and Chen, 2013; Liu, Zhang, Li, Miao, and Wu, 2008; Cuy, Mann, Livi, Teaford, and Weihs, 2002; Waite, and Broomell, 2012; Bozec, de Groot, Odlyha, Nicholls, Nesbitt, Flanagan, and Horton, 2005; Zhang, Niebur, and Ovaret, 2008; Klosowski, et al., 2015; McNally, Nan, Botton, and Schwarcz, 2013; Rho and Pharr, 1999; Bertassoni, and Swain, 2012; and Rodriguez-Florez, Oyen, and Shefelbine, 2013). Furthermore, Table 3.1 provides a systematic means to critically evaluate experimental methods that may be useful in interpreting the structural, chemical, and mechanical processes when descending the hierarchical scales of highly complex heterogeneous composite materials.

Table 3.1 DOE—Methods used for characterizing fish scale, bone, tooth, and other biomineralized composites.

	Hierarchal Length Scale Measurable Range [>1] mm											
	Characterization											
	Purpose						Phases			Measurement Type		Reference
Method	Structural		Chemical		Mechanical							
	Class Deter	Family Speciat.	Class Deter.	Family Speciat.	Class Deter.	Family Speciat.	Cryst.	Prot.	Cryst. + Prot.	Global	Local	
Unaided Eye Observation in Visible Light	No	No	No	No	No	No	No	No	No	Yes	No	N/A
Water Absorption and Desorption[1]	No	No	No	No	No	No	No	No	Yes	Yes	No	(Torres, 2008)
Drop Tower Impact	No	No	No	No	No	No	No	No	No	Yes	No	(Lee, 2011)
Uniaxial Compress	No	No	No	No	No	No	No	No	No	Yes	No	(Yang. 2013b)
Uniaxial Tension	No	No	No	No	No	No	No	No	No	Yes	No	(Garrano, 2012)

[1]Measure permeability of bulk structure.
[2]Provides structural arrangement of surface and internal structure.
[3]Provides structural arrangement and texture of structure surface.
[4]Provides structural and chemical content.
[5]Provides structural surface texture only.
[6]Provides mapping of pore structure in bulk system.
[7]Provides high-magnification view of structural orientation of crystal and proteins.

Table 3.1 DOE—Methods used for characterizing fish scale, bone, tooth, and other biomineralized composites (continued).

Method	Structural Class Deter	Structural Family Speciat.	Chemical Class Deter.	Chemical Family Speciat.	Mechanical Class Deter.	Mechanical Family Speciat.	Cryst.	Prot.	Cryst + Prot.	Global	Local	Reference
μm-XCT[2]	No	No	No	No	No	No	Yes	Yes	Yes	Yes	Yes	(Yang. 2013b)
FTIR	Yes	No	Yes	No	No	No	Yes	Yes	Yes	No	Yes	(Song, 2010)
Optical Microscopy[3]	No	No	No	No	No	No	No	No	No	Yes	Yes	(Song, 2010)
EMPA	Yes	No	Yes	No	No	No	Yes	No	No	No	Yes	(Cuy, 2002)
μm-XEDS	Yes	No	Yes	No	No	No	Yes	No	No	No	Yes	(Lin, 2011)
μm-XRD	Yes	No	Yes	No	No	No	Yes	No	No	Yes	No	(Song, 2010)
μm-XANES	Yes	Yes	Yes	Yes	No	No	Yes	No	No	Yes	Yes	(Waite, 2012)
μm-XRF	Yes	No	Yes	No	No	No	Yes	No	No	Yes	Yes	(Waite, 2012)
TGA[4]	Yes	No	Yes	No	No	No	Yes	No	No	Yes	No	(Liu, 2008)
HR-SEM[2]	No	No	No	No	No	No	Yes	Yes	Yes	Yes	Yes	(Yang. 2013b)
Vickers Microindentation	No	No	No	No	No	No	No	No	No	Yes	No	(Bruet, 2008a)

Columns above are grouped as: *Hierarchal Length Scale Measurable Range [0.001-1] mm* → *Characterization* → **Purpose** (Structural: Class Deter / Family Speciat.; Chemical: Class Deter. / Family Speciat.; Mechanical: Class Deter. / Family Speciat.) | **Phases** (Cryst. / Prot. / Cryst + Prot.) | **Measurement Type** (Global / Local) | **Reference**

[1]Measure permeability of bulk structure.
[2]Provides structural arrangement of surface and internal structure.
[3]Provides structural arrangement and texture of structure surface.
[4]Provides structural and chemical content.
[5]Provides structural surface texture only.
[6]Provides mapping of pore structure in bulk system.
[7]Provides high-magnification view of structural orientation of crystal and proteins.

Table 3.1 DOE—Methods used for characterizing fish scale, bone, tooth, and other biomineralized composites (continued).

	Hierarchal Length Scale Measurable Range [0.001-1] mm											
	Characterization											
	Purpose							*Phases*			*Measurement Type*		
Method	*Structural*		*Chemical*		*Mechanical*								*Reference*
	Class Deter	Family Speciat.	Class Deter.	Family Speciat.	Class Deter.	Family Speciat.	Cryst.	Prot.	Cryst + Prot.	Global	Local	
Surface Profilometry[5]	No	No	No	No	No	No	No	No	No	No	Yes	(Song, 2010)
Mercury Porosimetry[6]	No	No	No	No	No	No	No	No	No	Yes	Yes	(Song, 2010)
SS-NMR	Yes	Yes	Yes	Yes	No	No	Yes	Yes	Yes	Yes	No	(Waite, 2012)
Raman Spectroscopy	Yes	Yes	Yes	Yes	No	No	Yes	Yes	Yes	No	Yes	(Waite, 2012)
μm-Uniaxial Comp.	No	No	No	No	No	No	No	No	Yes	No	Yes	(Zhang, 2008)
Hierarchal Length Scale Measurable Range [0.3-1] μm												
HR-SEM[2]	No	No	No	No	No	No	Yes	Yes	Yes	Yes	Yes	(Bruet, 2008a)
TEM[3]	No	No	No	No	No	No	Yes	Yes	Yes	Yes	Yes	(Garrano, 2012)

[1]Measure permeability of bulk structure.
[2]Provides structural arrangement of surface and internal structure.
[3]Provides structural arrangement and texture of structure surface.
[4]Provides structural and chemical content.
[5]Provides structural surface texture only.
[6]Provides mapping of pore structure in bulk system.
[7]Provides high-magnification view of structural orientation of crystal and proteins.

Table 3.1 DOE—Methods used for characterizing fish scale, bone, tooth, and other biomineralized composites (continued).

	Hierarchal Length Scale Measurable Range [1-300] nm										
	Characterization										
	Purpose						*Phases*			*Measurement Type*		
Method	*Structural*		*Chemical*		*Mechanical*							*Reference*
	Class Deter	Family Speciat.	Class Deter.	Family Speciat.	Class Deter.	Family Speciat.	Cryst.	Prot.	Cryst + Prot.	Global	Local	
Nanoindentation	No	No	No	No	No	No	No	No	Yes	No	Yes	(Bruet, 2008a)
Atomic Force Microscopy[3]	No	No	No	No	No	No	Yes	Yes	Yes	No	Yes	(Bozec, 2005)
TEM[2]	No	No	No	No	No	No	Yes	Yes	Yes	Yes	Yes	(Garrano, 2012)
STEM- HAADF[7]	No	No	No	No	No	No	Yes	Yes	Yes	No	Yes	(McNally, 2013)
STEM-EELS[7]	No	No	No	No	No	No	Yes	Yes	Yes	No	Yes	(Klosowski, 2015)

[1]Measure permeability of bulk structure.
[2]Provides structural arrangement of surface and internal structure.
[3]Provides structural arrangement and texture of structure surface.
[4]Provides structural and chemical content.
[5]Provides structural surface texture only.
[6]Provides mapping of pore structure in bulk system.
[7]Provides high-magnification view of structural orientation of crystal and proteins.

Below are the critical aspects the experimental methods should address:

(i) Structural Determination Considerations

- Usually microscopy techniques are used to elucidate physical features of materials. The methods should be able to provide details regarding the geometry in terms of weight, density distribution, feature size, orientation, surface texture, pores, pore connectivity, position, and assemblage junction points. The following methods that have been successfully used to identify the physical features of materials are: (1) unaided eye observation in visible light, (2) micro x-ray computed tomography (μm-XCT), (3) optical microscopy, (4) high magnification scanning electron microscopy (HR-SEM), (5) transmission electron microscopy (TEM), (6) scanning transmission electron microscopy-high angle annular dark field (STEM-HAADF), (7) atomic force microscopy (AFM), (8) surface profilometry, (9) mercury porosimetry, and (10) water absorption and desorption.

- Spectroscopy methods use analytic techniques to measure diffraction patterns or spectral wavelength scattering/absorption of materials. The measures are then compared to known standards and used for identifying the structural materials class. The following methods that have been successfully used to identify the structural patterns and spectral features of materials are: (1) microcomputed synchrotron x-ray diffraction (μm-XRD), (2) microcomputed synchrotron x-ray absorption near edge structure (μm-XANES), (3) fourier transform infrared spectroscopy (FTIR), (4) raman spectroscopy, (5) thermal gravimetric analysis (TGA), and (6) solid-state nuclear magnetic resonance (SS-NMR).

(ii) Chemical Determination Considerations

- Typically analytical spectroscopy techniques are used to discern elemental composition of materials. The spectroscopy methods should be capable of identifying between

minerals/metals elemental composition. In addition, the experimental methods should be able to spatially resolve, using either stand-alone spectroscopy methods or can be coupled with microscopy, techniques to map the elemental distribution. The following methods that have been successfully used to identify the chemical/elemental composition of materials are:

(1) microcomputed x-ray energy-dispersive spectroscopy (μm-XEDS), (2) Electron microprobe analyzer (EMPA), (3) microcomputed synchrotron x-ray fluorescence (μm-XRF), and

(4) scanning transmission electron microscopy- Electron Energy Loss Spectroscopy (STEM-EELS).

- The experimental methods should also be capable of deciphering between inorganics/organics, classify/speciate family and classes of chemical compounds and molecules. The following methods provide overlap/confirmation and can be used to determine structural characteristics and also speciate the compounds and molecules in the system: (1) microcomputed synchrotron x-ray diffraction (μm-XRD), (2) microcomputed synchrotron x-ray absorption near edge structure (μm-XANES), (3) fourier transform infrared spectroscopy (FTIR), (4) raman spectroscopy, (5) thermal gravimetric analysis (TGA), (6) solid-state nuclear magnetic resonance (SS-NMR).

(iii) Mechanical Property Determination Considerations

- Experimental mechanical methods should be capable of providing a profile analysis of strength, toughness, and hardness that is representative of the structural composition. The methods should consider the effects of bulk irregular geometrical shape, local property grading, and antistrophic structural reinforcement. The following mechanical methods have been used to measure materials response, when externally loaded: (1) Vickers microindentation, (2) micropillar uniaxial compression (μm-UC), and (3) nanoindentation.

- In addition, the experimental measures should provide the means for spatially correlated spectroscopy and microscopy methods that help resolve the structural characteristics and chemical composition. The following mechanical method that has been successfully used to map mechanical response to structural characteristics and chemical composition is nanoindentation.

- Experimental mechanical methods should also consider measurements that can lead to the design and manufacturing of materials. Often the mechanical experiments that consider both analysis and design for manufacturing purposes provides an index for the average measured bulk response. Useful mechanical measurement techniques are: (1) drop tower impact (DTI), (2) uniaxial compression (UC), and (3) uniaxial tension (UT).

3.4.2 Down Selection of Experimental Methods for Testing Hypothesis (H)

The previous section outlined the criteria for selecting experimental methods for meeting the requirements for testing *H*. The selection criteria were applied to Table 3.1. Upon applying the criteria, some of the experimental characterization methods were reclassified as contingent supplemental methods while others were completely removed from the DOE plan.

Experimental methods that have been either designated as contingent supplemental methods or eliminated from the DOE plan are provided below.

(a) Raman spectroscopy has been designated as contingent supplemental structural/ chemical speciation methods. Raman spectroscopy or data sets of similar structural and chemical characteristics will be employed only if FTIR cannot adequately identify the constituents in the fish scale.

(b) The following mechanical characterization methods eliminated from the DOE plan were: DTI, UC, μm-UC, and UT. The methods were eliminated because they only

will provide an indexed average of bulk mechanical response. Furthermore, sample preparation would require removal of materials to meet the appropriate geometrical aspect ratio standards. Altering the inherent geometry of the specimen will provide mechanical results that would not be representative of the fish scale and negates the beneficial attributes gained from the composite structure.

Also eliminated from the DOE plan was the Vickers microindentation. Since the specimen has a non-uniform thickness, applying uniform external loading is not possible without major modification to the experimental specimen mounting procedure. Along with procedure modification, finite element analysis (FEA) will need to be conducted to understand the non-linear mechanical response caused by the non-uniform loading distribution. Moreover, to effectively obtain useful information from FEA the exact specimen geometry, material property identification/distribution, indenter geometry, and appropriate material model selected must be known while simultaneously accounting for the numerical instabilities/inaccuracies due to mesh development.

Additionally considered, when conducting forensic analysis for post failure mechanism identification, there is not a reasonable method to section the specimen without causing further damage. Consequently, sectioning the specimen for the forensic investigation will more than likely mask the damage caused by external loading. Thus, the mechanical characterization methods that were eliminated from the DOE plan are less likely to provide sufficient information of how the structural arrangement and chemical composition affect the mechanical response or insight to what is attributing to the fish scale delamination resistance.

(c) The remaining experimental methods that were removed from the DOE plan are surface profilometry, AFM, mercury porosimetry, water absorption, and desorption

measurements. Additionally, eliminated from the DOE were the topographical

measurements obtained from surface profilometry and AFM, which are redundant

measurements that can be obtained from HR-SEM and TEM. Unlike HR-SEM and

TEM, surface profilometry and AFM cannot be readily coupled to other

characterization methods used for structural/chemical class identification and

family speciation.

In regard to water absorption/desorption methods, they will only provide information for

bulk density. The measurements cannot quantify solid and pore volume fractions nor provide

information regarding the pore geometry and size distribution for the structure. Unlike the water

absorption/desorption characterization technique, mercury porosimetry measurements do well in

spatially resolving pore geometry and pore size distribution for surface pores. Surface pores are

voids that occur on the external face of the structure, have limited penetration depth, but do not

proliferate through the entire structure. Unfortunately, the mercury porosimetry method lacks the

capability to identify internal pores and pore connectivity. Pore connectivity identification is

used to quantify the permeability of the structure. If surface pores, internal pores, and/or

connected pores are present in the structure neither pore measurement methods can adequately

describe the functional role they play in transporting fluids for growth, energy dissipation,

structural and mechanical property grading in the biomineralized fish scale composite.

3.5 Relevance of Selected Experimental Methods for Characterizing Materials Hierarchies

The remaining experiments are thought to be the best suited for testing *H*. Additionally

considered, when combined, the remaining methods can be used to provide information at

descending levels of the fish scale's hierarchy. The selection of experimental methods to

ascertain what's structurally, chemically, and mechanically relevant for the discovery/

identification of mechanisms necessary for hypothesis testing is forever challenging. Still

problematic will be the interpretation of results obtained from the physical measurements. To

reduce the variability in data interpretation the experiments were conducted in dry state. As

shown in Figure 3.1, an illustration I developed shows when descending hierarchical length

scales from high to low of highly complex heterogeneous composite materials, the uncertainty of

results increases. The uncertainty is attributed to increasing unknown variables effecting

measurements of chemical, structural, and mechanical process. Therefore, the interpretation of

results from individual experiments can become very subjective. The selected experiments have

been combined in such a way that they can provide empirical evidence and for the most part

eliminate subjectivity. Empirical evidence will lead to conclusions that are objectively

determined.
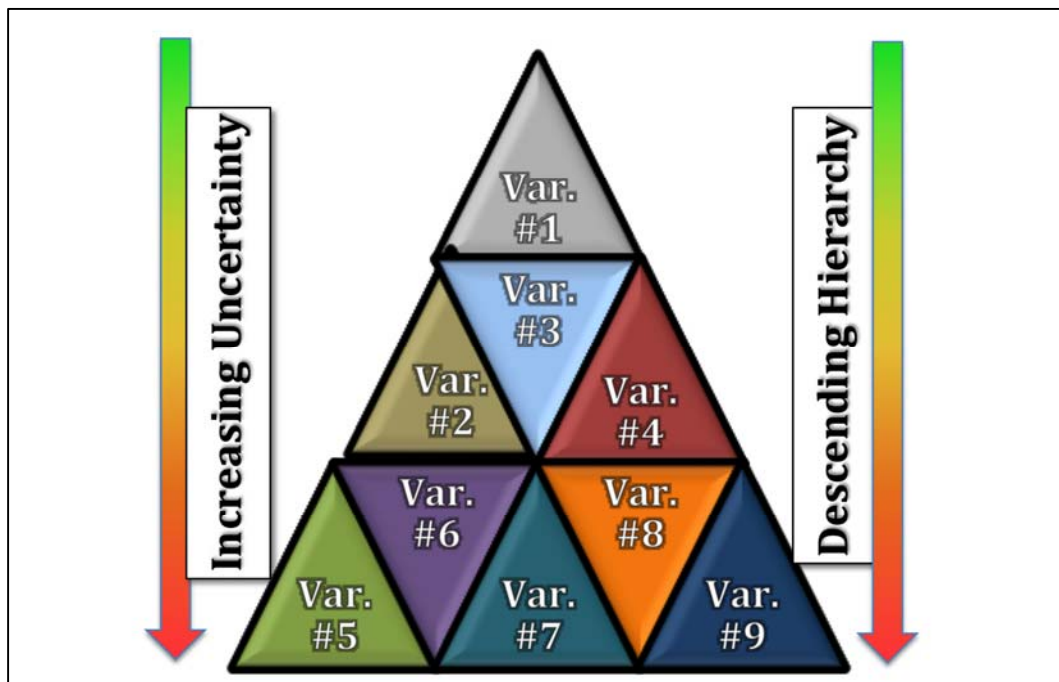
Figure 3.1 Illustration of increasing uncertainty due to increasing unknown variables
effecting measurements of chemical, structural and mechanical process when
descending hierarchical scales of highly complex heterogeneous
composite materials.

3.6 Description of Experimental Methods Used for Testing Hypothesis (*H*)

The experimental methods commissioned by this research provide a systematic top down approach, which can be used to probe the length scales. Most of the techniques are either based on visible light, infrared, electron, or x-ray diffraction/absorbance. As shown in Figure 3.2, when the electromagnetic spectral wavelength decreases, the wavelength's signal frequency increases (The Electromagnetic Spectrum, 2015). The increase in signal frequency increases heat generation (Callister Jr., and Rethwisch, 2008; Kim, 2013; Coates, 2000; Gunther, 2013; Willimott, 2011; Leng, 2008; Williams, and Carter, 2009; and Henderson, Neuville, and Downs, 2014).
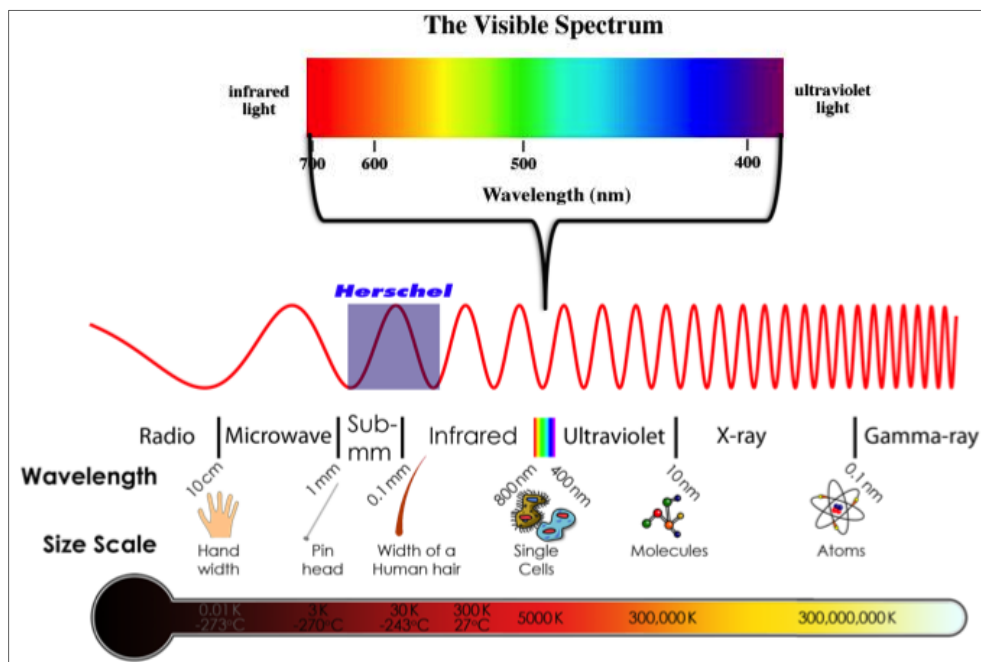
Figure 3.2 Illustration of electromagnetic spectral wavelength ranges
(The Electromagnetic Spectrum, 2015).

As a result, careful/detailed specimen preparation methods are used to minimize heat damage, caused by x-rays and electrons, such as mineral recrystallization and excessive cracking due to drying (Kim, 2013; Coates, 2000; Gunther, 2013; Willimott, 2011; Leng, 2008; Williams,

and Carter, 2009; and Henderson, Neuville, and Downs, 2014). Furthermore, careful specimen preparation helps minimize the variables when making observations along the various length scales. Provided below is a summary description of methods and sample preparation techniques.

3.7 Summary of Experimental Methods

3.7.1 Unaided Eye Observations (Measurements Taken at Length Scale [>1] mm):

Unaided eye observations can provide a sense of the specimen's size, shape, and texture. Specimens are viewed in visible light without the aid of a microscope. The eye observations are useful for deciding which length scale based experimental measurements and required specimen preparation techniques may be useful for characterizing the fish scale.

3.7.2 Nanoindentation (Measurements Taken at Length Scale [1-1000] nm):

Nanoindentation is a mechanical characterization method that can be used to measure the near surface local average elastic modulus and hardness of biological materials (Oyen, 2011; Cuy, Mann, Livi, Teaford, and Weihs, 2002; Waite, and Broomell, 2012; Balooch, Marshall, Marshall, Warren, Asif, and Balooch, 2004; Rho, and Pharr, 1999; Tai, Qi, and Ortiz, 2005; Pharr, Strader, and Oliver, 2009; Pharr, Herbert, and Gao, 2010; and Rho, Zioupos, Currey, and Pharr, 2002). Nanoindentation is used to map the mechanical properties across the fish scale and observe the evolution of mechanical properties across the interface. The experimental protocol uses dynamic indentation during the test to characterize the evolution of mechanical properties as the indenter tip penetrates into the surface of the sample; the indentation technique is further described in Oliver and Pharr's pioneering work (Oliver and Pharr, 1992; Oliver Pharr, 2004).

3.7.3 Thermo-Gravimetric Analysis (TGA) (Measurements Taken at Length Scale [N/A]):

Thermo-gravimetric analysis (TGA) uses heat to force reactions and physical changes in materials. The experimental method provides quantitative measurement of mass change in

materials associated with transition and thermal degradation. The measurements allow rapid and precise determination of weight losses due to moisture or loss of crystal water. TGA records change in mass from dehydration, decomposition, and oxidation of a sample with time and temperature. Characteristic thermo-gravimetric curves are given for specific materials and chemical compounds due to unique sequence from physicochemical reactions occurring over specific temperature ranges and heating rates (Leng, 2008).

3.7.4 Optical Microscopy (Measurements Taken at Length Scale [1-1000] μm):

The optical microscope uses visible light and a system of lenses to magnify images of small samples. Since microscope optics are static, different magnification objective lens are used to focus at different focal depths. In addition, visible light-sensitive cameras are usually used to capture the image from the optical microscope; however, the image's resolution is limited to the wavelength of visible light (Leng, 2008).

3.7.5 Solid-State Nuclear Magnetic Resonance (SS-NMR) Spectroscopy (Measurements Taken at Length Scale [1-1000] μm):

The Solid-State Nuclear Magnetic Resonance (SS-NMR) spectroscopy method can be used to identify/speciate the organic chemical-structural phases in fish scales. SS-NMR spectroscopy is used to determine the resonance frequency that causes the nuclear spin state in solid media. In solid media with little or no mobility (e.g., crystals, powders, large membrane vesicles, molecular aggregates), anisotropic interactions have a substantial influence on the nuclear spin state. In this context "nuclear spin" is defined as the magnetic state of the nuclei when the electromagnetic radiation is absorbed and re-emitted. The technique works by inducing the alignment of nuclear spins. Nuclear spin alignment is achieved by placing the specimen in a strong homogenous magnetic field and then exciting the chemical structure's nucleus by using

computer-controlled resonance frequency (RF) manipulation (Gunther, 2013; Henderson, Neuville, and Downs, 2014).

3.7.6 Raman Spectroscopy (Measurements Taken at Length Scale [1-1000] μm):

Raman spectroscopy uses a laser beam to irradiate a spot on the specimen. The scattered radiation produced by the Raman provides information about the molecular vibrational and rotational energies. The energies depend on the particular atoms or ions that comprise the molecule, the chemical bonds connecting them, the symmetry of their molecule structure, and the physico-chemical environment where they reside. The analytical technique is often used to identify/speciate either mineral or organic phases in materials (Coates, 2000; Leng, 2008; and Henderson, Neuville, and Downs, 2014).

3.7.7 Fourier Transform Infrared Spectroscopy (FTIR) (Measurements Taken at Length Scale [1-1000] μm):

Fourier Transform Infrared Spectroscopy (FTIR), sometimes complementary to Raman spectroscopy, is an analytical technique often used to identify/speciate either mineral or organic phases in materials. It provides information about the chemical bonding and molecular structure. The operating principle for FTIR is based on the fact that bonds and groups of bonds vibrate at characteristic frequencies; that are slightly higher than what's typically used in Raman spectroscopy. A molecule that is exposed to infrared rays absorbs infrared energy at frequencies that are characteristic to that molecule. During FTIR analysis, a spot on the specimen is subjected to a modulated IR beam. The specimen's transmittance and reflectance of the infrared rays at different frequencies is translated into an IR absorption plot consisting of reverse peaks. The resulting FTIR spectral pattern is then analyzed and matched with known signatures of identified materials in the FTIR library. The FTIR measurements can be used to identify

unknown materials present in a specimen when coupled with EMPA (Cuy, Mann, Livi, Teaford, and Weihs, 2002; Coates, 2000, Leng, 2008; and Henderson, Neuville, and Downs, 2014).

3.7.8 High Resolution Scanning Electron Microscopy (HR-SEM) (Measurements Taken at Length Scale [1-1000] μm):

High Resolution Scanning Electron Microscopy (HR-SEM) uses an electron probe that is scanned across the sample producing secondary and back-scattered electrons that can be detected and recorded as an image. The penetration depth is generally less than one micron, so the images produced are of the sample surface. The backscattering of electrons increases with increasing atomic number so that imaging with this method can produce images of heavier elements (Leng, 2008).

3.7.9 Microcomputed X-ray Energy-Dispersive Spectroscopy (μm-XEDS) (Measurements Taken at Length Scale [1-1000] μm):

Microcomputed X-ray Energy-Dispersive Spectroscopy (μm-XEDS) makes use of the X-ray spectrum emitted by a solid sample bombarded with a focused beam of electrons to obtain a chemical analysis. Mapping is most commonly used to produce 2D elemental distribution images within a sample. Images are collected from x-ray intensities that are measured by counting photons. Commonly μm-XEDS devices are coupled to either HR-SEM or TEM equipment. Usually, in conjunction with microscopy investigation, μm-XEDS is conducted to measure the individual elements in the material at the micron scale. The individual elemental distribution maps can be used for both quantitative/qualitative assessments if calibrated with material control standards (Nieto and Livi, 2013).

3.7.10 Electron Microprobe Analyzer (EMPA) (Measurements Taken at Length Scale [1-1000] μm):

Electron Microprobe Analyzer (EMPA) is an analytical technique often used to identify/speciate elemental constituents. EMPA can provide information to the degree of

impurity with respect to chemical composition of single particles. When coupled with TEM, spatial mapping of elements is possible. EMPA can also be used to examine the inorganic/ organic interface and determine chemical variation from the micron to nanometer scale (Cuy, Mann, Livi, Teaford, and Weihs, 2002).

3.7.11 Transmission Electron Microscopy (TEM) (Measurements Taken at Length Scale [1-1000] nm):

Transmission electron microscopy (TEM) is a microscopy technique in which a beam of electrons is transmitted through a thin specimen. Generally a specimen must be thinner than one micron to obtain a useful image. TEM provides information through the thickness of an electron-transparent specimen (Leng 2008; Williams and Carter, 2009; Henderson, Neuville, and Downs, 2014; and Nieto and Livi, 2013).

3.7.12 Scanning Transmission Electron Microscopy (STEM) (Measurements Taken at Length Scale [1-1000] nm):

Scanning transmission electron microscopy (STEM) is a type of TEM. In TEM electron beam is spread to image thin sections. However, for STEM the electron beam is focused into a narrow spot, which is scanned over the specimen in a raster pattern. The rastering of the beam across the sample makes STEM suitable for coupling spectroscopy and microscopy analysis techniques, such as EELS, and HAADF. The EELS and HAADF spectral signals can be obtained simultaneously, allowing direct correlation of image and quantitative data. When a hi-angle detector is used with STEM, it is possible to form atomic magnification images where the contrast is directly related to the elemental atomic number (z-contrast image). STEM has been used to image biological materials using dark-field microscopy. Dark-field microscopy is used to show high contrast images in heterogeneous biological samples without requiring staining (Leng

2008; Williams and Carter, 2009; Henderson, Neuville, and Downs, 2014; and Nieto and Livi, 2013).

3.7.13 Electron Energy Loss Spectroscopy (EELS) (Measurements Taken at Length Scale [1-1000] nm):

Electron energy loss spectroscopy (EELS) is a technique that provides elemental information on a nanometer scale when coupled with STEM. The energy of the incident electrons is altered as they pass through the sample. These energy loss spectra can be characterized using EELS to provide elemental identification. Because EELS provides improved spatial magnification (down to 1 nm), the energy magnification (<1 eV for EELS) technique is capable of measuring lower atomic number elements (e.g., H, O, Na, Mg, P, Ca). In addition, the low-angle inelastically scattered electrons used in EELS compliments the high-angle scattered electrons in HAADF images by allowing both signals to be acquired simultaneously (Leng 2008; Henderson, Neuville, and Downs, 2014; and Nieto and Livi, 2013).

3.7.14 High-Angle Annular Dark-Field (HAADF) (Measurements Taken at Length Scale [1-1000] nm):

High-Angle Annular Dark-Field (HAADF) is used to show atomic number contrast for high scattering angles of the electrons. The purpose of measurement is to determine local thickness of a specimen. When STEM is combined with both EELS and HAADF the scattered electrons can be used to discern structural and elemental composition from discrete spectral interfaces at the lowest nanometer scale, such as those measured in hydroxyapatite + collagen boundaries (Leng, 2008; Nieto and Livi, 2013; and Carlino, and Grillo, 2006).

3.7 15 Micro X-ray Computed Tomography (µm-XCT) (Measurements Taken at Length Scale [1-1000] µm):

Micro X-ray Computed Tomography (µm-XCT) is a nondestructive technique that uses x-ray spectra to visualize the interior of objects. The µm-XCT scans can be used to resolve fine

cross-sectional details. The thin two-dimensional scans are reconstructed using computed tomography, to form three-dimensional volumes. With the μm-XCT, reconstructed volumes can be imaged with a voxel magnification down to micron range (Song, Reichert, Kallai, Gazit, Wund, Boyce, and Ortiz, 2010; Allison, et al. 2013; Allison, et al. 2014; Yang, Gludovatz, Zimmermann, Bale, Ritchie, and Meyers, 2013b; and Chang and Chen, 2013).

3.7 16 Synchrotron X-ray Methods (μm-XRD/μm-XANES/μm-XRF-CT) (Measurements Taken at Length Scale [1-1000] μm):

The next three experimental methods involve the use of x-rays. As opposed to using bench top spectroscopy techniques exclusively, synchrotron x-ray methods were also included. Since Synchrotron uses much stronger energy to produce x-rays, the methods can be used to identify and sufficiently spatially map structural and elemental composition that could not otherwise be obtained from μm-XEDS, and EMPA. Additionally, by combining Synchrotron x-ray with the μm-XEDS and EMPA spectroscopy methods, most of the periodic elements that are common to biomineralized composites may be measured. Thus the differing energy range levels for each complimentary technique provides some overlapping information that can be used for confirmation.

Synchrotron X-rays are electromagnetic radiation that is emitted when charged particles are accelerated radially. Synchrotron radiation is produced when accelerated electrons pass radially through magnetic fields. The radiation has a characteristic polarization and the frequencies generated can range over the entire electromagnetic spectrum. As a result of the wide range electromagnetic spectrum a variety of synchrotron x-ray measurements can be made. The current research used microcomputed x-ray diffraction (μm-XRD), absorption near edge structure (μm-XANES), and florescence (μm-XRF) synchrotron based methods to determine the structural and elemental composition for the fish scale (Willmott, 2011; Kennedy, et al., 2012).

Synchrotron μm-X-ray Diffraction, μm-XANES, and μm-X-ray Fluorescence Mapping using μm-CT experiments were conducted on Beamlines X2B, X26A and X27A at the National Synchrotron Light Source at Brookhaven National Lab (NSLS) in Upton, NY. X-ray microprobes for the beamlines are designed to provide elemental distribution and speciation information for heterogeneous solid samples. The beamlines are powerful because they couple a number of analytical techniques thus providing information about complex samples that cannot be achieved using any other tool.

μm-XRF mapping is most commonly used to produce 2D elemental distribution images within a sample. Images are collected from many angles by rotating the specimen through small, evenly spaced, angular increments between 0 and 180 degrees. The number of images needed is proportional to the width of the specimen. These individual 2D images are then reconstructed into a 3D image. A magnification of [3~5] microns is achievable. Elemental correlations and changes in sample composition on the micron scale can be monitored using μm-XRF. Once the elemental composition of the sample is determined, μm-XANES and μm-XRD are collected on the same specimen to aid in identifying any major compounds present within the material.

μm-XRD is not element specific and provides information about any crystalline or well structured compounds within a sample. μm-XRD is excellent at identifying minerals (e.g., carbonates, phosphates, silicates) within a completed matrix on a micron-level scale. The techniques were used to monitor changes in chemical or mineral composition moving across the cross section of the scale (>10 micron step intervals). Because the sections within the fish scale differ in chemical composition, the transition boundary between these sections could be monitored using these tools.

µm-XANES is an element specific technique which provides chemical information about oxidation state and the environment surrounding the element (how and to what it is bound, and how tightly it is bound). µm-XANES was used to identify Ca compounds within the gar scales. Changes in Ca complexion from the outermost layer to the inner boney section of the scale were monitored.

3.8 Summary of Sample Preparation Methods

3.8.1 Animal Care Guidelines and Specimen Preservation:

Prior to conducting any studies using animals, regardless whether the subjects are living or deceased, permission must be granted by the appropriate wildlife and safety management authority. Permission was obtained by providing written animal care guidelines to the proper authority. In addition, researchers were provided fish scale specimens used in this current investigation by the U.S. Army Engineer Research and Development Center (ERDC). As a result, the University of Arkansas granted written permission based on the specimens being provided by ERDC researchers from ERDC's ongoing in-house research efforts. The research conducted in this dissertation is secondary to ERDC's, and ERDC provided federal government approved animal care guidelines listed under #EL-6009-2011-5. The ERDC's approved animal care guidelines encompass the National Institutes of Health (NIH) Guide for Care and Use of Laboratory Animals. For further detailed information please contact ERDC. The ERDC provided specimens that were immersed in a phosphate-buffered saline (PBS) solution. The PBS solution was used to maintain the fish scale's full hydration state during storage.

3.8.2 Initial Sample Preparation:

The ERDC provided scales they dissected from the middle region of the alligator gar fish and with its epidermis skin layer intact, Figure 3.3. After procurement, scales were further
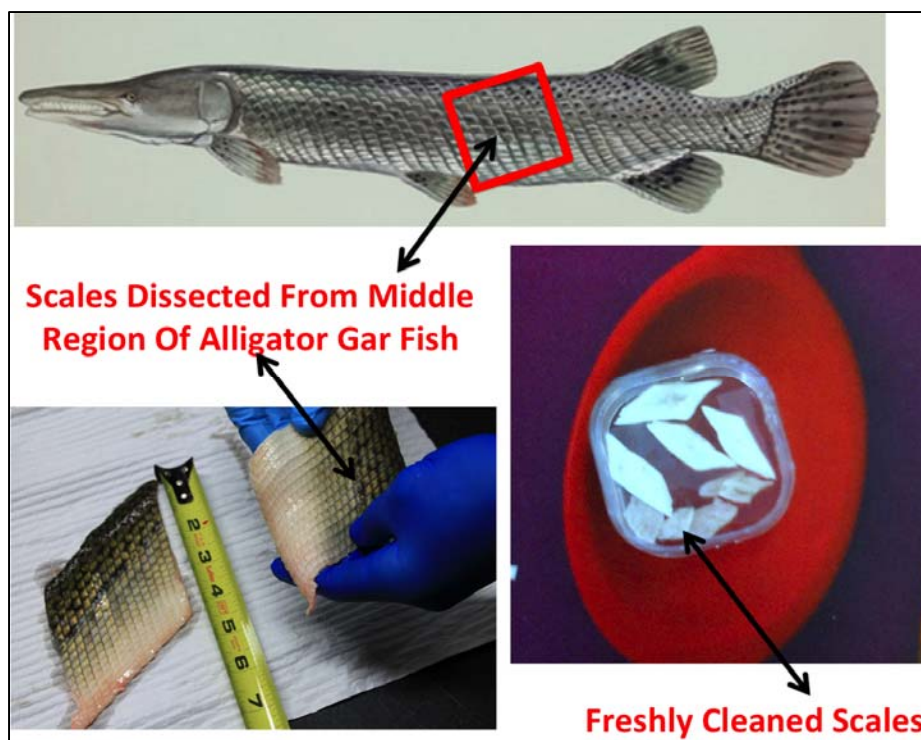
Figure 3.3 Freshly cleaned scales dissected from middle
region of alligator gar fish.

sectioned into individual fish scales. Next, the epidermis soft tissue layer was removed using a

razor blade. The scales were then sonicated in deionized water to remove any remaining soft

tissue particles and mucus. The cleaned scales, shown in Figure 3.3, were then placed in fresh

PBS to prevent cross contamination and stored for future specimen preparation and

characterization. The details are provided below for methods used to prepare specimen for

experimental characterization, unless further explained, in Chapter 4 during data analysis and

presentation of experimental results.

3.8.3 Unaided Eye Observations, Optical Microscope, and HR-SEM Sample Preparation:

Since the purpose of the unaided eye observations and optical microscope were to

provide a sense of the specimen's size, shape, and texture, no further sample preparation was

needed after the scales were freshly cleaned.

3.8.4 Cross-Sectional Analysis Using Optical Microscope, Nanoindentation and FTIR Sample Preparation:

Individual fish scales were mounted in 38-mm inner diameter molds. The stiff medium optically transparent epoxy, product name EPO-TEK™ 301-2, which consists of a two-component resin and hardener, was used to mount the sample. The samples were allowed to cure in ambient conditions at an average temperature [25±5]°C. The samples were de-molded after they had cured for a minimum of 72 hours. To expose the interior fish scale layer(s) for experimental characterization and to meet the recommended specimen height by equipment vendor a, Buehler Isomet ™ 2000 model cut-off precision diamond bladed, saw cut was made across the short axis "A" at near the midline of the sample, Figure 3.4.
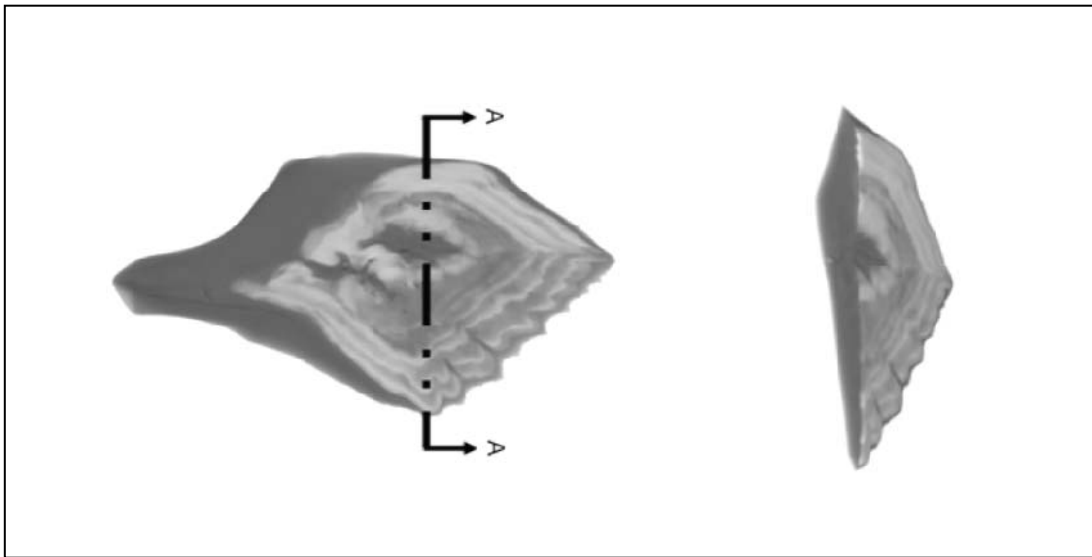
Figure 3.4 Cross-section of μm-XCT images of alligator gar scale depicting the short-axis "A" transverse section examined in this study by optical microscope, nanoindentation and FTIR techniques (Images courtesy of the U.S. Army's Engineer Research and Development Center (ERDC)-Geotechnical and Structures Laboratory (GSL) located in Vicksburg, Mississippi).

After cutting, the sample was sonicated in water for 15 minutes to remove any loose fragments and residual traces of cutting lubricant. The specimens were manually polished, with slight modification of the procedure described in textbook reference *Materials Characterization:*

Introduction to Microscopic and Spectroscopic Methods by Leng, on a Buehler Handimet ™ I Strip Grinder, sequential from coarse to fine by using #240, 320, 400, and 800-silicone carbide grit paper (Leng, 2008). In all grinding steps water was used as the lubricant. Before proceeding to the next smaller size grit, the sample was placed under a microscope to determine if scratches were all unidirectional. Unidirectional scratches were achieved by rotating the specimen clockwise one-quarter turn after every 50 forward hand strokes until four-quarter rotations have been completed. Following the 800-silicone carbide grit polishing, fine polishing using 1- and 0.03-micron Alumina water based suspensions on a Buehler Ecomett ™ II mechanical rotating polisher was conducted. The samples cross-sections were polished until the uniform unidirectional scratch width was less than 3 nanometers. Finally, the specimens were oven dried at 25 degrees Celsius for 24 hours. The samples were dehydrated to ensure consistent measurements were taken.

3.8.5 μm-XCT Sample Preparation:

Specimens were initially cleaned and dried as described above in Section 3.8.2. After cleaning the specimens were mounted to a holder using standard double-sided tape. No further preparation was needed.

3.8.6 Cross-Sectional Analysis Using TEM, STEM, EELS, HAADF, μm-XEDS and EMPA, Sample Preparation:

First follow the same sample preparation methods explained in the "Cross-Sectional Analysis Using Optical Microscope, Nanoindentation and FTIR Techniques" Section 3.8.4, with the exception that the specimens were mounted in a 25-mm inner diameter mold. The purpose for using a smaller specimen is to minimize outgassing effects, caused by the excited electrons heating the epoxy and/or biological materials. Excessive outgassing can cause distortions when electron based measurements are taken. After the specimens have been oven dried, the specimens

were then ion milled, using a PIPS ™ II - Precision Ion Polishing System, at cryo-temperature. Ion milling was used to cut the short-axis "A" transverse slices of whole specimens that are each [~10-nm] uniformly thick. Finally, to minimize ion charging, overheating, and recrystallization, the samples are carbon coated.

3.8.7 FIB Sample Preparation:

Focused ion beam prepared specimens can provide serial thin x-sections [~ 10 – 30 nm] for site-specific μm-CT images that can better resolve geometrical features at the surface, near surface. Specimens were initially cleaned and dried as previously described. Since every specimen reacts differently during the local milling, there is no specific guidance for preparing FIB specimens. The suggested practice used was the application of a palladium surface coating to minimize ion charging, overheating, and recrystallization. Also used was a "wedge" sectioning technique (Nalla, Porter, Daraio, Minor, Radmilovic, Stach, Tomsia, Ritchie, 2005; Jantou, Turmaine, West, Horton, and McComb, 2009; Grandfield, McNally, Palmquist, Botton, Thomsen, and Engqvist, 2010; Grandfield, and Engqvist, 2012; McNally, Schwarcz, Botton, and Aresnault, 2012; Resnikov, Natalie, Shahar, Weiner, 2014; and Kizilyaprak, Daraspe, and Humbel, 2014).

3.8.8 TGA Sample Preparation:

Freshly cleaned scales are oven dried at 25 degrees Celsius for 24 hours. Wire cutters were then used to cut the whole fish scale into smaller pieces. The smaller pieces were placed into several weigh pans. The weigh pans were filled until each had a minimum weight of 50 mg. The weight average of the pans was used to determine the overall TGA value. The temperature range used was [35 to 1550] degrees Celsius with a heating rate of 10-degrees Celsius/minute as recommended by Liao, Lin, Chen, and Sun 1999).

3.8.9 SS-NMR Spectroscopy Sample Preparation:

Freshly cleaned scales are oven dried at 25-degrees Celsius for 24-hours. Individual specimens were prepared by using a mortar and pestle to pulverize them into powder form. Approximately 50 mg by weight of powder was then packed into a 4-mm zirconium rotor. For the fish scales, analysis was conducted via solid-state 400 MHz NMR and spun at what is termed the "magic angle" within the magnetic field at speeds ranging from 5-12 kHz to eliminate spectral artifacts such as spinning side bands (How To Make A NMR Sample, 2015).

3.8.10 Synchrotron X-ray Methods (μm-XRD/μm-XANES/μm-XRF-CT) Sample Preparation:

Freshly cleaned scales are oven dried at 25-degrees Celsius for 24-hours. Synchrotron x-ray analysis samples were prepared by slicing serial thin cut sections from whole intact scales using a diamond tip knife attached to an ultramicrotome device. The cut sections were each approximately [3-5-μm] thick. Each serial section was mounted on separate Mylar™ films.

3.9 Overall Experimental Design Methodology Summary

The experimental design methodology was developed to provide a systematic top down approach, which can be used to probe the length scales. The outcome of the primary questions raised from the hypothesis *(H)* may lead to the development of secondary and ancillary questions as research progresses. The questions will be addressed based on the predefined research scope previously discussed in Chapter 1 and DOE strategy outlined earlier in Chapter 3.

The experimental characterization starts with the largest length scale as knowledge is learned but further questions may be raised. Shown in Figure 3.5, are locations probed and the experimental techniques used to examine the fish scale's hierarchy. As the successive length scales are examined some research questions are answered while additionally others are raised. The process stated above will continue until the lowest measurable length scale has been
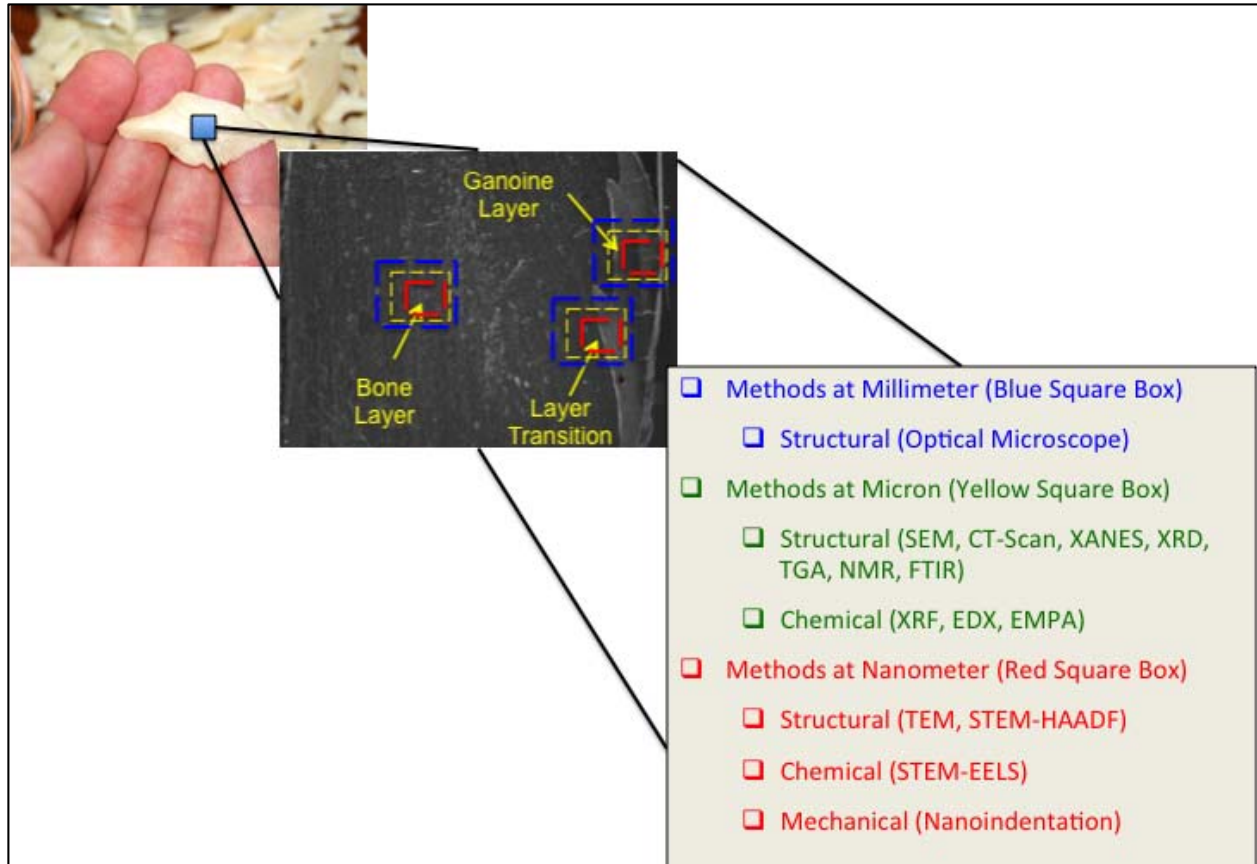
Figure 3.5 Locations probed and the experimental techniques
used to examine the fish scales hierarchy.

examined. The individual data sets will be analyzed first based on the discrete length scales and

then assembled. When combining the experiments, they can fill knowledge gaps that may not be

possible from individual experiments alone. In addition, some of the experiments provided

overlap and serve as confirmation for the others. The combined experiments used to characterize

each length scales will ultimately lead to the identification of mechanisms. The identification of

mechanisms will also lead to new discoveries that inherently describe the attribute that governs

the fish scale hierarchy mechanical response as a function of chemical composition and

structural arrangement.

After resolving the data relevance the experiments will be used to test the hypothesis *(H)*. If the hypothesis is true, then an appropriate DOE methodology has been established by this overall research effort. In addition to testing *(H)*, the research findings will be used to establish a suggested framework and requirements for incorporating bioinspired design. The attributes of alligator gar's biomineralized exoskeleton fish scales can be used to develop nature inspired advanced superior performing composite prototypes. Chapters 4 and 5 will present and discuss results to address questions developed from hypothesis *(H)*. Recommendations will also include pertinent concepts that have been identified because of this research effort. Also provided will be a recommended strategy for manufacturing and prototyping model systems.

CHAPTER 4: RESULTS

Presented in Chapter 4 are the experimental results that are used to discuss the questions developed from hypothesis *(H)*. The presentation of results begins with the largest length scale and continues until the lowest measurable length scale has been explained. After the individual results have been discussed, they will be assembled to determine what may be the attribute(s) that govern the fish scale hierarchy mechanical response as a function of chemical composition and structural arrangement.

Where possible, two weight classes for the alligator gar fish were examined. Since the exact ages of the fish could not readily be determined by the ERDC researchers, acquired scales are classified by fish weight. The first set of alligator gar fish scales were procured from one fish that fell in the weight range of [1 to 30 pounds]. The second set of alligator gar fish scales were procured from one fish that fell in the weight range of [31 to 70 pounds]. The scales used in this study were obtained from alligator small and medium fish that weighed 2.5 and 38 pounds, respectively. Both sets of scales were harvested from the middle region of the fish scale's body as illustrated in Figure 3.3. The purpose for examining two-distinct fish weight classes was to infer how the mechanical, structural, and chemical properties evolve as the fish grows.

4.1 Investigation of Length Scale [>1] mm

Unaided Eye Observations. The fish scales were first visually inspected using unaided eye observations. Shown in Figure 4.1 are whole small and medium unpolished biomineralized fish scales. From observation the scales have long and short axis. The scales' shape appears to have subtle curvature around its perimeter that converges at the vertices to form sharp points similar to arrowheads. The curved perimeter of the scales is thinner on the edge and overlap

67
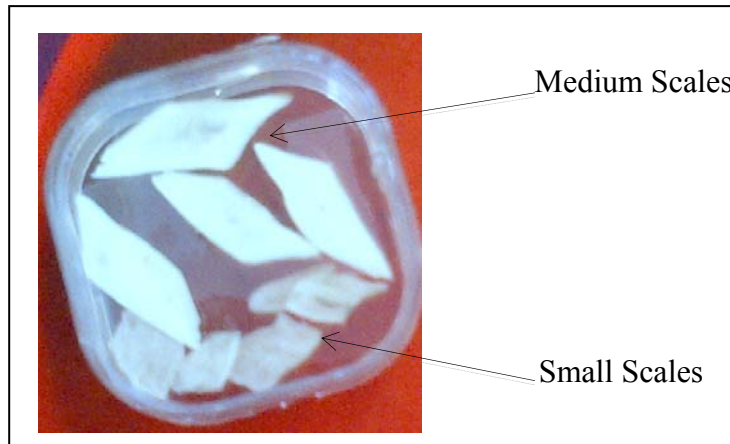
Figure 4.1 Whole biomineralized small and
medium alligator gar fish scales.

when connected to other scales with sharper fibers as previously described in Chapter 2 and

shown in Figure 2.6.

The small scale seems to grow more in the long axis direction. In addition, the small scale

looks and feels smooth on top while the bottom side of the scale seems to have a depression

containing pits on the surface, Figure 4.2. The bottom side of the scale is nearest the face that is

attached to the fish's body. As the small scale grows to the medium size, the top surface appears

and feels as if there is a crown forming or a subtle ledge near its center. Yet, the pitted area

remains present as the fish scale grows. The exact purpose and function of the depressed pitted

area is not known; however, the depressed region is somewhat concave. One possibility why

nature maintains the aspect ratio throughout the growth process for the concave geometry is the

scales can form fit the fish's body shape assisting with insulation and maneuverability through

water, similar to a deep-sea diver wearing a wet suit (Bartol, Gharib, Weihs, Webb, Hove, and

Gordon, 2003). The questions raised from unaided eye observations were (a) what are the fine

details of the surface textures when viewed at the next lower length scale, and (b) does the

surface texture percolate outward from the scales' internal structure.

68
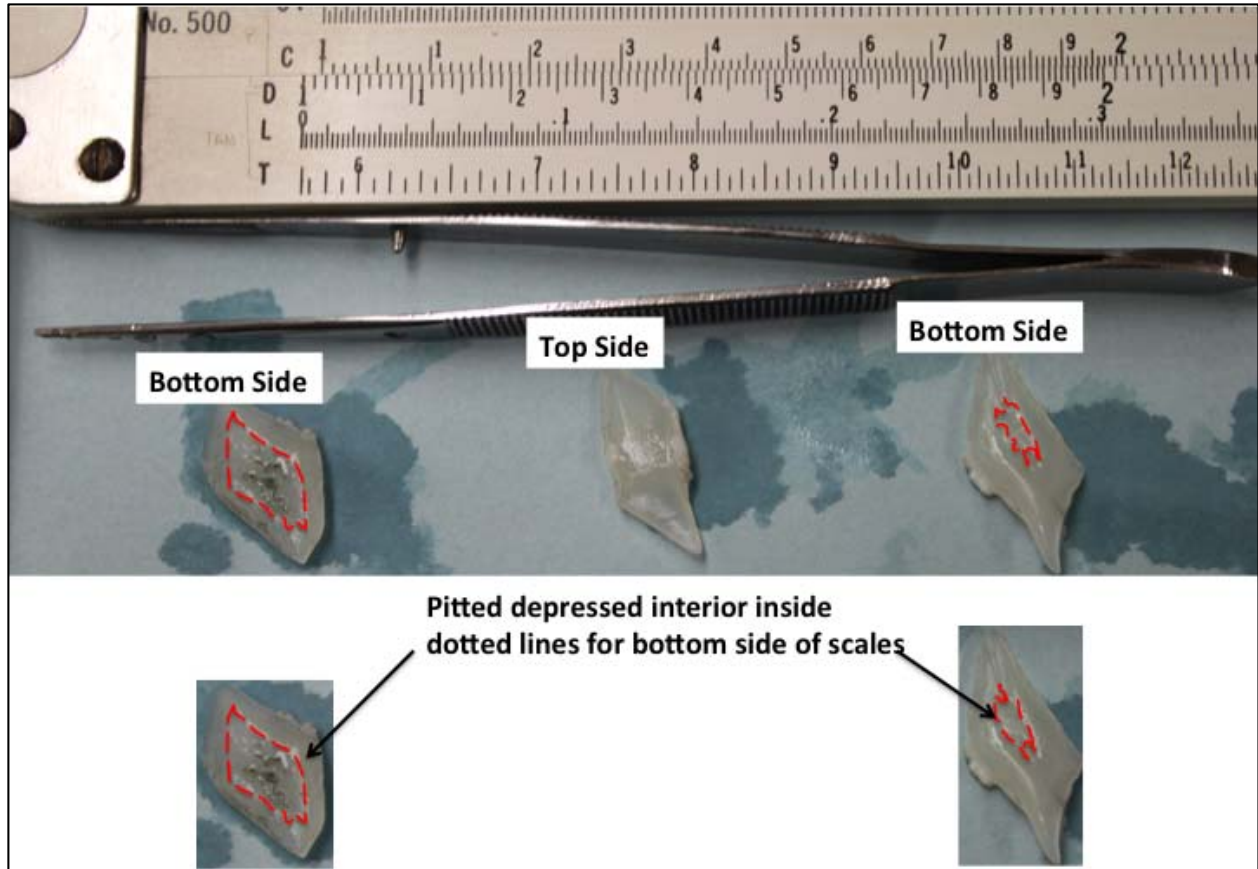
Figure 4.2 Medium size biomineralized fish scale with concave depression containing pits on the bottom side of the alligator gar scale.

4.2 Investigation of Length Scale [1-1000] μm

4.2.1 HR-SEM Observations

To investigate the questions (a) and (b) raised during the investigation of length scale [>1] mm, further observations were made at the [1-1000] μm length scale. Only the medium scale surface topology was investigated, using a JOEL™ HR-SEM, since the geometry and textures were more pronounced than the small scale when inspected by the naked eye in visible light. The HR-SEM images were able to show surface details at higher magnification. In Figure 4.3, the top of the medium alligator gar scale at one-millimeter magnification clearly shows a non-smooth and non-level surface. The specimen appears to have at least two distinct
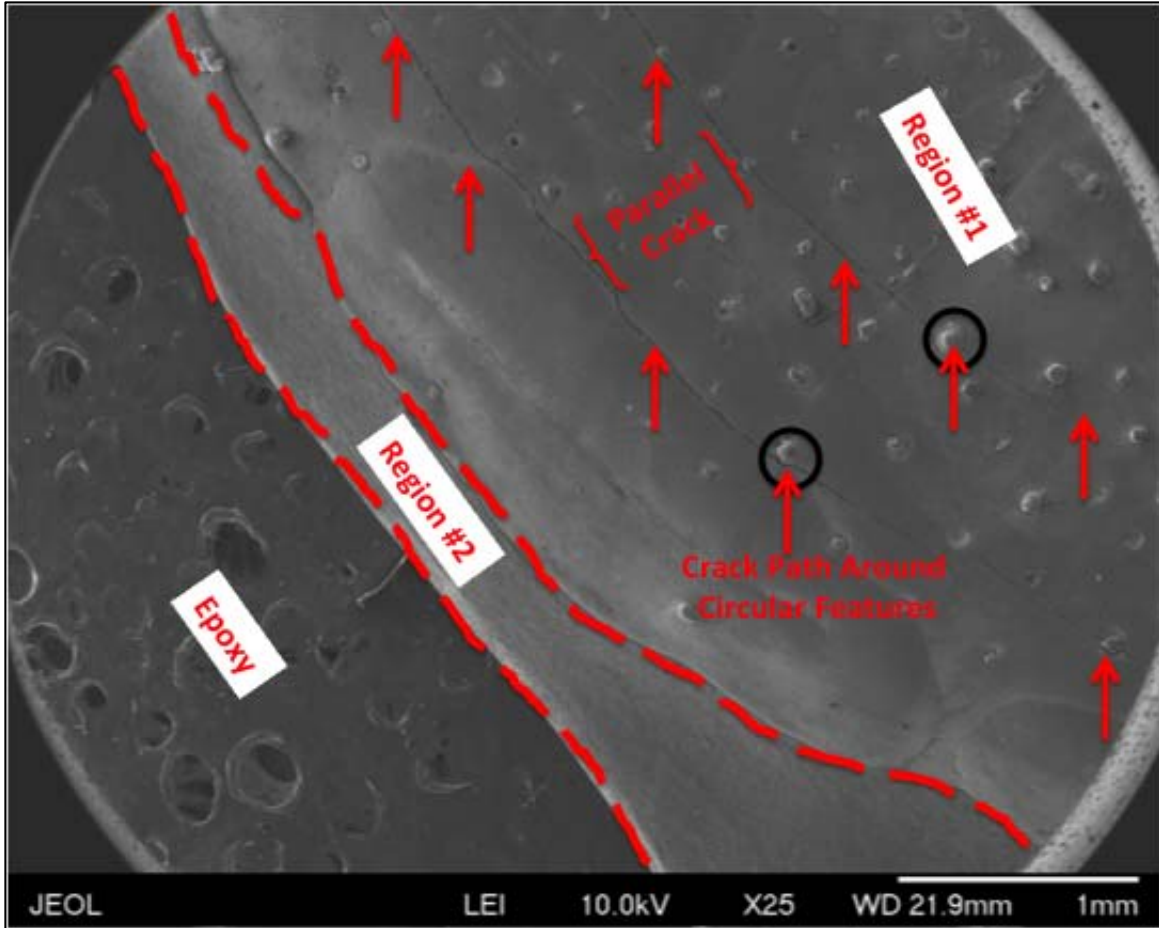
Figure 4.3 Top surface of medium size gar fish scale at one-millimeter magnification using HR-SEM backscatter mode.

texture regions, as highlighted by the dotted lines, along the surface. The backscattered gray-scale surface image indicates that at least two regions that have differing material densities. There is a smoother surface for Region 2 when compared to Region 1. However, the surface of Region 2 shows a gradual surface textural transition from Region 1 to Region 2.

Also observed in Region 1 are circular features that are uniform in size inside the black circles. On the outer edge of the circle features is a crack propagating linearly. Similarly, the specimen has two cracks running parallel near the edges of the circular feature in Region 1. The specimen has yet to be loaded or polished so the cracking may be due to shrinking caused by

drying. In addition, the cracks are consistently appearing near the edges of the circular

formations as if there is a zone of discontinuity for the material.

Region 2 has a smoother topology that is more or less defect free and sloping/

transitioning downward and away from Region 1. Unlike Region 1, the surfaces of Region 2 do

not show cracks. Further examination of the surface is needed to understand the details of

cracking occurring near the circular feature.

To further investigate the fine details of the circular feature, finer HR-SEM images were

taken at the higher magnifications of 100 microns in Figure 4.4 and 10 microns, shown in

Figures 4.5 and 4.6. Shown in Figure 4.4 is the top surface of medium size gar fish scale at

100-micron magnification. There are several features that are observed at the finer magnification.

For instance, when viewing the surface Regions 1 and 2 at their interface, barbs are propagating

out of the surface. The barbs are equally spaced and hook over toward the Region 1 direction.

Another important discovery illustrated in Figure 4.4 is the barbs are hollow.

At the 10-micron magnification the hollow barbs appear to be transport channels that are

self-contained and serve some unknown function, Figure 4.5. On the surface of the fish scale are

bumps/pores similar to the human skin which hair fibers grow from. Here the fibers may have

been used to attach the soft tissue to the surface. Furthermore, what appeared as circles at the

1-millimeter range there are actually remnants of the hollow barb's base. The researcher believes

these are only remnants left because during cleaning the scales' surface most of the barbs were

unknowingly scraped off.

In Figure 4.6, also at the 10-micron magnification, are surface damage sites for the areas

where the barbs were scraped off. Notice the barb channel area has become detached from the
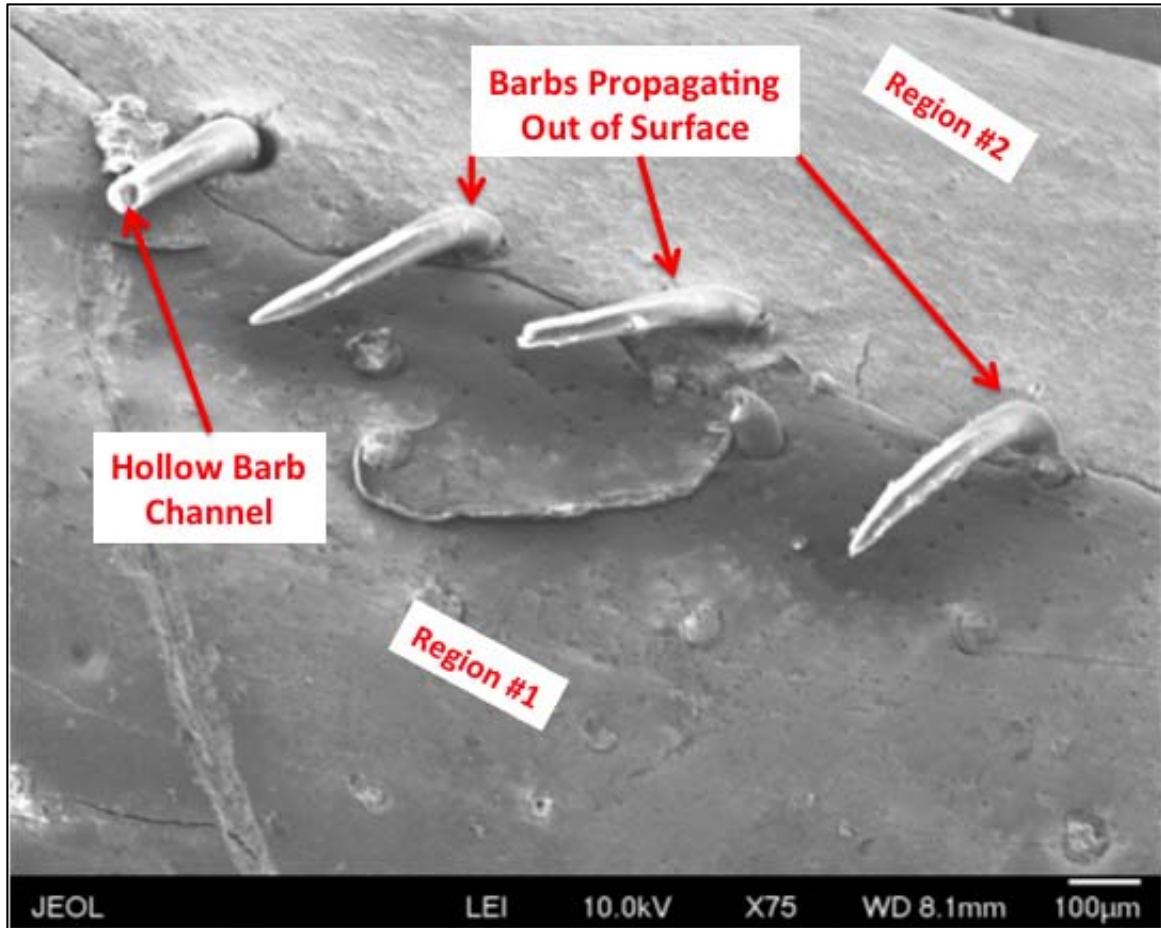
Figure 4.4 Top surface of medium size gar fish scale at 100-micron
magnification using HR-SEM backscatter mode.

surrounding materials. The surrounding area has cracked. Crack paths seem to follow along the

detached area and surface imperfections.

The unanswered question (b) raised during the investigation of length scale [>1] mm of

whether the surface texture percolates outward from the scales internal structure is still unknown

and cannot be answered from surface observations alone. The additional questions now raised

during the investigation of length scale [0.001-1] mm are: (c) Do the layers exist through the

thickness of the fish scale? (d) Do the hollow barbs observed at the surface extend through the

entire thickness of the fish scales' internal structure?
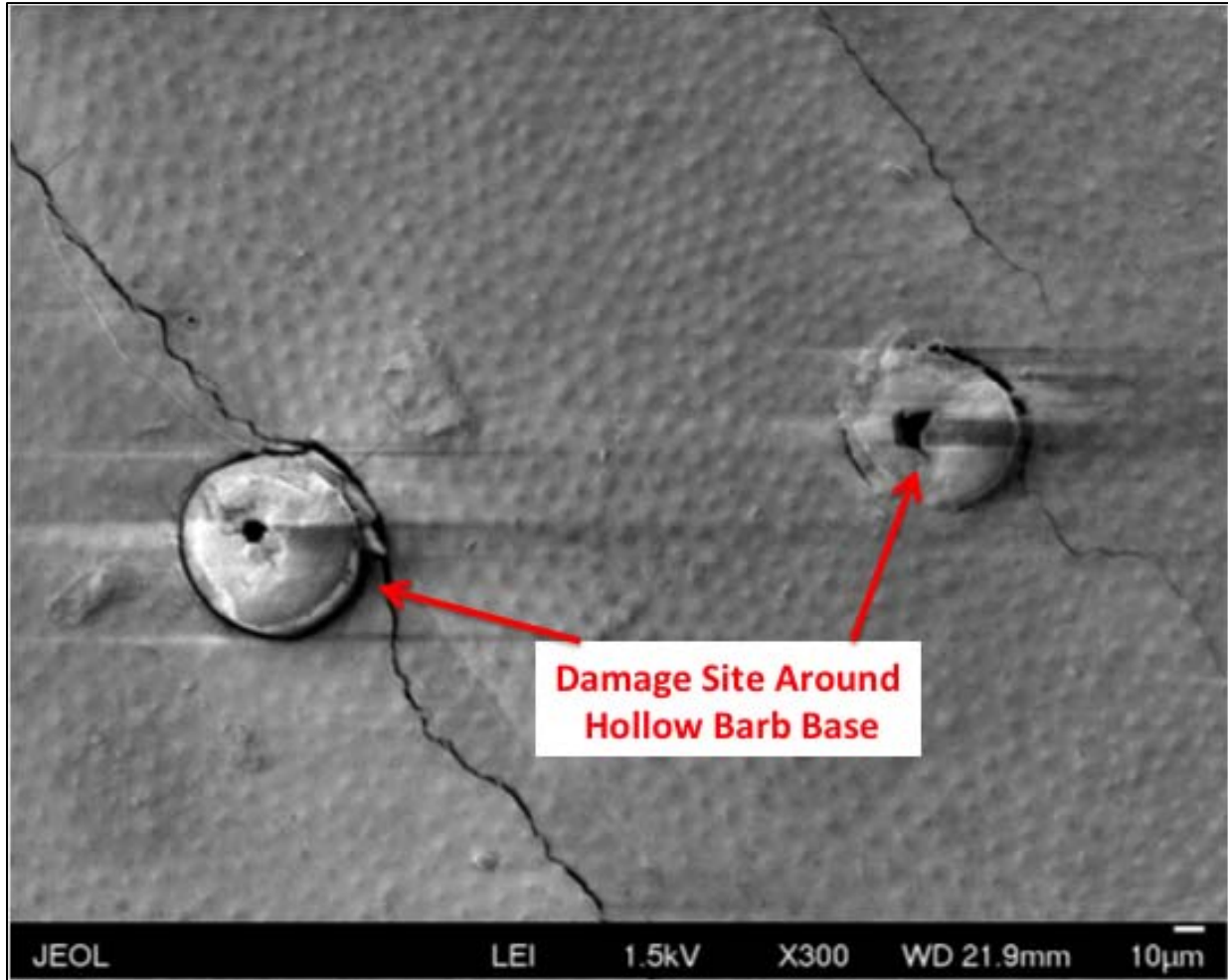
Figure 4.5. Top surface of medium size gar fish scale at 10-micron
magnification showing damage site around hollow barb base
using HR-SEM backscatter mode.

To be able to determine if the internal structure contributes to the surface layering,

texturing, and cracking, both fractured and polished cross sections surface were imaged using

HR-SEM. The fish scale specimen was fractured by using two-sets of needle nose pliers to apply

sufficient manual force to break the specimen. The direction of the applied force was selected

based on previous literature that showed hardness decreased with depth along with collagen fiber

content increased with depth across the short axis (Allison, et al. 2013). Therefore, to better

capture images that contain fibers that may be pulled out during fracture, the concave external
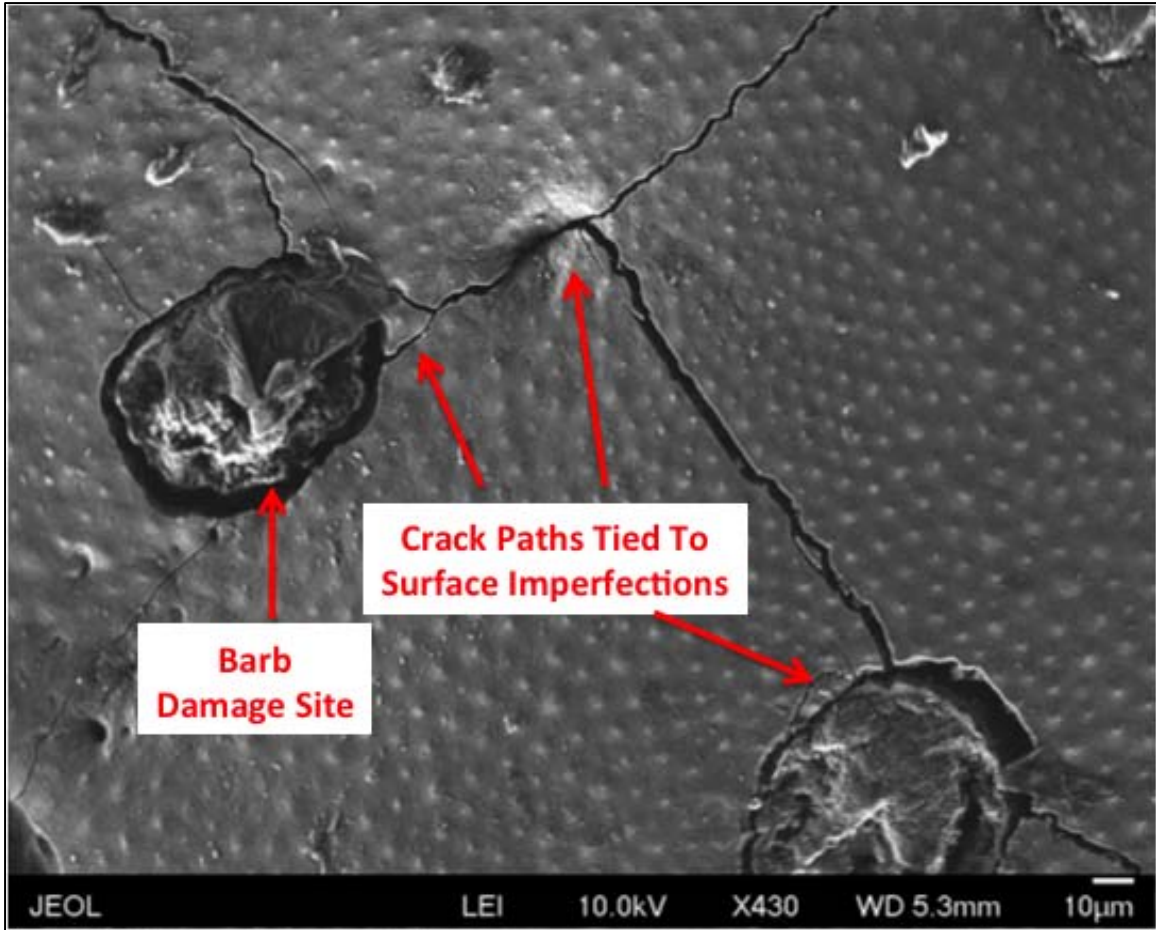
Figure 4.6 Top surface of medium size gar fish scale at 10-micron
magnification showing crack paths tied to surface imperfections
using HR-SEM backscatter mode.

forces were applied upward (weakest direction) using the needle nose pliers as shown in

Figure 4.7.

After breaking the fish scale, the fracture surface images were taken. Figure 4.8 shows

the overall facture surface at one-millimeter in the HR-SEM. There are two distinct layers

identified by backscattered gray-scale in the cross section. The answer to question (c), formed by

the hypothesis is yes, layers do exist. Likewise, the layers are present through the thickness of

the fish scale. Additionally, Layer 1 is a lighter gray than the darker gray shown in Layer 2. The

lighter gray image is an indication Layer 1 has a higher material density than Layer 2. Similarly
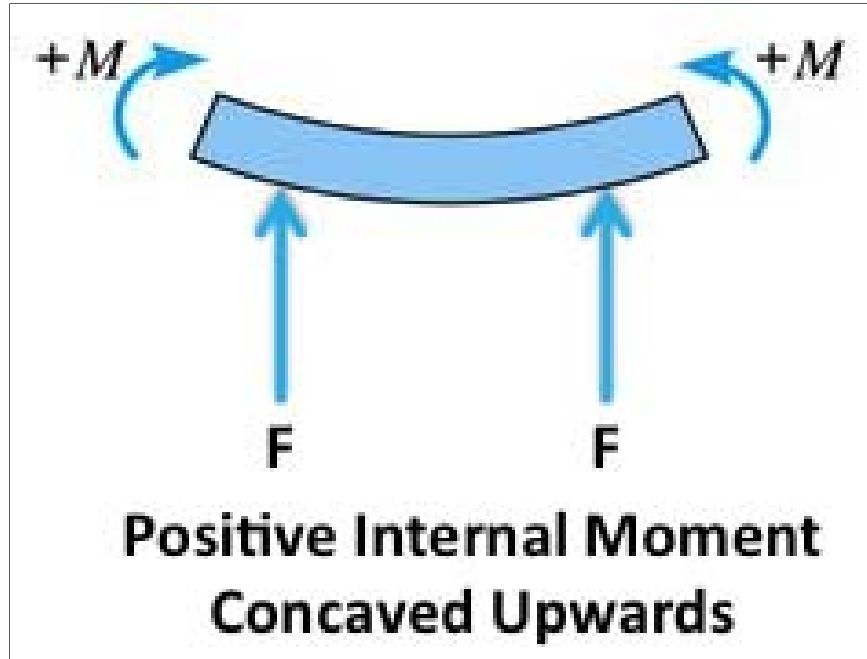
Figure 4.7 Schematic of applied force and
direction used to fracture fish
scale specimen.
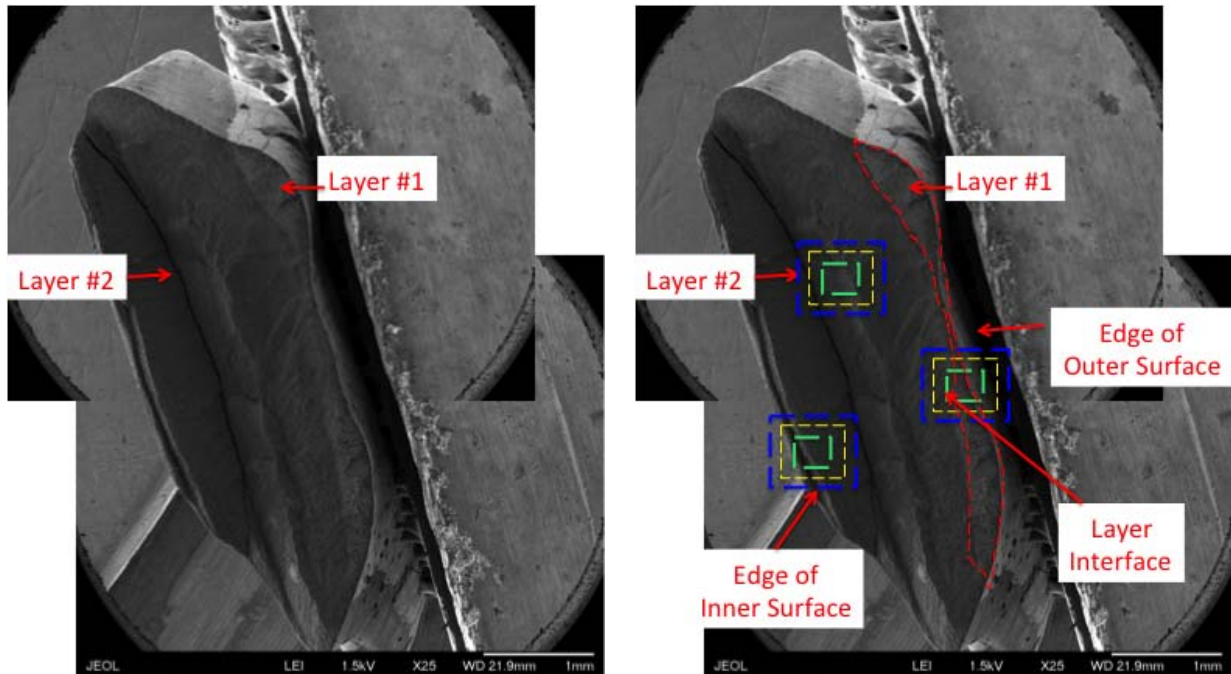
Figure 4.8 Overall facture surface at one-millimeter magnification
using HR-SEM backscatter mode.

the gray scale fracture surface appears to correspond to the gray scale surface images seen in Figure 4.3. Also, in Figure 4.8, the backscattered image shows Layer 2 is much thicker than Layer 1. Layer 2's fracture surface starts at the edge of the inner surface and stops at the dotted red line. Layer 1 is the shown to be inside the red dotted line and does not have a uniform thickness. Within Layer 1, the layer is thinnest near the center of the outer surface and progressively becomes thicker at the edges of the outer surface.

Next, the inner layer fracture surfaces were investigated for Layer 1, Layer Interface (ITZ), and Layer 2 at finer magnifications. The blue, yellow, and green dotted boxes, in Figure 4.8, identify investigated sites. The blue, yellow, and green dotted boxes represent 100-, 10-, and 1-micron magnification levels, respectively.

At 100-micron magnification, Figure 4.9 enhances the linear cracking found in the ITZ. The linear (parent) crack path, outlined by the yellow dashed line, in the ITZ seems to be continuous along the interface of Layers 1 and 2. Since there does not appear to be branch (child) cracking emanating from the linear (parent) crack, then cracking does not seem to be related to mechanically interface shearing. Instead the parent crack is likely occurring due to environmental dehydration, leading to debonding of the layers. Debonding is an indication of a change in structural arrangement and/or chemical composition.

When observing the fractured cross-sectioned barb damage site at a 50-micron magnification, displayed in Figure 4.10, for the surface damaged areas in Figure 4.6 and Figure 4.9 at one millimeter and 100-microns, respectively, the higher fidelity image provides no evidence the barb is embedded or does a hollow region exist directly below the surface of Layer 1. Nor do cracks seem to penetrate far below the surface. Also shown by the fracture surface for Layer 1 side of interface is a texture that appears to be dense/compact with very few

76
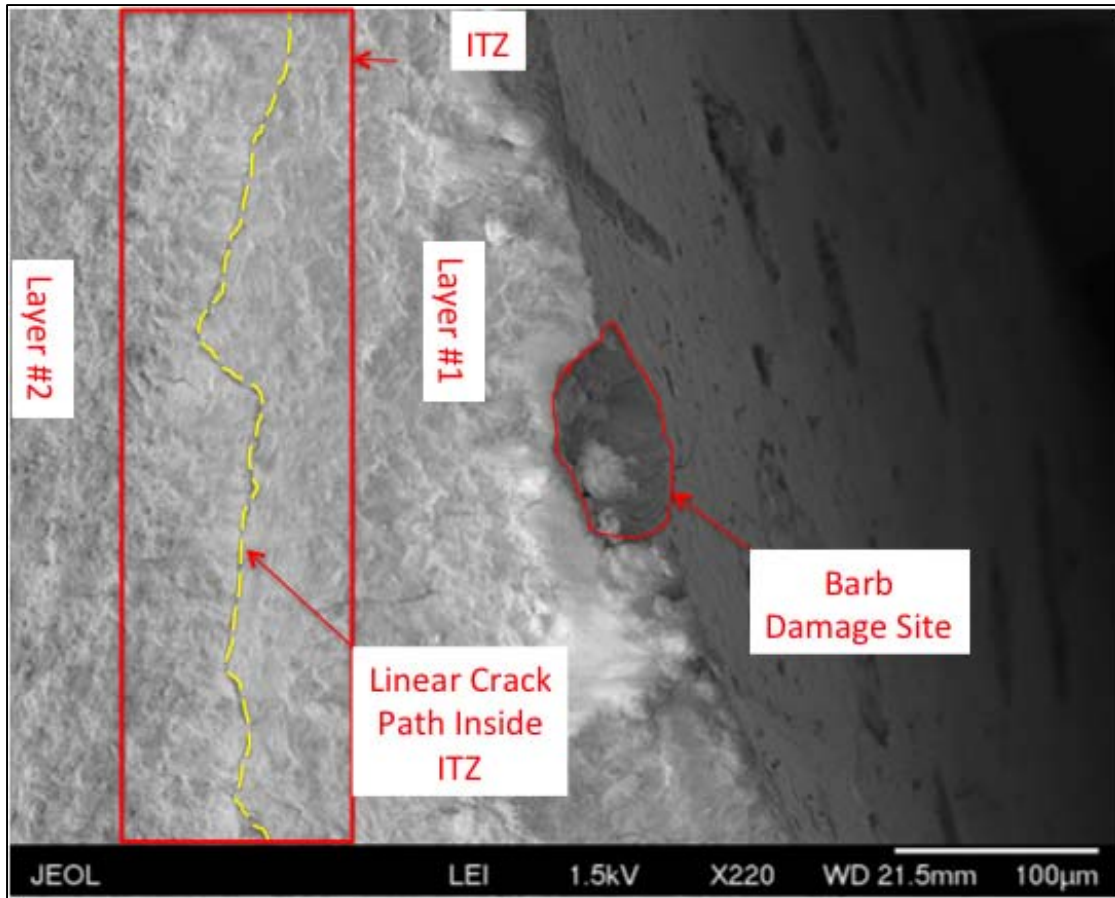
Figure 4.9 Cross-section for fracture surface at a 100-micron magnification using HR-SEM backscatter mode.

pores. At 10-microns, Figure 4.11, the fracture surface for Layer 1 side of interface illustrates a

roughened, unleveled surface texture. At the even more refined 1-micron magnification,

Figure 4.12 displays the fracture pattern, lineated by the red-dotted arrows, for the roughened

topology.

Immediately adjacent to the ITZ is Layer 2, Figure 4.13, illustrating the fracture surface

that does not appear to be densely compact as found in Layer 1. The pore volume increased when

approaching the innermost edge of the fish scale. In addition, the surface contains several

identifiable pore structures that are visible at the 100-micron magnification. The image shows

there are several pore sites having a varying distribution of sizes. Additionally, some of the pore
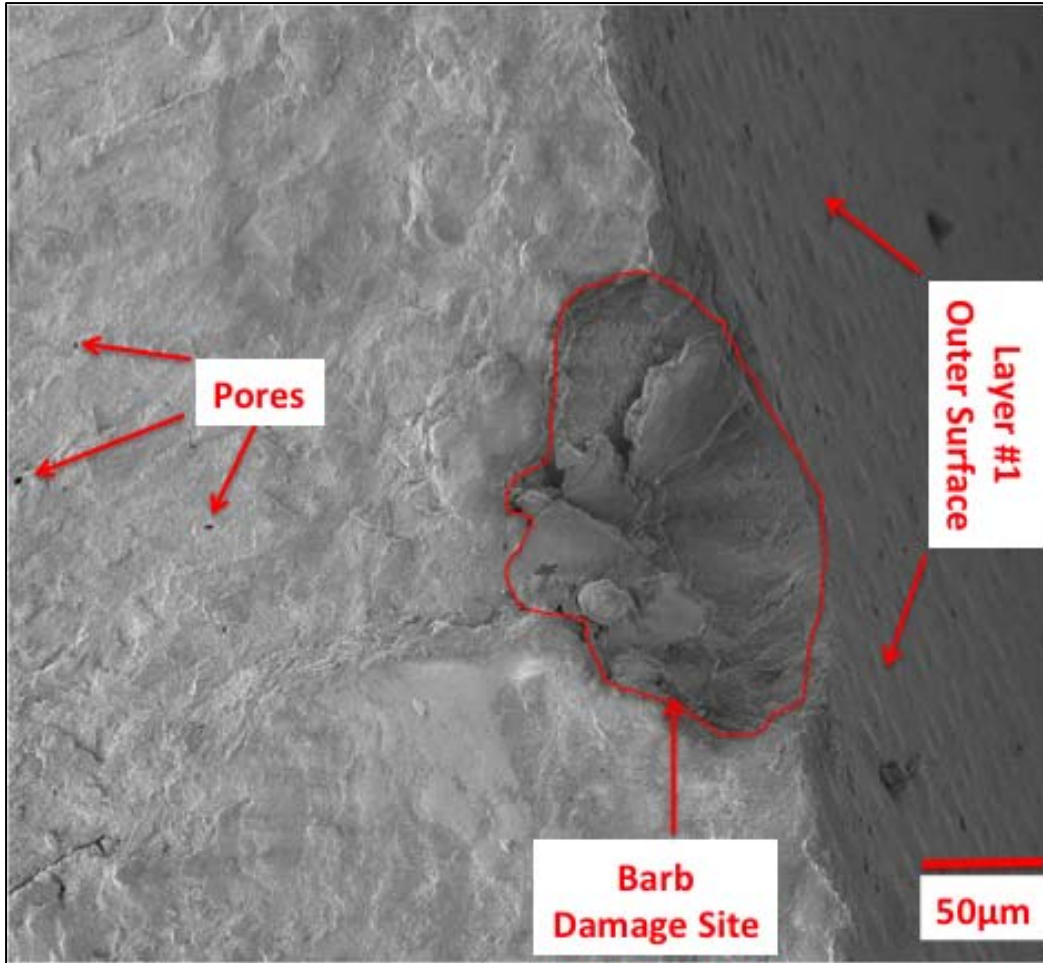
Figure 4.10 Cross-section of the barb damage site at a 50-micron magnification using HR-SEM backscatter mode for Layer 1.

sites seem to be connected. Also shown was that connected pore sites can form pore channel structures. Upon further investigation, at the 1-micron range, the pore channel was found to have a fibrous interior, Figure 4.14.

The innermost edge of the fish scale was next examined. Shown in Figure 4.14, is a vastly different structural arrangement than what was observed in Layer 1 and the ITZ. At 10-micron magnification the image shows a loosely compacted surface, Figure 4.15. Furthermore, the pullout of fibers shows they were previously embedded in the loosely compacted solid phase prior to fracturing the surface. At the finer 1-micron magnification,

78
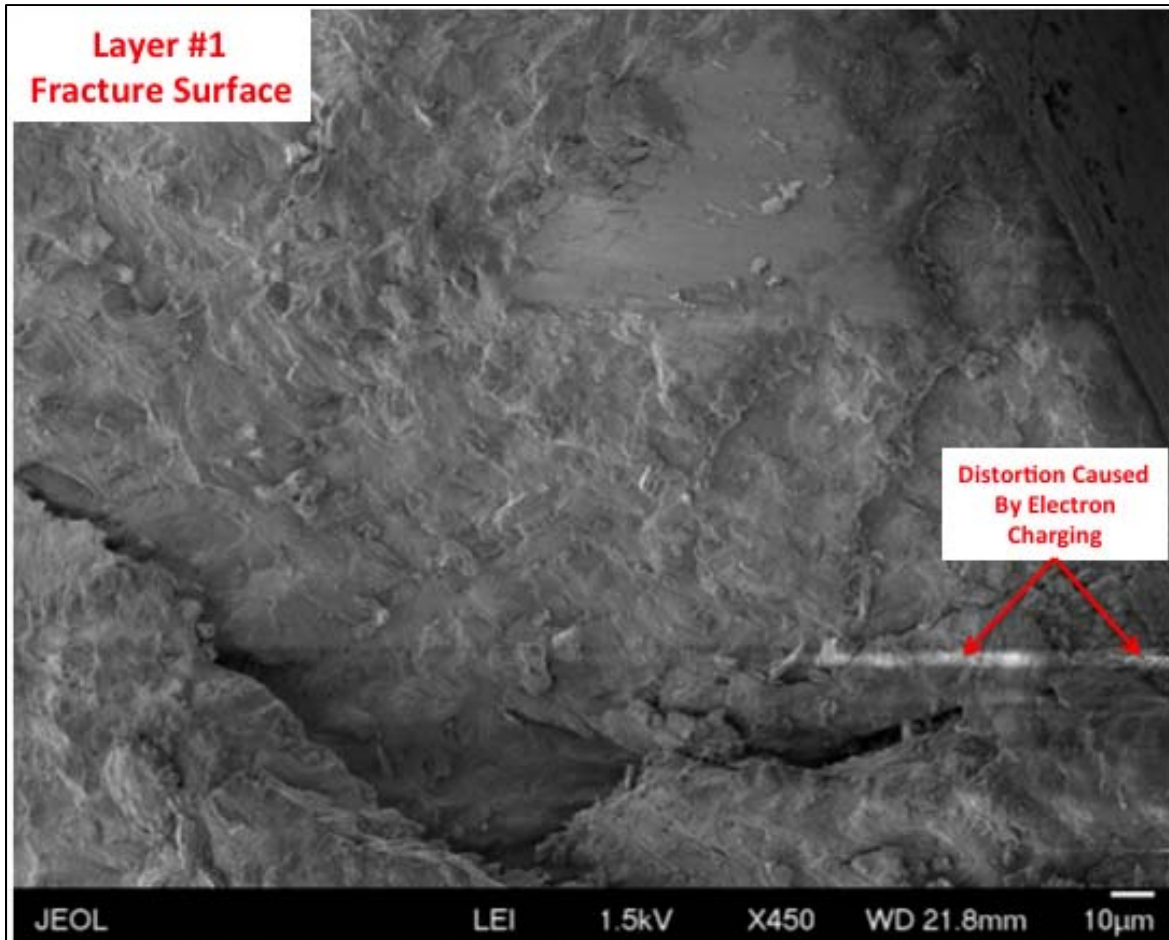
Figure 4.11 Cross-section for roughened fracture surface at a 10-micron
magnification using HR-SEM backscatter mode for Layer 1.

Figure 4.16, elucidate the hierarchical fibrous structure. Collections of individual fibrils are

woven to form individual fiber strands. The individual fiber strands become entwined to form

fibrous bundles. By observation, the solid fractions appear to be individual minerals that are

much smaller than individual fibers.

So far the research has presented and discussed the structure for the fish scales' fracture

surface. Next, HR-SEM will be used to elucidate the structural details for both the small and

medium polished cross sections. There are distinct differences and similarities for the two fish

scale sizes, shown in Figure 4.17, at 200-micron magnification.
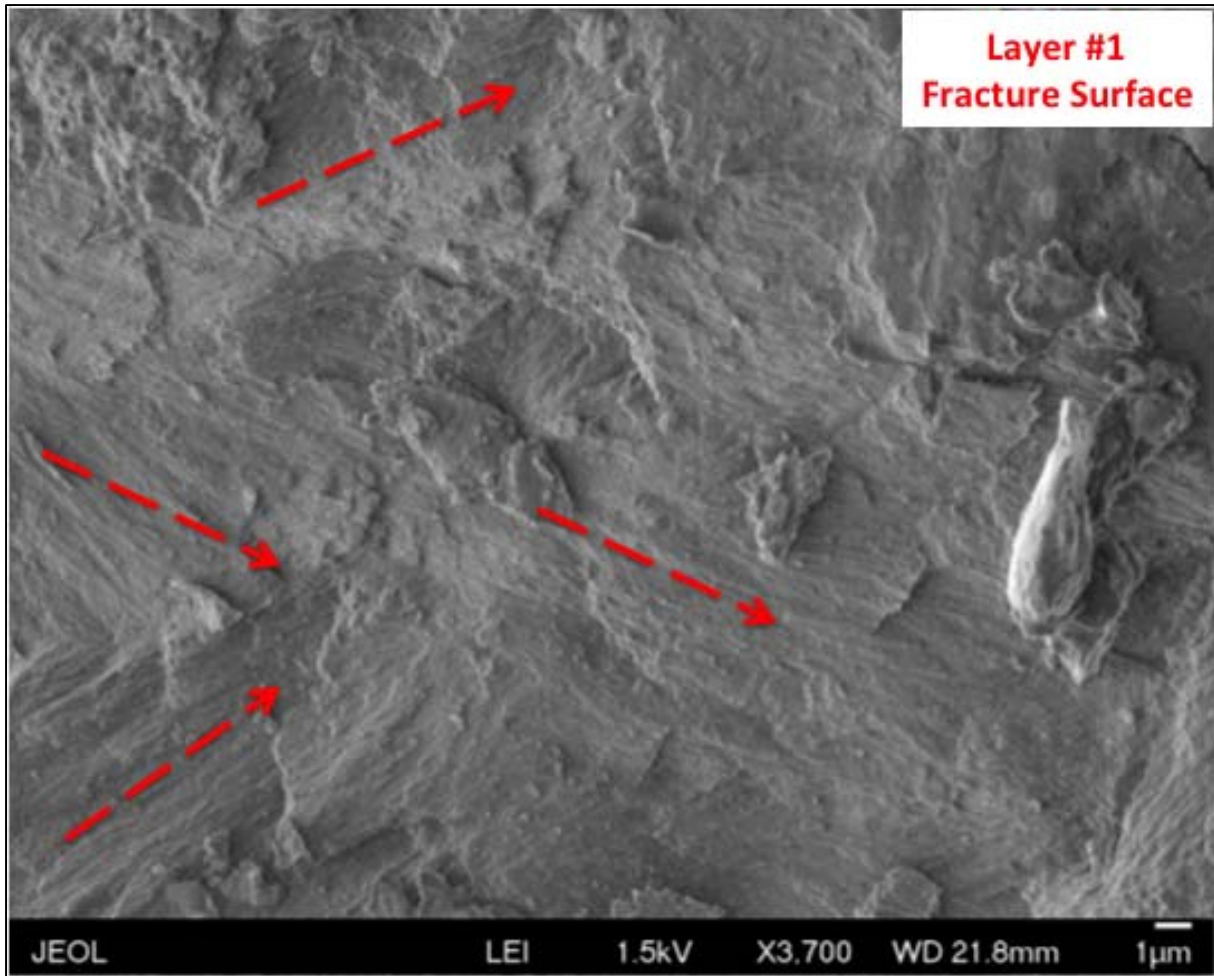
Figure 4.12 Cross-section showing surface, delineated by red-dotted arrows, at 1-micron magnification using HR-SEM backscatter mode for Layer 1's roughened fracture surface.

There are few differences in the small and medium scales. However as the fish grow, the scale seems to be prone to more defects/damage. The HR-SEM image for the medium scale shows cavities (also known as tubules or canals), outlined by the red dotted circles, and is present near the center of the scale. Also observed was outermost dense-layer fractured and flaking occurred. Further analysis will be the discussed later in Chapter 4 that helps determine if the differences in the two scales are caused by a change in chemical, structural, and/or mechanical properties.
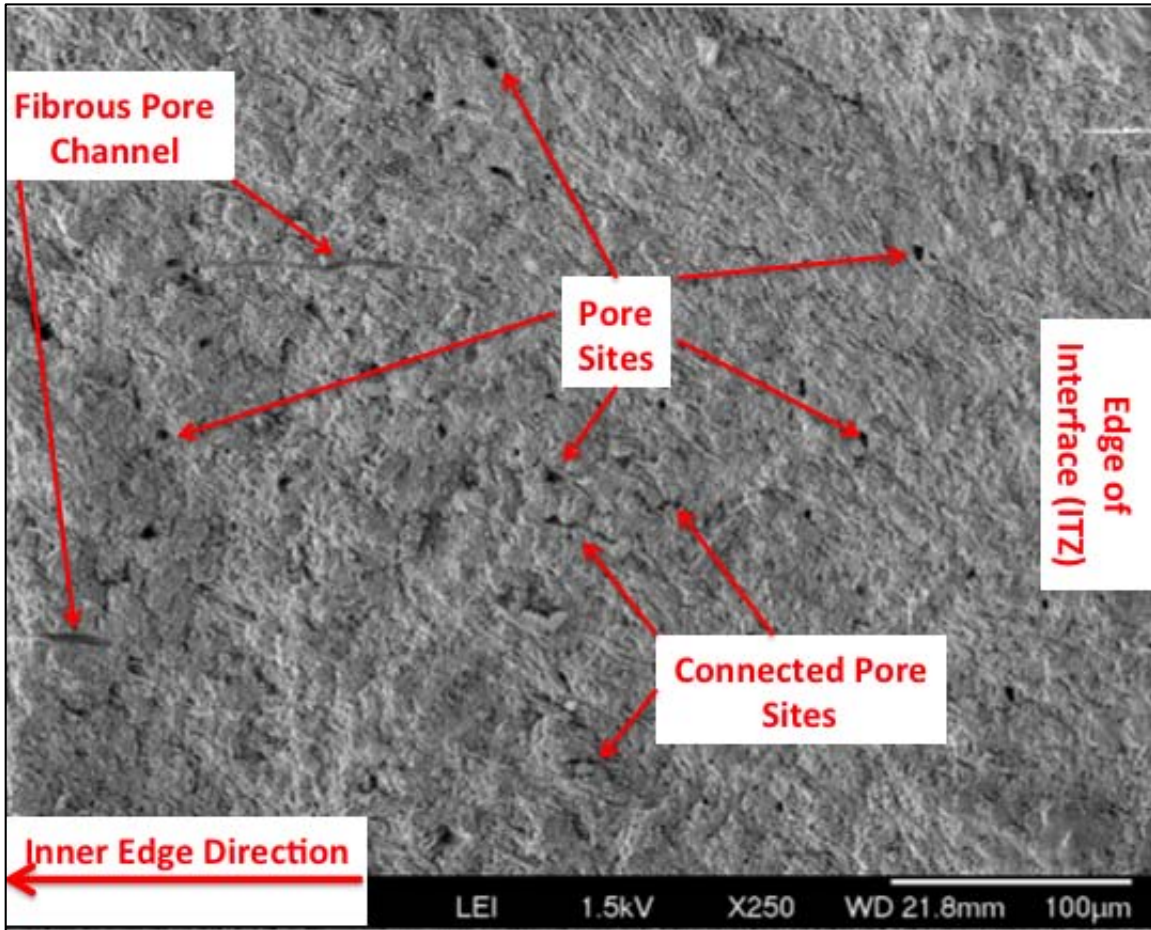
Figure 4.13 Cross-section of fracture surface immediately adjacent to ITZ, using HR-SEM backscatter mode, at 100-micron magnification.

The fish both have dense exterior layer thickness, which appear to grow proportionally with the underlying layer. The outer layer does not extend to the edge of the scale. Furthermore, the layer is thicker at the edge and gradually becomes thinner toward the center of the layer. At the center of the dense layer there is a noticeable depression. The exterior layer appears to provide little to no coverage for the underlying layer at the depression zone. The dense layer is connected to the underlying layer by what seems to be a saw tooth geometrical interlocking interface. In addition, the interface seems to be mainly bonded by mechanical means, rather than chemically, because of saw tooth geometries, Figure 4.17. Since saw tooth geometries are used to
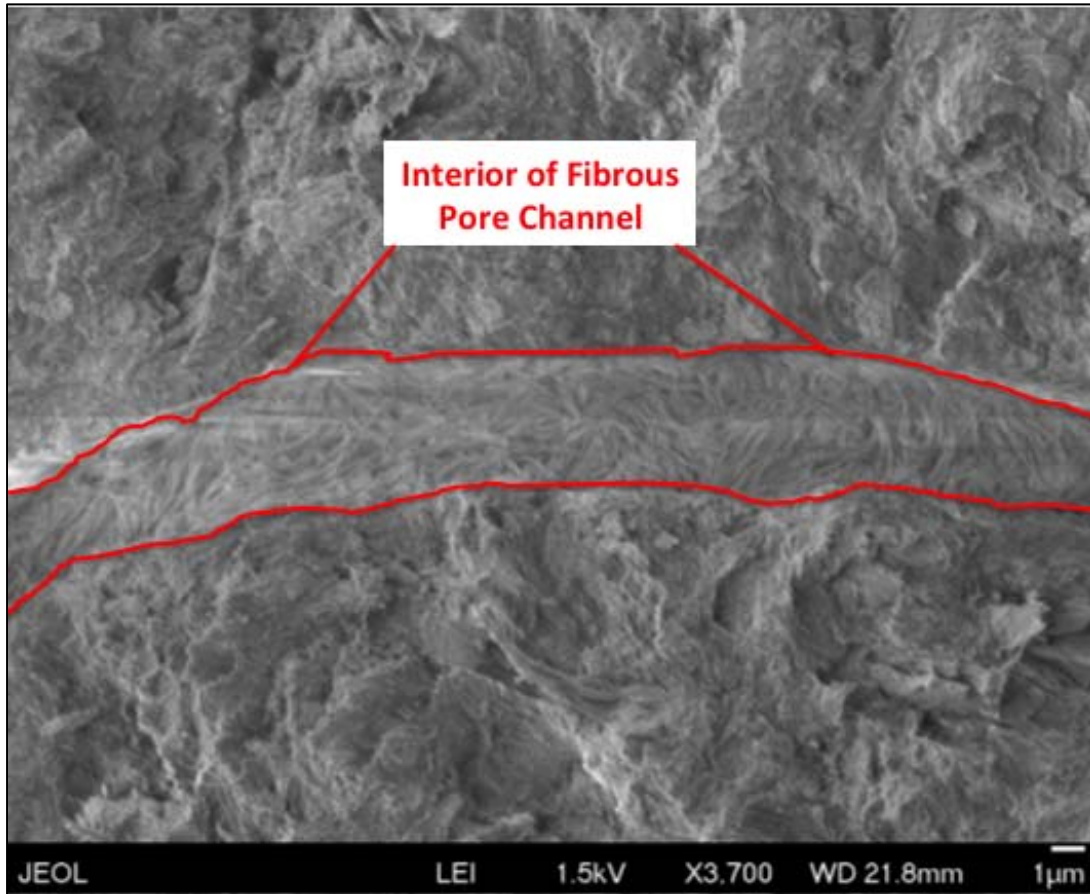
Figure 4.14 Cross-section of fracture surface showing a fibrous interior for the pore channel, using HR-SEM backscatter mode, at 1-micron magnification.

secure the layers' interfaces, the layers are not discreetly bonded like layers in engineered laminates. Within the saw tooth regions the material overlaps and is embedded at various depths within each layer to form periodic "repeating" bonded connections. The saw tooth connections perhaps provide enhanced shear resistance at the interface when the full hydration state is maintained and helps inhibit debonding. Evidence for mechanically bonding is shown in the medium fish scale. At the interface for the medium fish scale there is some indication shrinkage cracking has occurred. More than likely, shrinkage cracking was caused by sample preparation. The image for the medium fish scale shows the two layers have separated, however, they maintain the saw tooth shape at the junction sites.
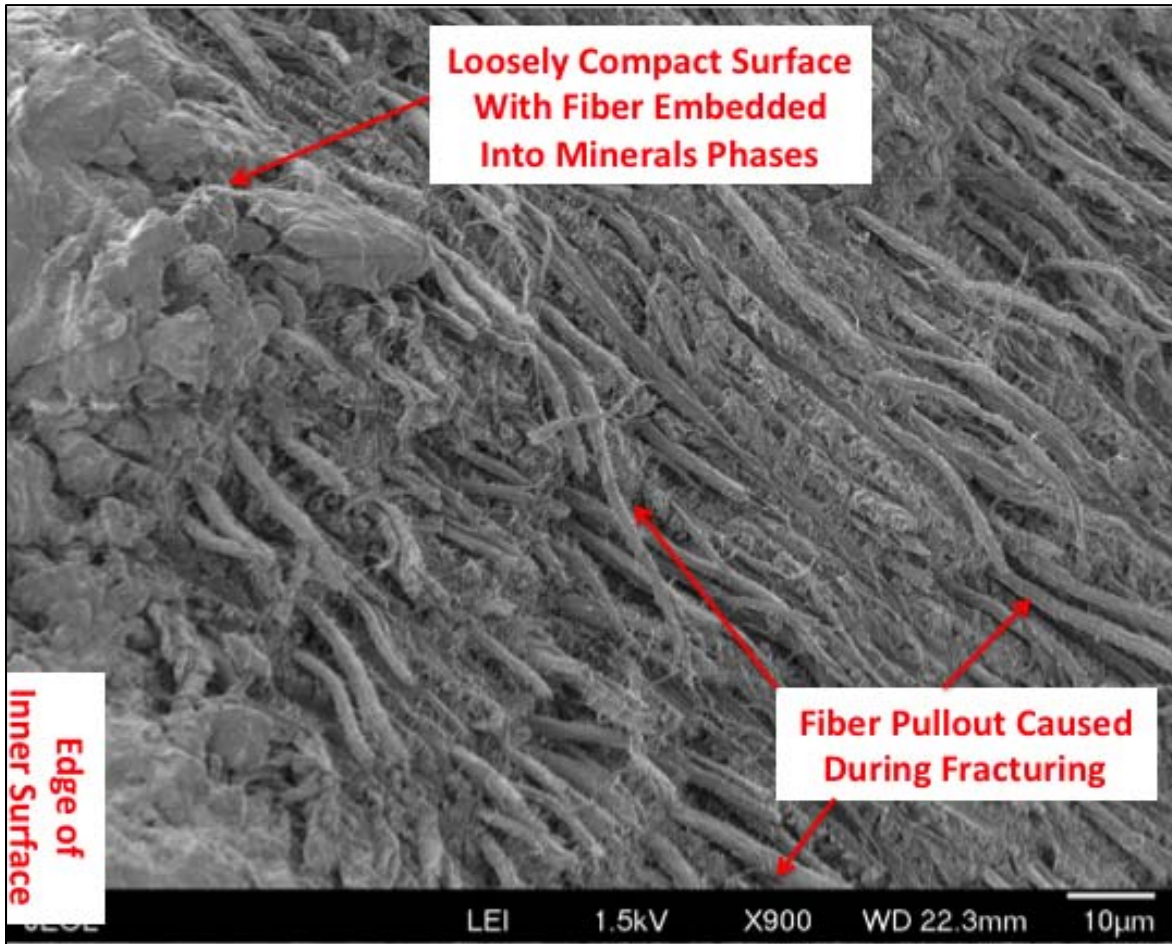
Figure 4.15 Cross-section of inner fracture surface elucidating mineral-fiber
structure, using HR-SEM backscatter mode, at 10-micron magnification.

As illustrated in Figure 4.18, for the small and medium scales, the enhanced image

highlights linear cracks occur through the short axis for dense layer. The lateral spacing between

the cracks seems to be directly proportional to the change in thickness. In the images as the layer

thickens the lateral spacing between cracks widens.

Figure 4.17, also shows repeating contrasting gray-scale concentric rings occurring

throughout the scale. The highlighted layers, in Figure 4.19, show contrasting rings tend to

follow the contours of the scale. Upon zooming into the denser outer layer, Figure 4.20, the

image shows an increase in contrast. Each sub-layer has a bright bottom and darker top. Each
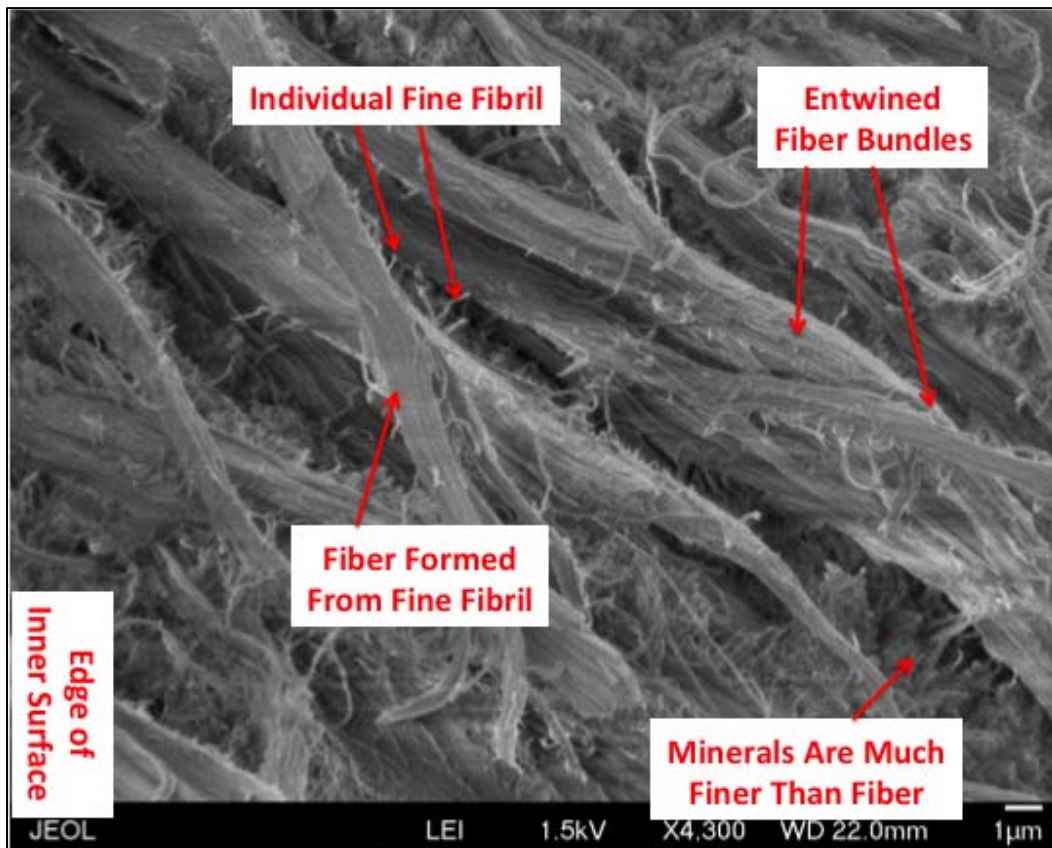
Figure 4.16 Cross-section of inner fracture surface elucidating mineral-fiber structure, using HR-SEM backscatter mode, at 1-micron magnification.
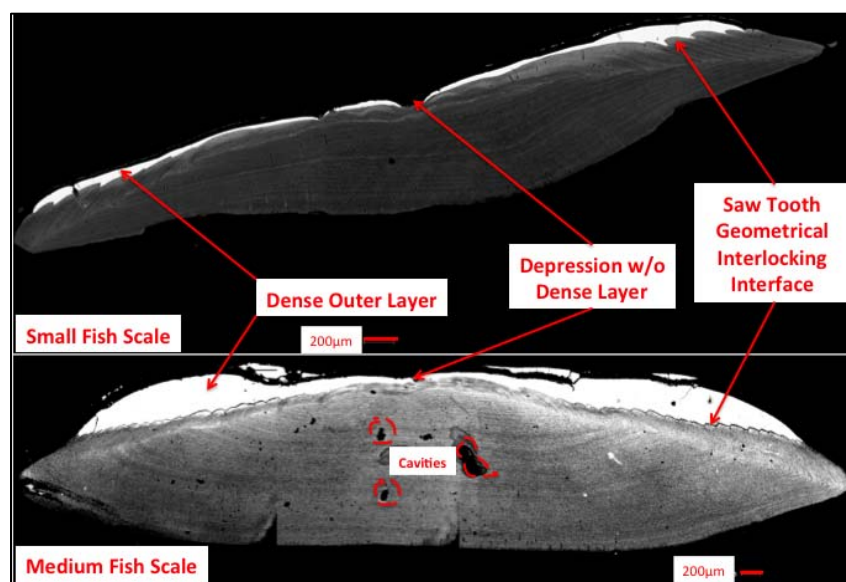
Figure 4.17 Cross-section for small and medium polished fish scale surfaces at a 200-micron magnification using HR-SEM backscatter mode.
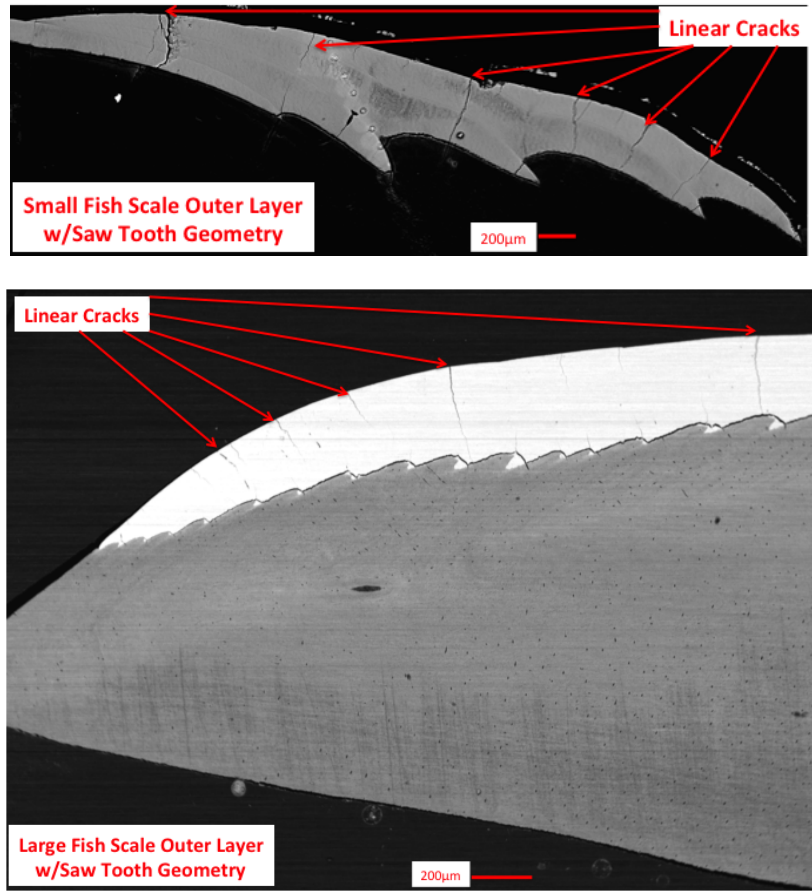
Figure 4.18 Enhanced HR-SEM backscatter image at 200-micron magnification, for small and medium scales, highlighting linear cracks occurring through the short axis for dense layer.
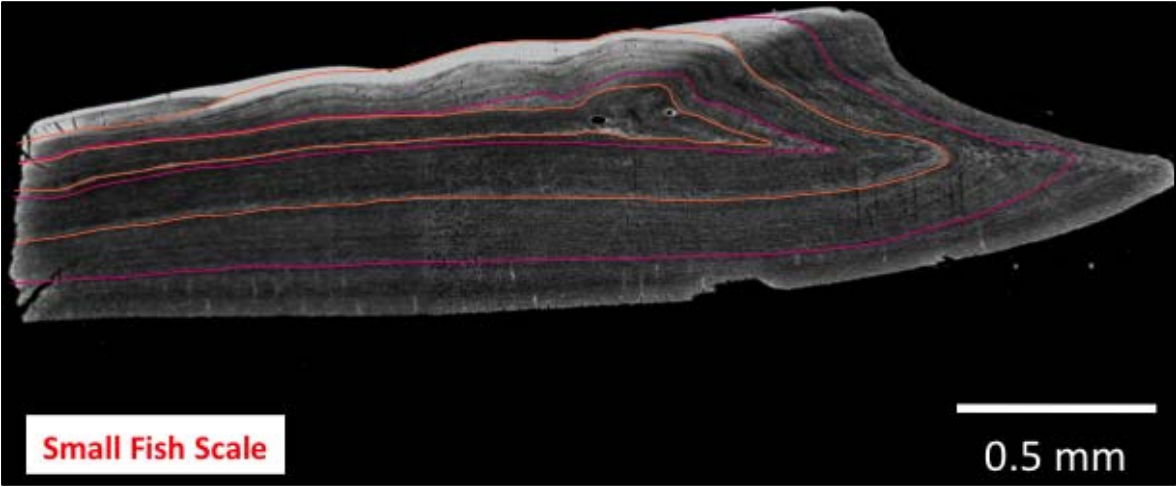
Figure 4.19 Enhanced HR-SEM backscatter image at 500-microns magnification, for small fish, highlighting the gray-scale concentric rings occurring throughout scales layers.
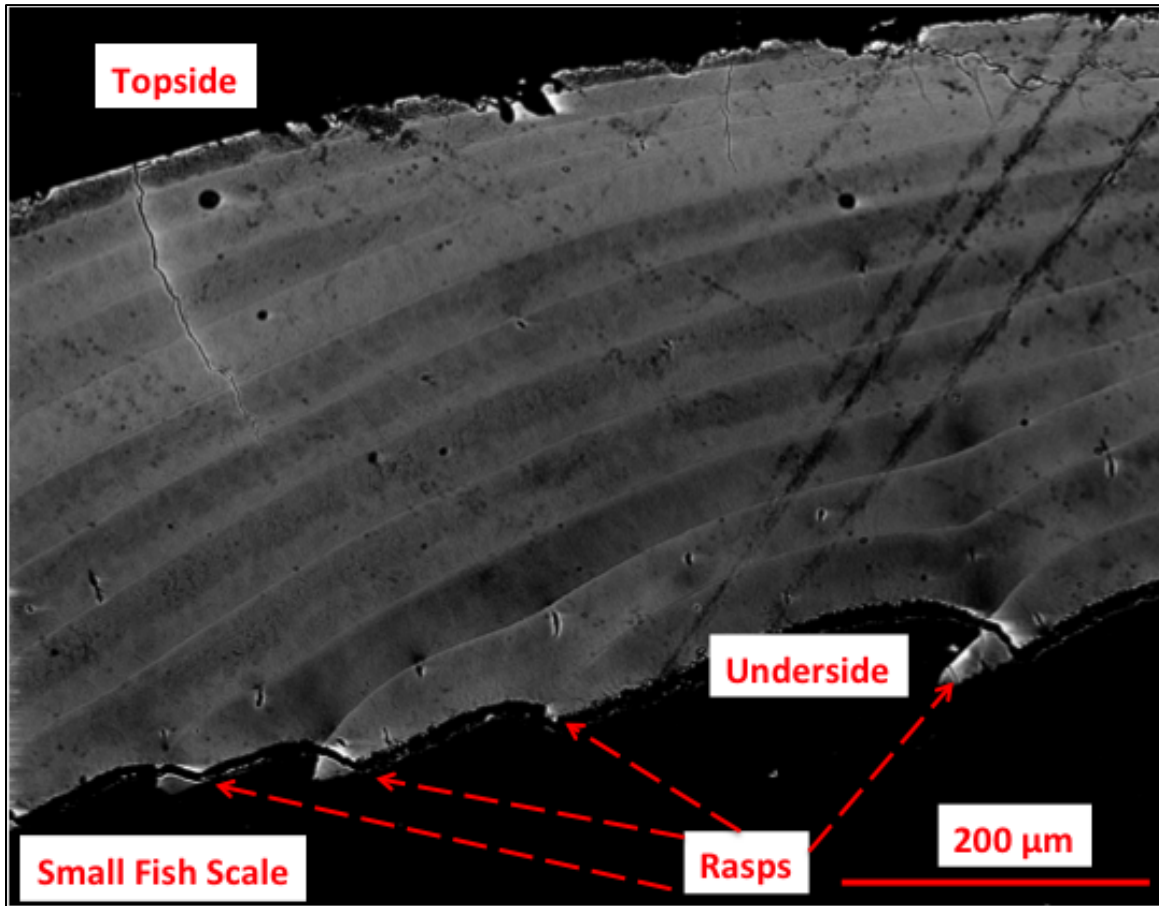
Figure 4.20 Enhanced HR-SEM backscatter image at 200-micron magnification, for small fish, highlighting the gray-scale sub-layers occurring within the denser outer layer.

sub-layer grades from a dense underside to a less dense upper layer. Each sub-layer ends in a rasp shape.

The contrast in the image indicates there is high likelihood that density is changing within the layers. The contrasts revealed by HR-SEM enhanced backscatter image for the medium fish scale, shown in Figure 4.21, indicates within the ITZ (yellow dashed lines) at the center top of scale is the oldest. Both layers become less dense (younger) further away from top center.

The significance of gray scale contrasting provides more evidence the density likely changes with age. The change in density and the repeating contours provides an indication the scale's composition and structure may be evolving with growth. To obtain greater knowledge of
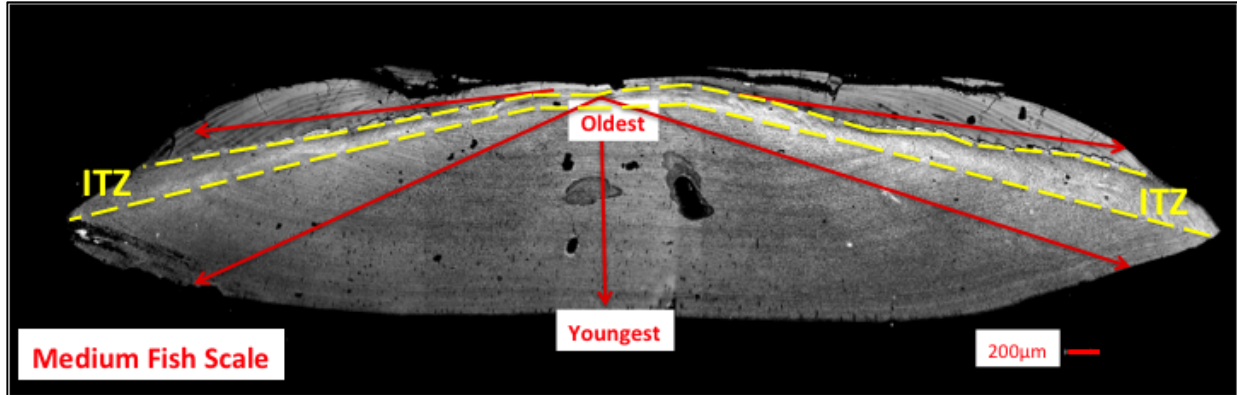
Figure 4.21 Enhanced HR-SEM backscatter gray-scale image, at 200-microns, highlighting the growth initiation and direction for the medium fish scale layers.

how the scales are evolving during growth further optical microscopy, μm-XCT, structural, and chemical analysis was conducted at the micron level.

The questions that arose with no definitive answers: (e) Why does the lateral spacing between cracks widen as the layer becomes thicker (No Answer)? (f) Also what may be the reason for linear cracking occurring within the layer of what appears to be like materials (Stress Release Due To Drying)? Both of these questions are addressed in the next sections.

4.2.2 Optical Microscopy Observation

A Carl-Zeiss Imager Z1m ™ optical light microscope was used to measure average layer thickness for the small and medium size scales. Shown in Figure 4.22, is the average thickness in the small fish scale for Layer 1 and Layer 2, which are 44.87 and 287.59 microns, respectively. Additionally in Figure 4.23, is the average thickness in the medium fish scale for Layer 1 and Layer 2, which are 1575.40 and 11804.40 microns, respectively. The nominal ratio for *Layer 1 Thickness-to-Total Scale Thickness* for the small and medium fish scales are13.3 and 15.6 percent, respectively. The ratio was used to show how the individual layers for the fish scale tend to grow. As the fish scale grows, the ratio indicates the layer thicknesses remain constant.
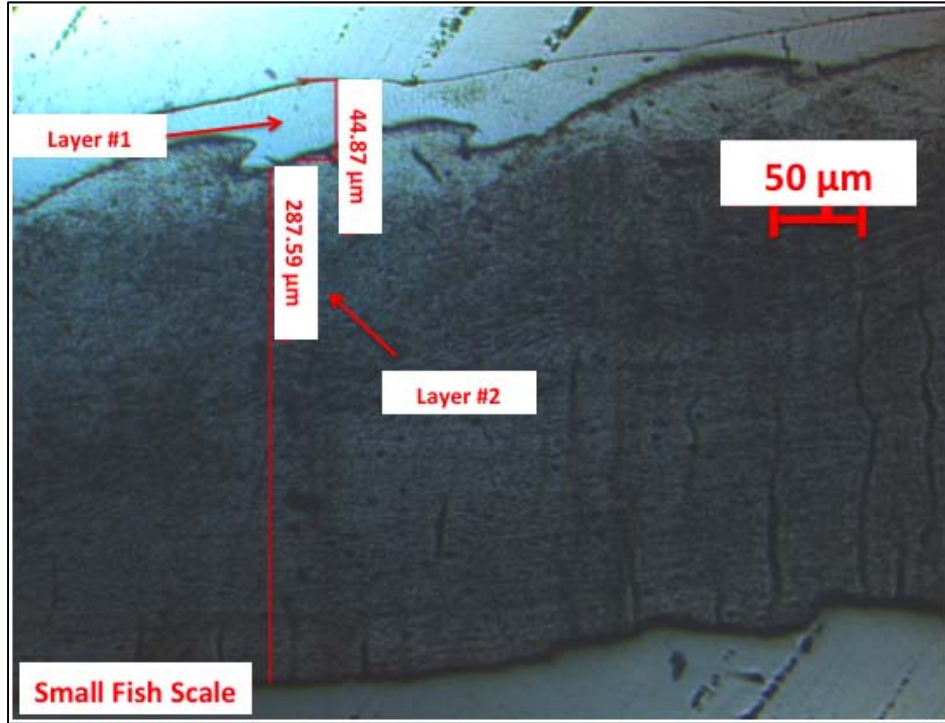
Figure 4.22. Optical microscopy image showing the average layer thickness for small fish scale.
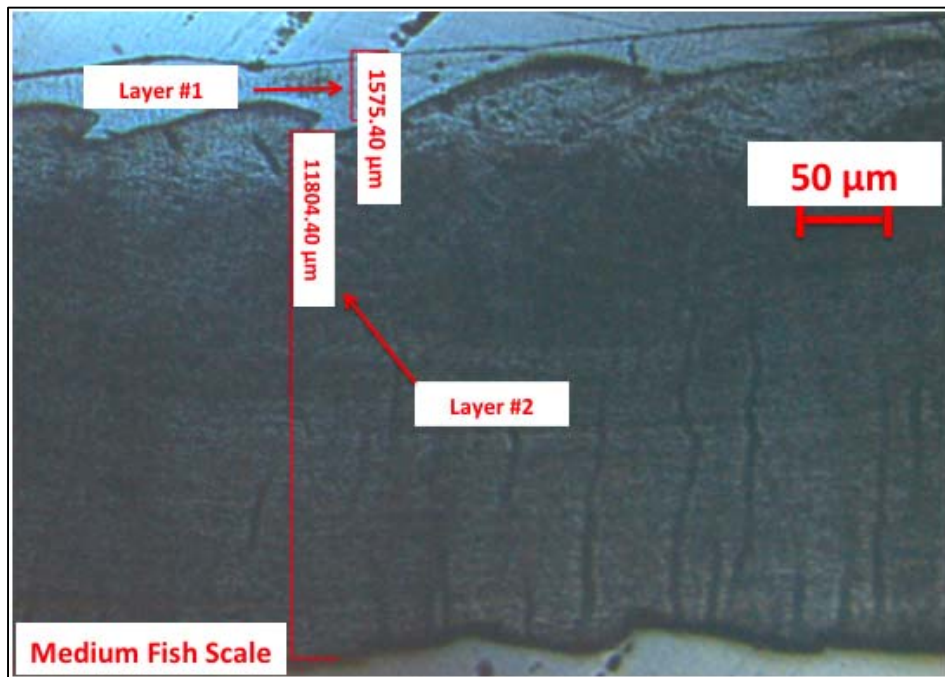
Figure 4.23 Optical microscopy image showing the average layer thickness for medium fish scale.

4.2.3 μm-XCT Observations

Displayed in Figure 4.24 is the μm-XCT image for a medium-size fish scale. The

reconstructed three-dimensional image volume for the whole intact scale provides
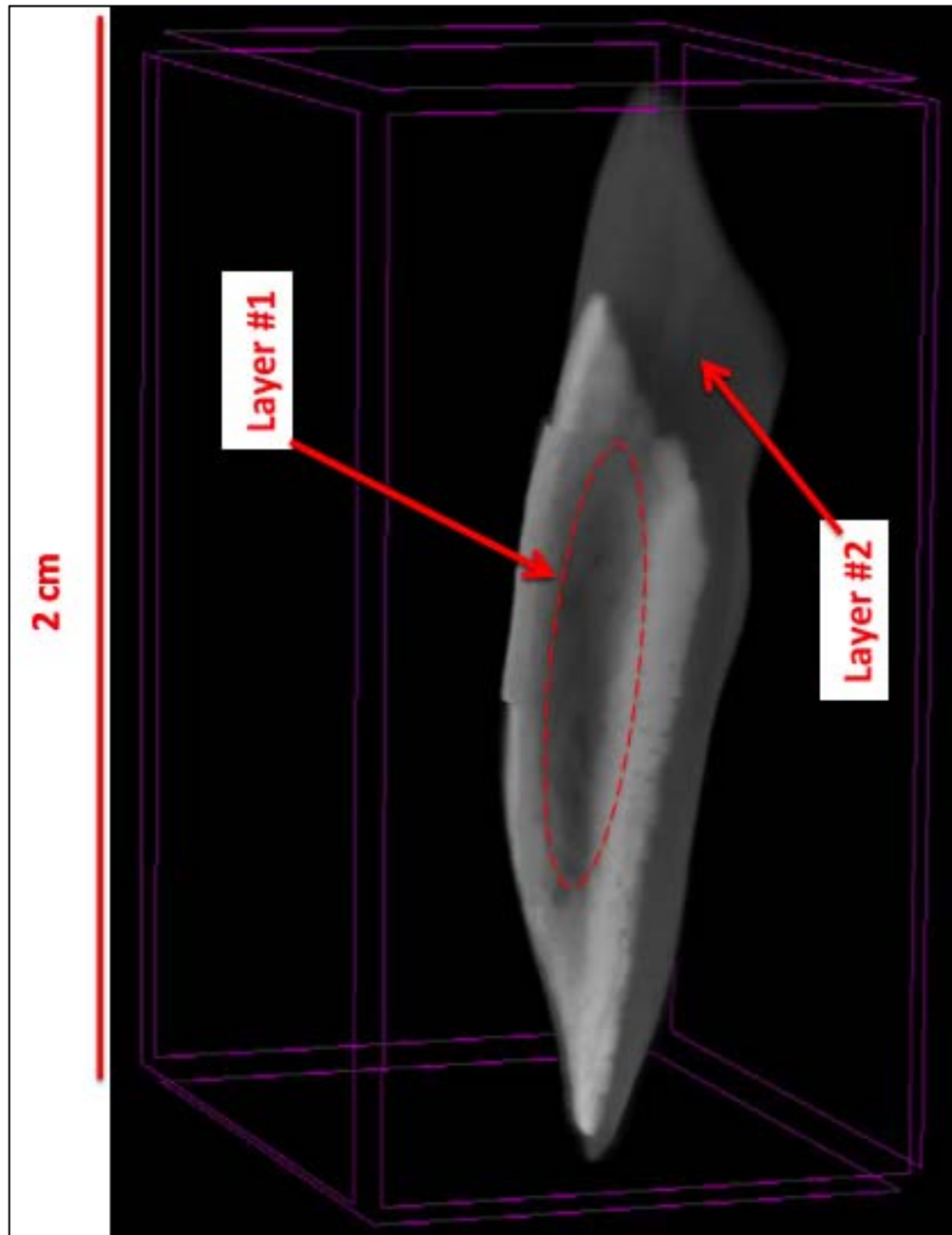
Figure 4.24 Reconstructed 3-D volume μm-XCT
image for a medium-size whole intact fish scale.

verification there exists a dense outer Layer 1 which does not fully cover the underlying Layer 2. Inside the dotted red line shows the scale does not have a uniform thickness indicated by concave sloping surface occurring toward the center.

The reconstructed three-dimensional scale was digitally sliced at the bottom of Layer 1 near the interface, Figure 4.25, to show ridges that were formed. The ridges are analogues to the grooves seen in Tupperware™ storage container lids. The grooves point in opposite directions going down and outward, indicated by the red dotted arrows, from the scales' center. The sawtooth rasps observed in HR-SEM and optical microscope cross-section images, for Figures 4.17, 4.22, and 4.23, are formed from the ridges. The μm-XCT image also confirms the interface uses geometry to form a mechanical bond when anchoring Layer 1 to the underlying Layer 2. At the center of the scale, indicated by the blue interior, is the hollow area. The hollow
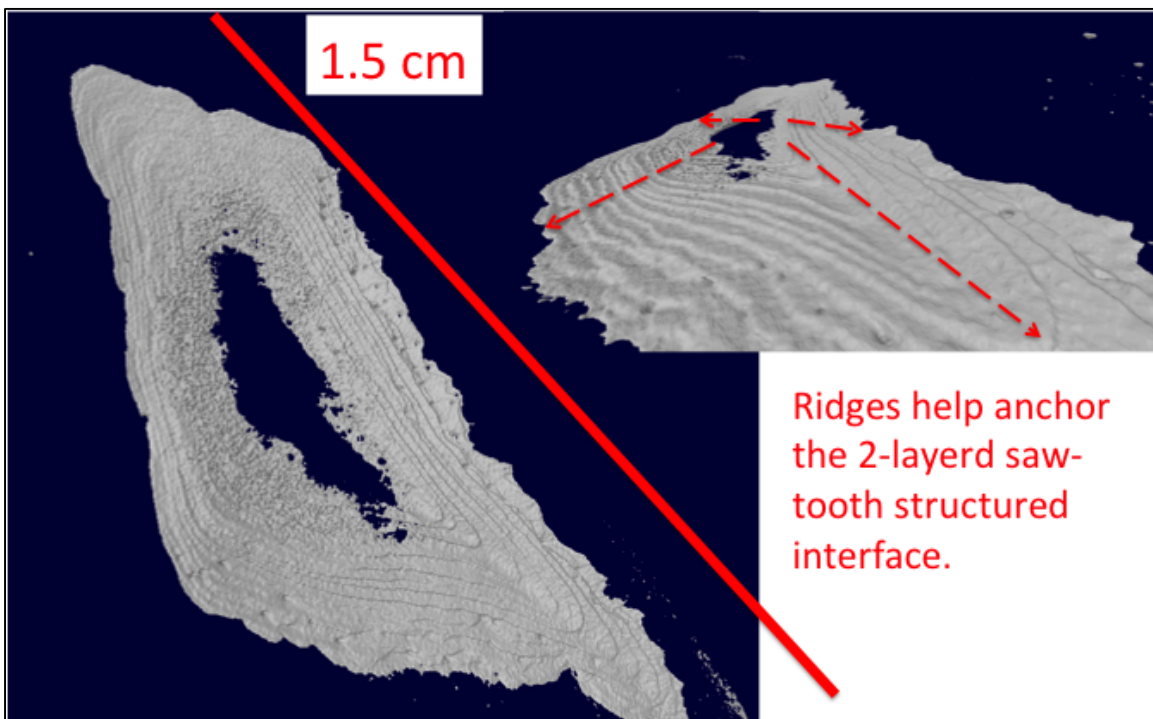
Figure 4.25 Reconstructed fish scale image from 3-D μm-XCT volume at the bottom of Layer 1 near the interface, where ridges are formed.

area corresponds to the pitted area previously discussed for Figure 4.2 and the non-uniform thickness seen in the μm-XCT image for Figure 4.25. Still uncertain is reason for cracking, crack spacing, and how the ridges form. Perhaps the ridges represent growth rings as individual sub-layers, which were previously discussed in HR-SEM cross-section image, Figure 4.19.

So far the results have discussed how the structural layers are assembled geometrically at micron level. The remaining sections will discuss the use of analytical techniques for identifying the chemical composition and elemental distribution that are measured at the [1-1000] μm length scale. The information was used to determine what are components that make up the fish scale's structure.

4.2.4 Synchrotron X-ray Analysis (μm-XRF- CT/μm-XANES/μm-XRD)

Synchrotron μm-XRF-CT, μm-XRD, and μm-XANES microprobe analysis was conducted to determine the elemental distribution and provide speciation information for heterogeneous solid fish scale. The analysis was performed at beamline X26A, X27A, and X2B at the National Synchrotron Light Source at Brookhaven National Laboratory in Upton, NY. At the time of this research beamline X27A was the only synchrotron x-ray energy source in the USA calibrated uniquely for the x-ray properties of calcium. Previously, researchers have shown calcium, by percent dry weight, is one of the main elements that are responsible for the degree of mineralization in bone, tooth, and even fish scales (Currey, 1999; Mann, 2001; Ochsner, 2011; Olszta, Cheng, Jee, Kumar, Kim, Kaufman, Douglas, and Gower, 2007; Fratzl, Fratzl-Zelman, Klaushofer, Vogl, and Koller, 1991; Boskey, 1991; Boskey, 2007; Canton and Tucker, 2009; Sahi and Schoonen, 2006; Jantou-Morris, Horton, and McComb, 2010; Schonborner, Meunier,. and Castanet, 1981; Weiner, Veis, Beniash, Arad, Dillion, Sabsay, and Siddiqui, 1999; Ratner, Hoffman, Schoen, and Lemons, 2013; Shapiro, Byers, Glorieux, and Sponseller, 2014).

Two-dimensional elemental distribution images were produced from the five-micron thick serial sliced scale sections for the small and medium fish only, using μm-XCT mapping. The beam size on the sample was approximately 7 μm × 10 μm using Rh-coated Kirkpatrick-Baez focusing optics. X-rays were selected using a water-cooled channel-cut Si (111) monochromator. Changes in elemental compositions for the serial sections were monitored using μm-XRF and correlations were made between elemental composition and location. Once the elemental composition was determined, the same specimens were then analyzed, using μm-XANES and μm-XRD analytical techniques to aid in identifying any major compounds present within the biomineralized fish scale.

The μm-XRF data were collected at energies either 4100 electron volt (eV), 11000 eV, or 13000 eV using a four-channel Silicon drift detector. To maximize the detection for the light element of calcium μm-XRF data was collected at 4100 eV. The same sample was scanned a second time at a higher energy (11000 or 13000 eV) to collect data on the trace elements present in the samples. For the current investigation bio/geo chemistry trace element interpretations were used. Specifically, to be considered a trace element for a given energy range, a chemical element has an average concentration which is less than 1000 parts per million (ppm) of a material's composition and is usually measured in counts per arbitrary unit (Albarede, 2003; Reinhardt, 2001; Rakovanm Luo, and Borkiewicz, 2008). Each individual atomic count represents a single x-ray photon entering the energy detector (Faust, Johnston, and Reed, 1998; Levinson, Berry, Johnston, Osborne, and Pack, 2001; Leng 2008; Willmott, 2011).

The μm-XRF multi channel analyzer plot (MCA), shown in Figure 4.26, for elements that fluoresce in the [3,000 -10,000] eV energy range. The energy peaks were used to identify the periodic elements. Each element has known x-ray properties. The x-ray properties were
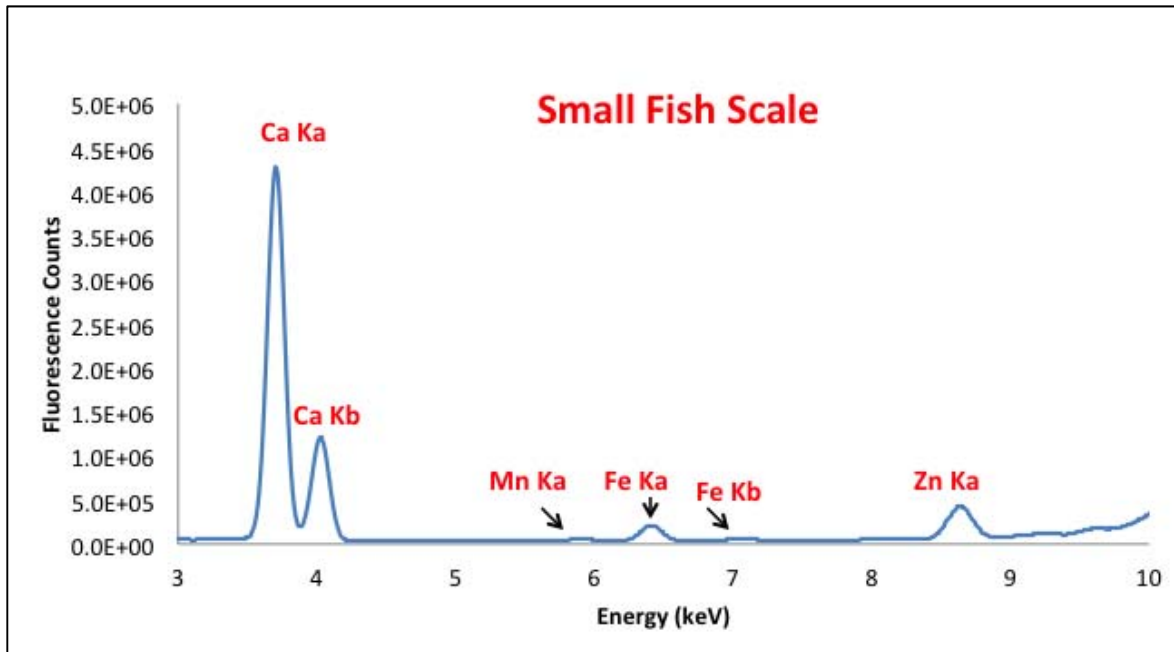
Figure 4.26 Synchrotron µm-XRF multi channel analyzer plot showing periodic elements that fluoresce in the [3000 -10000] eV energy range, for the small fish scale.

identifying using Lawrence Berkeley National Laboratory's website that provides a

downloadable PDF document titled "X-RAY DATA BOOKLET" that contains information for

all elements (X-RAY DATA BOOKLET, 2015). The "Ka" and "Kb" are shell emission lines in

electron volts that were compared to those listed in the x-ray properties of elements found in the

"X-RAY DATA BOOKLET."

The MCA-plot identified calcium and zinc as the main elements found in the small fish

scale. The trace elements found were iron and manganese. Observed in Figure 4.27 are the

µm-XCT elemental two-dimensional distribution maps for Ca and Zn. The warmer colors

(red/yellow) indicate areas of higher concentration. The Ca and Zn distribution appear in the

concentric ring as sub-layers throughout the scale. The darker yellow area on Ca map indicates

an increase in Ca concentration. When comparing the light white region to the synchrotron

µm-XCT two-dimensional density map, Figure 4.28, to the yellow region in the µm-XRF

93
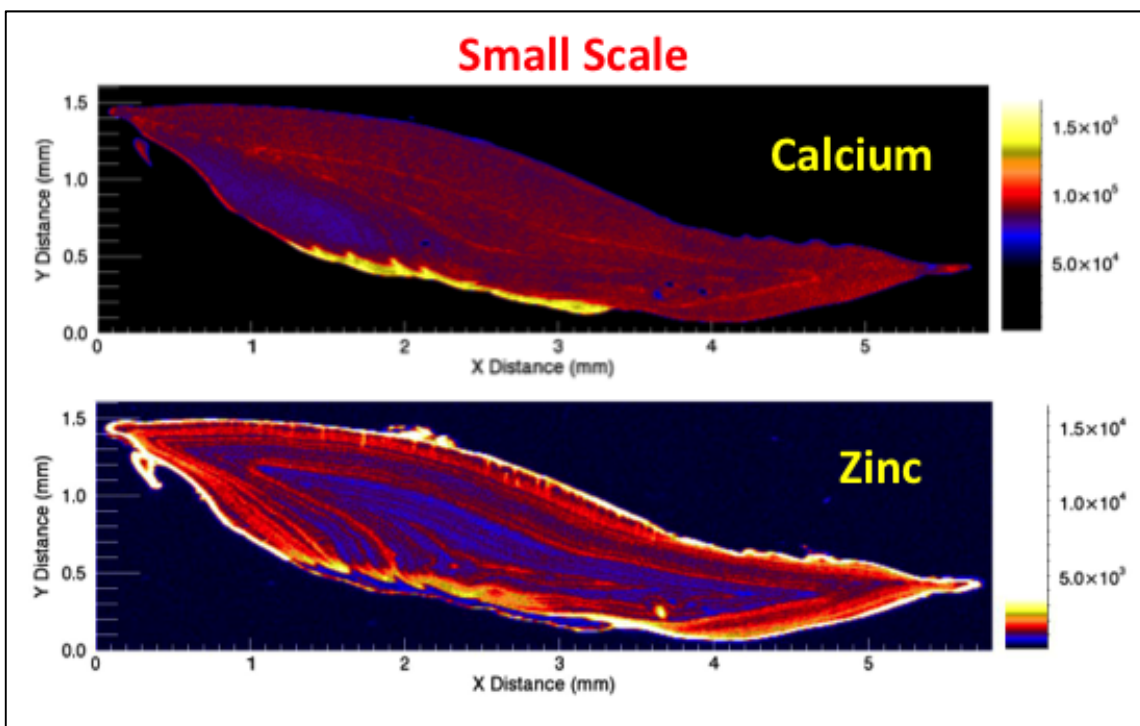
Figure 4.27 Synchrotron μm-XCT 2-D elemental distribution
maps for Ca and Zn for the small fish scale.

calcium maps, Figure 4.27, the area is most likely the densest for the fish scale. Since the

medium scale was much denser, the ultramicrotomy technique caused crinkling of the specimen

during preparation. The μm-XRF measurements and maps obtained from the damaged specimens

provided results that were inconclusive, Figure 4.29.

The μm-XANES spectroscopy was next collected for both the small and medium

biomineralized scale for mineral speciation. The beamline was calibrated to 4,038 eV for calcium

μm-XANES/XRF analysis and to 9,659 eV for Zinc μm-XANES/XRF analysis using standard

metal compounds (X-RAY DATA BOOKLET, 2015). μm-XANES data was processed using a

combination of the X27A data software and Athena software packages.

In Figure 4.30, μm-XANES spectroscopy is used to compare the collected experimental

fish scale data to known Ca-standards for energy absorbance. Calcium μm-XANES was used as
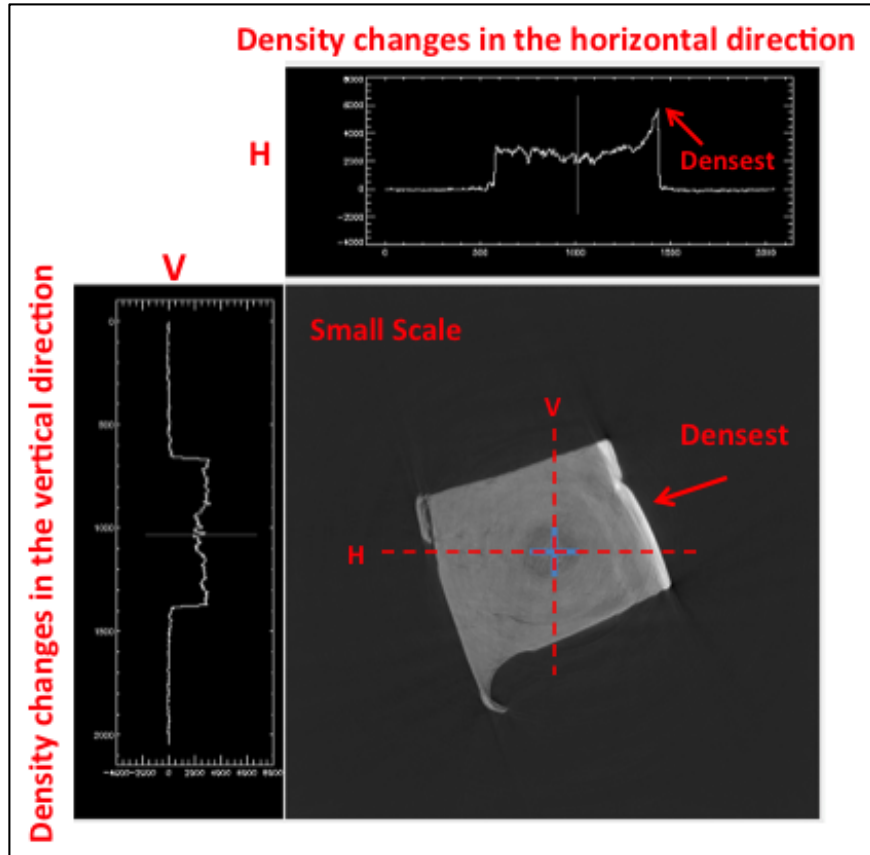
**Figure 4.28 Synchrotron μm-XCT 2-D density map
for the small fish scale.**
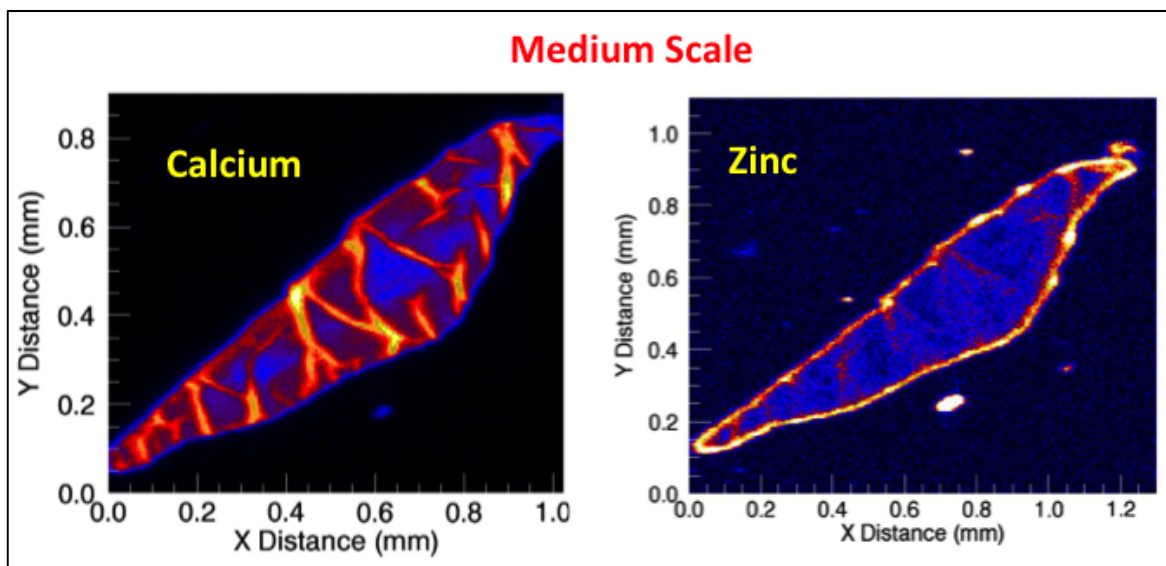
Figure 4.29 Synchrotron μm-XCT 2-D elemental distribution maps
for Ca and Zn for the medium fish scale.

95
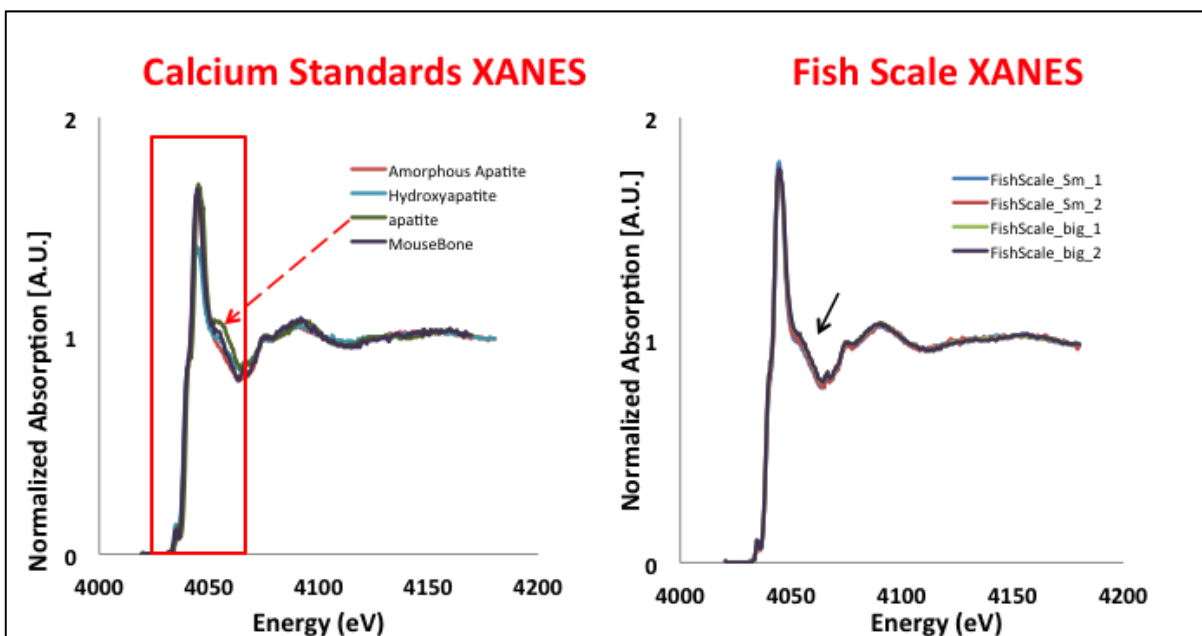
Figure 4.30. Synchrotron μm-XANES spectroscopy plots for comparing the collected experimental fish scale data to known Ca-standards.

a fingerprinting technique to determine the form of Ca in the fish scale. On the left are μm-XANES scans of only Ca-standards—notice the differences between these compounds—this is critical when looking at μm-XANES plots. On the right are μm-XANES collected on a larger and smaller fish scale—note the similar structure—indicating that there is little difference in Ca-speciation between the scales as they age.

The energy absorbance spectra, in Figure 4.31, are nearly identical to the bio-apatite (mouse bone) minerals as opposed to the pure inorganic Ca-minerals. The comparison further indicated that Alligator gar fish scale is composed of a biogenic- Ca-Phosphate mineral. Additionally, the amorphous Ca-phosphate mineral is a better fit than the pure apatite; therefore, the inorganic portion of the scale may be composed of amorphous Ca-phosphate.

When comparing fish scale μm-XANES data to known bio-apatite (mouse bone) and Zn-standards, Figure 4.32, an interesting trend was observed for the Zn. Zinc is distributed

96
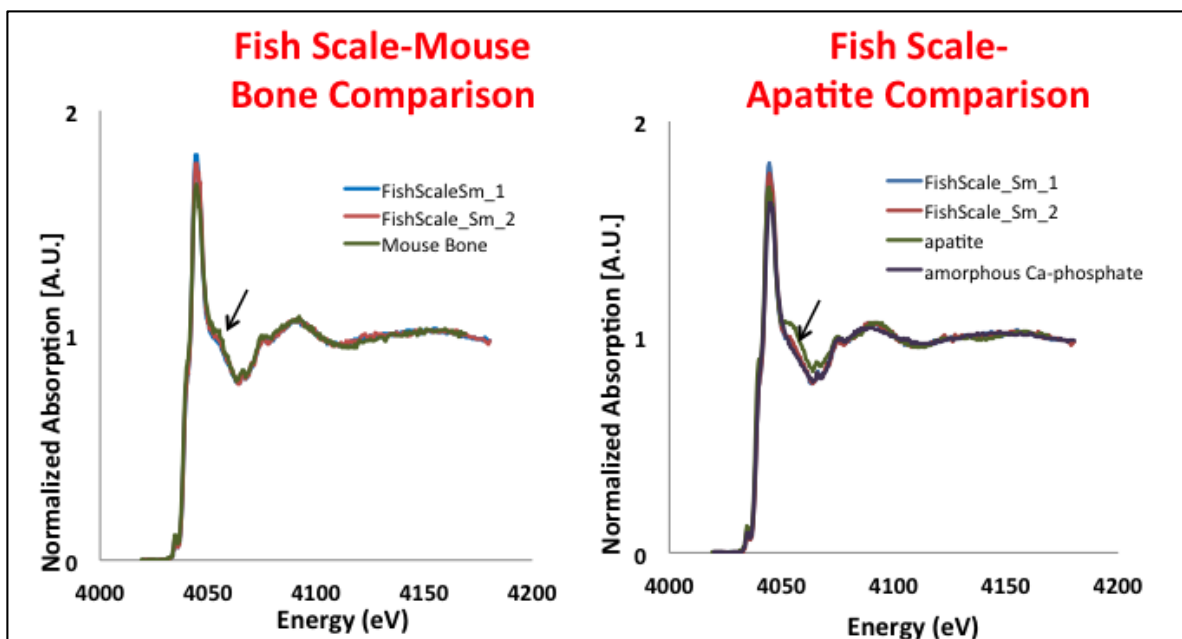
Figure 4.31 Synchrotron μm-XANES spectroscopy plots for comparing the collected experimental fish scale data to known apatite and bio-apatite (mouse bone) standards.

throughout the fish scale—it appeared to correlate closely with the Ca levels. The Zn XANES also indicates that the Zn in the Alligator Gar scale is much more closely related to Zn found in bio-minerals than pure inorganic phases. Chemistry suggests that Zn could replace Ca in the Ca-phosphate structure (Mucalo, 2015). The role Zn plays in biomineralized bio-apatite is not well understood.

After completing Synchrotron μm-XANES measurements the μm-XRD data was collected at 0.7093λ with aluminum oxide (α-Al_2O_3) and silver behenate ($AgC_{22}H_{43}O_2$) as calibration standards. Data was fit using Fit2D ™ and Match! ™ software packages. Once collected the μm-XRD spectra for the fish scale was compared to four-mineral types: Hydroxylapatite-(Carbonate), Apatite-Human Dental, Apatite-(F), and Apatite-(MnF). Provided in Figure 4.33, are the crystallographic structures along with calculated stoichiometry for the relative quantities of reactants and products in chemical reacted apatite minerals used for

97
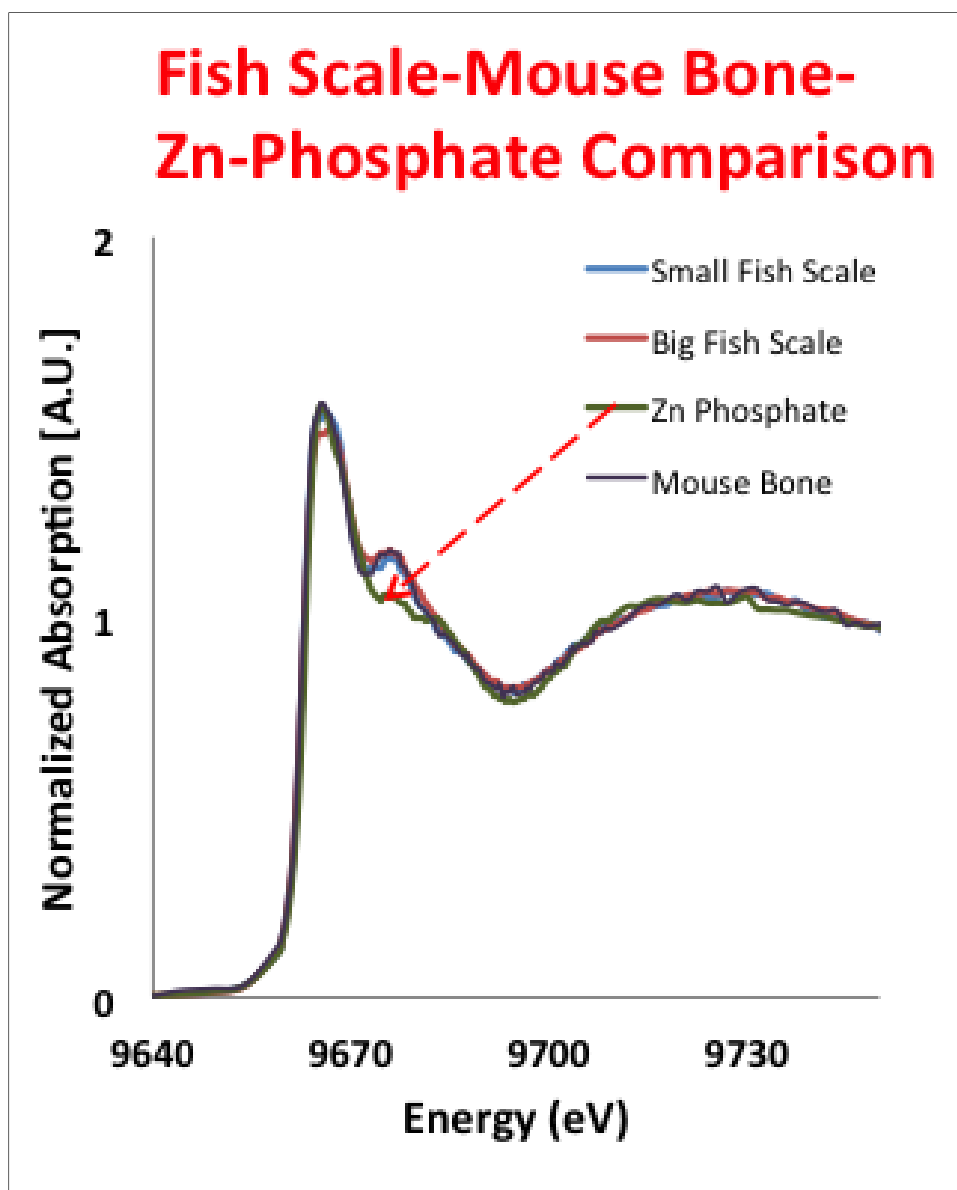
Figure 4.32 Synchrotron µm-XANES spectroscopy plots for comparing the collected experimental fish scale data to known bio-apatite (mouse bone) and Zn-standards.

comparison (Wilson, Elliot, and Dowker, Rietveld, 1999; Fleet, Liu, and King, 2004; Hughes, Cameron, and Crowley,1989; and Hughes, Cameron, and Crowley, 1991). As an aside, usually present in all matter is carbon but is difficult to measure so the reacted oxidation state is normally assumed in stoichiometric calculations.
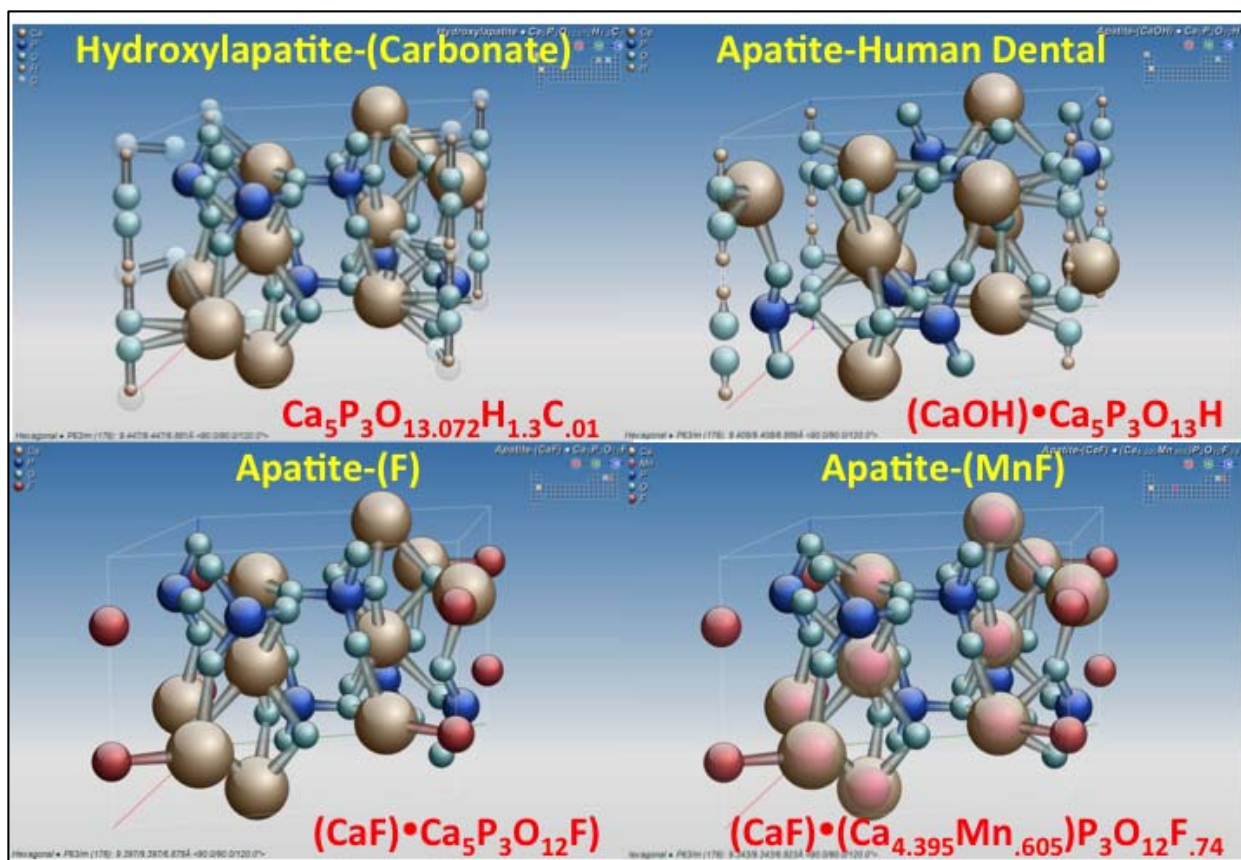
Figure 4.33 Crystallographic structures and calculated stoichiometry for apatite minerals used in fish scale XRD comparisons (Wilson, Elliot, and Dowker, Rietveld, 1999; Fleet, Liu, and King, 2004; Hughes, Cameron, and Crowley,1989; and Hughes, Cameron, and Crowley, 1991).

The mineral phase speciation for the small fish scale structure was proven to be an apatite based mineral, Figure 4.34. In general, there were no discernible differences for the varying apatite structures shown by the comparison. Equally, the apatite minerals with elemental substitutions (Carbonate, Ca, F, and Mn) retain a similar pattern. Meanwhile, the µm-XRD crystallographic comparison with other apatites illuminated the P and F periodic elements in the fish scale structure. Recall, µm-XRF mapped the presence of Ca, Zn, Mn, and Fe elements. Since synchrotron x-ray experimental methods could be coupled, they were able to show distribution and speciation for major and trace elements for the fish scale structure. Data were not collected
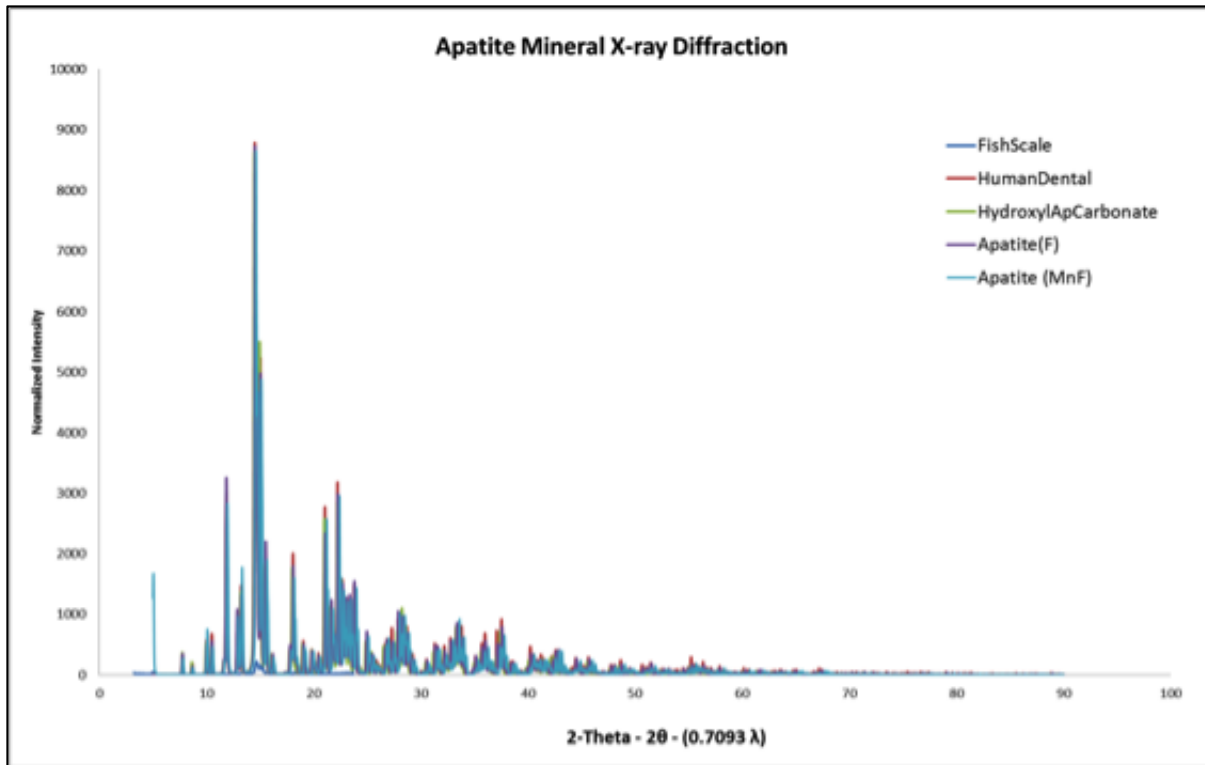
Figure 4.34 Synchrotron μm-XRD spectra for the small fish scale compared
to several known varying apatite crystallographic structures.

for the medium fish scale because μm-XRD experiment showed there was very little variation in

apatite structures.

4.2.5 TGA

Phase changes and decomposition of apatite structure was studied by means of thermal

gravimetric analysis. The TGA experimental technique measures total mineral and organic

contents, including carbonated mineral and non-collagenous proteins, providing additional

insight into bulk composition. Thermal response depends on the heating rate, amount of sample,

and phase purity (Haines, 1995; Bigi, Cojazzi, Panzavolta, Ripamonti, Roveri, Romanello, Noris

Suarez, and Moro, 1997; Bahrololoom, Javidi, Javadpour, and Ma, 2002; and Markovic, Fowler,

and Tung, 2008).

Prior to TGA, the fish scales were wiped with filter paper to absorb the excess water on the scale surface. The experiment was conducted for both the small and medium scales. The initial mass for the small and medium fish scales were 55.3 and 46.3 milligrams, respectively. The samples were heated in alumina (Al_2O_3) crucibles. Using a Netzch™ system the scanning temperature range was from 35 to 1550°C with a heating rate of 10°K /min, balance flow of 20 mL/min and a sample flow of 50 mL/min of ultra-purity N_2.

The results for TGA, shown in Figure 4.35, indicate there are three thermally identifiable processes. Water (free and physi-sorbed) loss due to evaporation occurs between [35 -250]°C. Calcination of the carbonated hydroxyapatite biomineral phase resulting from thermal decomposition and subsequent loss of chemically-bound H_2O ($2HPO_4^{-2} \rightarrow P_2O_7^{-4} + H_2O$ (gas)) and CO_2 ($P_2O_7^{-4} + CO_3^{-2} \rightarrow 2PO_4^{-3} + CO_2$ (gas)) occurs between 250-1000°C. During calcination, the decomposition of collagen and combustion of the residual organic components occurs between [250 - 450]°C, and removal of carbonate ions from the inorganic phase between [450 and 1000]°C.

The assumption made from μm-XRD crystallographic comparison was that the chemical composition of the fish scale structure produces a carbonated bio-apatite structure (B-Ap); thus the decomposition beyond 1000°C is uncertain. The uncertainty is due to lacking full knowledge of the starting composition. Earlier discussed, trace elements measured at a given energy state depend on their measurable molar concentrations being below 1000-ppm; therefore all elements in the structure may not be detectable.

Previous research has described carbonate is liable in apatite-based minerals and can be substituted with cations and anions (Tonsuaadu, Gross, Pluduma, and Veiderma, 2012). Depending on the element type and molar concentration used to modify the atomic structure, the
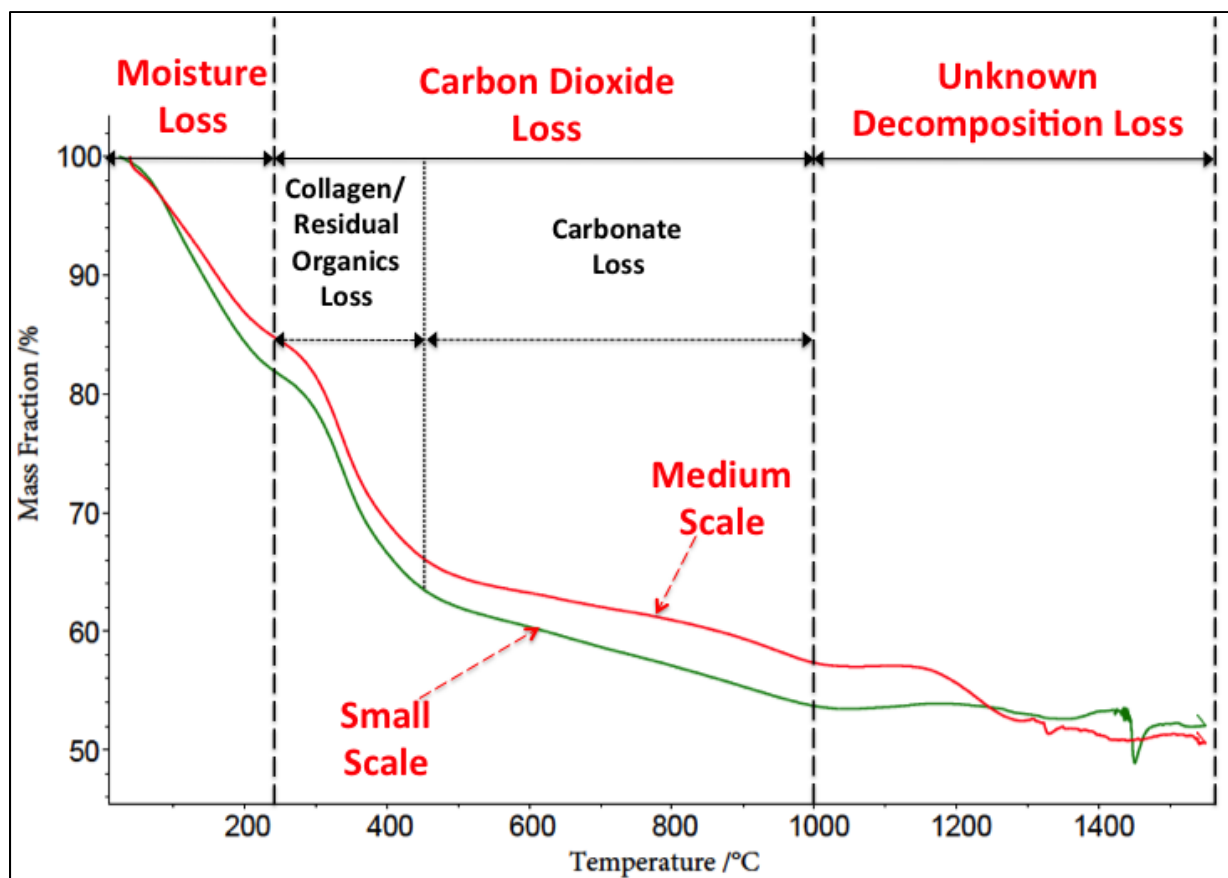
Figure 4.35 Thermal gravimetric analysis for the small
and medium fish scales.

carbonate may either produce apatites that range from thermally unstable to highly stable molecules. Ion exchange has been explained to occur more freely in calcium-based bio-apatites with Al, Si, Cl, Na, Mg, Zn, P, Mn, F, Fe, and K periodic elements (Fleet, 2015; Liou, Chen, Lee, and Bow, 2004; Mathew and Takagi, 2001; and Young, 1974). Also provided in this dissertation is evidence, obtained from TGA, that can be used to postulate how calcium carbonate allows nature to substitute elements based on availability and can evolve as needed to maintain a stable biomineralized structure.

Additionally, TGA was able to support the assumption made for the carbonate presence, because of the reported temperature range for mass loss, so the difference in the small and

medium fish scale results can be elucidated. For biological materials that have composite layers with graded calcium concentrations that cause a density distribution, the rate of calcination will vary. As shown in teeth, which are akin to fish scales, there exists an outer denser layer with higher calcium concentrations than the underlying layer (Nieto and Livi, 2013). Unlike the teeth, but similar to bone, the fish scale layers become denser with growth/age thereby requiring elevated temperatures to calcine the medium scales when compared with the small scales.

4.2.6 SS-NMR Analysis

Solid-state nuclear magnetic resonance was used to investigate the organic phase contained in the biomineralized fish scale structure. The organic phase is the proteinaceous fibrous components that are assembled from amino acid groups. The molecular structure for the amino acid group is defined by bond length, angles, and orientation of atoms. The resonant frequency for atoms can be used to identify/speciate the bound elemental constituents in the organic carbonate phase.

For heterogeneous structures, SS-NMR results are inherently anisotropic. The measured peaks are often broad, with substantial overlap among the different carbon functional groups. To overcome the ambiguous overlapping for the carbon groups, "selective" Cross-Polarization (CP) techniques were used to dephase some groups over others. The following five SS-NMR one-dimensional cross-polarization techniques, "(a)-(e)," were used to amplify the carbon compounds: (a) Total Carbon Speciation (CP-TOSS) can be used to determine the carbon group type, (b) Dipolar De-phasing (CP-DD) can be used to identify "unprotonated" and "mobile" carbon segments, such as quaternary carbons and rotating CH_3 groups respectively, (c) Chemical Shift Anisotropy (CP-CSA) can be used to search specifically for sp^3-orbital-hybridized carbons, (d) Dipolar De-phasing Difference (CP-DDD) can be used to find explicitly the protonated

carbons, and (e) Carbon-Hybridized (CP-CH) can be used to select only sp^2-orbital-hybridized carbon groups while de-phasing all other groups.

The SS-NMR experiment was performed on the small fish scale only. The results from TGA showed both fish small and medium scales had similar organic thermal decomposition rates; therefore the chemical structure does not drastically change with age. The results from the one-dimensional SS-NMR spectra, shown in Figure 4.36, provide the biopolymeric composition for the small-mineralized fish scales.

The cross-polarization diagnostic examination of carbon nuclei, within the complex fish scale structure, shows strong evidence for carboxyl (COOH) groups within the samples, indicating the presence of organic acids. The spectra greater than 150 ppm were truncated due to substantial carbon overlapping. However, not shown at 172 ppm, a strong/narrow peak occurs which suggests the proteinaceous materials are formed from amino acids. Below 150-ppm CP-TOSS spectra resembles collagen. Also seen is a strong absorbance at 24 and 16 ppm indicating alkyl-bearing (nonpolar) fatty acids.

The CP-DD pulse spectra cannot efficiently dephase the "mobile" CH_3 groups within the samples. Yet, peaks at approximately 75 ppm suggest the carbon is associated with the hydroxy-proline amino acid group. Identical peaks appear as quaternary carbons and sp^3 quaternary carbons; however, the latter is scaled differently in plots labeled CP-DD. The CP-CH selection technique emphasizes absorbance between 40 and 70 ppm, indicating highly substituted sp^3-hybridized carbons with only one hydrogen atom. The relatively high chemical shift (>40 ppm) suggests that the substituents (single and double bonds) are largely oxygen, not nitrogen, to carbon.
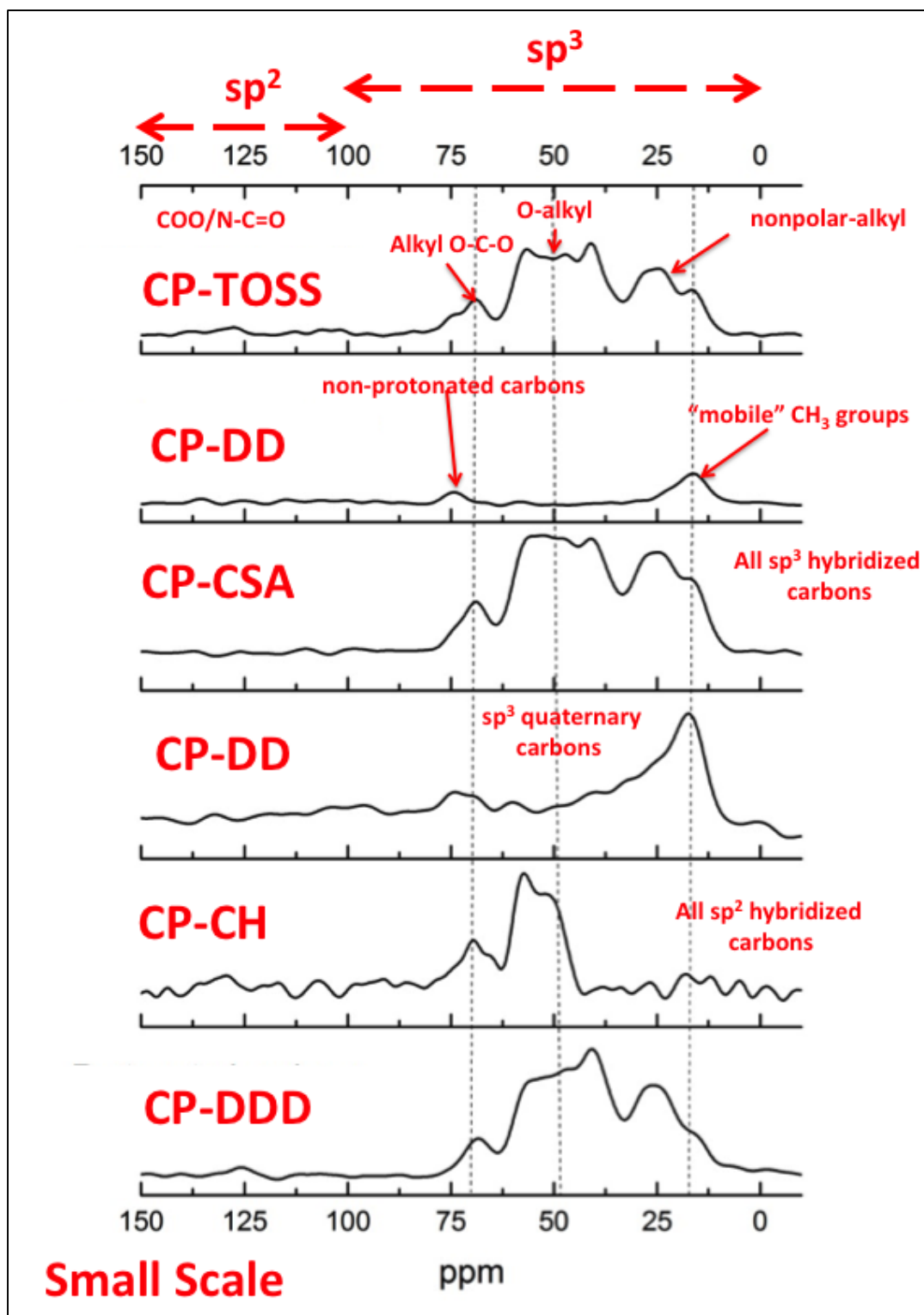
Figure 4.36 SS-NMR 1-D spectra showing the biopolymeric composition for the mineralized small fish scale.

The widths of the absorbance bands suggest the organic material is relatively non-crystalline. There are a wide variety of organic molecule types, combination of amino acid residues, polysaccharides, and fatty acids. No aromatic compounds were found. However, the SS-NMR instrument could not produce a sufficiently higher resonant frequency so uncertainty lies whether any aromatic-bearing amino acids are present. Knowing the type of amino acids could specify the collagen type. Higher resonance frequencies are needed to better detect the presence of aromatic carbons, which usually can be seen at approximately 120 ppm. But because the hydroxyl-proline amino acid group could be identified, it is likely Type-I collagen is present in the fish scale.

4.2.7 FTIR Analysis

The FTIR analysis was used to further investigate the inorganic/organic molecular phase compounds. The mechanical behavior for carbonated bioapatites containing mineralized collagen fibers is a function of the atomic inter/intra atomic bonds strength for the (Chang, and Tanaka, 2002). The vibrational frequencies, produced by FTIR, excite the atomic bonds and were used to identify/speciate the different phase compounds. Spectral FTIR analysis, also, provided spatially resolved information concerning the chemical and structural composition of the fish scale.

The FTIR spectra for bioapatites are very complex, so researchers mainly focus on the phosphate, carbonate, and collagen bands (Grunenwald, Keyser, Sautereau, Crubezy, Ludes, and Drouet, 2014). Usually, the spectra from the amide functional groups are used to specify collagen types. Supplemental to the phosphate, carbonate, and collagen bands; the vibrational spectra for hydrocarbons (CH_X) and hydroxide (OH^-) compound classes are sometimes measured as well.

A Nicolet 6700 ™ FT-IR spectrometer interfaced with Continuum FTIR microscope equipped with a single bounce Attenuated Total Reflectance (ATR) attachment was used to

collect FTIR spectra for the polished fish scale cross-section. The ATR attachment included a germanium (Ge) internal reflection element (IRE), and mid-range spectra were collected between [750-4000]-cm^{-1} with 4-cm-^{1} magnification, and averaging 512 scans. Using the same justification provided during the SS-NMR results presentation in Section 4.2.5 on TGA only the small fish scale was examined. Spectra was collected on the outer layer and the less dense internal layer of the small fish scale, at seven line-scan locations, to determine differences between and within the layers.

The FTIR results, in Figure 4.37, for the small fish scale were compared to published research. Previous researchers compared ATR-FTIR spectra for the three reference materials of cortical bone, hydroxyapatite, and Type-I collagen (Figueiredo, 2015). The pertinent chemical and structural details used for comparison were extracted from the [750-1800]-cm^{-1} spectral range, inside the red dotted rectangular box. The FTIR spectra for the fish scales' outer [Locations 1 through 5] and inner [Locations 6 and 7] layers identify the main functional groups present as amide, carboxylic, phosphate and carbonyl. Specifically, a strong absorbance band at ~1000 cm^{-1} signifies phosphate (PO_4) stretching was occurring in both layers of the fish scale spectra. Also, distinctive absorption bands characteristic of carbonate substitution for phosphate in apatite were present at ~870, ~1420, and ~1450 cm^{-1} in both layers. The spectra of inner layer of the fish scales showed peaks at ~1660, ~1520, ~1225 cm^{-1} which denotes amide I, II, and III absorption bands common to Type-I collagen.

When comparing the compounds for fish scale to the three reference materials the ATR-FTIR spectra most closely resembles as an analogue to either the cortical bone or Type-I collagen structures. Generally speaking all spectra beyond 1800 cm^{-1}, for fish scale, were nearly identical to cortical bone. Interestingly, the spectra collected in this study, not only differ between the two
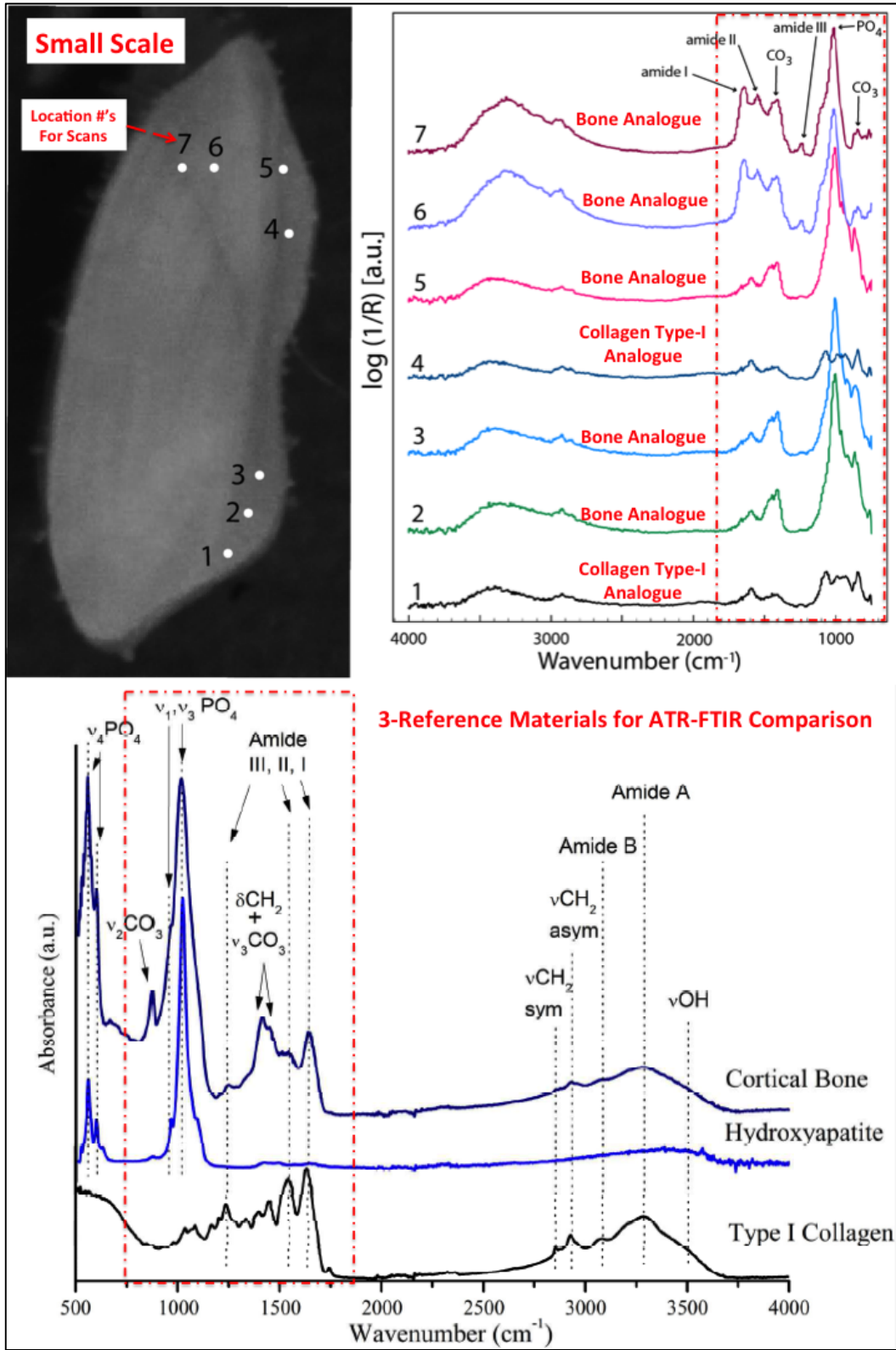
Figure 4.37 FTIR results for the small fish scale compared to that of cortical bone, hydroxyapatite, and Type-I collagen reference materials.

layers, but within the individual layers. Limited conclusions can be drawn for the quantity of individual compounds within different layers of the fish scale from FTIR data. However, the results suggest the carbonate (CO_3) present in the two-layers might differ either in chemical composition or in concentration that depending on location within the fish scale. Moreover, the carbonate phase might either be highly mineralized or amorphous and liable for anion substitution at lower degrees of mineralization (Chang, and Tanaka, 2002).

Also detected in both layers were the amide peaks, which are associated with Type-I collagen. The peaks were shown to be much less prominent in the denser outer layer than the inner layer. Yet, the spectra at locations 1 and 4 appear different than other spectra in the denser layer. The cause for the differences are uncertain but could be attributed to morphology changes in the structure. A review of locations 1 and 4, in Figure 4.37, indicated the measurements were taken at the layers interface. Shown during the SEM investigation separation at the interface, caused by fracture or shrinkage, can occur exposing fibrous collagen. Recall, the FTIR analysis was conducted on fully de-hydrated specimens, the hydration dependent collagen rich inner layer may have contracted, thus exposing the separated collagen fibers at the layer interface leading to the differing spectral measurements.

4.2.8 μm-XEDS and EMPA

The μm-XEDS and EMPA were used to identify the lighter periodic elements, by molar concentration (M), which could not be measured from Synchrotron X-ray, TGA, SS-NMR, and FTIR experiments. First, μm-XEDS data was collected to identify the bulk composition followed by EMPA, which was used for spatially correlating elemental distribution. The information gathered was used to assist with estimating the stoichiometric composition in the fish scale's structure. Typically, the electron signal for the micro-probe is calibrated to mineral standards.

109

The mineral standards were selected based on the likely compositional elements for carbonated bioapatites (Fleet, 2015; Iyengar, 1999). The premise for using known mineral standards with EMPA is two-fold (Russ, 1984; Marinenko, 1991; Reed, 1996; Sanchez-Quevedo, Nieto-Albano, Garacia, Gomez de Ferraris, and Campos, 1998; and Goldstein, Newbury, Joy, Lyman, Etchling, Lifshin, Sawyer, and Michael, 2007). Firstly, the mineral standards are used to identify unknown elements for a substance. Secondly, the standards are used to determine if there are impurities present in embedded inorganic-organic bound phases, based on electron signal loss that may not be straightforwardly measured directly (e.g., carbonates and phosphates). The minerals standards used were Albite, Zaby Enstatite, and Chlorapatite. Collectively the mineral standards represent known molar concentrations for periodic elements of aluminum (Al), calcium (Ca), chlorine (Cl), chromium (Cr), fluorine (F), iron (Fe), potassium (K), magnesium (Mg), manganese (Mn), sodium (Na), oxygen (O), phosphorous (P), silicon (Si), and titanium (Ti). Notice elements of carbon (C), hydrogen (H), and nitrogen (N) are not represented. The C, H, and N elements are essential for maintaining life in organic matter, because of oxidation or storage states, accurate measurements tend to be difficult to achieve and not taken.

The mineral standards discussed above were used to calibrate a JOEL 8600™ microprobe, interfaced with Philips EM 420™ TEM, and equipped with an Oxford™ EDS detector. To detect the elements in the biomineralized fish scale structure, 15-keV at 40x-magnification was used. Both the small and medium fish scales were investigated using EMPA. Three line scans per polished fish scale cross-section were collected to spatially resolve elemental composition. Each location in the line scan had a 20-μm diameter spot size.

Prior to conducting line scans the entire fish scale's cross-section was mapped to identify any periodic elements that are common for most biomineralized structures. The elemental

compositional μm-XEDS maps for the gray-scale backscattered small fish scale image are shown in Figure 4.38. The individual elemental maps, for Al, Ca, C, Cl, Mg, N, O, P, Si, Na, Sr, S, and Zn, are interpreted as the lighter colors are the highest concentration areas while the darker shaded colors being the least concentrated areas for the same color bands. The maps show periodic elements of C, N, Si, Sr, S, and Zn were not detectable. However, the trace elements that could be detected were Al, Cl, and P. The element of aluminum may be an artifact caused by the alumina suspension remnants used during polishing. Higher Cl concentrations are in the less dense layer whereas the concentrations for P elements are observed in the densest upper layer. The major electron signals of Ca, Mg, Na, and O elements were detected. The highest concentrations of Ca and Na were identified in the densest upper layer compared to the highest concentrations of Mg and O in the less dense lower layer.

In addition to mapping the individual elements, EMPA was used to measure the atomic percent of molar concentrations. The atomic unit for each element was based on electron energies that could be sufficiently measured in the medium fish scale's cross-section by line scans and are shown in Figure 4.39. The combined results from Synchrotron X-ray, TGA, SS-NMR, FTIR, μm-XEDS and EMPA indicate the fish scale structure is a carbonated bioapatite that contain periodic elements of Al, C, Ca, Cl, Fe, H, Mg, Mn, N, Na, O, P, and Zn. The experiments delineated the elements contributing to the fish scales' structural formation, now the overall chemical compound can be estimated. The measured units can be used to determine the first approximated stoichiometric relationship for the assumed molecular formulation of $Ca_{(10-x)} \bullet []_x [(PO_4)_{(6-x)} (CO_3)_x] \bullet (OH)_{(2-x)} \bullet []_x$ (Tonsuaadu, Gross, Pluduma, and Veiderma, 2012; Wopenka, and Pasteris, 2005). To allow for equation balancing the carbon oxidation state is fixed
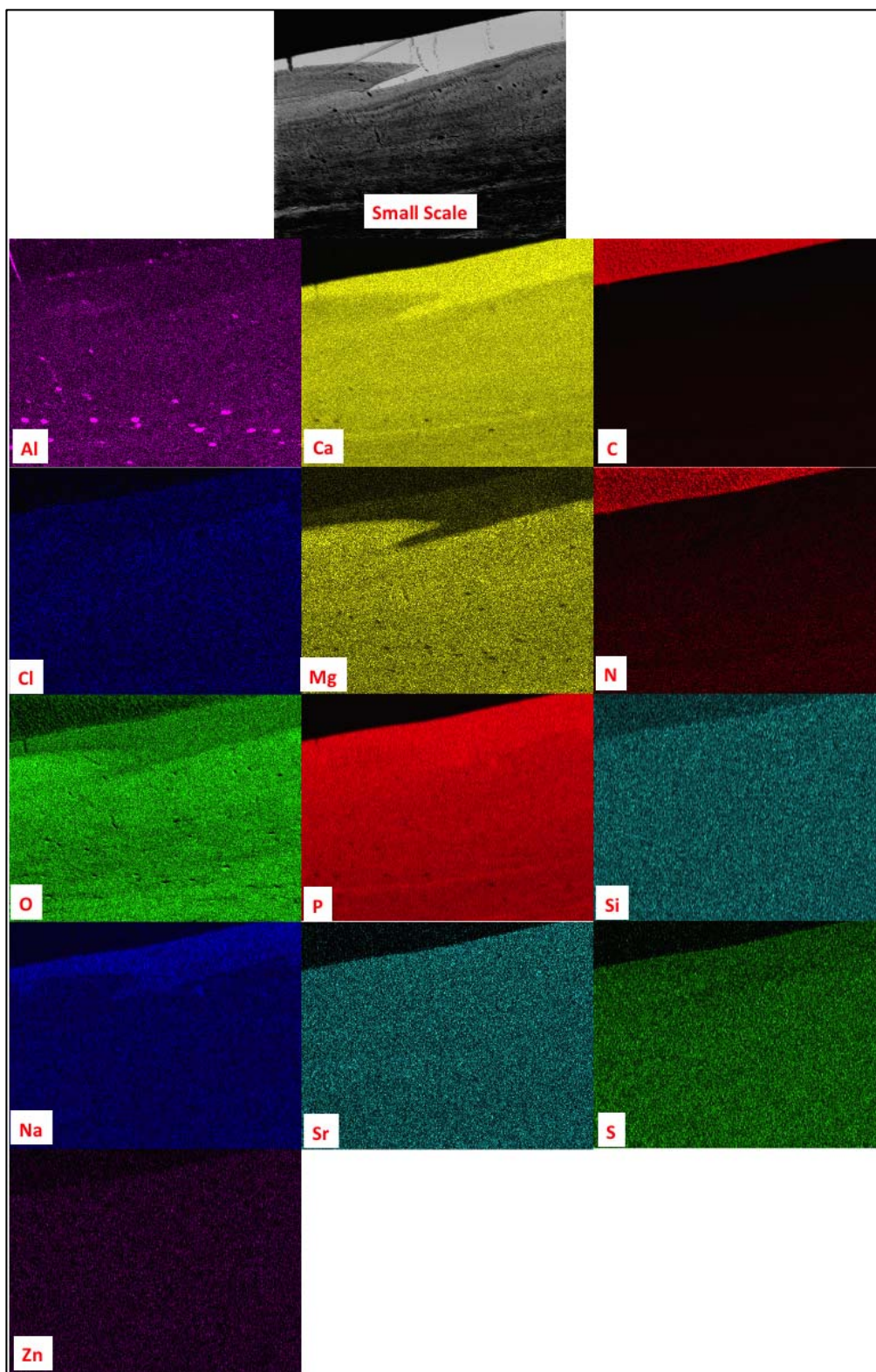
Figure 4.38 μm-XEDS elemental distribution maps for
small fish scale's cross-section.
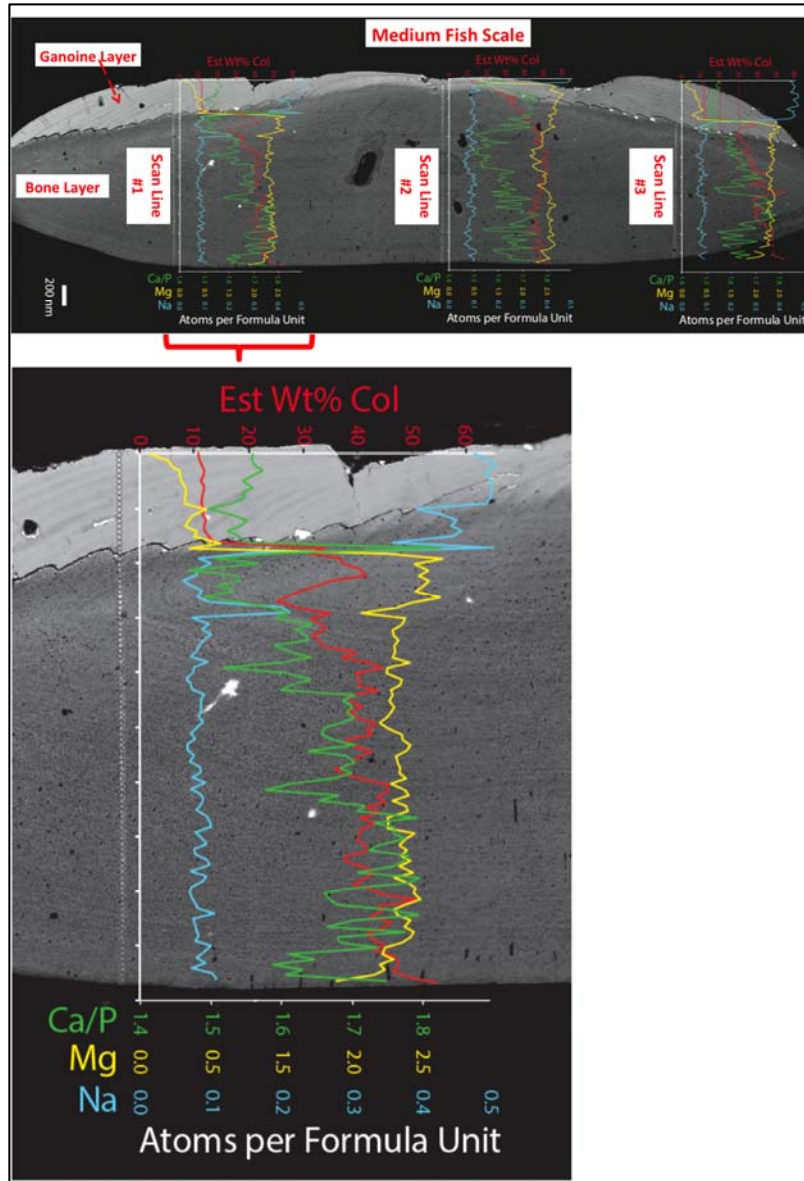
Figure 4.39 EMPA line scan elemental maps for medium fish scale's cross-section.

with a 2^+ charge. The shortcoming for the assumption is directly determining what atomic units are bound to both inorganic and organic phases is not trivial.

Plotted from the line scans, in Figure 4.39, are calculated mineral formulae for the inorganic hydroxyapatite (HAp) reported as atoms per formula unit at the bottom. On the top, in red, is plotted a first approximation of the collagen content, which is estimated by subtracting the

sum of the inorganic oxides from one hundred percent. Because line scans were able to confirm the layer elemental concentrations the structural layers can be identified by layer names as defined by previous researchers (Yang, Chen, McKittrick, and Meyers, 2012; Yang, Chen, Gludovatz, Zimmermann, Ritchie, and Meyers, 2013a; Yang, Gludovatz, Zimmermann, Bale, Ritchie, and Meyers, 2013b). The denser outer layer is known as ganoine while the inner less dense layer is bone. The three traverse scans across the scale are each somewhat different. The commonalities are: the ganoine is higher in Na, lower in Mg and collagen, and has a lower Ca/P ratio than the bone regions. The Ca/P ratio in the ganoine layer range was [1.55 -1.66] while in the bone layer [1.55 -1.90].

Of the three calculated mineral formulae Ca/P ratio is the most informative. The ratio is used to determine the degree of mineralization. In the extracellular matrix the mineralized tissues contain phosphorus, which is highly anionic and hence has the ability to bind to calcium. As a result, the strength and density for the biomineralized structure depends on the degree of binding for calcium in the presence of the phosphorus (Boskey, 1991; Shapiro, Byers, Glorieux, and Sponseller, 2014; Fleet, 2015; Chang and Tanaka, 2002; Grunenwald, Keyser, Sautereau, Crubezy, Ludes, and Drouet, 2014). The ideal calcium-to-phosphorus ratio for the standard geological apatite is 1.67. When Ca/P ratios are less than 1.67, usually the mineralization is decreasing whereas for higher ratios mineralization is increasing (Fleet, 2105). In bio-applications the Ca/P ratio is typically used as a diagnostic parameter to evaluate health of vertebrate or determination for biosynthesis stability/compatibility (Boskey, 1991; Shapiro, Byers, Glorieux, and Sponseller, 2014; Mucalo, 2015; Fleet, 2015). For the fish scale investigation the Ca/P ratio was used to interpret the biomineralization process and identify the difficult to measure supplementary carbonate phase. Carbonate ions are found to substitute

anions in biological apatites. The carbonates can substitutes ions for OH$^-$ (type A carbonate) and PO$_4^{3-}$ (type B carbonate), which can possibly be quantified by the Ca/P ratio.

Focusing on the ITZ that corresponds to just under the ganoine where the structure is densest, as shown earlier in Figure 4.21, the HAp and collagen there are highly oriented and densely packed. Further away from the ganoine, beyond the transition zone, the estimated collagen (Est. Col.) content increases and the overall Ca/P ratio increases. However, as the microprobe samples bands of bright intensity, in general, the collagen and Mg content drop while the Ca/P and Na increase.

Remember, until now all experimental evidence has shown the densest layer is in the ganoine regions, so why does Bone HAp + Collagen have a higher Ca/P? The following reasons are provided: (a) CO$_3^{-2}$ substitutes for PO$_4^{-3}$ in HAp. CO$_3^{-2}$ could be increasing away from the Ganoine interface, lowering P, raising Ca/P. The substitution is consistent with other reported findings that young HAp has more CO$_3^{-2}$ than mature HAp (Fleet, Liu, and King, 2004; Tonsuaadu, Gross, Pluduma, and Veiderma, 2012; Fleet, 2015; Figueiredo, 2015). (b) The level of carbonation is also known to increase with the maturity of the HAp, see TGA result in Figure 4.35, so more vacancies in P is expected to occur further away from the (higher mineralized) ganoine, with aging vacancies decreases.

Apatite compounds are often nonstoichiometric due to the presence of vacancies in calcium and hydroxide sites. Still unknown are the effects of CO$_3^{-2}$ and vacancy content on the physical/mechanical properties of HAp versus collagen. The presence of carbonation ions can clearly influence crystallization processes. The ions may also provide stabilization for the collagen embedded inside the apatite crystalline structure. Furthermore, the phosphates are related to mineral crystallinity as well. An increase in the mineral crystallinity is indicative of an

increase in mineral size and/or decrease in the non-stoichiometric substitutions (Boskey, 1991; Fleet, Liu, and King, 2004; Bigi, Cojazzi, Panzavolta, Ripamonti, Roveri, Romanello, Noris Suarez, and Moro, 1997; Bahrololoom, Javidi, Javadpour, and Ma, 2009; Grunenwald, Keyser, Sautereau, Crubezy, Ludes, and Drouet, 2014; and Figueriredo, 2015). To better understand the effects that chemistry has on the fish scale's crystalline structure and mechanical properties, further analysis was conducted at the nanometer length scale using TEM, STEM-HAADF, STEM-EELS, and nanoindentation.

4.3 Investigation of Length Scale [1-1000] nm

4.3.1 TEM Observations

To this point the discussion of results, for the current research effort, have illuminated pertinent information with respect to the fish scale's chemical content and structure at both the millimeter and micron length scale. However, information is lacking for the description of the biomineralized structure at the nanometer length scale. Therefore, TEM will be used to better clarify the structural details for the individual biomineralized collagen-HAp units for the composite system.

The fish scales have been shown to be an extremely complex biological system in itself with anticipated complexity increasing when exploring the lower nanometer length scale. As a result only the medium fish scale's cross-section was investigated. The thought process for only selecting the medium fish scale for exploration was based on the required detailed investigative efforts to probe the nanometer scale that are very extensive along with specimen preparation being quite rigorous. So the main objective set forth was to use TEM efficiently to examine the fish scale, specifically at the nanometer range, to define geometries for subunits of collagen and HAp. Contingent to TEM and as continuation of the main objective, STEM based experiments

116

are better suited to identify the assemblages and chemistry for the combined subunits of the layered system if there is greater disparity. Ultimately, the medium fish scale is thought to offer the greatest disparity because of its size and age, which were used to interpret formation processes for the layers when both STEM and TEM experimental results are combined.

Shown in Figure 4.40 is an electron image produced using the Philips EM 420 ™ TEM instrument. The specimen was prepared using the FIB sectioning technique from an osmium tetroxide (OsO₄) stained fish scales' cross-section. Staining was used to irradiate the collagen (soft tissue) fibers within the biomineralized scale. The image indicates there are three distinctly different layers. From top to bottom is the highly-mineralized-densely-packed ganoine, densely woven ganoine-bone interface, and loosely woven bone layers.
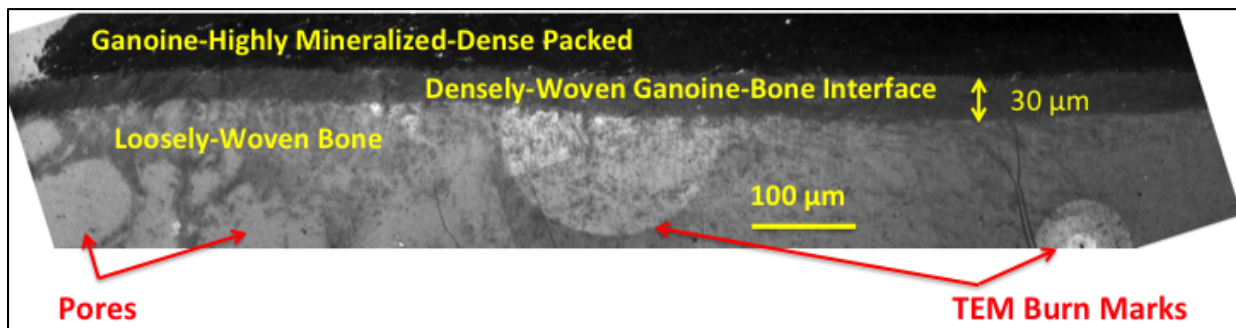
Figure 4.40 TEM image prepared using FIB sectioning
technique from an osmium tetroxide stained
medium fish scale's cross-section.

At the finer 5-µm magnification, in Figure 4.41, is a TEM montage image showing the ITZ for the ganoine and bone layers. To highlight the stained collagen fibers, the contrast for each layer was set independently. The contrasting identifies the packing arrangement for the collagen fibers. The darker region, from staining, indicates the highest packing density occurs in the ganoine for the collagen. Also from contrasting at 1-µm magnification, in Figure 4.42, there
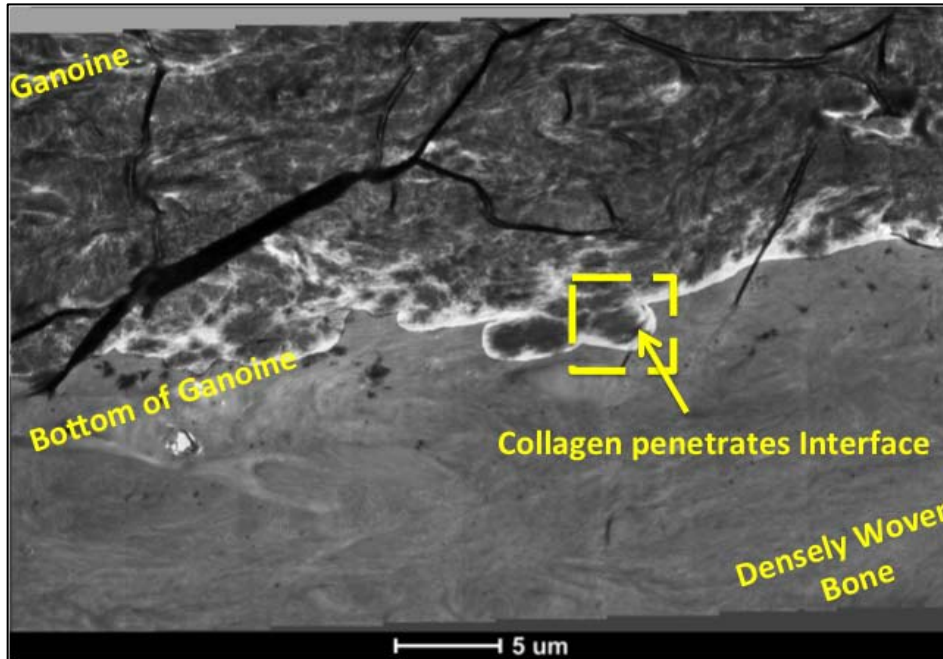
Figure 4.41 TEM montage image showing the ITZ for the ganoine and bone layers from a stained medium fish scale's cross-section at the finer 5-µm magnification.
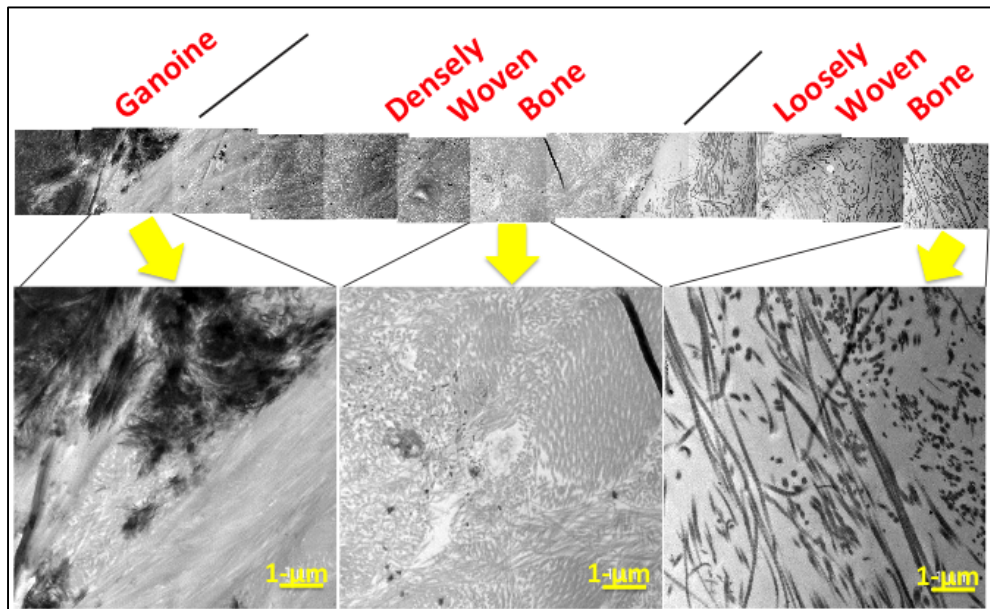
Figure 4.42 TEM montage image showing the collagen packing density gradient for a medium fish scale layers from the stained cross-section at 1-µm magnification.

seems to be a packing density gradient and shows collagen packing decreasing when progressing

from the highly mineralized ganoine, through the densely woven ITZ, into the loosely woven

bone layers. Collagen fibers have 67-nm periodicity subunits within the chain and are

approximately 70-nm in diameter with an unidentifiable total length. Additionally, in

Figure 4.41, the dark ITZ region inside the yellow dashed box was investigated at a much finer

magnification. When viewing the ITZ at the 200-nm magnification, Figure 4.43, the collagen

appears to bridge the interface and penetrate both layers.
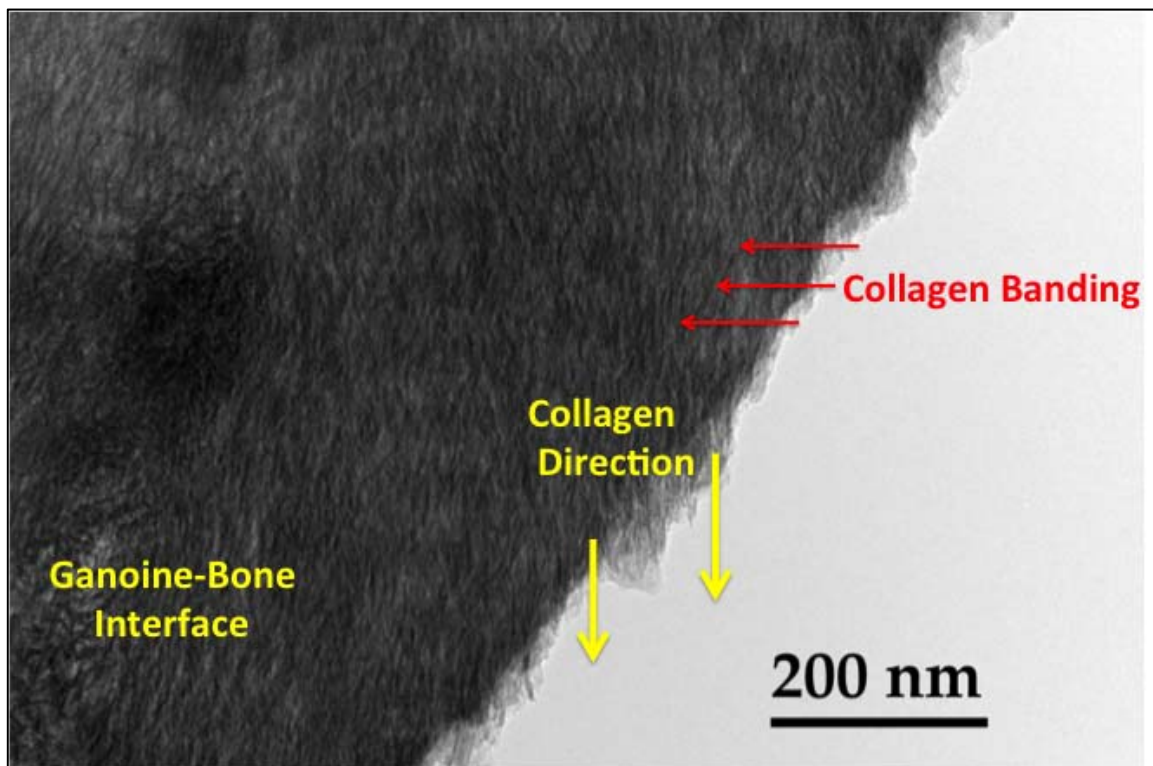
Figure 4.43 TEM image showing the highly ordered collagen
arrangement in the ITZ at the finer 200-mm magnification.

The collagen arrangement is highly ordered at the ganoine-bone interface. Yet, illustrated

by Figure 4.44, the collagen arrangement much further into the bone layer seems to be more

chaotically ordered. Further away from the ganoine, the bone become less dense, more open and

119
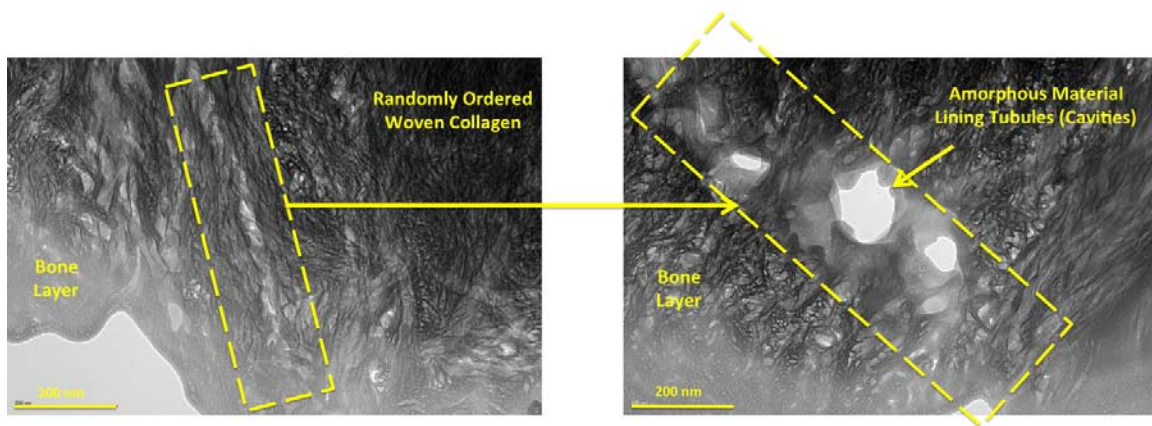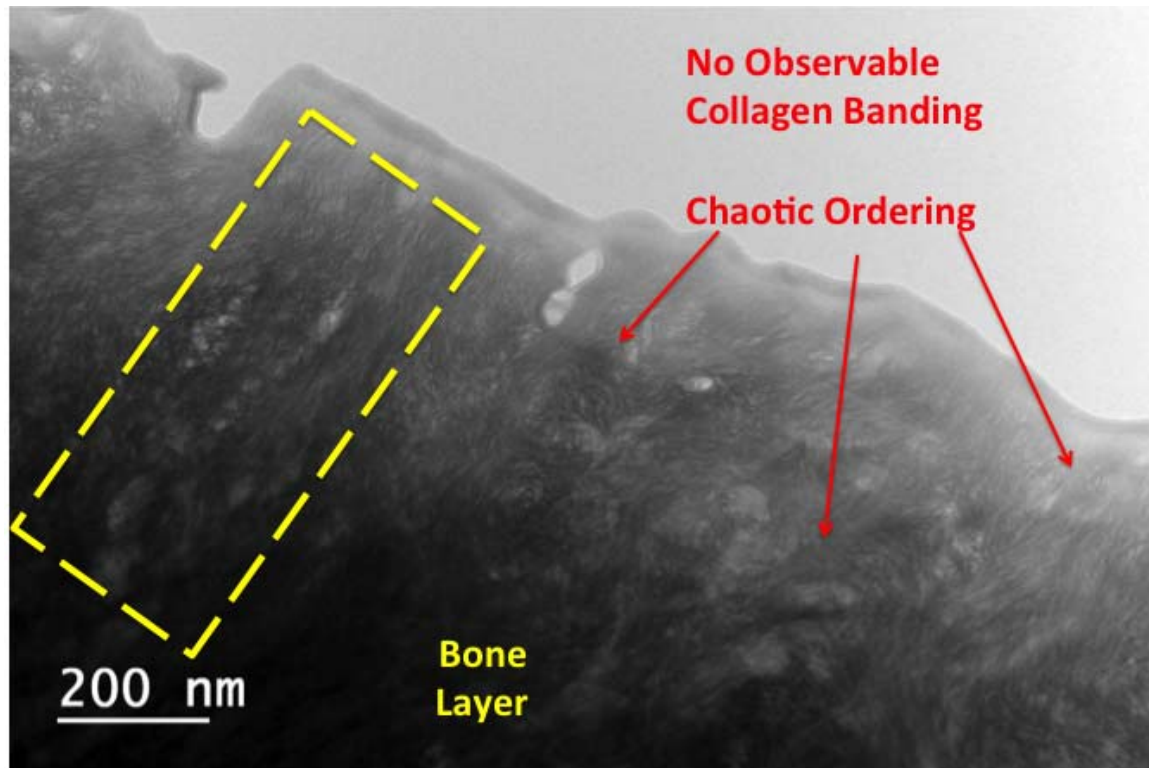
Figure 4.44 TEM image showing the chaotic ordered collagen arrangement
in the bone layer at the finer 200-mm magnification.

having collagen-HAp composite fibrils that are more twisted. After zooming into the rectangular

dashed sections there are randomly woven patterns visible. Inside the woven patterns there are

tubules (cavities) that are lined with amorphous materials. The tubules may be related to cavities

and canals discussed earlier in Figures 4.14 and 4.17.

To better identify the HAp crystals, unstained specimen were cryo-milled from fish scales' cross-section. The scales were cold-treated with a hydrazine inorganic compound. The hydrazine treatment was used to chemically remove the collagenous (proteins) bound materials (Bigi, Cojazzi, Panzavolta, Ripamonti, Roveri, Romanello, Noris Suarez, and Moro, 1997). Before further TEM analysis was performed, FTIR experiments were conducted to verify the HAp crystalline atomic structure was not altered. Shown in Figure 4.45, are FTIR spectra measured in both the ganoine and bone layers for untreated and hydrazine treated fish scales. When comparing untreated to hydrazine-treated ganoine and bone layers for fish scale show, there are no appreciable differences in FTIR spectra. Therefore, the hydrazine inorganic compound did not affect the HAp crystalline atomic structure.

The de-collagenized HAp structure has differing crystal sizes. The HAp platelets in Figure 4.46 appear to show larger non-uniform sizes are present in the ganoine layer and they tend to be ovals with smooth outlines. In the bone layer the platelets have irregular outlines and are linked together to form a porous film structure. The primary bone HAp particles have a narrower size distribution. The average HAp oval sheets have dimensions that are approximately $[20-?] \times [60-200] \times 5$ nm. The sheets have irregular rolling "cornflake-like" topologies. As previously stated, researchers believe the crystalline size/maturity is a function of the degree on mineralization, which is controlled by the distribution of carbonate concentration (Fleet, Liu, and King, 2004; Fleet, 2015; Mathew, and Takagi, 2001; Grunenwald, Keyser, Sautereau, Crubezy, Ludes, and Drouet, 2014; and Figueriredo, 2015). Now that TEM has successfully identified the individual subunits for collagen and HAp crystals the combined parts will be investigated using STEM techniques.
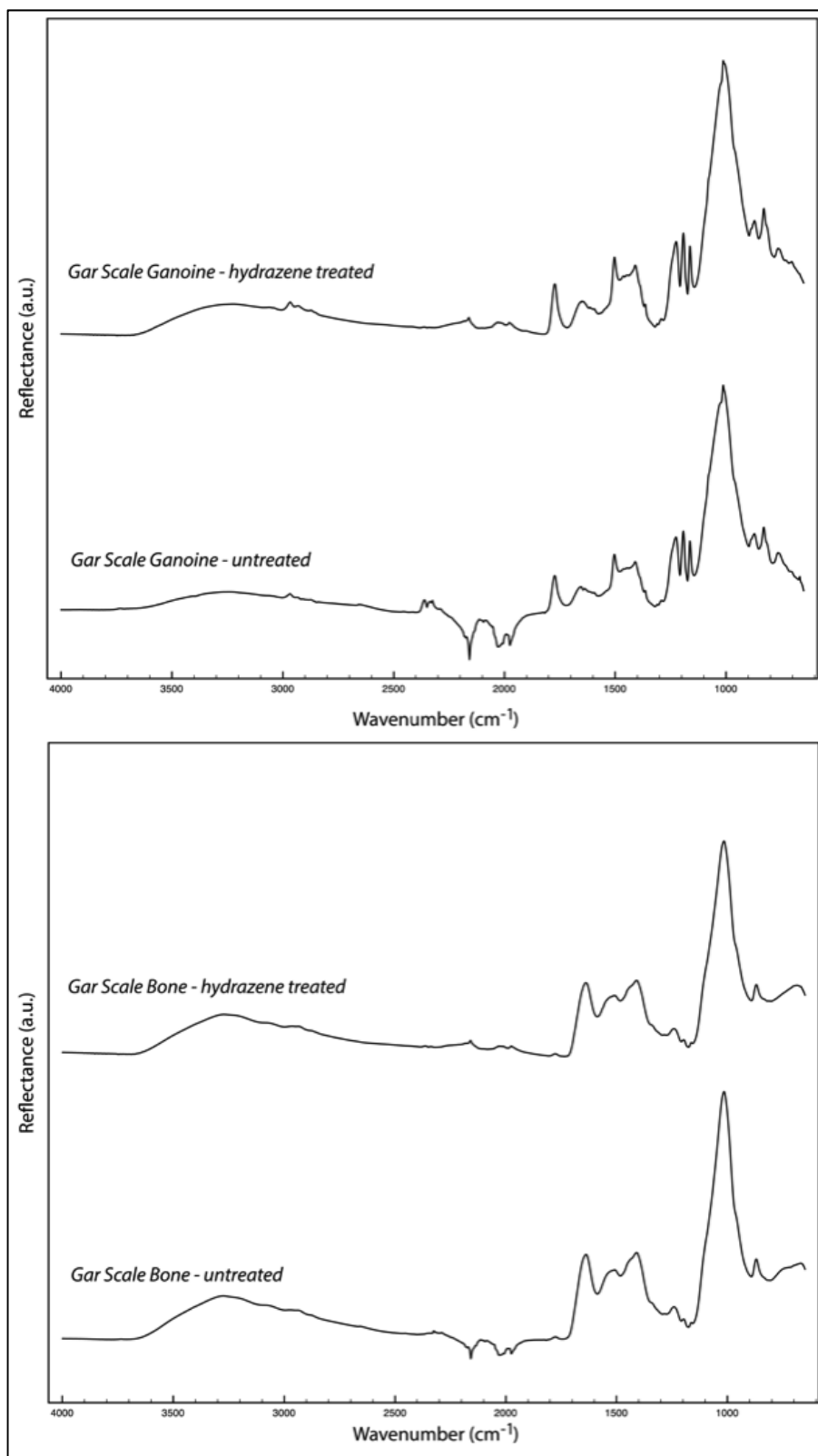
Figure 4.45 FTIR spectra comparing untreated/hydrazine-treated ganoine and bone layers for gar fish scale.

122
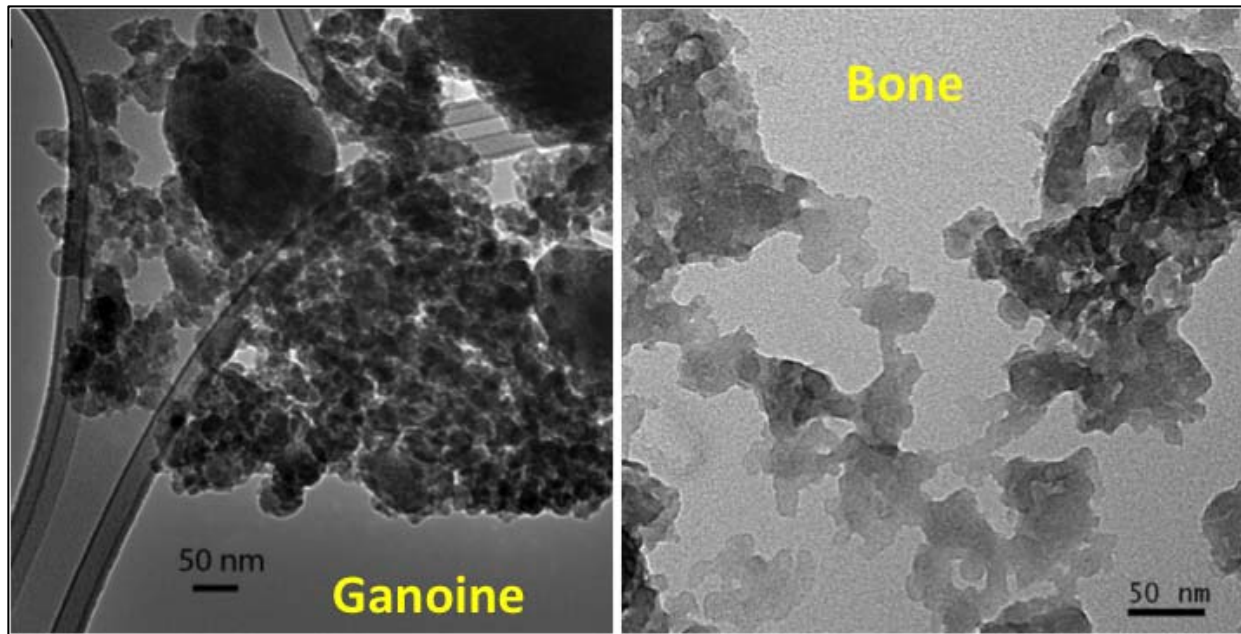
Figure 4.46 TEM image comparing de-collagenized hydrazine-treated HAp crystals in ganoine and bone layers for gar fish scale.

4.3.2 STEM-HAADF-EELS

One of the challenges of probing the biomineralized fish scale structure is the ability to identify the embedded mineral and fiber compositions at the nanometer scale. Moreover, when using TEM the HAp crystals do not readily diffract when combined with the collagen because the crystal thickness (5-nm) for the individual crystals are 14 orders of magnitude smaller than collagen. Because the subunits for collagen and HAp interfaces are difficult to delineate, the combined STEM-HAADF-EELS experimental techniques are helpful at lower nanometer range for probing biomineralized chemical composition and structural arrangement for the fish scale.

Scanning transmission electron microscopy (STEM), when combined with high angle annular dark-field can produce images from contrasting intensities that correlate with the mean atomic number (Z) for known periodic elements. Typically electron energy-loss spectroscopy (EELS) data is simultaneously collected with STEM-HAADF. The addition of EELS allows the

investigation of the chemical state and electron density at the nanoscale. The combined experiments uses the secondary electron signatures to identify the periodic elements, based on their mean atomic number, which provide contrast for structures that have opaque interfaces when imaged.

The current STEM investigation used a FEI CM 300™ FEG equipped with Gatan 200 EELS™, Oxford™ EDS, and HAADF detectors. The CM 300™ instrument has a 300 keV atomic magnification with a field emission gun capable of point-to-point characterization of material at the nanoscale (<0.2 nm). The instrument is also equipped with a high current probe capable of extremely high-magnification (~1 nm) chemical analyses.

The STEM-HAADF-EELS study was conducted at the highest magnification. Shown in Figure 4.47, is the correlated STEM-HAADF-EELS image of the medium fish scale's bone layer. The bright contrasting intensity means there is high occurrence for mean atomic number. In this case the mean atomic number is used to identify HAp are inside collagen and also align along the collagen long axis. The gap and overlap banding have very sharp boundaries. HAp crystals run vertically, but not exactly parallel with the collagen fibers, and cut through both the GAP and OVERLAP bands. On the right are STEM (K and $L_{3,2}$) Electron Energy-Loss Spectroscopy Maps of C, O, P and Ca. Here, the light bands correspond to Ca-rich, C-poor GAP bands, while the dark band is C-rich OVERLAP band. The STEM imaging contrast is the opposite of conventional TEM images of bone layers. Even though Ca is greater in the GAP band, there are immense amounts of Ca in the OVERLAP bands and also lots of C in the GAP band. So Ca is not simply limited to the GAP-band of collagen. In fact, the majority of Ca may be in HAp platelets that are larger than the GAP or OVERLAP bands. Additionally, the ordering for GAP and OVERLAP banding for collagen is unique to Type-I Collagen (Nudelman, Pieterse, George,

124
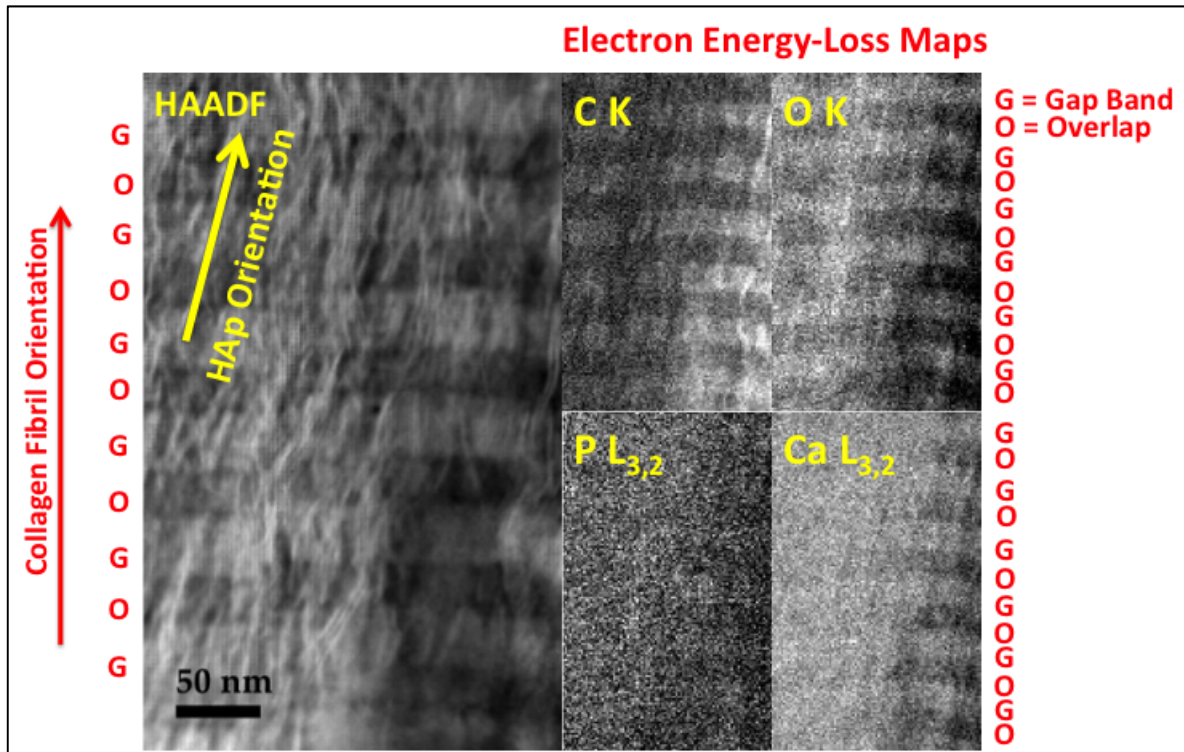
Figure 4.47 STEM-HAADF-EELS image of the medium
fish scale's bone layer.

Bomans, Friedrich, Brylka, Hilbers, de With, and Sommerdijk, 2010; Jantou-Morris, Horton, and

McComb, 2010; McNally, Schwarcz, H. P., Botton, and Aresnault, 2012; McNally, Nan, Botton,

and Schwarcz, 2013). Inferred from the STEM-HAADF-EELS analysis, the calcium

concentrations are embedded in collagen. The concentration of calcium is not all part of the HAp

mineral phase, some are contributing to the collagen phase but even more contributes to the

carbonate phase.

4.3.3 Nanoindentation Mechanical Analysis

Thus far Chapter 4 has been dedicated to discussing the hierarchical description of the

chemical composition and structural assemblage. Nanoindentation experiments were used to

provide further details of how the biomineralized ganoine and bone layers respond to external

loading. Additionally, the experimental measurement was used to interpret how collagen fiber and HAp mineral structural phases contribute to the fish scales mechanical strengthening.

Analysis of nano-indentation experiments assumes the measured response is that of a linear homogenous or near homogenous material system (Constantinides, Ravi Chandran, Ulm, and Van Vliet, 2006). The assumption permits interpretation of physical measurement using *classical continuum mechanics* based on elasticity, plasticity, and/or viscoelasticity, all three of which assume material parameters do not depend on specimen size (Ostojic and McPherson, 1987). For heterogeneous materials this assumption breaks down, especially when the material is composed of discrete components that are large compared to the size of the probe. For example, most materials exhibit size-dependent phenomena in the length scale range of 1–10 nm due to surface energy effects that become increasingly appreciable due to the large surface-to-volume ratios available at the nanoscale (Maranganti, and Sharma, 2007). The practical application of *classical continuum mechanics* assumes the length scale over which deformation varies is much larger than the discrete size of the particles. Further, the assumption of size-invariant properties for discrete and heterogeneous systems breaks down when the experiments are analyzed *using the equations for homogeneous material* in conjunction with averaged material parameters (Brandstatter, 1963; Pethica, and Oliver, 1989). Properties so determined depend on specimen size unless there is a large separation between specimen size and the size of material components. Moreover, such materials display scale dependent features such as wave dispersion, force chains, and finite sizes of shear bands and fractures whereas continuum mechanics tells us wave velocities should be independent of wave length and force chains, shear bands, and fractures should have zero size. Accordingly, the governing equations for homogenized discrete and heterogeneous systems must be based on non-local stress-strain relationships, which impart a

characteristic scale not available using the locality assumption of classical continuum mechanics. Such relationships are essential for proper modeling of material damage and softening. However, the relationships have yet to be sufficiently developed by the community of practice.

Biological materials cannot be considered homogenous due to their hierarchical structure. The key issue is the difference (or scale separation) between the discrete components and domain size. Here the discrete components are minerals and fibers with separation of length scale for the domain being attributed to the much larger radius of curvature for the indenter probe used to conduct the indentation experiment (Rettler, Hoeppener, Sigusch, and Schubert, 2013). Since the minerals and fibers are much smaller than the probe size, further considerations are needed when interpreting the mechanical response from nanoindentation measurements. Specifically, for biomineralized composite materials that have bound compliant soft (fibers) fixed inside rigid (mineral) nano phases, capturing the energy dissipative response is difficult. Therefore, it is important to understand the suitability of experimental techniques used to capture the discrete elastic and viscous properties for highly heterogeneous material systems. For the fish scale, the instrumented nanoindentation (INI) techniques were selected as the most appropriate technique that could best capture the effects of the hierarchical structure.

The primary advantages of the INI technique are the ability to characterize small volumes of material and measure properties with high spatial resolution. However, characterizing small volumes of materials creates a conflict when attempting to capture the heterogeneity attributes for the fish scale. That is, to get meaningful properties, we need to average over some representative volume, but doing so masks the mechanical property attributes gained from the local material variation. The viscoelastic properties are of critical importance in the fish scales' structure because they can describe how the bone layer stores energy (storage modulus), like a

127

spring, and how the internal network of collagen fibers uses friction to convert mechanical energy into heat (loss modulus)–the energy that is lost/dissipated through heat generation.

The (INI) experiments were carried out using strain-rate-displacement controlled, dynamic indention measurements. Strain-rate controlled, dynamic indention measurements are sensitive to small deformations (less than one-micron). To correctly capture the small deformations, a two-step process was carried out during the experiment for the small and medium dehydrated fish scales. During polishing, the specimen's surface is typically and unavoidably work hardened. The work-hardened layer is roughly one third to one-half the size of the particle size used for polishing. As a result, the measured elastic modulus could reflect the value of the work hardened layer, or the underlying substrate or some combination thereof thus giving a false reading. Moreover, the false reading can give a false sense of layering. So the first step for conducting INI experiments is to determine what is the minimum displacement needed to penetrate the work hardened polished surface.

The experiments were conducted using a Nanomechanics iNano™ nanoindenter with the setup parameters listed in Table 4.1. A Berkovich grid indented array was used to map the fish scales' cross-section, Figure 4.48. The converged penetration depth determined in Step 1 was extracted from the elastic modulus-penetration depth and hardness-penetration depth plots for the small and medium scales, in Figures 4.49 and 4.50, respectively. The mechanical properties show excellent convergence in the ganoine and bone regions by 300 nm of surface penetration.

Next, for Step 2 the data for mechanical properties in each experiment were analyzed over the penetration range from [500 - 800] nm and used spatially resolved line plots and surface maps to report the measured mechanical properties. Using the dynamic indentation technique allowed for the continuous acquisition of hardness and elastic modulus as the tip penetrated

Table 4.1 Nanoindentation setup parameters for determining minimum
penetration depth, modulus, and hardness.

Input Parameter	Value
Tip Geometry (Angle/Curvature)	Berkovich (142.3°/~150 nm)
Tip Material Type	Diamond
Indentation Strain Rate	0.2 s^{-1}
Maximum Indention Depth, (D$_{Max}$)	1-μm
Spacing Between Indents, 10x(D$_{Max}$)	10-μm
Poisson's Ratio, (ν)	0.35
Penetration Range for Averaging Results	[500-800]-μm
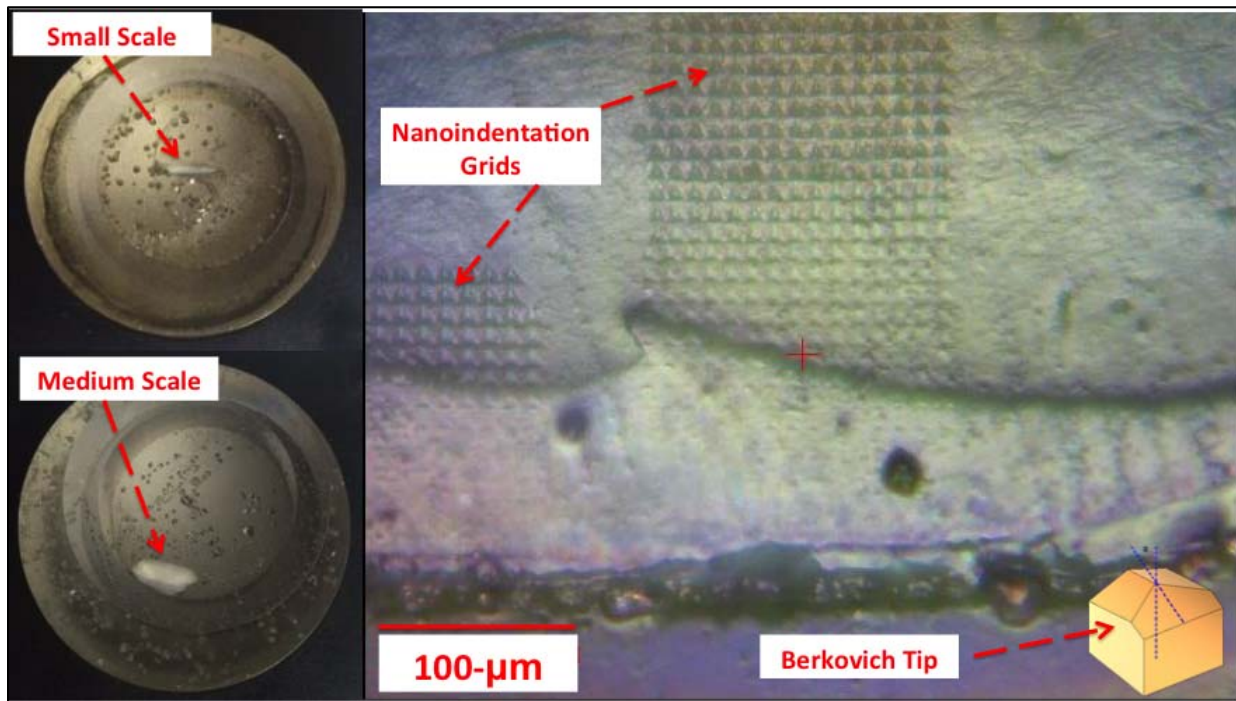
Figure 4.48 Berkovich indented array for mapping
the fish scales the cross-section.
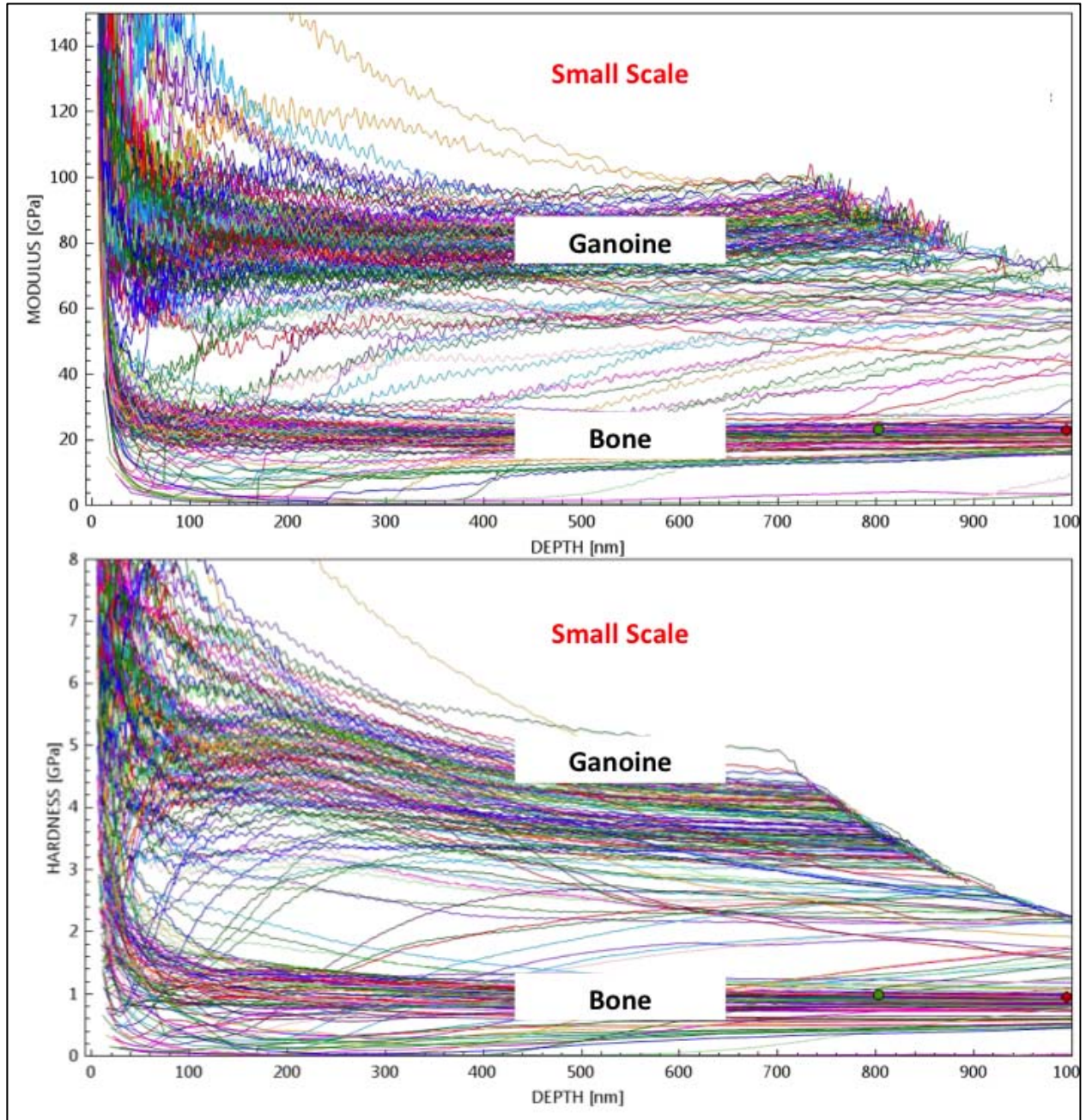
Figure 4.49 Nanoindentation elastic modulus-penetration depth
and hardness-penetration depth plots for the
small dehydrated fish scale.
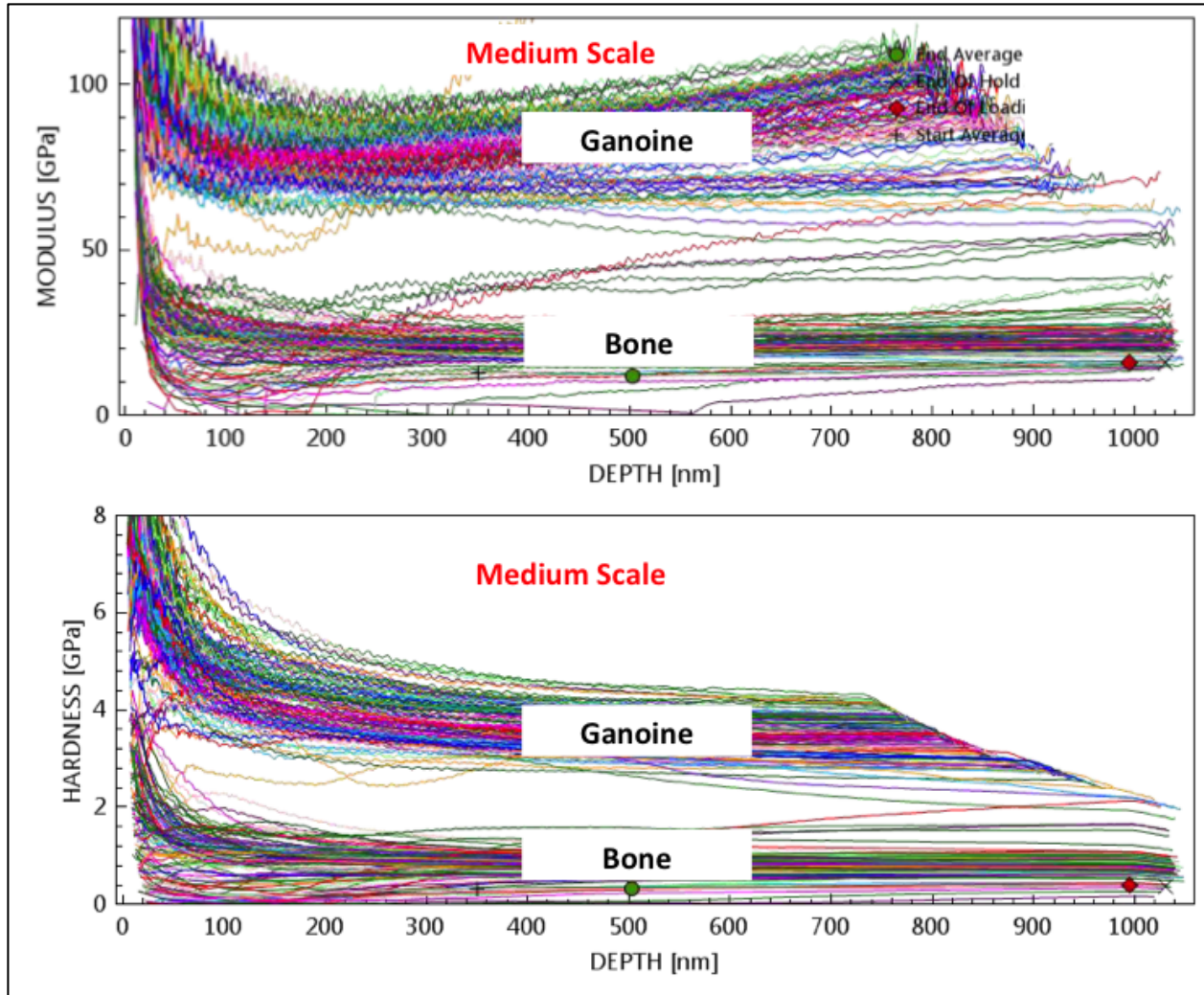
Figure 4.50 Nanoindentation elastic modulus-penetration depth
and hardness-penetration depth plots for the
medium dehydrated fish scale.

through the surface of the sample. An array totaling 1680 and 3600 indents with a 10-μm spacing

between indents were used to map the small and medium fish scale's cross-sections, respectively.

Shown in Figures 4.51 and 4.52, are the measured elastic moduli and hardness for both the small

and medium scales. Also, illustrated in Figures 4.51 and 4.52, are snapshots showing how the

mechanical properties transitions across the ganoine-bone interface.
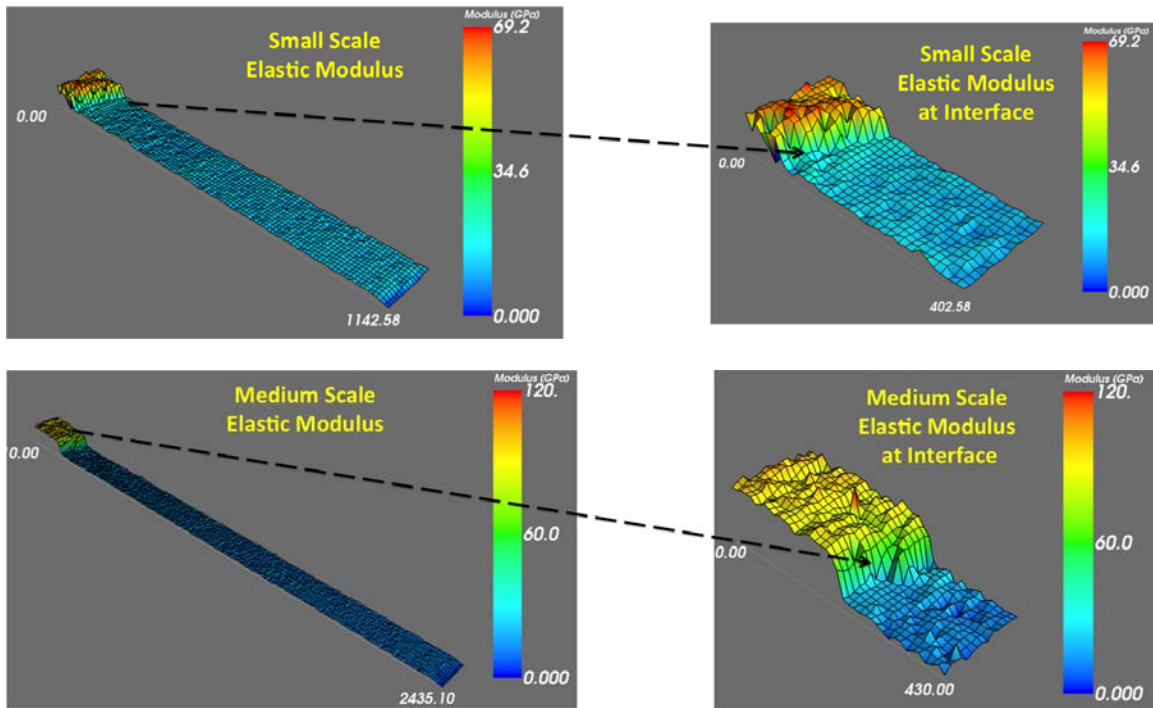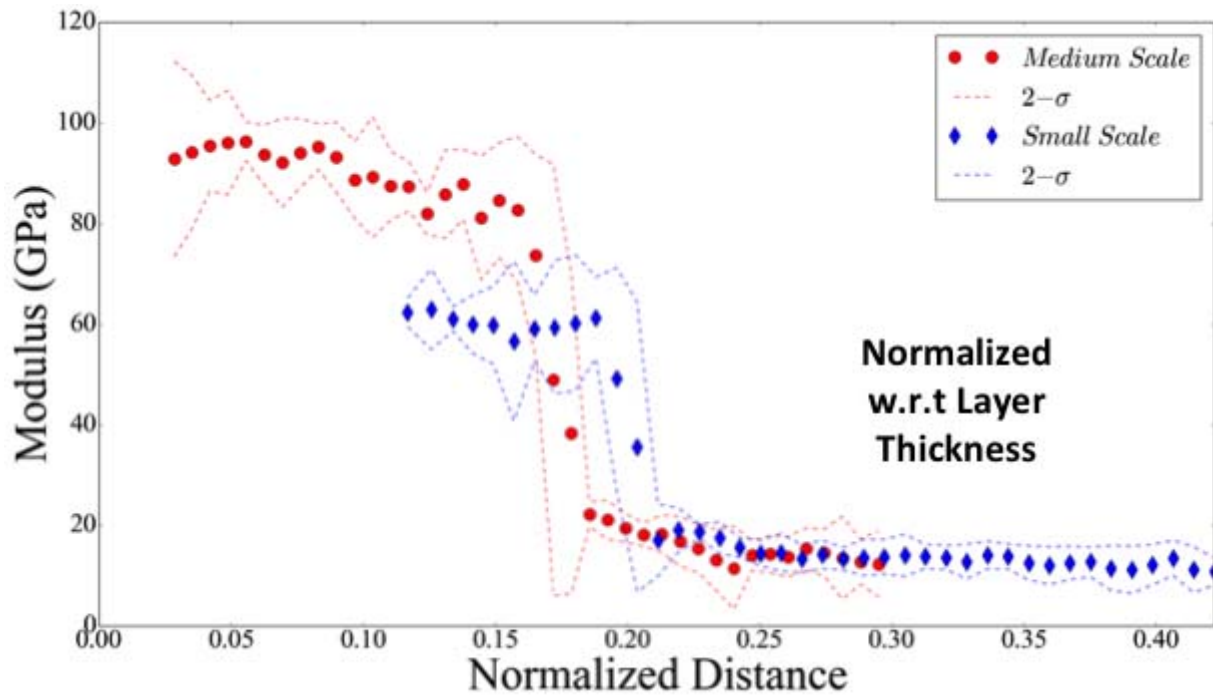
Figure 4.51 Nanoindentation elastic modulus for dehydrated small and medium fish scale.
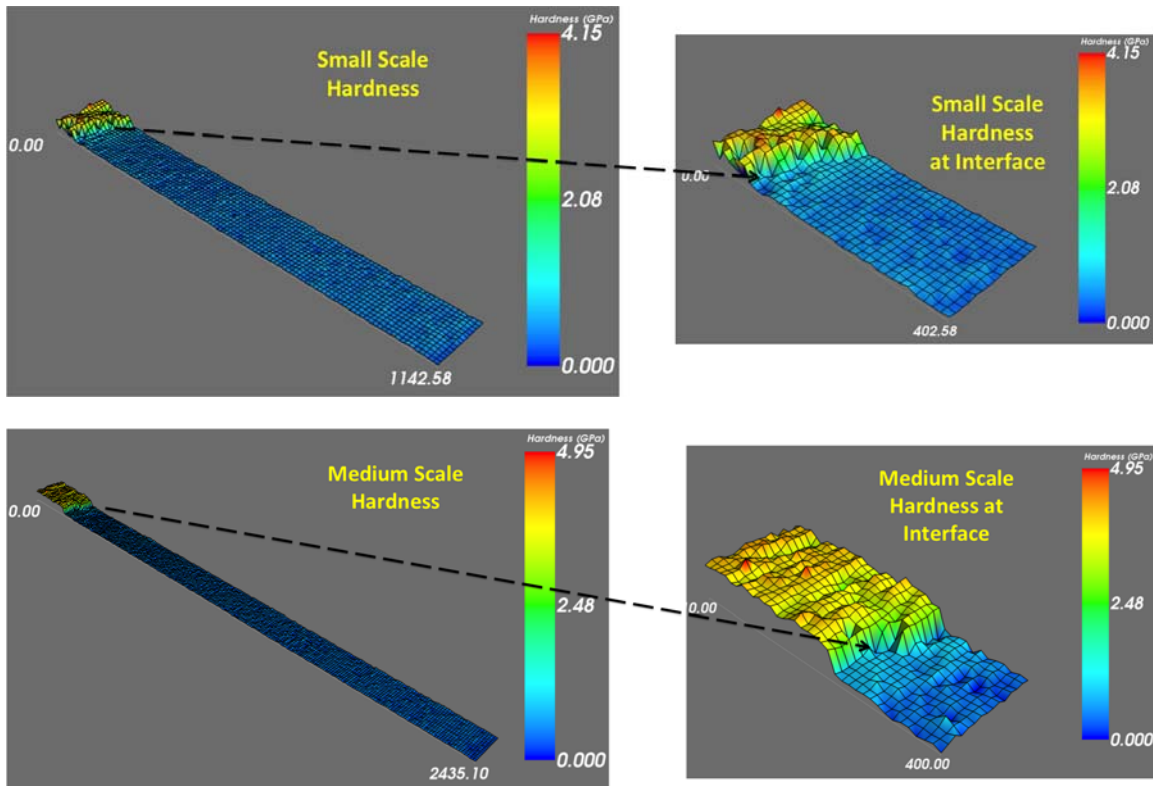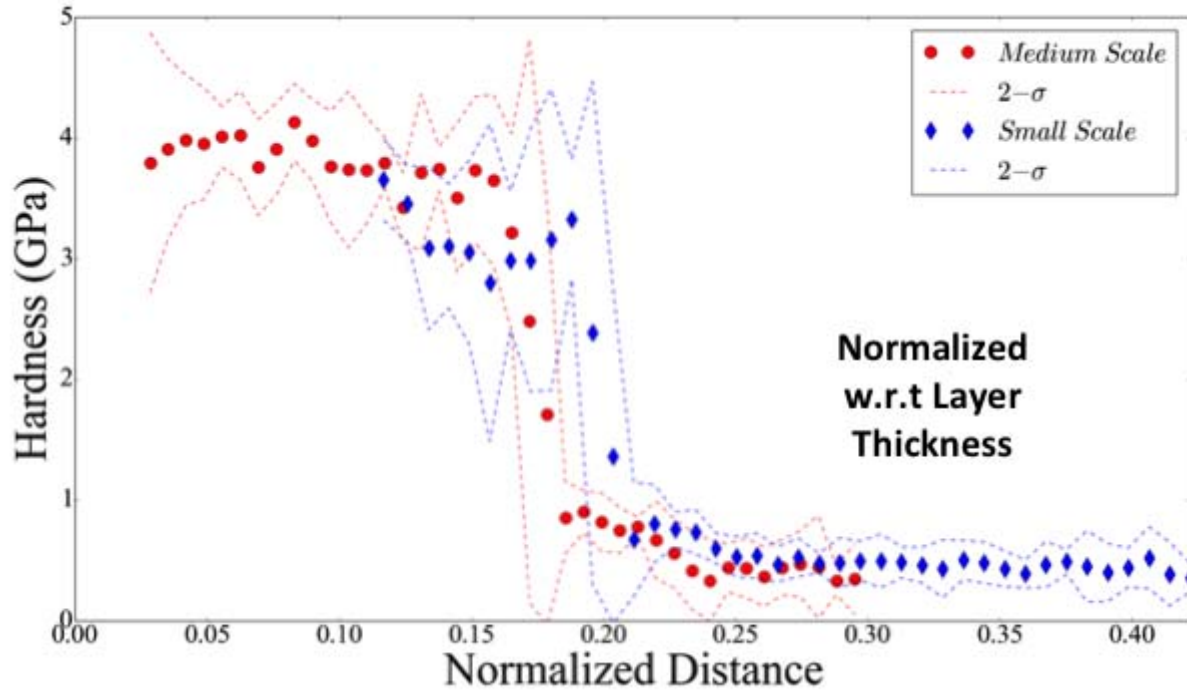
Figure 4.52 Nanoindentation hardness for dehydrated
small and medium fish scale.

Both elastic moduli and hardness have property gradients occurring through the ITZ from [0.11 – 0.25] and [0.02 – 0.23] normalized distances, with respect to layer thickness, for the small and medium fish scales, separately. In the outset of each line plot, the median properties for small and medium scales are shown using blue diamonds and red circles, respectively. Each data point represents the average measured mechanical property positioned equidistant from the interface. The corresponding colored dashed line represented by two standard deviations (2σ) show the upper and lower bound for the orthogonal property grading. Meaning the upper and lower lines are respectively twice the standard deviations from the mean making the zone between four standard deviations. The surface plots better show three-dimensional variation for the local maxima and minima results.

In the line plots elastic modulus in the ganoine layer for the medium scale shows a continuous decrease as the interface is approached with the maximum measured elastic modulus occurring at the outer edge of the ganoine layer. Whereas, the small scale shows an increase in elastic modulus as the interface is approached, with the maximum elastic modulus in the bone layer occurring at the interface. The hardness shows the same trend as compared to the elastic modulus for both fish scale sizes.

Noticeably the ganoine layer has elastic moduli ranging from [60-66] GPa in the small scale compared to [98-80] GPa in the medium scale; while both scales' bone layer have an average elastic modulus of 18 GPa. Similarly, the ganoine layer have hardness values ranging from [3.0-3.4] GPa in the small scale compared to [3.6-4.0] GPa in the medium scale; while both scales' bone layer have an average elastic modulus of 0.5 GPa. For comparison purposes, shown in Chapter 1 by Figure 1.3, the elastic modulus for the fish scale's ganoine layer closely resemble human tooth enamel while the bone layer has comparable modulus as human bone. As a

reminder, the tooth has a fixed 2-layer structure with harder outer protective enamel layer covering a less dense softer dentin layer. While the bone has a more woven medium compact structure containing osteon gap zones that are used for constant bone remolding throughout life.

Continuing with the indentation analysis both fish scale sizes have comparable slopes occurring in the ITZ with average elastic modulus changing from [60-18] GPa in the small scale compared to [80-16] GPa. However, the average hardness shows much less change ranging from [3.4-0.5] GPa in the small scale compared to [3.6-0.5] GPa. Even more interesting, both the medium and small scales show similar mechanical properties in the bone layer over the same distance from the interface, suggesting that size and age of the scale does not influence the size of the transition zone in the bone layer. Yet in the ganoine layer an increase in the elastic modulus is observed for the medium scale with an additional steady increase in elastic modulus as the outer edge of the scale is approached. The overall findings, from modulus and hardness, indicate the fish scale grows from the bone-ganoine interface as the fish grows and the scale becomes more mineralized and denser/stronger in the ganoine layer while the bone layer maintains a consistent lower modulus and hardness.

Recall, from the analytical chemical speciation and structural characterization the bone layer is much less compact, than at the interface and ganoine layers, leading to the much lower elastic modulus and hardness. In addition, the bone layer has a collagen rich, chaotic, randomly ordered structure. To better capture the heterogeneity effects collagen has on viscoelastic response in the ganoine and bone layer, dynamic mechanical measures were also taken during the INI experiments for elastic modulus and hardness. The current study used the phase lag (tan Φ), determined using dynamic mechanical analysis (DMA), to map the viscoelastic response

for the corresponding indenter locations for both the small and medium fish scales in Figures 4.51 and 4.52.

To note the calculated values of E' and E'' can be affected by the uncertainties in accuracy for the measured the contact area, especially at lower indentation depth where full contact may not have been established. However, the Berkovich indenter tips usually maintain full contact for at least the "***unhydrated case***" allowing for an accurately determined contact area (Sneddon, 1965; Rho, Zioupos, Currey, and Pharr, 2002; Swadener, George, and Pharr, 2002; Bei, George, Hay, and Pharr, 2005; Fischer-Cripps, 2006; Pharr, Strader, and Oliver, 2009; Pharr, Herbert, and Gao, 2010; and Randall, Vandamme, and Ulm, 2011). Thus the dynamic INI experimental technique is ideally suited for measuring the viscoelastic effect of the indented materials at shallow depths (Oliver, and Pharr, 1992; Hay and Pharr, 2000; VanLandingham, 2003; Oliver, and Pharr, 2004; Golovin, 2008; Pharr, Strader, and Oliver, 2009; Hay, 2009; Ryou, Romberg, Pashley, Tay, and Arola, 2012; and Sun, Ling, Wang, Chen, Zhang, Tong, and Wang, 2014).

Viscoelastic materials are commonly characterized by their E' and E'' moduli where the former represents the stored energy or the elastic response, and the latter corresponds to the amount of energy dissipated or the viscous response, as well as their ratio – the loss tangent is calculated as the ratio of loss to storage. During the dynamic INI experiment as the indenter tip penetrates the specimen, illustrated in Figure 4.53, a harmonic force oscillation is applied to the tip, which generates an oscillatory harmonic displacement response at the same frequency of force application. A phase locked harmonic oscillating force is applied to measure the frequency specific harmonic displacement response, and determine the phase angle (Φ)—also termed the phase lag—between the two harmonic signals, Figure 4.54. The phase locked harmonic
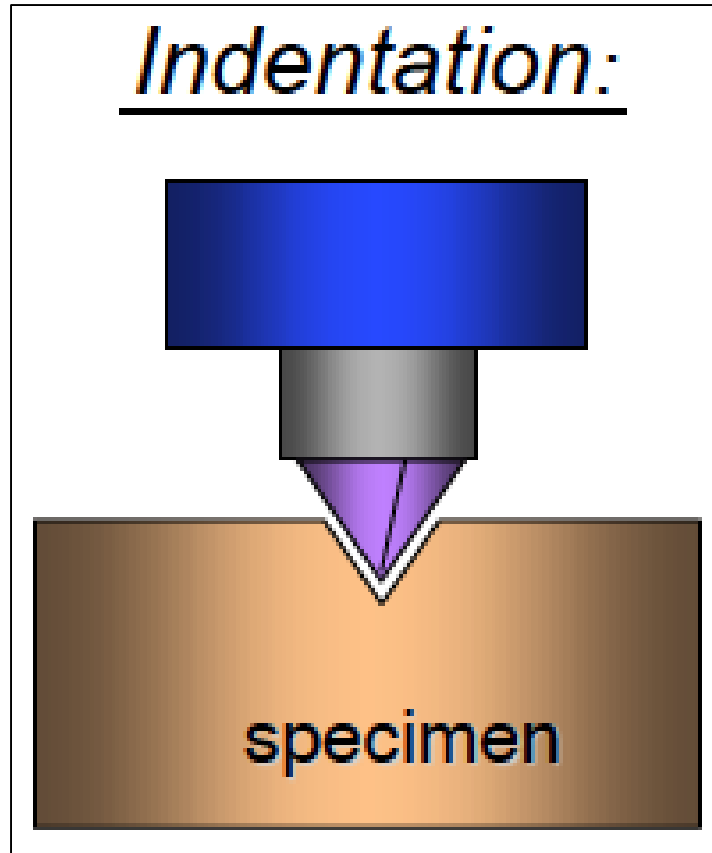
Figure 4.53 Illustration of indenter tip penetrating
a specimen (Pharr and Strader, 2009).
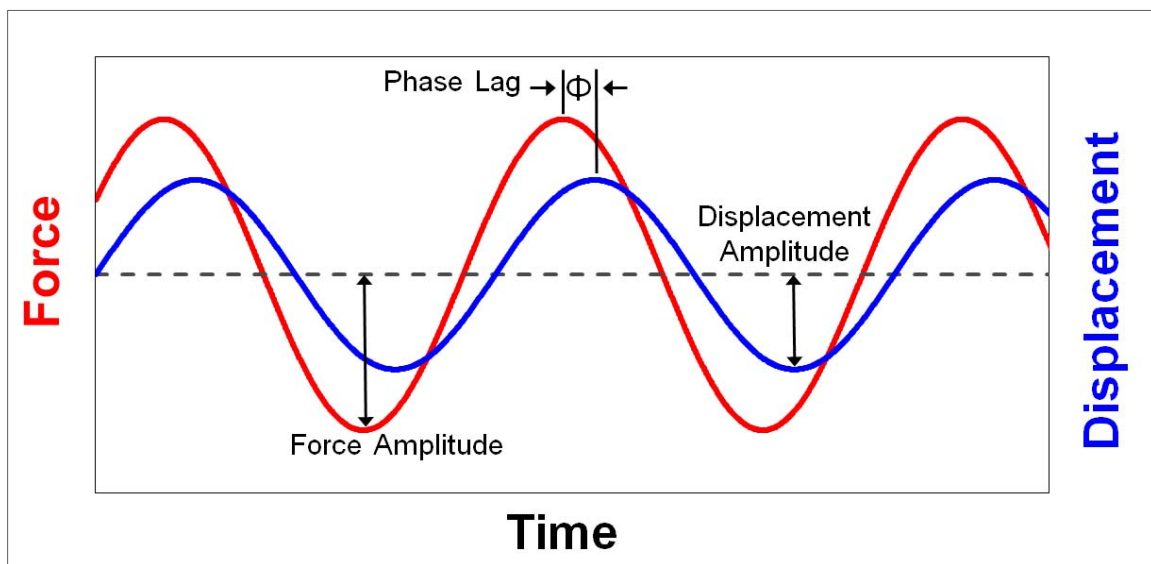
Figure 4.54 Phase lag (tan Φ) determined from storage and loss modulus
for viscoelastic behaving materials (Hay and Crawford, 2011).

137

oscillation allows the harmonic displacement to be in phase with the applied harmonic force causing an instantaneous displacement response due to the external force application. As damping is introduced into the sample, through the viscoelastic collagen fibers, the displacement response starts to lag behind the force application. The lag is measured through the phase angle separation between the harmonic force application and the frequency specific displacement response. To isolate the response of the sample, the instrument is modeled as a force, damped oscillator with a modified *Voigt* model to capture the viscoelastic behavior (Wright, Maloney, and Nix, 2007; Herbert, Oliver, and Pharr, 2008; Jager, and Lackner, 2008; and Hay and Crawford, 2011).

The schematic viscoelastic model used when conducting the INI experiment is a modified Voigt solid model, having a spring in series with a spring and dashpot that are in parallel and connected in parallel with a simple spring with an adjacent parallel dashpot, illustrated by Figure 4.55 (Golovin, 2008). Where in the Voigt model denoting the mass (m), contact stiffness (S), contact damping, (D_S), machine damping (D_m), finite stiffness (k_f), and spring stiffness (k_s), as shown in Wright, Maloney, and Nix (2007). The models' configuration allows for determination of the energy dissipative behavior for differing storage and loss modulus relaxation times as a function of $\tan(\phi)$.

Assuming (1) the instrument can be modeled as a forced, damped oscillator that is limited to one-degree of freedom, (2) the contact measurements must be made in the linear viscoelastic regime of the sample, and (3) measurements are only performed under conditions of steady-state harmonic motion linear viscoelastic behavior, then the phase lag ($\tan \Phi$) for the sinusoidal
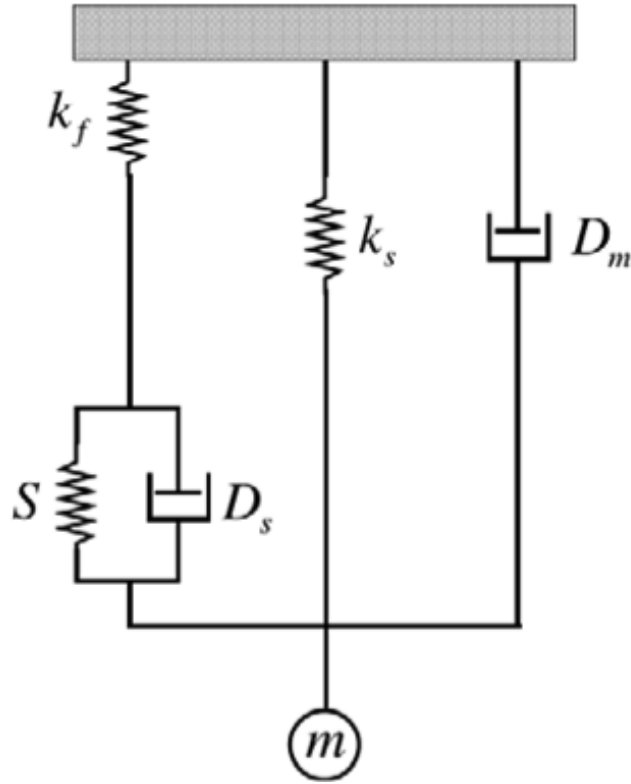
Figure 4.55 Illustration of modified Voigt
model used for dynamic instrumented
indentation analysis (Wright,
Maloney, and Nix, 2007).

phases, show in Figure 4.54, can be computed from the data using the following the calculations

(Herbert, Oliver, and Pharr, 2008):

$$S = \frac{F_0}{h_0} \cos \varphi \quad (1),$$

$$C\omega = \frac{F_0}{h_0} \sin \varphi \quad (2), \text{ and}$$

$$\frac{C\omega}{S} = \tan \varphi \quad (3),$$

where F_0 is the harmonic force amplitude, h_0 is the harmonic displacement amplitude, and ϕ is

the phase angle between the two harmonic signals. To isolate the response of the sample, the

instrument is modeled as a force, damped oscillator.

To better elucidate the instantaneous dampening response in the dynamic INI experiment, a single frequency in the lower quasi-static frequency range of 5-Hz was used as opposed to traditionally conducting a full frequency sweep for DMA. Although, the biomineralized fish scale has complex highly heterogeneous structure conducting the INI-DMA experiment at a single frequency is sufficient and a novel approach to use the measured tan ϕ parameter to show energy dissipative response. Shown in Figure 4.56, is the calculated phase angle both the small and medium scales.
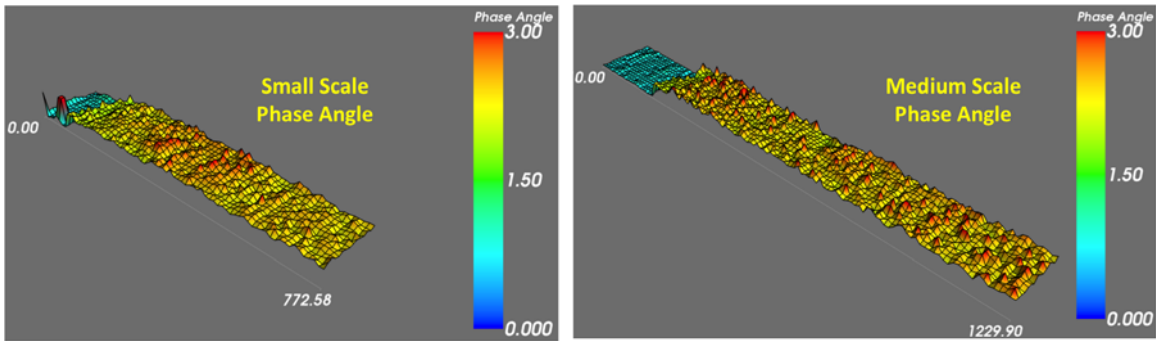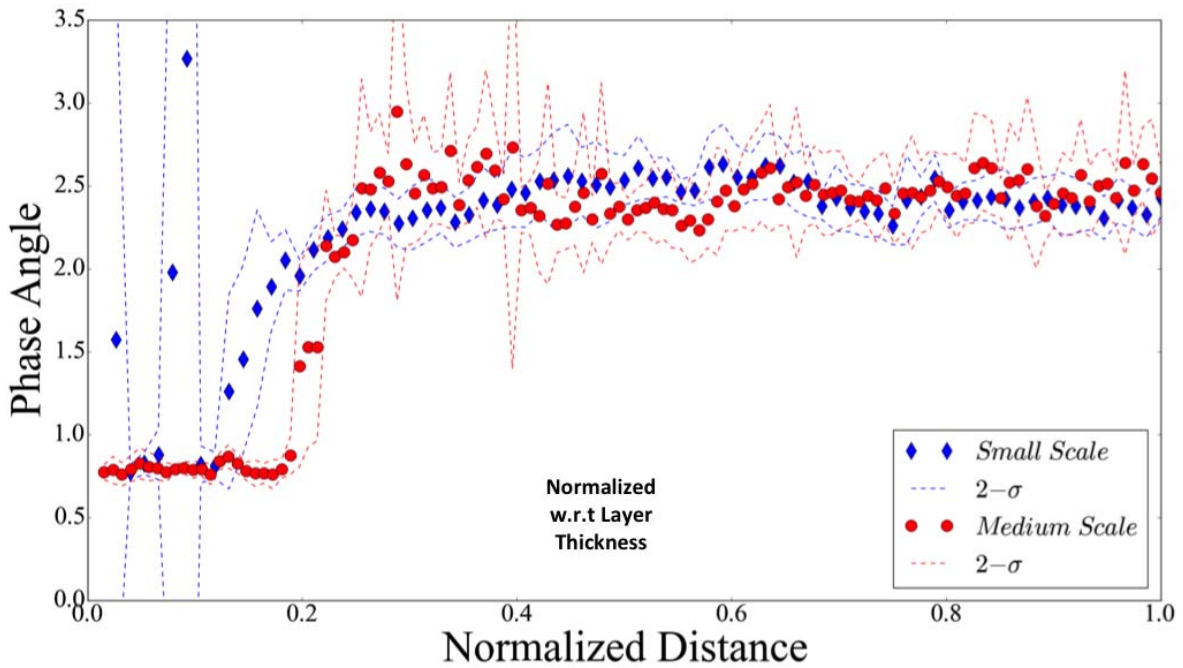
Figure 4.56 Nanoindentation phase angle, tan (ϕ), for storage and loss modulus for small and medium dehydrated fish scale.

Like, the previously measured mechanical properties, the phase angle gradients are occurring through the ITZ from [0.20 to 0.40] and [0.10 to 0.40] normalized distances, with respect to layer thickness, for the small and medium fish scales, separately. In the outset of each line plot, the median properties for small and medium scales are shown using blue diamonds and red circles, comparatively. Each data point represents the average calculated. The corresponding colored dashed lines represented by two standard deviations (2σ) show the upper and lower bound for the orthogonal phase angle parameter grading. Meaning the upper and lower lines are respectively twice the standard deviations from the mean making the zone between four standard deviations. The (tan Φ) value is interpreted as the higher the value the more energy dissipative at the local indention site and vice versa. The surface plots better show three-dimensional variation for the local maxima and minima results.

The line plots in the ganoine layer for the medium scale shows a near constant but much lower (tan Φ) away from the interface; whereas, the small-scale plots show lower (tan Φ) that have large variations in the ganoine layer when crossing the interface. Shown in the surface plots, for the bone layer the average phase angle is comparable for both scale sizes with the difference being the medium scale has a wider variation nearer to the interface. Distinctively the ganoine layer has a phase angle ranging from [0.75-3.5$^+$]° in the small scale compared to [0.75-0.80]° in the medium scale. But in the bone layer the small and medium scales consistently have much higher phase angles with ranges of [2.30-2.40]° and [2.25-2.50]°, comparably.

The medium fish scale has a sharp slope occurring in the ITZ with average phase angle changing from [0.75-2.00]° unlike the small fish scale which has more of a gradual slope with the same phase angle values. The phase angles for the medium and small scales show an interesting trend in the bone layer over the same distance from the interface. The trend tends to

141

show as the fish scale grows; the bone layer for the medium scale becomes more energy dissipative with a higher variation than the small scale in the bone layer. Unlike in the ganoine layer for the medium scale there is much lower energy dissipative behavior observed with the minimal variation. For the small scale in the ganoine layer the dampening behavior is fairly inconsistent and changing. The trends also suggest the ITZ is the key and heavily influences the maturation of the layers. With aging the ganoine layer becomes more mineralized, shown by the sharper phase angle gradient thus being denser/stiffer whereas the bone layer becomes more porous/compliant. There is much greater variation in the energy dissipative behavior than suggested by the measured elastic and hardness properties, suggesting the material in the ITZ is not as discrete as the measured mechanical properties might indicate. This difference is marked by an increased energy response occurring on the bone side immediately adjacent to the interface. Evidently the difference grows with age. Thus, the geometrically connected saw tooth structured interface, combined with the additional energy dissipative/damping effect, might minimize stress localization and delamination in the ITZ. When the layers are combined, the outer ganoine layer achieves high strength and is possibly used as a protective layer whereas the interior layer achieves high toughness, a combination that produces an advanced high performance composite material provided delamination is resisted. Understanding delamination resistance allows the development of better composites.

While there remains a level of uncertainty for identifying all contributors to the energy dissipative/damping behavior in the fish scale, the phase angle results indicate the loosest compact biomineralized region in the fish scale exhibits much higher energy dissipative potential. The higher dampening behavior is unique to the bone layer and is more than likely attributed to the loosely packed chaotically ordered collagen fibers. The loosely packed bone

layer identified throughout the hierarchal chemical/structural analysis appears to mostly use collagen fiber bundles to introduce anisotropic reinforcement at the nanoscale. The nanoscale collagen fiber reinforcement seems to dampen/dissipate energy at the largest length scale for the composite when loaded externally.

4.4 Summary of Findings

A systematic detailed approach was used to identify controlling mechanisms by discovering the scale-dependent fish scale structure that governs its mechanical response as a function of chemical composition and hierarchal structural arrangement. The fish scale was found to be a robust advanced composite, having a simple elemental composition. Subtle differences in chemical processes appear to form the fish scale's layered structure while using elements that remain relatively uniform throughout the scale. Within the fish scales the structural hierarchy takes on several morphological arrangements that are not obvious from individual microscopy techniques (Optical, HR-SEM, or TEM) when used alone. Innovative experimental and data analysis techniques were employed for interpreting the relationship between these chemically based differences with differences in mechanical response. A novel application of nano-scale engineering measurements was used to isolate and better understand the extremely complex contributions for the assembled structural components and their subunits. For better clarity the scientific and engineering results presented in Chapter 4 will be discussed in greater detail in Chapter 5. Also addressed in Chapter 5 are the specific questions raised by the hypothesis, insight provided for the biological design principles, and suggested methodologies for developing bioinspired engineered composite designs that exhibit advanced high-performance.

CHAPTER 5: DISCUSSION

The results discussed in Chapter 4 provided sufficient evidence to test the hypothesis *(H)*. The hypothesis *(H)* stated was the fish scales are effective in resisting cracks, dissipating energy, and transferring loads across interfaces because of the grading of the composite layer properties. The hypothesis is found to be consistent with the data and from the comprehensive experimental investigation the results verified the following: (a) interfaces exist and (b) the layers are graded. The test of, *H*, there is a significant difference in the material above, below, or between layers and the difference in material arrangement is the reason for the fish scale's attributes. To further expand on how the results were used to test and prove the hypothesis to be true a discussion addressing the overall research objective is provided for the remainder of Chapter 5.

The overall objective was to use experimentation to provide insight on what are the inherent chemical, structural, and mechanical attributes of bio-engineered fish scale composites found in the alligator gar's exoskeleton. Experiments were used to determine (a) how is the natural composite system assembled, (b) how do the layer thickness and the functionalized gradient properties interact to achieve high toughness, (c) what are the design principles of natural armor systems, and (d) how can these design principles be applied to the design of man-made engineered composite systems. The pertinent information gathered helped provide the necessary details to allow an adequate assessment of the biomineralized fish scale attributes as a superior performing advanced composite.

5.1 Discussion

5.1.1 Natural Composite System Assembly

The fish scale's composite system is assembled using periodic elements most often found in nature. The fish scale uses eight elements to develop, maintain, and evolve its structure. The elements of carbon, phosphorus, oxygen, nitrogen, and hydrogen are used to form the amide, phosphate, and carbonate chemical groups. The carbonate compound controls the degree of mineralization by substituting with magnesium and sodium. Finally, calcium is the primary element used to mineralize the bio-structure.

The fish scale was observed to use at least 3-levels of length scale hierarchy to form its structure. The biomineralized composite uses the chemical groups to form the two structural sub-units of bioapatite (B-Ap crystals) and Type I-Collagen (fibrils) phases at the nanoscale. Although the geometric dimensions of the collagen are 14-order of magnitudes larger than the bioapatite crystals, by volume the crystals occupy at least 90-percent of the fish scale's space. Furthermore, at the nanoscale, the collagen and B-Ap crystals are not attached by their surfaces. Rather the crystal subunits are embedded, at sharp angles, along the collagen fiber strands length.

At the micron level the collagen bundles + B-Ap crystals (C/B-Ap) form a distinctive two-layered system that is connected by what is described as sawtooth geometrically structured interface. The outermost layer for the fish scale is called ganoine while the inner layer called bone. The ganoine layer does not provide full coverage over the bone layer. Additionally, as the layers grow the ratio of their thicknesses remain relatively constant. As an aside, the current research effort has provided never before shown proof that collagen does not tend to appear as ridged/stiff rods at any length scale as reported by many previous researchers (Bruet, Song, Boyce, and Ortiz, 2008a; Bruet, 2008b; Chen, Lin, Yang, Lopez, Li, Olevsky, and Meyers, 2011;

Allison, et al. 2013; Yang, Gludovatz, Zimmermann, Bale, Ritchie, and Meyers, 2013b; and Han, Wang, Song, Boyce, and Ortiz, 2011). In fact collagen fibers were shown to possess degrees of freedom that allow for bending, stretching, and twisting and therefore cannot be appropriately described as having a rigid needle structure. What has been interpreted as the needle-like collagen strands are actually the hidden fine nanometer cornflake-structured B-Ap crystals passing through the banded collagen bundles. As a result, when conducting morphological studies using HR-SEM at the micron scale, the magnification is too coarse and the results are easily misinterpreted. However, at the nanometer length scale, with the use of TEM and STEM-HAADF-EELS, the true morphology was uncovered.

Finally, at the millimeter length scale the fish scales have long and short axis. The scale's shape appears to have subtle curvature around its perimeter that converges at the vertices to form sharp points similar to arrowheads. The layer thickness seems to lead to its overall shape. Also, the curved perimeter of the scales is thinner on the edge and overlap when connected to other scales.

5.1.2 Functionalized Gradient Properties

Overall the fish scale structure uses the same limited mineralogical constituents throughout the structure. The mineralogical constituents are used to form the two structural sub-units of bioapatite (B-Ap crystals) and Type I-Collagen (fibrils) in the two-layered structure. Independently the collagen fibers and hydroxyapatite minerals phases are weak. However, the ganoine and bone layers uniquely use the subunits, along with the controlling the collagen fibers and hydroxyapatite volume fractions, combined with optimizing morphological arrangements materials within in its structural hierarchy to functionally grade the properties. Additionally, the geometrically connected saw tooth structured interface, combined with the additional viscous

146

damping effect, might minimize stress localization and delamination in the ITZ. When the layers are combined, the outer much thinner ganoine layer achieves high strength and is possibly used as a protective layer whereas the interior's much thicker layer achieves high toughness, a combination that produces an advanced high performance composite material provided delamination is resisted and the system is fully hydrated. The fish scale structure has the likeness of a steel plate attached to a bed of springs with varying spring stiffnesses.

5.1.3 Design Principles of Natural Armor Systems

This investigation has made new discoveries of mechanisms that can inherently describe the attributes that govern the fish scale hierarchy mechanical response as a function of chemical composition and structural arrangement. The design principles of natural armor system are as follows:

(a) The structure of the biomineralized fish scale composite has both short and long range order. The ganoine layer is highly ordered. Densely compact the layer contains an abundance of B-Ap minerals and very little collagen fibrous material leading to the layer's high strength. This ordered structure is in contrast with the bone layer, which is chaotically ordered, loosely compact, and containing an abundance of collagen with similar volumes of B-Ap minerals, leading to the layers with high toughness.

(b) The structure grows from the ganoine-bone curved saw-tooth geometrically structured interface outwards. The ganoine-bone interface is the oldest of the layers, therefore has shown to be the densest region in the fish scale structure. Because of geometrically mechanical interlocking and similar material densities, a less discrete (graded) interface exists which might provide durability and delamination resistance.

(c)   The fish scale structure uses the same limited mineralogical constituents throughout the structure. Since the fish scale uses limited constituents, the selected materials tend to be indigenous and are routinely abundant in nature. Consequently, the same limited mineralogical constituents allow for chemical, structural compatibility, and may evolve when queued by external stressors.

(d)   The fish scale creatively uses the minimal components of collagen fibers and bioapatite minerals materials to efficiently optimize the structural composite. Remember the fish scale's structure is efficiently produced at ambient conditions using minimal material types. Nature focuses mainly on making use of the structural hierarchy to optimize the geometric arrangement, the volume fractions, and grading of properties for the components during the growth processes. The resulting structure ultimately dictates the mechanical response at the system level.

As a result of the aforementioned design principles for the natural armor fish scale system, a high-performance advanced composite structure is formed. The simple two phases are used to form a very robust complex hierarchal functionally property-graded composite structure. The exoskeleton fish scale is very attractive to the design community because layered composite possesses the attributes of being lightweight, high-strength, high-stiffness, and energy absorbent/ dissipative. In addition the fish scale appears to be delamination resistant when fully hydrated.

5.1.4 Application of Bio-Inspired Design for Designing Man-made Engineered Composite Systems

Shown in Figure 5.1, is the illustration I develop for an effective application of the biological design principles to design man-made engineered composites is made possible by the evolving additive manufacturing technology, in concert with a computational test bed for optimizing material properties for the structural design.
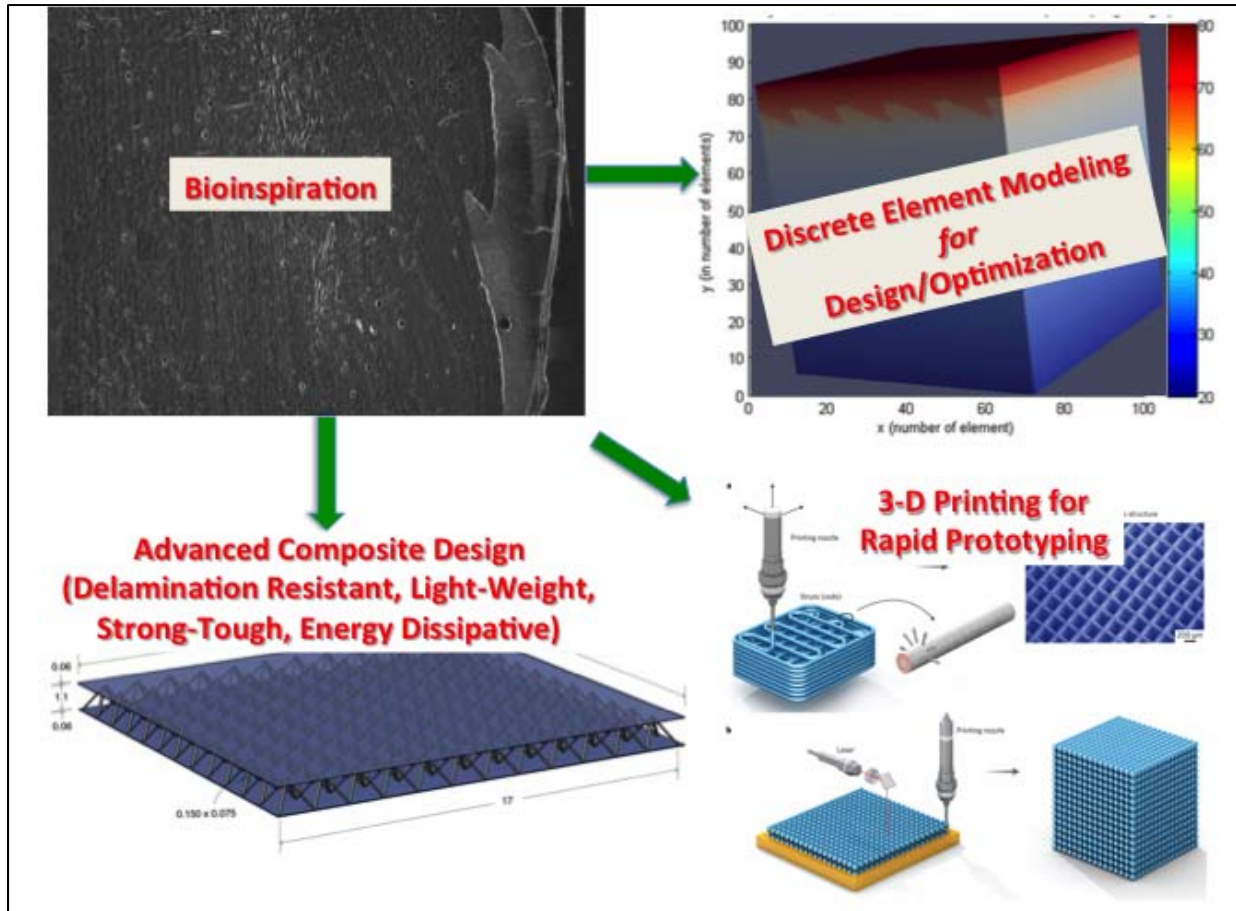
Figure 5.1 Illustration of how research findings can make use of modeling and rapid prototyping methods to better understand mechanisms that transfers stress across interfaces.

The results in Chapter 4 showed the fish scale is highly detailed due to the complex biological formation processes at the lower nanometer range. Because the formation processes are not well understood attempting to incorporate the intricate details from the nano to millimeter length scale in manufacturing is not feasible at present. However, building the layered system, observed at the micron scale, with the structured interface, which included property grading, is an ideal controllable approach when employing additive manufacturing technologies.

Additive manufacturing technologies such as three-dimensional (3-D) printing allows the flexibility to *"control the manufacturing process"* down to tens of microns. Another advantage

149

of 3-D printer bench scale designs can be rapidly prototyped in less than one day unlike

subtractive (traditional) manufacturing process that require retooling and resetting dyes each

time designs are changed. Also worth mentioning is laminated composite, the current industry

standard, are design/manufactured to at best to include orthotropic reinforcement. The current

3-D printing technologies also accommodate the use of a variety of multiple materials (e.g.,

polymers and plastics) that have variance in mechanical properties, allowing for the design/

manufacturing anisotropic strengthened composites beyond simple composite designs.

Specifically, 3-D printing could be used as means to manufacture a scaled up geometric

model for the fish scale, using the principles of similitude and dimensional analysis, to isolate

and study the role the layer thickness and structured interface plays in transferring load across

the layers for a single material type. Also, by using a computational test bed, the structural design

can first be optimized for the irregular geometry.

As a first approximation of the averaged mechanical properties using finite element

modeling may be sufficient when optimizing single material type in a one-controllable structural

parameter design. However, finite element modeling (FEM) is not adequate to discern the four

attributes of functionally graded properties found in the fish scale: varied multilayered thickness,

anisotropic reinforcement structures, heterogeneous material system and a structured saw-tooth

interface. Each attribute is a discrete feature having its own length scale and to some extent

interacts in an imbricated structure that is difficult to capture in an averaged representative

volume as required by a continuum approach such as FEM. A more appropriate modeling

technique for optimizing the multi-structural parameters, using the computational test bed, is the

discrete element method (DEM) to ascertain the relevance of each structural parameter

describing fish scale.

As discussed in Chapter 4 in the nanoindentation results Section 4.3.3, the local variation of properties are often masked with averaging techniques derived from continuum mechanics, which are primarily used to determine constitutive relationships for the global stress and strains in FEM. Although DEM uses similar phenomenological relationships to define interactions, the method is based on discrete systems rather than discrete approximations to continuous partial differential equations. In DEM, as in the actual material, incompatible degrees of freedom acting at multiple scales can interact, whereby it is possible to analyze particle-scale deformation, stress, rotations and couples that develop within locally grouped particle. Additionally, DEM can be used to identify the internal connectivity of the systems using coordination number to determine where force chains are likely to occur before shear banding percolates to the surface as an observable defect. Therefore the discreteness of DEM allows for a thorough sensitivity analysis to determine which discrete combinations of structural design parameters have the most effect over the mechanical response.

The optimization process using DEM and 3-D printing as complimentary tools can be further used to reduce the composite's weight while maintaining the same strength-to-weight ratio. The materials can be varied in 3-D printing to match the microstructures designed using DEM. The caveat is the materials used should be chemically compatible to minimize the debonding.

Additionally, civil engineers are interested in incorporating multifunctional materials. During the manufacturing process electronic materials could be used in 3-D printing of the structure. For instance biopolymers, carbon nanotubes, or graphene sheets could be used in the design as a self-sensing material and used as a means to self-report undesired detrimental deterioration cause by the environment or external loading conditions.

151

5.2 Summary of Discussion

The research findings support the hypothesis that the favorable mechanical properties of fish scale is enabled by graded layer structures existing over a range of length scales. The biomineralized fish scale composite is complex and hierarchically structured. Nature does not design structures rather it designs for functionality using whatever materials are indigenous to the geographical location. In the fish scale, nature appears to have focused on optimizing the geometry of the structure to serve some unknown function. From a design perspective, nature created a composite structure that seems to be resilient and can evolve on as needed basis, to tailor its structure to obtain the most favorable mechanical attributes. There are only two individual structural components that are used in the biological composite.

The lessons learned from the current investigation are thought to be transferable to other biomineralized composites and also valid for the bioinspired design of man-made engineered composites. Furthermore, the bioinspired design space can make use of the emerging 3-D printing additive manufacturing technologies along with using computational test bed with DEM modeling as a proving ground to optimize both the structure and materials. The future is also promising for adding multifunctionality by adding electronic materials to the design space for self-monitoring and self-reporting on structural health. In the next chapter, Chapter 6, the major conclusions discovered and innovation that has been produced from this compressive research effort will be explained.

CHAPTER 6: SUMMARY/CONCLUSIONS/FUTURE WORK

6.1 Summary

The focus of this study was to learn how nature integrates hard and soft materials at each length scale to form a layered composite that is lightweight, has high-strength with good fracture toughness but does not delaminate. Previous research conducted by others had suggested that from the nano-to-millimeter length scale the individual components of the fish scale are glued rather than being integrated to form layers in the composite. My research provided a detailed description, using novel experiments, to explain how hard and soft materials are mixed and integrated at each length to form a layered structure. In addition, my research provided details on how the hard and soft materials have been optimized by volume fractions, spatial proximity, and directional placement within the layers. Furthermore, the material variations were compared to mechanical properties of modulus, hardness, and, for the first time, energy dissipation was used to explain why fish scale has high strength, good toughness, and may not delaminate.

6.2 Contributions/Conclusions

The research contributions from my work for the first time provided from experimental measurements the following conclusions of how the fish scale has high-strength, good toughness, and may be delamination resistant when individual hard (inorganic minerals) and soft (polymer-like organic collagen fibers) materials are used:

(a)   The combination of hard (inorganic minerals) and soft (polymer-like organic collagen fibers) materials are integrated instead of being glued at nano length scale. At the micron scale for the two-layered composite materials, the outer dental enamel (hard) layered interface uses a saw tooth geometrical shaped joint to connect to the inner bone (hard open-like

foam) layer. At the millimeter scale the material and mechanical properties are gradually graded through the thickness, away from the enamel-bone saw tooth connected interface, for approximately 150 microns into each individual layer.

(b)   Within each layer, at the micron scale, there are subtle variations in the spatial proximity, and directional placement of the hard and soft materials. However, the outer enamel (hard) layer has 90 percent hard (inorganic minerals), 10 percent soft (polymer-like organic collagen fibers) by volume and the materials in the layer are densely packed. Whereas, the inner bone (hard open-like foam) layer contains 60 percent hard (inorganic minerals) and 40 percent soft (polymer-like organic collagen fibers) by volume, and materials in the layer are loosely packed.

(c)   My research developed a new experimental technique that was used to map the local viscoelastic (energy dissipative) response, attributed to the mixing/integrating of hard (inorganic minerals) and soft (polymer-like organic collagen fibers) volume fractions, within the layers at the nano length scale. The instrumented nanoindentation-dynamic mechanical analysis experimental method was modified and was used to show variation due to change in material volume fractions and local placement of materials within the layers. For the outer enamel (hard) layer there was minimal variation of the local viscoelastic property and there was minimal viscoelastic contribution provided by the soft (polymer-like organic collagen fibers) within the layer. For the inner bone (hard open-like foam) layer there was major variation of the local viscoelastic property and there was major viscoelastic contribution provided by the soft (polymer-like organic collagen fibers) within layer.

(d)   If fully hydrated, the fish scales may resist cracks and delamination because of how the hard and soft materials are mixed/integrated within the layers from the nano-to-micro length

scales, along with the way the two layers grade the properties away from the interface at the millimeter scale. Evidently, the fish scale has optimized the hard (inorganic minerals) and soft (polymer like organic collagen fibers) material volume fractions, variations within the layers, and uses gradual layer property transitions to reduce the local stresses that lead to delamination and crack formation caused by impact/penetration.

6.3 Future Work

The current research identified the main materials in the two-layered composite as hard (inorganic minerals) and soft (polymer-like organic fibers). The materials are integrated at the nano scale and are likely to contribute to the superior delamination resistance. The two integrated materials and the layers should be modeled using the discrete element method to rank which aspects are most important:

(a)   How do gradual transitions between layers that contain the same components, but with different concentrations and textures of these components, distribute load, and increase desired physical properties?

(b)   Is the geometric saw tooth joint at the micron scale the best design to connect the two layers?

(c)   How can the variations in material volume fraction, layer thickness, or layer density be optimized and possibly lead to the creation of stronger, lighter, tougher, more delamination resistant composite systems?

REFERENCES

Aizenberg, J., Weaver, J. C., Thanawala, M. S., Sundar, V. C., Morse, D. E., and Fratzl, P. (2005). "Skeleton of Euplectella Sp.: Structural Hierarchy from the Nanoscale to the Macroscale." *Science* 309: 275-278.

Albarede, F. (2003). Geochemistry: An Introduction. Cambridge, UK:Cambridge University Press.

Alfaro, R. M., Gonzales, C. A., and Ferrara, A. M. (2008). "Gar Biology and Culture: Status and Prospects." *Aquaculture Research* 39: 748 – 763.

Allison, P. G., Chandler, M. Q., Rodriguez, R.I., Williams, B.A., Moser, R.D., Weiss, C.A. Jr., Poda, A.R., Lafferty, B. J., Kennedy, A. J., Seiter, J. M., Hodo, W. D., and Cook, R. F. (2013). "Mechanical Properties and Structure of the Biological Multilayered Material System, Atractosteus Spatula Scales." *Acta Biomaterialia* 9(2): 5289-5296.

Allison, P. G., Rodriguez, R. I., Moser, R. D., Williams, B. A., Poda, A. R., Seiter, J. M., Lafferty, B. J., Kennedy, A. J., and Chandler, M. Q., (2014). "Characterization of Multi-layered Fish Scales (*Atractosteus spatula*) Using Nanoindentation, X-ray CT, FTIR, and SEM." *Journal of Visualized Experiments* 89: doi: 10.3791/51535.

American Association of State Highway and Transportation Officials (AASHTO). (1993). AASHTO Guide for Design of Pavement Structures. Washington, DC: AASHTO.

Ashby, M. F., Shercliff, H., and Cebon, D. (2007). Materials Engineering, Science, Processing and Design, First Edition, Massachusetts: Elsevier Ltd.

Ashish, W., Mehta, Y., Cleary, D., Guo, E., Musumeci, L., Zapata, A., and Kettleson, W. (2011). "Load-Transfer Efficiencies of Rigid Airfield Pavement Joints Based On Stresses and Deflections." *Journal of Materials in Civil Engineering* 23(8): 1171–1180.

Bahrololoom, M. E., Javidi, M., Javadpour, S., and Ma, J. (2009). "Characterization of Natural Hydroxyapatite Extracted From Bovine Cortical Bone Ash." *Journal of Ceramic Processing Research* 10(2): 129-138.

Balooch, G., Marshall, G. W., Marshall, S. J., Warren, O. L., Asif, S. A., and Balooch, M. (2004). "Evaluation of a New Modulus Mapping Technique to Investigate Microstructural Features of Human Teeth." *Journal of Biomechanics* 37: 1223–1232.

Baohua, J., and Huajian, G. (2010). "Mechanical Principles of Biological Nanocomposites." *Annual Reviews of Materials Research* 40: 77 – 100.

Barthelat, F. (2007a). "Biomimetics for Next Generation Materials." *Philosophical Transactions of The Royal Society: A* 365: 2907 – 2919.

Barthelat, F., and Espinosa, H. (2007b). An Experimental Investigation of Deformation and Fracture of Nacre–Mother of Pearl. *Experimental Mechanics* 47: 311–324.

Bartol, I. K., Gharib, M., Weihs, D., Webb, P. W., Hove, J. R., and Gordon, M. S. (2003). "Hydrodynamic Stability of Swimming in Ostraciid Fishes: Role of the Carapace in the Smooth Trunkfish Lactophrys Triqueter (Teleostei: Ostraciidae)." *Journal Experimental Biology* 206: 725–44.

Bauerlein, E., Behrens, P., Epple, M., and Pickett-Heaps, J. (2007). Handbook of Biomineralization: Biological Aspects and Structure Formation, 3 Volume Set, Wiley-VCH.

Bei, H. B., George, E. P., Hay, J. L., and Pharr, G. M. (2005). "Influence of Indenter Tip Geometry on Elastic Deformation During Nanoindentation." *Physical Review Letters* 95: 4-pp.

Beniash, E. (2011). "Biominerals-Hierarchical Nanocomposites: The Example of Bone." *Wiley Interdisciplinary Reviews: Nanomedicine and Nanobiotechnology* 3(1): 47-69.

Bertassoni, L. E. and Swain, M. V. (2012). "Influence of Hydration on Nanoindentation Induced Energy Expenditure of Dentin." *Journal of Biomechanics* 45: 1679-1683.

Bhushan, B. (2009). "Biomimetics: Lessons from Nature – An Overview." *Philosophical Transactions of The Royal Society: A* 367: 1445—1486.

Bigi, A., Cojazzi, G., Panzavolta, S., Ripamonti, A., Roveri, N., Romanello, M., Noris Suarez, K., and Moro, L. (1997). "Chemical and Structural Characterization of the Mineral Phase from Cortical and Trabecular Bone." *Journal of Inorganic Biochemistry* 68: 45-51.

Boskey, A. L. (1991). "The Role of Extracellur Matrix Components in Dentin Mineralization." *Critical Reviews in Oral Biology and Medicine* 2(2): 369-387.

Boskey, A. L. (2007). "Mineralization of Bones and Teeth." *Elements* 3(6): 385—391.

Bozec, L., de Groot, J., Odlyha, M., Nicholls, B., Nesbitt, S., Flanagan, A., and Horton, M. (2005). "Atomic Force Microscopy of Collagen Structure in Bone and Dentine Revealed by Osteoclastic Resorption." *Ultramicroscopy* 105: 79-89.

Brandstatter, J. J. (1963). Theory of Elasticity of an Anisotropic Elastic Body. San Francisco, CA: Holden Day.

Brill, D. R., (1998). Development of Advanced Computational Models for Airport Pavement Design. FAA Technical Report DOT/FAA/AR-97/47. Washington, DC: Department of Transportation.

Bruet, B., Song, J., Boyce, M., and Ortiz, C. (2008a). "Materials Design Principals of Ancient Fish Armour." *Nature Materials* 7: 748 – 756.

Bruet, B. J. F. (2008b). Multiscale Structural and Mechanical Design of Mineralized Biocomposites. *PhD. Dissertation*. Massachusetts Institute of Technology, Boston, Massachusetts, USA

Buehler, J. (2007). "Nano- and Micromechanical Properties of Hierarchical Biological Materials and Tissues." *Journal of Materials Science* 42: 8765–8770.

Bull, J. W., and Singh, A. (1990). "A Comparison Between the Stresses Computed for Finite Sized Precast Concrete Pavement Units Using Westergaard's Equations and a Numerical Design Method." *Computers and Geotechnics*, 9(4): 325-340.

Callister, Jr., W. D., and Rethwisch, D. G. (2008). Fundamentals of Materials Science and Engineering: An Integrated Approach, 3rd Edition. USA: John Wiley & Sons Ltd.

Canton, J., and Tucker, A. (2009). "Current Knowledge of Tooth Development: Patterning and Mineralization of the Murine Dentition" *Journal of Anatomy* 214: 502-515.

Carlino, E., and Grillo, V. (2006). "Atomic Resolution STEM-HAADF Imaging in the Study of Interfaces." *Archives of Metallurgy and Materials* 51(1): 23-32.

Chandler, M. Q., Allison, P. G., Rodriguez, R. I., Moser, R. D., and Kennedy, A. J. (2014). "Finite Element Modeling of Multilayered Structures of Fish Scales." *Journal of the Mechanical Behavior of Biomedical Materials* 4: 375-389.

Chang, M. C., and Tanaka, J. (2002). "FT-IR Study for Hydroxyapatite/Collagen Nanocomposite Cross-Linked by Glutaraldehyde." *Biomaterials* 23: 4811-4818.

Chang-Yu, S., and Chen, P-Y. (2013). "Structural Design and Mechanical Behavior of Alligator (Alligator Mississippiensis) Osteoderms." *Acta Biomaterialia* 9(11): 9049-9064.

Chen, P.-Y., Lin, Y.-S.,Yang, W., Lopez, M. I., Li, J., Olevsky, E. A., and Meyers, M. A. (2011). "Predation versus Protection: Fish Teeth and Scales Evaluated by Nanoindentation." *Journal of Materials Research* 27(1): 100 – 112.

Chen, P., McKittrick, J., and Meyers, M. (2012). "Biological Materials: Functional Adaptations and Bioinspired Designs." *Progress in Materials Science* 57:1492—1704.

Chou, Y. T. (1997). Analysis of Permanent Deformations of Flexible Airport Pavements. WES TR S-77-8. Vicksburg, MS: US Army Engineer Waterways Experiment Station.

Chung, W., Oh, J., Kwak, K., Lee, B., Meyer, J., Wang, E., Hexemer, A., and Lee, S-W. (2011). "Biomimetic Self-Templating Supramolecular Structures." *Nature Materials* 478: 364-368.

Coates, J. (2000). Interpretation of Infrared Spectra, A Practical Approach. In Meyers, R. A. Encyclopedia of Analytical Chemistry. pp. 10815–10837. Chichester: John Wiley & Sons Ltd.

Columbia Accident Investigation Board. (2003). Vol. 1. Washington, DC: National Aeronautics and Space Administration and the Government Printing Office.

Constantinides, G., Ravi Chandran, K. S., Ulm, F.-J., and Van Vliet, K. J. (2006). "Grid Indentation Analysis of Composite Microstructure and Mechanics: Principles and Validation." *Materials Science and Engineering A* 430: 189-202.

Currey, J. (1999). "The Design of Mineralized Hard Tissues for Their Mechanical Functions." *The Journal of Experimental Biology* 202: 3285–3294.

Cuy, J. L., Mann, A. B., Livi, K. J., Teaford, M. F., and Weihs, T. P. (2002). "Nanoindentation Mapping of the Mechanical Properties of Human Molar Tooth Enamel." *Archives of Oral Biology* 47: 281–291.

Daget, J., Gayet, M., Meunier, F. J., and Sire J-Y. (2001). "Major Discoveries on the Dermal Skeleton of Fossil and Recent Polypteriforms: A Review." *Fish and Fisheries* 2: 113-124.

Das, B. M. (1990). Principles of Foundation Engineering 2nd Edition, Boston, MA: PWS Publishing Company.

Das, B. M. (1994). Principles of Geotechnical Engineering 3rd Edition, Boston, MA: PWS Publishing Company.

Domingo, L., Grimes, S. T., Soler-Gijón, R., and López-Martínez, N. (2009). "Analysis of the Geochemical Variability in Lepisosteid Scales from the Fontllonga-3 site (Early Danian, Tremp Formation, South Central Pyrenees, Spain): Implications for Palaeoenvironmental Studies." *Palaeogeography, Palaeoclimatology, Palaeoecology* 274: 204 – 214.

Dubey, D., and Tomar, V. (2010). "Role of Molecular Level Interfacial Forces in Hard Biomaterial Mechanics: A Review." *Annals of Biomedical Engineering* 38(6): 2040—2055.

Dunlop, J. W. C., and Fratzl, P. (2010). "Biological Composites." *Annual Review of Materials Research*. 20: 1 – 24.

Ehrilich, H. (2010). Biological Materials of Marine Origin Invertebrates. New York: Springer.

Faust, C. B., Johnston, J., and Reed, N. (1998). Modern Chemical Techniques. London, UK: Royal Society of Chemistry.

Figueiredo, M. M. (2012). Infrared Spectroscopy - Life and Biomedical Sciences, Chapter 18-Characterization of Bone and Bone-Based Graft Materials Using FTIR Spectroscopy. Accessed on November 10, 2015. http://www.intechopen.com/books/infrared-spectroscopy-life-and-biomedical-sciences.

Fischer-Cripps, A. C. (2006). "Critical Review of Analysis and Interpretation of Nanoindentation Test Data." *Surface and Coatings Technology* 200: 4153 – 4165.

Fleet, M. E., Liu, X., and King, P. L. (2004). "Accommodation of the Carbonate Ion In Apatite: An FTIR and X-ray Structure Study of Crystals Synthesized at 2-4 GPa" *American Mineralogist* (89):1422-1432.

Fleet, M. (2015). Carbonated Hydroxyapatite: Materials, Synthesis, and Application. Boca Raton, FL: Taylor and Francis.

Fratzl, P., Fratzl-Zelman, N., Klaushofer, K., Vogl, G., and Koller, K. (1991). "Nucleation and Growth of Mineral Crystals in Bone Studied By Small-Angle X-ray Scattering." *Calcium Tissue International* 48: 407-413.

Fratzl, P. (2007). "Biomimetic Materials Research: What Can We Really Learn From Nature's Structural Materials?" *Journal of The Royal Society Interface*, 4: 637—642.

Gao, H., Ji, B., Buehler, M., and Yao, H. (2004). "Flaw Tolerant Bulk and Surface Nanostructures of Biological Systems." *Mechanics and Chemistry of Biosystems* 1(1): 37-52.

Garrano, A. M. C., La Rosa, G., Zhang, D., Niu, L.-N., Tay, F. R., Majd, H., and Arola, D. (2012). "On The Mechanical Behavior of Scales From Cyprinus Carpio." *Journal of the Mechanical Behavior of Biomedical Materials* 7: 17-29.

Gayet, M., and Meunier, F. J. (1991). "First Discovery of Polypteridae (Pisces, Cladistia, Polypteriformes) Outside of Africa." *Geobios* 24: 463 – 466.

Gayet, M., Meunier, F. J., and Werner, C. (2002). "Diversification in Polypteriformes and special comparisons with the Lepisosteiformes." *Palaeontology* 45: 361–376.

Géraudie, J. (1988). "Fine Structural Peculiarities of the Pectoral Fin Dermoskeleton of Two Brachiopterygii, Polypterus Senegalus, and Calamoichthys Calabaricus (Pisces, *Osteichthyes*)" *The Anatomical Record* 221(1): 455-68.

Gibson, R. F. (1994). Principles of Composite Materials Mechanics. New York: McGraw-Hill.

Geubelle, P. H., and Baylor, J. S. (2008). "Impact-Induced Delamination of Composites: A 2D Simulation." *Elsevier Composites Part B: Engineering* 29 (5): 589 – 602.

Goldstein, J., Newbury, D., Joy, D., Lyman, C., Etchling, P., Lifshin, E., Sawyer, L., and Michael, J. (2007). Scanning Electron Microscopy and X-ray Microanalysis, 3rd Edition. New York, NY: Springer.

Golovin, Y. (2008). "Nanoindentation and Mechanical Properties of Solids in Submicrovolumes, Thin Near-Surface Layers, and Films: A Review." *Physics of the Solid State* 50(2): 2205–2236.

Goodrich, E. (1907). "On the Scales of Fish, Living and Extinct, and Their Importance in Classification." *Proceedings of The Zoological Society of London* 77(4): 751–773.

Goodsell, D. (2004). Bionanotechnology – Lessons from Nature. La Jolla, California: Wiley.

Gottfried, M. D., and Krause, D. W. (1998). "First Record of Gars *Lepissteidae Actionoterygii* on Madagascar Late Cretaceous Remains from the Mahajanga Basin." *Journal of Vertebrate Paleontology* 18[2]: 275 – 279.

Grandfield, K., McNally, E. A., Palmquist, A., Botton, G. A., Thomsen, P., and Engqvist, H. (2010). "Visualizing Biointerfaces in Three Dimensions: Electron Tomography of the Bone-Hydroxyapatite Interface." *Journal of Royal Society-Interface* 7(51): 1497-1501.

Grandfield, K., and Engqvist, H., (2012) "Focused Ion Beam in The Study of Biomaterials and Biological Matter." *Advances in Materials Science and Engineering* 2012: 6-pp.

Grunenwald, A., Keyser, C., Sautereau, A. M., Crubezy, E., Ludes, B., and Drouet, C. (2014). "Revisiting Carbonate Quantification In Apatite (Bio)Minerals: A Validated FTIR Methodology." *Journal of Archaeological Science* 49:134-141.

Gunther, H. (2013). NMR Spectroscopy: Basic Principles, Concepts and Applications in Chemistry, 3rd Edition. New Jersey: Wiley.

Gururaja, M. N. (2012). "A Review on Recent Applications and Future Prospectus of Hybrid Composites." *International Journal of Soft Computing & Engineering* 1(6): 352 - 355.

Haines, P. J. (1995). Thermal Methods of Analysis. Principles, Applications and Problems, 1st Edition. London, UK: Chapman & Hall.

Hammons, M. I., and Ioannides, A. M. (1997).Advanced Pavement Design: Finite Element Modeling for Rigid Pavement Joints. Report 1: Background Investigation. FAA Technical Report DOT/FAA/AR-95/85. Washington, DC: US Department of Transportation.

Hammons, M. I. (1998). Advanced Pavement Design: Finite Element Modeling for Rigid Pavement Joints, Report II: Model Development. FAA Technical Report DOT/FAA/AR-97/7. Washington, DC: Department of Transportation.

Han, L., Wang, L., Song, J., Boyce, M. C. and Ortiz, C. (2011). "Direct Quantification of the Mechanical Anisotropy and Fracture of an Individual Exoskeleton Layer via Uniaxial Compression of Micropillars." *Nano Letters* 11(9): 3868-3874.

Hanus, M. J., and Harris, A. (2013). "Nanotechnology Innovations for the Construction Industry." *Progress in Materials Science* 58(7): 1056-1102.

Hay, J. L., and Pharr, G. M. (2000). Instrumented Indentation Testing, Kuhn, H., and Medlin, D., (eds), ASM Handbook Volume 8: Mechanical Testing and Evaluation, 10th Edition. Materials Park, OH: ASM International. pp. 232–243.

Hay, J. L. (2009). "Introduction to Instrumented Indentation Testing." *Experimental Techniques* 33(6): 66-72.

Hay, J., and Crawford, B. (2011). "Measuring Substrate-Independent Modulus of Thin Films." *Journal of Materials Research*. 26(6): 727-738.

Henderson, G. S., Neuville, D. R., and Downs, R. T. (2014). "Spectroscopic Methods in Mineralogy and Materials Sciences." *Reviews in Mineralogy and Geochemistry* 78.

Herbert, E. G., Oliver, W. C., and Pharr, G. M. (2008). "Nanoindentation and the Dynamic Characterization of Viscoelastic Solids." *Journal of Physics D: Applied Physics*. 41(7): 074021, 9-pp.

Hoa, S. V., (2009). Principles of the Manufacturing of Composite Materials. Pennsylvania: DEStech Publications.

How to Make A NMR Sample. Accessed on November 10, 2015. http://chem.ch.huji.ac.il/nmr/preparation.html.

Huang, Y. H. (1993). Pavement Analysis and Design. Englewood Cliffs, NJ: Prentice Hall.

Hughes, J. M., Cameron, M., and Crowley K. D. (1989). "Structural Variations in Natural F, OH, and Cl Apatites." *American Mineralogist* 74: 870-876.

Hughes, J. M., Cameron, M., and Crowley K. D. (1991). "Ordering of Divalent Cations in the Apatite Structure: Crystal Structure Refinements of Natural Mn- and Sr-Bearing Apatite." *American Mineralogist* 76: 1857-1862.

Ikoma, T., Kobayashi, H., Tanaka, J., Walsh, D., and Mann, S. (2003). "Microstructure, Mechanical, and Biomimetic Properties of Fish Scales from Pagrus Major." *Journal of Structural Biology* 142: 327-333.

Ioannides, A. M., and Korovesis G. T. (1990). "Aggregate Interlock: A Pure-Shear Load Transfer Mechanism." *Transportation Research Record* 1286: 14–24. Washington, DC: Transportation Research Board of the National Academies.

Iyengar, G. V., and Tandon, L. (1999). Minor and Trace Elements in Human Bones and Teeth. Vienna, Italy: International Atomic Energy Agency (IAEA) -- Nutritional and Health-Related Environmental Studies (NAHRES), 39.

Jager, A., and Lackner, R. (2008). "Identification of Viscoelastic Model Parameters By Means of Cyclic Nanoindentation Testing." *International Journal of Materials Research*. 99(8): 829-835.

Jantou, V., Turmaine, M., West, G. D., Horton, M. A., and McComb, D. W. (2009). "Focused Ion Beam Milling and Ultramicrotomy of Mineralized Ivory Dentine for Analytical Transmission Electron Microscopy." *Micron* 40: 495-501.

Jantou-Morris, V., Horton, M. A., and McComb, D. W. (2010). "The Nano-Morphological Relationships Between Apatite Crystals and Collagen Fibrils In Ivory Dentine." *Biomaterials* 31: 5275-5286.

Joint Light Tactical Vehicle. Accessed on December 10, 2015. https://en.wikipedia.org/wiki/Joint_Light_Tactical_Vehicle.

Kennedy, A. J., Johnson, D. R., Seiter, J. M., Lindsay, J. H., Boyd, R. E., Bednar, A. J., and Allison, P. G. (2012). "Tungsten Toxicity, Bioaccumulation, and Compartmentalization into

Organisms Representing Two Trophic Levels" *Environmental Science and Technology* 46: 9646-9652.

Kim, S-K. (2013). Marine Biomaterials: Characterization, Isolation and Applications. Philadelphia, PA: CRC Press, Taylor and Francis.

Kizilyaprak, C., Daraspe, J., and Humbel, B. M. (2014). "Focused Ion Beam Scanning Electron In Biology." *Journal of Microscopy* 254(3): 109-114.

Klosowski, M. M., Friederichs, R. J., Nichol, R., Anolin, N., Carzaniga, R., Windl, W., Best, S. M., Shefelbine, S. J., McComb, D. W., and Porter, A. E. (2015). "Probing Carbonate in Bone Forming Minerals On The Nanometer Scale." *Acta Biomaterrialia* 20: 129-139.

Kumar, K., Rana, R. S., and Paliwal, B. S. (2005). "Osteoglossid and Lepisosteid Fish Remains from the Paleocene Palana Formation, Rajasthan, India" *Palaeontology* 48(6): 1187—1209.

Lambe, T. W., and Whitman, R. V. (1969). Soil Mechanics. London, UK: John Wiley and Sons.

Landis, W. J. (1995). "The Strength of a Calcified Tissue Depends in Part on the Molecular Structure and Organization of its Constituent Mineral Crystals in their Organic Matrix." *Bone* 16(5): 533-544.

Lee, S., Novitskaya, E., Reynante, B., Vasquez, J., Urbaniak, R., Takahashi, T., Woolley, E., Tombolato, L., Chen, P., and McKittrick, J. (2011). "Impact Testing of Structural Biological Materials." *Materials Science and Engineering: C* 31(4): 730-739.

Leng, Y. (2008). Materials Characterization: Introduction to Microscopic and Spectroscopic Methods. Chichester: John Wiley & Sons Ltd.

Levinson, R., Berry, M., Johnston, J., Osborne, C., and Pack, M. (2001). More Modern Chemical Techniques. London, UK: Royal Society of Chemistry,

Liao, C-J., Lin, F-H., Chen, K-S., and Sun, J-S. (1999). "Thermal Decomposition and Reconstruction of Hydroxyapatite In Air Atmosphere." *Biomaterials* 20(19): 1807-1813.

Lin, Y. S., Wei, C. T., Olevsky, E. A., and Meyers, M. A. (2011). "Mechanical Properties and the Laminate Structure of Arapaima Gigas Scales." *Journal of the Mechanical Behavior of Biomedical Materials* 4: 1145-1156.

Liou, S-C., Chen, S-Y., Lee, H-Y., and Bow, J-S. (2004). "Structural Characterization of Nano-Sized Calcium Deficient Apatite Powders." *Biomaterials* 25: 189-196.

Liu, W. T., Zhang, Y., Li, G. Y., Miao, and Wu, X. H. (2008). "Structure and Composition of Teleost Scales from Snakehead Channa Argus (Cantor) (Perciformes: Channidae)." *Journal of Fish Biology* 72: 1055-1067.

Luz, G., and Mano, J. (2009). "Biomimetic Design Material Biomaterial Inspired by the Structure of Nacre." *Philosophical Transactions of The Royal Society: A* 367: 1587—1605.

163

Makhecha, D. P. (2005). Dynamic Fracture of Adhesively Bonded Composite Structures Using Cohesive Zone Models. *PhD. Dissertation*. Virginia Polytechnic Institute and State University, Blacksburg, VA, USA.

Mallick, R. B., and El-Korchi, T. (2009). Pavement Engineering: Principles and Practice Boca Raton, FL: CRC Press Taylor and Francis Group.

Mann, S. (2001). Biomineralization Principles and Concepts in Bioinorganic Materials Chemistry. New York: Oxford University Press.

Maranganti, R., and Sharma, P. (2007). "Length Scales at Which Classical Elasticity Breaks Down for Various Materials." *Physical Review Letters* 98(19):195504.

Marinenko, R. B. (1991). Standards for Electron Probe Microanalysis, in Electron Probe Quantitation (K. F. J. Heinrich and D. E. Newbury, ed), Plenum, pp.251-260.

Markovic, M., Fowler, B. O., and Tung, M. S. (2004). "Preparation and Comprehensive Characterization of a Calcium Hydroxyapatite Reference Material." *Journal of Research of the National Institute of Standards and Technology* 109(6): 553-568.

Mathew, M., and Takagi, S. (2001). "Structures of Biological Minerals in Dental Research." *Journal of Dental Research* 106(6): 1035-1044.

McNally, E. A., Schwarcz, H. P., Botton, G. A., and Aresnault, A. L. (2012). "A Model for the Ultrastructure of Bone Based on Electron Microscopy of Ion-Milled Sections." *PLoS ONE* 7(1): e29258. doi:10.1371/journal.pone.0029258.

McNally, E. A., Nan, F., Botton, G. A., and Schwarcz, H. P. (2013). "Scanning Transmission Electron Microscopic Tomography of Cortical Bone Using Z-Contrast Imaging." *Micron* 49: 46-53.

Meyers, M., Chen, P., Lin, A., and Seki, Y. (2008). "Biological Materials: Structure and Mechanical Properties." *Progress in Materials Science*. 53: 1—206.

Meyers, M., Chen, P., Lopez, M., Seki, Y., and Lin, A. (2011). "Biological Materials: A Materials Science Approach." *Journal of The Mechanical Behavior of Biomedical Materials* 4(5): 626 – 657.

Mine-Resistant Ambush Protected. Accessed on December 10, 2015. https://en.wikipedia.org/wiki/MRAP.

Mucalo, M. (2015). Hydroxyapatite (HAp) for Biomedical Applications, 1st Edition. Cambridge, UK: Woodhead Publishing Series in Biomaterials-Elsevier.

Nalla, R. K., Porter, A. E., Daraio, C., Minor, A. M., Radmilovic, V., Stach, E. A., Tomsia, A. P., and Ritchie, R. O. (2005). "Ultrastructural Examination of Dentin Using Focused Ion-Beam Cross-Sectioning and Transmission Electron Microscopy." *Micron* 36: 672-680.

Needleman, A. (1989). "An Analysis of Decohesion Along an Imperfect Interface." *International Journal of Fracture* 42(1): 21 – 40.

Nieto, F., and Livi, K. J. T. (2013). "Minerals at the Nanoscale." *European Mineralogical Union: Notes In Mineralogy* 14.

Nudelman, F., Pieterse, K., George, A., Bomans, P. H., Friedrich, H., Brylka, L. J., Hilbers, P. A., de With, G., and Sommerdijk, N. A. (2010). "The Role of Collagen in Bone Apatite Formation in the Presence of Hydroxyapatite Nucleation Inhibitors." *Nature Materials* 9: 1004—1009.

Ochsner, A., and Ahmed, W. (2011). Biomechanics of Hard Tissues Modeling, Testing, and Materials (4th Edition). Hoboken, NJ, USA: Wiley-VCH.

Oliver, W. C., and Pharr, G. M. (1992). "An Improved Technique for Determining Hardness and Elastic Modulus Using Load and Displacement Sensing Indentation Experiments." *Journal of Materials Research* 7(6): 1564-1583.

Oliver, W. C., and Pharr, G. M. (2004). "Measurement of Hardness and Elastic Modulus by Instrumented Indentation: Advances in Understanding and Refinements to Methodology." *Journal of Materials Research* 19(1): 3-20.

Olszta, M., Cheng, X., Jee, S., Kumar, R., Kim, Y-Y., Kaufman, M., Douglas, E., and Gower, L. (2007). "Bone Structure and Formation: A New Perspective." *Materials Science and Engineering: R: Reports* 58(3–5): 77-116.

Ostojic, P., and McPherson, R. (1987). "A Review of Indentation Fracture Theory: Its Development, Principles and Limitations." *International Journal of Fracture* 33: 297-312.

Oyen, M. L. (2011). Handbook of Nanoindentation with Biological Applications. Singapore, China: Stanford Publishing.

Pethica, J. B., and Oliver, W. C. (1989). "Mechanical Properties of Nanometer Volumes of Material: Use of the Elastic Response of Small Area Indentations." *Materials Research Society Symposium Proceedings* 130: 13-23.

Pharr, G. M., Strader, J. H., and Oliver, W. C. (2009). "Critical Issues in Making Small-Depth Mechanical Property Measurements by Nanoindentation with Continuous Stiffness Measurement." *Journal of Materials Research* 24(3): 653-666.

Pharr, G. M., Herbert, E. G., and Gao, Y. (2010). "The Indentation Size Effect: A Critical Examination of Experimental Observations and Mechanistic Interpretations." *Annual Review of Materials Research* 40: 271-292.

Qiao, P., Yang, M., and Bobaru, F. (2008). "Impact Mechanics and High-Energy Absorbing Materials: Review." *Journal of Aerospace Engineering* 21(4): 235-248.

Rakovan, J., Luo, Y., and Borkiewicz, O. (2008). "Synchrotron Microanalytical Methods in the Study of Trace and Minor Elements in Apatite." *Mineralogia* 39(1-2): 31-40.

Randall, N. X., Vandamme, M., and Ulm, F-J. (2011). "Nanoindentation Analysis As A Two-Dimensional Tool For Mapping the Mechanical Properties of Complex Surfaces." *Journal of Materials Research* (24): v679-690.

Raschi, W., and Tabit, C. (1992). "Functional Aspects of Placoid Scales: A Review and Update" *Australian Journal of Marine and Freshwater Research* 43(1): 123 – 147.

Ratner, B. D., Hoffman, A. S., Schoen, F. J., and Lemons, J. E. (2013). Biomaterials Science: An Introduction to Materials in Medicine, 3rd Edition. London, UK: Elsevier.

Reed, S. J. B. (1996). Electron Microprobe Analysis and Scanning Electron Microscopy in Geology. Cambridge, UK: Cambridge University Press.

Reinhardt, C. (2001). Chemical Sciences in the 20th Century: Bridging Boundaries. Weinheim, Germany: Wiley-VCH.

Resnikov, N., Shahar, R., and Weiner, S. (2014). "Three-Dimensional Structure of Human Lamellar Bone: The Presence of Two Different Materials and New Insights Into the Hierarchical Organization." *Bone* 59: 93-104.

Rettler, E., Hoeppener, S., Sigusch, B. W., and Schubert, U. S. (2013). "Mapping the Mechanical Properties of Biomaterials on Different Length Scales: Depth-Sensing Indentation and AFM Based Nanoindentation." *Journal of Materials Chemistry B* 1: 2789-2806.

Rho, J-Y., and Pharr, G. M. (1999). "Effects of Drying on the Mechanical Properties of Bovine Femur Measured by Nanoindentation." *Journal of Materials Science: Materials in Medicine* 10: 485-488.

Rho, J. Y., Zioupos, P., Currey, J. D., and Pharr, G. M. (2002). "Microstructural Elasticity and Regional Heterogeneity in Human Femoral Bone of Various Ages Examined by Nano-Indentation." *Journal of Biomechanics* 35: 189-198.

Richter, M., and Smith M. (1995). "A Microstructural Study of the Ganoine Tissue of Selected Lower Vertebrates." *Zoological Journal of the Linnean Society* 114(2): 173 – 212.

Ritchie, R. (2011). "The Conflicts Between Strength and Toughness." *Nature Materials* 10(11): 817-822.

Rodriguez-Florez, N., Oyen, M. L., and Shefelbine, S. J. (2013). "Insight Into Differences in Nanoindentation Properties of Bone." *Journal of the Mechanical Behavior of Biomedical Materials* 18: 90-99.

Russ, J. C. (1984). Fundamentals of Energy Dispersive X-ray Analysis. London, UK: Butterworths.

Ryou, H., Romberg, E., Pashley, D. H., Tay, F. R., and Arola, D. (2012). "Nanoscopic Dynamic Mechanical Properties of Intertubular and Peritubular Dentin." *Journal of the Mechanical Behavior of Biomedical Materials* 7: 3-16.

Sahi, N., and Schoonen, M. A. A. (2006). "Medical Mineralogy and Geochemistry." *Reviews in Mineralogy and Geochemistry*, 64.

Salonitis, K., Pandremenos, J., Paralikas, J., and Chryssolouris, G. (2010). "Multifunctional Materials: Engineering Applications and Processing Challenges." *International Journal of Advanced Manufacturing Technology* 49: 803 – 826.

Sanchez-Quevedo, M. C., Nieto-Albano, O. H., Garacia, J. M., Gomez de Ferraris, M. E., and Campos, A. (1998). "Electron Probe Microanalysis of Permanent Human Enamel and Dentine. A Methodological and Quantitative Study." *Histology and Histopathology* 13: 109-113.

Sarikaya, M., Fong, H., Frech, D., and Humbert, R. (1999). "Biomimetic Assembly of Nanostructured Materials." *Material Science Forum* 293: 83—98.

Schonborner, A. A., Meunier, F. J., and Castanet, J. (1981). "The Fine Structure of Calcified Mandl's Corpuscles in Teleost Fish Scales." *Tissue and Cell* 13(3): 589-597.

Shapiro, J. R., Byers, P. H., Glorieux, F. H., and Sponseller, P. D. (2014). Osteogenesis Imperfecta: A Translational Approach to Brittle Bone Disease. London, UK: Elsevier.

Shark. Accessed on November 10, 2015. http://www.britannica.com/EBchecked/topic/53bb51/shark.

Sire, J-Y. (1989a). "Scales in Young Polypterus Senegalus are Elasmoid New Phylogenetic Implications. *American Journal of Anatomy* 186(3): 315 – 323.

Sire, J-Y. (1989b). "From Ganold to Elasmoid Scales in the Actinopterygian Fishes." *Netherlands Journal of Zoology* 40(1-2): 75 – 92.

Sire, J-Y. (1995). "Ganoine Formation in the Scales of Primitive Actinopterygian Fishes, Lepisosteids and Polypterids." *Connective Tissue Research* 33(1-3): 213 – 222.

Smith, J. B., Grandstaff, B. S., and Abdel-Ghani, M. S., (2006). "Microstructure of Polypterid Scales (*Osteichthyes: Actinopterygii: Polypteridae*) From the Upper Cretaceous Bahariya Formation, Bahariya Oasis, Egypt." *Journal of Paleontology* 80(6): 1179—1185.

Sneddon, I. N. (1965). "The Relation Between Load and Penetration in the Axi-Symmetric Boussinesq Problem for a Punch of Arbitrary Profile." *International Journal of Engineering Science* 3(1): 47-57.

Song, J., Reichert, S., Kallai, I., Gazit, D., Wund, M., Boyce, M., and Ortiz, C. (2010). "Quantitative Microstructural Studies of the Armor of the Marine Threespine Stickleback (*Gasterosteus aculeatus*)." *Journal of Structural Biology* 171: 318–331.

Song, J., Oriz, C., and Boyce, M. C. (2011). "Threat-Protection Mechanics of an Armored Fish." *Journal of the Mechanical Behavior of Biomedical Materials* 4(5): 699-712.

Srinivasan, A.V., Haritos, G. K. and Hedberg, F. L. (1991). "Biomimetics: Advancing Man-Made Materials Through Guidance From Nature." *Applied Mechanical Reviews* 44(11): 463-481.

Strong, A. B. (2008). Fundamentals of Composites Manufacturing - Materials, Methods, and Applications, Second Edition. Dearborn, Michigan: Society of Manufacturing Engineers.

Structural Composites and Sandwhich Panels. Accessed on November 10, 2015. http://www.engineeredmaterialsinc.com/products/structural-composites-and-sandwhich-panels/.

Sudo, S., Tsuyuki, K., Ito, Y., and Ikohagi T. (2002). "A Study on the Surface Shape of Fish Scales." *JSME International Journal. Mechanical Systems, Machine Elements and Manufacturing* 45(4): 100 – 1105.

Sun, J., Ling, M., Wang, Y., Chen, D., Zhang, S., Tong, J., and Wang, S. (2014). "Quasi-Static and Dynamic Nanoindentation of Some Selected Biomaterials." *Journal of Bionic Engineering* 11: 144-150.

Swadener, J. G., George, E. P., and Pharr, G. M. (2002). "The Correlation of The Indentation Size Effect Measured with Indenters of Various Shapes." *Journal of the Mechanics and Physics of Solids* 50: 681-694.

Tai, K., Qi, H. J., and Ortiz, C. (2005). "Effect of Mineral Content on the Nanoindentation Properties and Nanoscale Deformation Mechanisms of Bovine Tibial Cortical Bone" *Journal of Materials Science: Materials In Medicine* 16: 947-959.

Terzaghi, K. (1943). Theoretical Soil Mechanics, London, UK: John Wiley and Sons.

The Electromagnetic Spectrum. Accessed on November 10, 2015. http://herschel.cf.ac.uk/science/infrared.

Timoshenko, S., and Lessels, J. M. (1925). Applied elasticity. Pittsburg, PA: Westinghouse Technical Night School Press.

Tippetts, T. (2005). "Non-Linear Models of Composite Laminate." *Proceedings of the 23rd Conference*.

Tonsuaadu, K., Gross, K. A., Pluduma, L., and Veiderma, M. (2012). "A Review on the Thermal Stability of Calcium Apatites." *Journal of Thermal Analysis and Calorimetry* 110: 647-659.

Torres, F. G., Troncoso, O. P., Nakamatsu, Grande, C. J., and Gomez, C. M. (2008). "Characterization of the Nanocomposite Laminate Structure Occurring in Fish Scales From Arapaima Gigas." *Materials Science and Engineering C* 28: 1276-1283.

Unified Facilities Criteria (UFC), Pavement Design for Airfields. (2001b).UFC 03-260-02. Construction Criteria Base. Washington, DC: National Institute of Building Sciences.

VanLandingham, M. R. (2003). "Review of Instrumented Indentation." *Journal of Research of the National Institute of Standards and Technology* 108(4): 249–265.

Waite, J. H., and Broomell, C. C. (2012). "Review: Changing Environments and Structure–Property Relationships in Marine Biomaterials." *The Journal of Experimental Biology* 215: 873-883.

Wegst, U. G. K., and Ashby, M. F. (2004). "The Mechanical Efficiency of Natural Materials." *Philosophical Magazine* 84(21): 2167 – 2181.

Wegst, U., Bai, H., Saiz, E., Tomsia, A., and Ritchie, R. (2015). Bioinspired Structural Materials. *Nature Materials* 14 (1): 23-36.

Wegst, U., Schecter, M., Donius, A., and Hunger, P. (2010). "Biomaterials by Freeze Casting." *Philosophical Transactions of The Royal Society: A* 368: 2099—2121.

Weiner, S., Veis, A., Beniash, E., Arad, T., Dillion, J. W., Sabsay, B. and Siddiqui, F. (1999). "Peritubular Dentin Formation: Crystal Organization and the Macromolecular Constituents in Human Teeth." *Journal of Structural Biology*, Vol. 126, pp. 27-41.

Weiner, S., Addadi, L., and Wagner, H. D. (2000). "Materials Design in Biology." *Materials Science and Engineering C* 11: 1-8.

Westergaard, H. M. (1925). "Computation of Stresses in Concrete Roads." *In Proceedings Highway Research Board. National Research Council* 5(1): 90–112.

Wheeler, A. J. and Ganji, A. R. (2001). Introduction to Engineering Experimentation. 2nd Edition. Upper Saddle River, NJ: Pearson-Prentice Hall.

Wiley, E. O. (1976). "The Phylogeny and Bio Geography of Fossil and Recent Gars (*Actinopterygii: Lepisosteidae)." University of Kansas Museum of Natural History Miscellaneous Publication* 64: 1-111.

Wright, W. J., Maloney, A. R., and Nix, W. D. (2007). "An Improved Analysis for Viscoelastic Damping in Dynamic Nanoindentation." *International Journal of Surface Science and Engineering* 1(2-3): 274-292.

Williams, D. B., and Carter, C. B. (2009). Transmission Electron Microscopy: A Textbook for Materials Science, 2nd Edition. New York, NY: Springer.

Williamson, W. C. (1849). "On the Microscopic Structure of the Scales and Dermal Teeth of Some Ganoid and Placoid Fish." *Philosophical Transactions-Royal Society of London. Physical Sciences and Engineering* 139: 435 – 475.

Willmott, P. (2011). An Introduction to Synchrotron Radiation: Techniques and Applications. Chichester: John Wiley & Sons Ltd.

Wilson, R. M., Elliot, J. C., and Dowker, S. E. P. (1999). "Rietveld Refinement of the Crystallographic Structure of Human Dental Enamel Apatites." *American Mineralogist* 84: 1406-1414.

Wopenka, B., and Pasteris, J. D. (2005). "A Mineralogical Perspective on the Apatite in Bone." *Materials Science and Engineering C* 25: 131-143.

X-RAY DATA BOOKLET. Accessed on November 10, 2015. http://xdbl.llbl.gov.

Yang, W., Chen, I. H., McKittrick, J., and Meyers, M. A. (2012). "Flexible Dermal Armor in Nature." *Journal of the Minerals, Metals & Materials Society* 64 (4): 475-485.

Yang, W., Chen, I. H., Gludovatz, B., Zimmermann, E. A., Ritchie, R. O., and Meyers, M. A. (2013a). "Natural Flexible Dermal Armor." *Advanced Materials* 25(1): 31-48.

Yang, W., Gludovatz, B., Zimmermann, E. A., Bale, H. A., Ritchie, R. O., and Meyers, M. A. (2013b). "Structure and Fracture Resistance of Alligator Gar (*Atractosteus Spatula*) Armored Fish Scales." *Acta Biomaterialia*, 9(4): 5876-5889.

Yoder, E. J., and Witczak, M. W. (1975). Principles of Pavement Design 2nd Edition, London, UK: John Wiley and Sons.

Young, R. A. (1974). "Implications of Atomic Substitutions and Other Structural Details in Apatites." *Journal of Dental Research*, 53(2): 193-203.

Zhang, J., Niebur, G. L., and Ovaret, T. C. (2008). "Mechanical Property Determination of Bone Through Nano- and Micro-Indentation Testing and Finite Element Simulation." *Journal of Biomechanics* 41: 267-275.

CURRICULUM VITAE

a. Name: Wayne D. Hodo

b. Current Position, Department and Division: Research Civil Engineer, Airfields and Pavements Branch, Geotechnical and Structure Laboratory, US Army, ERDC

c. Education:

- 2006 M.S. (Civil Engineering), Mississippi State University, Starkville, Mississippi, USA
- 1997 B.S. (Civil Engineering), Auburn University, Auburn, Alabama, USA

d. Professional Experience or Employment:

- 1998-present Research Civil Engineer, Airfields and Pavements Branch Geotechnical and Structure Laboratory
- 2005-2009 American Society for Civil Engineers – Local Chapter Chairman of Scholarship Committee
- 2003-2010 American Society for Testing and Materials – Chairman of Fundamental/ Mechanistic Test of Bituminous Mixtures
- 2009-2011 American Concrete Institute Member
- 2011-present American Society for Mechanical Engineers Member
- 2015-Co-Organizer for ASME's International Mechanical Engineering Congress and Exposition (IMECE) for Symposium 21-Mechanics and Material Science of Nanoengineered, Hierarchical, and Multi-Scale Materials.

e. Publications:

- Allison, P. G., Hodo, W. D., Rodriguez, R. I., Kennedy, A. J., Chandler, M. Q., Hidalgo, R. G., Moser, R. D., and Peters, J. P.. Structure and mechanical properties of biological multi-layered material systems. International Journal of Plasticity Conference 2012.
- Hodo, W. D., Allison, P. G., Rodriguez, R. I., Kennedy, A. J., Chandler, M. Q., Hidalgo, R. G., Moser, R. D., and Peters, J. P. Structure-Property Relationships of the Interface in Natural Multi-Layered Material Systems. International TMS Conference 2012.
- Moser R. D., Hodo, W. D., Weiss Jr., C. A., Malone, P. G., Chappell, M. A, Seiter, J. M., Lafferty, B., Rodriguez, R. I., Negron, O. R., Torres-Cancel, K. A., Allison, P. G., Chandler, M. Q., and Hidalgo-Hernandez, R. G. Application of Advanced Characterization Tools to the Study of Structural Biomaterials and Bio-Inspired Materials. NICOM 4: 4th International Symposium on Nanotechnology in Construction 2012.

f. Presentations/Poster Sessions:

- "Experimental Characterization of Bone and Exoskeleton Fish Scale Structures," Presented at The Minerals, Metals and Materials (TMS) Conference, March 2015

- "Structure and mechanical properties of biological multi-layered material systems," Paper Presented at International Journal of Plasticity Conference, January 2012
- "Structure-Property Relationships of the Interface in Natural Multi-Layered Material Systems," Poster Session and Paper Presented at The Minerals, Metals and Materials (TMS) Conference, March 2012
- "Application of Advanced Characterization Tools to the Study of Structural Biomaterials and Bio-Inspired Materials" Paper accepted for presentation at NICOM 4: 4th International Symposium on Nanotechnology in Construction, May 2012

g. Research Achievement and Recognition Awards:

- 2013 Army Award – Science and Technology Leader
- 2013 STEM-BEYA – Modern-Day Technology Leader
- 2012 ERDC Award for providing Outstanding Service and Leadership in the support of ERDC's Research Program on High-Performance Materials
- 2008 ERDC Award for Outstanding Team Effort in supporting the Air Force Semi-Prepared Runway Operations research program
- 2008 ERDC Award for Outstanding Team Effort in supporting the Army Joint Rapid Airfield Construction research program
- 2007 Superior Civilian Service award for the IPET Katrina effort in the validation of failure mechanism for the New Orleans Levee System, using centrifugal physical modeling concepts
- 2006 Army Award from John Paul Woodley, Assistant Secretary of the Army for Civil Works, for providing technical support for the IPET (Interagency Performance Evaluation Taskforce) research effort of the New Orleans Levee system
- 2000 Award from the General of the Royal Jordanian Air Force for outstanding performance in the reconstruction of a Jordanian airfield